For the lettering along the back of the bound copies

XENON YIELDS AND ISOMER RATIOS IN FISSION

J. H. FORSTER 1966

XENON YIELDS AND ISOMER RATIOS IN THE FISSION OF HEAVY ELEMENTS BY MEDIUM-ENERGY PROTONS

by

JOHN H. FORSTER

A thesis submitted to the Faculty of Graduate Studies and Research in partial fulfilment of the requirements for the degree of Doctor of Philosophy

Department of Chemistry,
McGill University,
Montreal,
Canada.

April 1966.

ACKNOWLEDGMENTS

I am very [redacted]ful t[redacted]fessor L. Yaffe for my rewarding and happy years at McGill University, and for his continual encouragement.

Dr. N.T. Porile gave very helpful direction during his period in this laboratory, from 1963-1965.

I sincerely appreciate the many things which I have learnt from my colleagues at McGill.

I thank my wife, Dorothy, for the invaluable assistance she has given me. She tirelessly and efficiently typed the drafts and final manuscript of this thesis.

The following contributions to the research are much appreciated.

At the beginning of the work, Dr. I. Dostrovsky generously advised us on experimental techniques.

Dr. R.E. Bell, Director of the Foster Radiation Laboratory, made the cyclotron available to us. Bob Mills cheerfully performed the irradiations.

McGill University Computing Centre efficiently executed the programs.

The National Research Council awarded the author a Scholarship from 1963-1966, and The Chemistry Department of McGill University provided Demonstratorships from 1961-1966.

ABSTRACT

The independent yields of ^{135}Xe, ^{133m}Xe and ^{133g}Xe and the cumulative yields of ^{135}I and ^{133}I have been measured for twenty-seven fission systems, consisting of the targets ^{232}Th, ^{238}U, ^{235}U and ^{233}U with protons of energies from 20 to 85 MeV. A radiochemical gas-sweeping technique was used and the xenon activities were measured by a gamma spectrometer calibrated with a gas-phase beta proportional counter. The experiments were designed primarily for a study of precise isomeric yield ratios of ^{133}Xe, but they also gave information on fission yields and their variations in mass chains 133 and 135.

Because of the large uncertainty in α_T for ^{133m}Xe, four possible values of this coefficient were used to report the isomer ratios. It is suggested that the existing experimental value of α_T is too low. For all the systems studied, the value of the isomer ratio of ^{133}Xe was remarkably constant, within the experimental relative uncertainty of 10-20%. It was concluded that the isomer ratio is apparently independent of the spin and type of the fission target. The present data suggest that the isomer ratio is more weakly dependent on fission energy than was generally thought.

Crude statistical computations were performed for three spin-pair classes of isomers, (9/2, 1/2), (11/2, 3/2) and (8,5). The theoretical results improved our understanding of the relative formation of isomers in fission and allowed a more quantitative discussion and survey of existing data.

For proton energies up to 55 MeV, charge distribution was studied in the chains 133 and 135. A Gaussian charge distribution curve was assumed in two methods used to determine empirically, from relative yield data, the values of Z_p and fractional chain yields. One method, developed here, uses the ratio of the cumulative yield of a beta parent to the independent yield of the daughter. The method proved reliable for the pairs $^{135}I/^{135}Xe$ and $^{133}I/^{133}Xe$. It should be useful in future work.

For ^{238}U and ^{232}Th, the variations with proton energy of Z_p for chains 133 and 135 showed the trends now fairly well established for this mass region. However, a considerably different behaviour was observed for ^{235}U and ^{233}U. The simplified CCR postulate was used to estimate roughly total yields of fission neutrons, from the empirical Z_p values.

Absolute cross sections, plotted as excitation

functions, were obtained from the irradiations of ^{232}Th, ^{238}U and ^{235}U, by monitoring the proton beam with the reaction $^{65}Cu(p,pn)^{64}Cu$.

Total chain yields were determined from the absolute and fractional yields in chains 133 and 135. They were consistent with a flat mass distribution curve in this mass region.

TABLE OF CONTENTS

		Page
1.	INTRODUCTION	
	1.1 General - - - - - - - - - - - - - - -	1
1A.	SECTION A. FISSION YIELDS AND THEIR VARIATIONS	
	1A.1 Nomenclature - - - - - - - - - - - - -	3
	1A.2 Measurement of Fission Yields - - - - - -	6
	1A.2.1 Fission Yields of Xenon and Krypton -	7
	1A.3 Variation of Fission Yields - - - - - - -	14
	1A.3.1 Mass Distribution - - - - - - - -	15
	1A.3.2 Charge Distribution - - - - - - -	27
	Postulate Correlation Method (A) - -	33
	Empirical Correlation Method (B) - -	39
	New Physical Methods - - - - - - -	49
	Summary of Present Knowledge - - -	51
	1A.4 Distributions of Isotopic Mass and Isotonic Charge - - - - - - - - - -	61
1B.	SECTION B. ISOMERIC YIELD RATIOS IN FISSION	
	1B.1 General - - - - - - - - - - - - - - -	62
	1B.2 Factors Deciding the Fission Isomer Ratio -	63
	1B.2.1 Spin Distribution of the Compound Nucleus - - - - - - - - - - -	64
	1B.2.2 Spin Changes Following Emission of Pre-fission Neutrons - - - - - -	66
	1B.2.3 Orbital Angular Momentum between Fragments - - - - - - - - - - -	67
	1B.2.4 Disposition of Angular Momentum between Fragments - - - - - - - -	68
	1B.2.5 Orientation of the Spins of Complementary Fragments - - - - - -	72
	1B.2.6 Modification of the Spin Distribution of Initial Fragments - -	73
	1B.2.6.1 Stage (1), Neutron Emission -	74
	1B.2.6.2 Stage (2), Gamma Ray Cascade	77
	1B.2.6.3 Choice of Input Parameters for Stages (1) and (2) - -	78
	1B.2.7 Effective Spin-pair of the Isomeric Species - - - - - - - -	85
	1B.3 Suitability of the Isomers of ^{133}Xe for this study - - - - - - - - - - -	89

1AB. PURPOSE OF THE PRESENT WORK 91

2. EXPERIMENTAL

2.0 Outline of Experimental Work - - - - - - - 93
2.1 Irradiations and Target Assembly - - - - - 94
2.2 Chemical Separations and Yields - - - - - - 99
2.2.1 Copper - - - - - - - - - - - - - - 99
2.2.2 Xenon - - - - - - - - - - - - - - 100
2.2.2.1 Gas-sweep (a) - - - - - - - 100
Part 1. Extraction of Xe and Kr 100
Part 2. Separation of Xe from Kr 106
Part 3. Preparation of Xe Sample 109
2.2.2.2 Gas-sweep (b) - - - - - - - 110
2.2.2.3 Miscellaneous Details - - - 110
2.3 Radiation Measurement - - - - - - - - - 112

3. TREATMENT OF DATA FROM THE ACTIVITY MEASUREMENTS

3.1 Analysis of Spectra and Decay Curves - - - 115
3.1.1 Copper - - - - - - - - - - - - - - 115
3.1.2 Xenon - - - - - - - - - - - - - - 117
Sample from Sweep (a) - - - - - - - 117
Sample from Sweep (b) - - - - - - - 122
3.2 Calculation of Relative and Absolute Cross Sections - - - - - - - - 124
3.3 Errors - - - - - - - - - - - - - - - - 125

4. RESULTS AND DISCUSSION

4A. SECTION A. FISSION YIELDS AND THEIR VARIATIONS

4A.1 Absolute and Relative Cross Sections - - - 132
4A.2 Determination of Empirical Z_p Values - - - 147
4A.2.1 Use of a Gaussian FUNCTION (1) - - - 148
4A.2.2 Method (1) - - - - - - - - - - - 151
4A.2.3 Method (2) - - - - - - - - - - - 155
4A.3 Empirical Z_p Values for Chains 133 and 135 - 156
4A.3.1 Variations in Z_p - - - - - - - - 158
4A.3.2 Conclusions on Variations of Z_p - - 162
4A.4 Z_p Values and the Maximum in Excitation Functions - - - - - - - - 167
4A.5 Fractional and Total Chain Yields for A = 133 and 135 - - - - - - - 175

4B. SECTION B. ISOMERIC YIELD RATIOS IN FISSION

4B.1 Experimental Isomer Ratios of ^{133}Xe - - - 179
4B.2 Theoretical Calculations of Spin Distributions during Fragment De-excitation - 184
4B.2.1 Input Data for Stages (1) and (2) - - 186
4B.2.2 Results for Stages (1) and (2) - - - 189
4B.2.3 Stage (3) - - - - - - - - - - -
4B.2.4 Theoretical Isomer Ratios - - - - 194
4B.2.5 Conclusion from Fragment De-excitation Calculations - - - - 200
4B.3 Calculation of the Spin Distribution of the Compound Nucleus - - - - - - - - 203
4B.4 Effect of Target Spin on the Fission Isomer Ratio - - - - - - - - - 206
4B.5 Effect of Projectile Energy on the Fission Isomer Ratio - - - - - - - - - 208
4B.6 Estimate of Fragment Spin from the Isomer Ratio - - - - - - - - - - - 211
4B.7 Comparison of Yield Ratios for an Isomer Pair Formed in Spallation and in Fission - - 216
4B.8 Prediction of Unmeasured Fission Isomer Ratios - - - - - - - - - - - - 219
4B.9 Limitations of the De-excitation Model - - 221
4B.10 Concluding Assessment of Fission Isomer Ratio Studies - - - - - - - - - 224

5. SUMMARY

5A. SECTION A. FISSION YIELDS AND THEIR VARIATIONS 230

5B. SECTION B. ISOMERIC YIELD RATIOS IN FISSION 233

APPENDIX A. Equations and Monitoring Used to Obtain Cross Sections

A.1 Equations used in Calculations of Cross Sections - - - - - - - - 235
A.2 Monitoring the Proton Beam - - - - 240

APPENDIX B. Photopeak Efficiencies and Measurement of Beta Activity

B.1 Photopeak Efficiencies - - - - - 242
B.1.1 Photopeak Due to ^{64}Cu - - - 242
B.1.2 Photopeaks Due to Xenon Isotopes - - - - - - 242
B.1.2.1 Beta Counting Equipment 243
B.1.2.2 Efficiency of Beta Counter - - - - - 248
B.1.2.3 Efficiency of Xe Photopeaks - - - - 249
B.2 Beta Counting of Xenon Produced in Fission - - - - - - - - - - 252

APPENDIX C. Method (2) to Determine Z_p. Bateman Equations for Growth and Decay in Chain 133 - - - - - - - 257

BIBLIOGRAPHY (230 References) - - - - - - - - - 267

1. INTRODUCTION

1.1 GENERAL

The main purpose of this thesis was to examine the relative yields of the isomers of ^{133}Xe formed in the fission of several heavy elements by medium-energy protons. The experiments were designed primarily for this purpose. It was possible from the same experiments to contribute to the study of the charge distribution in fission, and to obtain fractional and absolute yields for the nuclides of xenon and iodine, in the isobaric chains of mass, A, equal to 133 and 135. From these yields, total chain yields could be estimated for the two masses.

First, this Introduction outlines important general references on fission; then in SECTION A it reviews the study of fission yields and their variations with mass and charge; in SECTION B it surveys in some detail the study of the relative formation of isomers in fission; and finally it summarizes the purpose of this study. Although SECTIONS A and B are complementary to one another they have been written as self-contained introductions to their respective topics. This was achieved by allowing some repetition of subjects which

were important to both sections.

A satisfactory comprehensive theory does not exist for the complex process of fission; specific theoretical aspects of fission pertinent to the present study will be discussed in the appropriate sections of this thesis.

There is a very large experimental and theoretical literature on fission and this has been regularly collected and surveyed (COR 51, WHI 52, SPE 53, GLE 54, HAL 59, HYD 60, HYD 62, HYD 64, KAT 60, CRO 60, HUI 62).

Wheeler (WHE 56) outlined the development of fission theories up to 1956 and Leachman (LEA 62) reviewed fission mechanisms up to 1962. Swiatecki (SWI 65) has surveyed recent contributions to fission theory. He stressed the importance of the work of Nix and Swiatecki (NIX 65) which made an important contribution (discussed in Section 1B) to the theory of isomeric yield ratios in fission, and could be extended to discuss the charge distribution in fission fragments. The one hundred diverse papers presented at the recent I.A.E.A. Symposium on the Physics and Chemistry of Fission (Salzburg, March 1965) showed the wide interest that still exists in this complex process. They also illustrated that, although various theories and empirical prescriptions can now account for the main

features of some fission systems, many aspects of fission are not well defined experimentally and remain a mystery theoretically (NIX 65).

1A. SECTION A

FISSION YIELDS AND THEIR VARIATIONS

1A.1 NOMENCLATURE

The literature on fission yields contains nomenclature which is often ambiguous and confusing. In this thesis an attempt has been made to avoid this difficulty by using the following definitions.

FISSION FRAGMENTS are formed in the act of scission. FISSION PRODUCTS are formed after emission of prompt neutrons from the fragments, either before or after beta-decay from isobaric fission products.

Two types of fission product yields can be measured, independent and cumulative. THE INDEPENDENT YIELD of a fission product nuclide is the yield of a nuclide which is formed from fission fragments of the same isotopic chain, by the emission of 0, 1, 2 or more neutrons (neglecting any charged particle emission from fragments). THE CUMULATIVE YIELD of a fission product isotope is the sum of the

independent yields of that nuclide and of all the isobaric fission products leading to that nuclide.

A careful distinction must be made between two types of charge distribution.

(i) THE INITIAL CHARGE DISTRIBUTION will be used to refer to the charge distribution of isobaric fragments; obviously it is this distribution which shows how the nuclear charge divides itself between the two fragments at scission.

(ii) THE APPARENT CHARGE DISTRIBUTION will be used to refer to the charge distribution of isobaric fission products; this distribution shows how the independent fission yields of isobaric fission products vary along an isobaric chain.

Although some authors have reserved the term "charge dispersion" (FRI 65) for the apparent charge distribution, and then used the term "charge distribution" to refer only to the initial charge distribution, confusion is caused by the many authors who use the term charge distribution to describe either type of distribution. In this thesis no distinction is made between the words, distribution and dispersion, and the use of the latter word is avoided because of its occurrence in discussions of the

corrections made to physical data in mass distribution studies.

Consistent with the nomenclature for charge distribution, a careful distinction must be made between two types of mass distribution.

(i) THE INITIAL MASS DISTRIBUTION refers to the mass distribution of the fragments, and obviously shows how the mass divides at scission.

(ii) THE FINAL MASS DISTRIBUTION refers to the mass distribution of the fission products. It shows how the total isobaric chain yield, the sum of the independent yields in a chain, varies with the mass of the chain. The word "final" may be used in this context since the decay of fission products causes no change of mass number, A, except in the relatively rare event of decay by delayed neutron emission.

The adjectives "primary" and "secondary" have not been used here to qualify fission yields because of their ambiguous use in the literature.

1A.2 MEASUREMENT OF FISSION YIELDS

The measurement of fission yields has made a large contribution to the study of the fission process since its discovery (HAH 39). Most of the existing yield data for fission products have come from numerous radiochemical and mass spectrometric studies, but promising new physical methods are being developed and have already given valuable data for fission fragments as well as fission products. The fission products in low-energy fission and many of those in medium-energy fission are neutron-rich and therefore decay by negative beta-particle emission along an isobaric chain to the stable isobar. The early members of these chains are many charge units from stability and are so short-lived that it is usually possible to measure only cumulative yields of isobars near the stable end of a chain. However, independent yields can be measured directly, for the few shielded fission products which have stable isobaric precursors, and indirectly with suitable growth corrections, for those fission products which are semi-shielded or quasi-shielded by relatively long-lived precursors. The fractional yields of some very short-lived fission products have been measured by ingenious experimental techniques.

1A.2.1 THE FISSION YIELDS OF XENON AND KRYPTON

This thesis is concerned with the fission yields of xenon isotopes formed in the fission of heavy elements by protons of medium-energy.

An important part of the existing fission yield data has been collected for the rare gases, krypton and xenon. They are both formed in good yield in fission and are particularly suitable for quick, efficient chemical separation after or even during (APO 62, JAM 64) an irradiation. They are very suitable for study by mass-spectrometry. It will be seen in this thesis that they have made a considerable contribution to the understanding of charge distribution and it is of historic interest that in an early gas-sweep experiment (DIL 51) they gave the first experimental evidence for a distribution of initial nuclear charge for fission products of a particular mass number.

There have been a large number of experimental studies of krypton and xenon not only because of the convenience with which they may be measured, but also because of their importance industrially and in nuclear reactor technology. No attempt is made to discuss the technological aspects of radioactive rare gases beyond the very brief outline in the following paragraph.

Rare gases formed in fission cause "swelling" (WEB 63) of uranium fuel materials and may therefore rupture a fuel rod. They also cause a decrease in reactor efficiency (FIC 59) due to the extremely high capture cross section of ^{135}Xe for thermal neutrons ($\approx 3 \times 10^6$ barns). Many systems for testing failures in reactor fuel elements depend on the release of rare gas activities (KRI 61). Radioactive rare gases are very suitable (WIL 57) for industrial uses (e.g. static eliminators, leak detection, discharge initiators). The most suitable are the relatively long-lived ^{133}Xe (5.3 days) and ^{85}Kr (10.6 years). These have a very low radioactive toxicity and no contamination hazard because they are relatively inert gases, and have stable decay products. ^{85}Kr is extracted on a large scale from uranium slugs after their irradiation in a reactor. A standard source of ^{85}Kr was used in the present work to calibrate the gas-counting equipment.

Bergstrom (BER 52) reviewed the studies of krypton and xenon isomers, up to 1952. A monograph by Momyer (MOM 60) has reviewed, up to 1960, the extensive radiochemistry of the rare gases, including techniques for removal of these gases from fission targets, for separation and purification of krypton and xenon, and for measuring the

activity of their radioactive isotopes. Since then, many rare gas techniques have been used (KOC 61, AUB 61, FEL 62, KAP 61, STO 62, MCH 63, JAM 64, DOS 64). The experimental work in this thesis was based largely on the method used by Dostrovsky and Stoenner (DOS 62). More details are given in the experimental Section 2.2.2, but the main steps which are similar to those in many radiochemical studies of the rare gases are summarized here.

(i) The rare gases are removed from the target. This has been done by vacuum fusion (MCH 63) but more commonly by chemical dissolution of the target followed by sweeping with a non-radioactive gas (e.g. H_2, O_2, CO_2, N_2, He). A measured amount of inactive krypton and xenon carrier gas is usually injected into this sweep gas.

(ii) The gases are purified, particularly from halogens which are the beta-decay parents of krypton and xenon.

(iii) They are adsorbed at low temperature on activated charcoal (WEL 59) or other suitable material (e.g. silica gel, molecular sieves).

(iv) Krypton and xenon are separated by gas-chromatography (AUB 61, KOC 61).

(v) The separated gases are purified, measured to establish their recovery-yield, and then their activity is determined.

Information about the cumulative yields of the halogen parents can be obtained in later gas-sweeps, by "milking" the rare gas which has grown from the decay of these parents.

Gas-sweeping techniques cannot measure the yields of very short-lived rare gases. Very important data for the fractional cumulative yields of short-lived krypton and xenon have been obtained by the emanation technique of Wahl (WAH 58), which has been applied extensively to low-energy neutron fission (WAH 62, WAH 65), recently to fission by 14 MeV-neutrons (WOL 65), and will probably be adapted for fission by charged particles. In this technique, the fissionable material was covered with, or was itself, a stearate salt in an evacuated container lined with filter paper. A mixture of fission products recoiled into the stearate, but only the rare gases formed in fission, and fission products that decay to them, emanated from the salt into the container. After the emanated rare gases with short half-lives had decayed, the container was opened. Then the decay products on the liner, and the fission and decay

products in the stearate, were assayed by standard radiochemical procedures. The interpretation of data from the emanation method may be considerably influenced by uncertainties in the half-lives for the short-lived rare gases. These half-lives have been measured precisely by special techniques (PAT 65).

The first fission product yields to be measured with the mass spectrometer were those of the isotopes of krypton and xenon formed in thermal neutron fission of ^{235}U (THO 47, FRI 58). Since then numerous fission product yields have been measured using a combination of careful chemistry and mass spectrometry. McHugh (MCH 63) has collected a bibliography of about twenty of these investigations. The technique was used mainly for low-energy fission (FAR 62b), after long bombardments in a high neutron flux. However, the high sensitivity work of Gordon and Friedman (GOR 57), Chu (CHU 59) and later workers (BLA 60, MCH 63) has shown that the technique can also give precise relative isotopic abundances even for medium- and high-energy fission. The yields obtained at these energies are very low, because generally it is possible to use only a relatively low flux and relatively short irradiations. In practice the sensitivity of mass spectrometry is limited by

natural contamination, for which corrections must be made. The precise data of McHugh are of particular interest and are further discussed in other parts of this thesis.

As in radiochemical methods, it is usually necessary in the design and interpretation of mass spectrometric measurements of fission yields to have a good knowledge of the half-lives and branching ratios in the appropriate beta-decay chain. However, mass spectrometric techniques have the advantage that stable as well as radioactive fission products can be measured and that some errors inherent in all radiochemical methods are eliminated. These errors occur in the determination of chemical yields in often complex series of separations, in the finer details of the decay scheme, and in the efficiences of the activity measurement. Furthermore a main difficulty in radiochemical methods has been the resolution of complex decay curves, though their analysis has been simplified by specially designed computer programs and by spectrometry of X-rays, gamma-rays and beta-rays. Recently a powerful method has been developed which avoids the resolution of complex decay curves. First, a particular fission product element, for example iodine (RUD 65), is separated chemically and then fed to the ion source of an electromagnetic separator which

prepares samples of individual isotopes for standard activity measurements.

For proton-induced fission no fission yields have previously been reported for the xenon isotopes, ^{133}Xe and ^{135}Xe, measured in this work. For the fission of ^{232}Th by protons, Pate, Foster and Yaffe (PAT 58a) used an independent radiochemical method to obtain the cumulative yields of ^{133}I and ^{135}I. Their results will be compared with the corresponding data from this work.

For thermal neutron fission, the fission yield of ^{135}Xe has been measured previously (HOA 51, BRO 53, KAT 53, STO 62, BAY 61). For thermal neutron fission of ^{235}U, the independent fractional chain yield of ^{133}Xe is very small (0.1%) and only its cumulative yield has been measured (MAC 50, KAT 53).

For some medium-energy fission systems (Table 1), independent yields have been measured for ^{135}Xe (STO 62, MCH 63) and ^{133}Xe (STO 62). Cumulative yields were obtained for their respective iodine parents (COL 61, STO 62, MCH 63).

For the fission of ^{238}U by neutrons of energy 14.7 MeV, James, Martin and Silvester (JAM 64) measured the cumulative yields of ^{133}Xe and ^{135}Xe.

1A.3 VARIATION OF FISSION YIELDS

Important characteristics of fission are the distribution of fission fragments and products with their mass, A, and charge, Z. It is not surprising that only a partial description of these distributions has been obtained. The measurement of each fission product yield is a major research project. It would be very difficult to measure the yield of many of the approximately four hundred fission products that have been identified, because of their very low yields or because of inconvenient half-lives in their beta-decay chains. These practical difficulties demonstrate the importance of new physical methods for studying these distributions. After presenting some general references which discuss both types of distribution, separate discussions are presented of mass distribution and then of charge distribution. Although the two types of distribution are intimately connected it is convenient and has been customary to treat them separately, and in this order.

Hyde has comprehensively reviewed the studies of these distributions for low-(HYD 60), medium-(HYD 62) and high-(HYD 64) energy fission. More recently, Wahl (WAH 65) has surveyed these distributions for thermal neutron fission, about which most is known, and discussed the effects of the

type of fissioning nucleus and of the excitation energy, up to about 20 MeV. For high-energy fission induced by protons, Friedlander (FRI 65) recently surveyed the distributions, with emphasis on the GeV region.

1A.3.1 MASS DISTRIBUTION

Only a small contribution can be made to the study of this distribution from the present work, for the chains of mass 133 and 135, for fission induced by medium-energy protons. For this type of fission there have been only a few measurements of mass distribution (TEW 52, JON 55, STE 58) though about fifty other medium-energy studies of mass yields have been listed by Hyde (HYD 60). Fig. 1 (STE 58) shows the mass distribution of the fission products of ^{238}U bombarded with protons of increasing energy. It illustrates the well established trend with increasing energy; the yields corresponding to symmetric and very asymmetric fission increase.

The effect of target mass on the mass distribution is not well known at medium-energy. However, the many data (FOR 65, WAH 65) for different fissioning nuclei at low energy, shown in Fig. 2, demonstrate the remarkable constancy of the heavy peak, though the light peak moves to

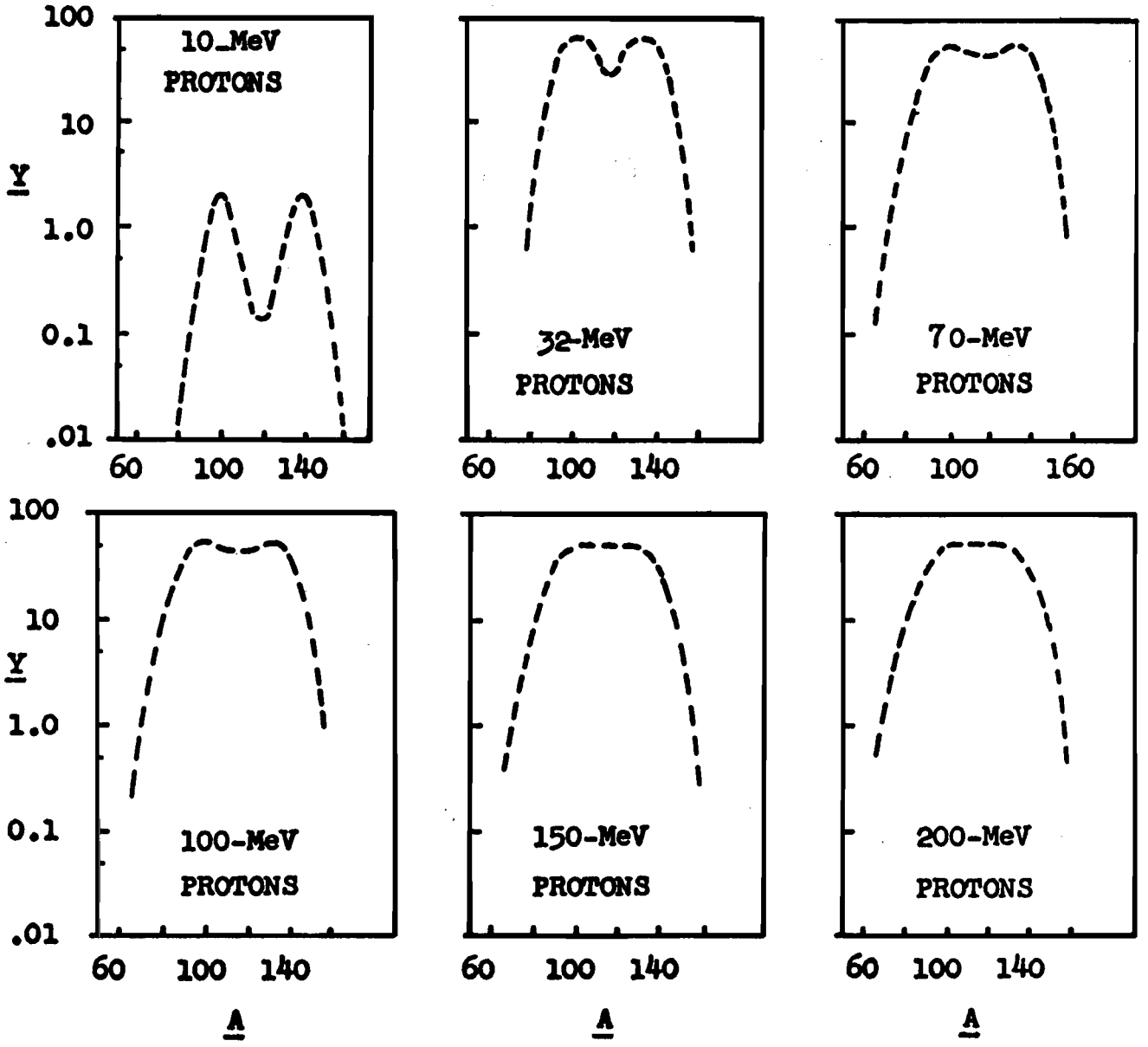

FIGURE 1. (STE 58) Mass Distribution Curves for the Fission Products of ^{238}U, with Protons of Different Energies. The Ordinate, Y, is the Total Chain Yield in mb.

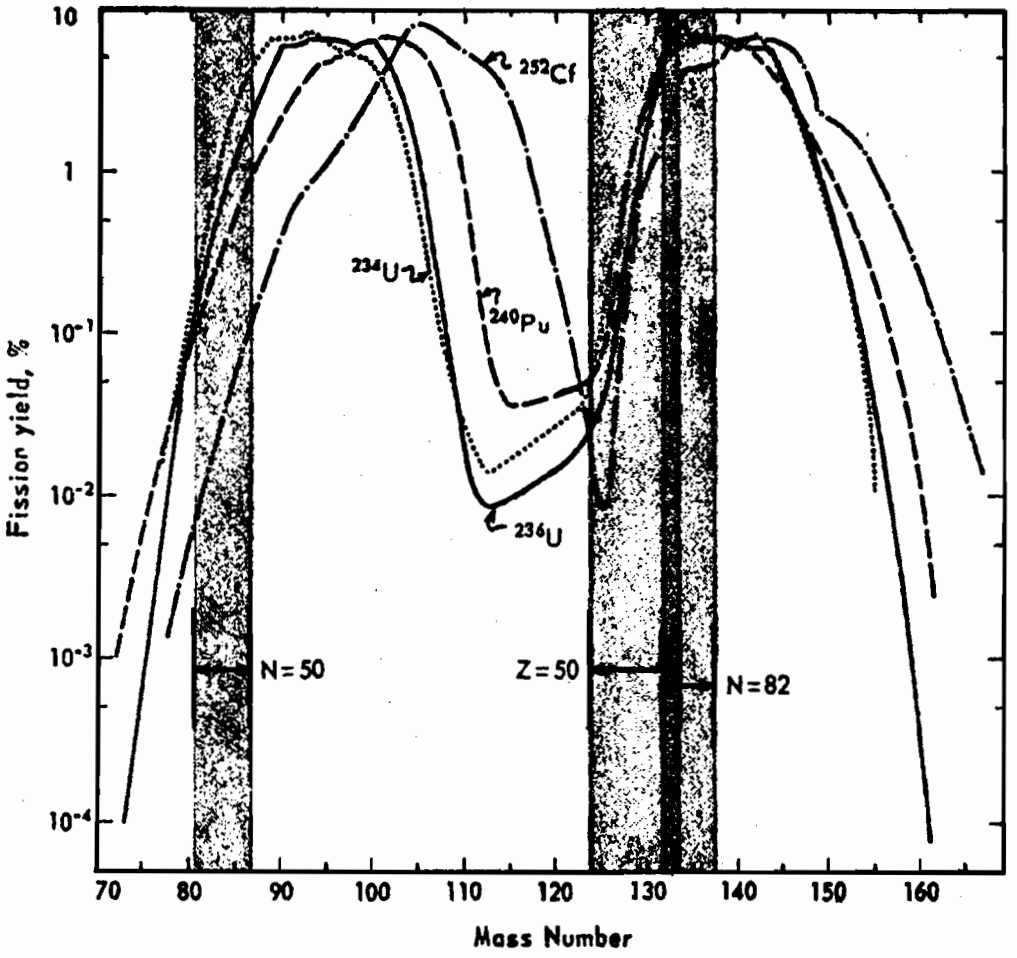

FIGURE 2. (WAH 65) Final mass distribution curves for thermal neutron fission of ^{233}U, ^{235}U, and ^{239}Pu and spontaneous fission of ^{252}Cf. Shaded areas indicate the approximate positions of nuclear shell edges.

higher values of A with increasing target mass.

Mass distribution studies by radiochemical and physical methods give not only fission yield data but also give other information which is pertinent to the present study. These other aspects of fission include fission energetics, neutron emission and shell effects. Although radiochemical and mass spectrometric methods have given most of the existing data for the mass distribution of fission products many of the future data will probably come from improved physical methods. The latter have already been extensively applied to low-energy fission and have been shown to be applicable to medium-, medium-high- (KOW 64) and very high- (FRI 65) energy fission. The newer physical methods are briefly surveyed here because of their rapid advance and because they give much detailed information about fission processes. Physical methods have some advantages over radiochemical methods. The radiochemical determination of a mass distribution for one fission system involves a very long, tedious study of many elements; errors in these yields can be large though the mass of the fission product is known exactly. In physical measurements, although the mass is not known exactly, one experiment can give data for an entire mass distribution curve. This

distribution can be obtained not only for the fission products, but also for the fragments.

Terrell has comprehensively surveyed (TER 65) one of the most interesting aspects of these methods. The average number of neutrons emitted by individual fragment masses can be determined by comparing (TER 62) initial and final mass distribution curves. The results of these comparisons are discussed later in this section.

For pairs of coincident fragments, the velocities have been measured by time-of-flight methods (MILF 62, MIL 65, WHE 64) and the kinetic energies have been measured by solid state detectors (BRI 64, STE 65, THOGP 65). These methods have fairly good mass resolution (~2 mass units) though this cannot be improved beyond the small lower limit imposed by the recoil of prompt neutrons (TER 62). In these accurate methods the fragment velocities, which are essentially independent of neutron emission from the fragments, and the measured kinetic energies were related to mass distributions by the conservation of mass and momentum. Mass distribution and prompt neutron data have also been obtained using ionization chambers as fragment detectors, but their mass resolution was poor (FRA 54, APA 60).

A wealth of physical data now exists for the spontaneous fission of ^{252}Cf (TER 62, BOW 63, BOW 65, STE 65, FRA 65, THOGP 65). ^{252}Cf has been a very useful source of fission for developing and calibrating physical methods because it avoids the difficulties involved in measurements performed inside a reactor or accelerator. The techniques have also been applied to thermal neutron fission (MILF 62, MIL 65, THOGS 65). No physical yield data are yet published for medium-energy proton fission, but Whetstone and Britt have used double-velocity time-of-flight (WHE 64) and double-energy semiconductor (BRI 64) methods to measure the coincident fragment pairs in fission of ^{230}Th, ^{232}Th, ^{233}U induced by alpha particles of 22-30 MeV.

For ^{252}Cf and thermal neutron fission, Terrell (TER 62) found that the prompt-neutron data which he derived from mass distributions agreed with those from other methods. His neutron yields were obtained by comparing final mass distributions, measured radiochemically, with initial distributions measured in time-of-flight studies with a correction for dispersion. Fig. 3 is taken from Terrell's work on thermal neutron fission of ^{235}U. It shows initial and final mass distributions, with their well known strong asymmetry, and also shows the derived number of

FIGURE 3.

Initial and final mass distributions for thermal-neutron-induced fission of ^{235}U, and the derived post-fission neutron yields, ν_f, as a function of fragment mass. Here, f = H or L, for heavy or light fragments. Shell edges are indicated (cf. Fig. 2, p.17). (TER 65)

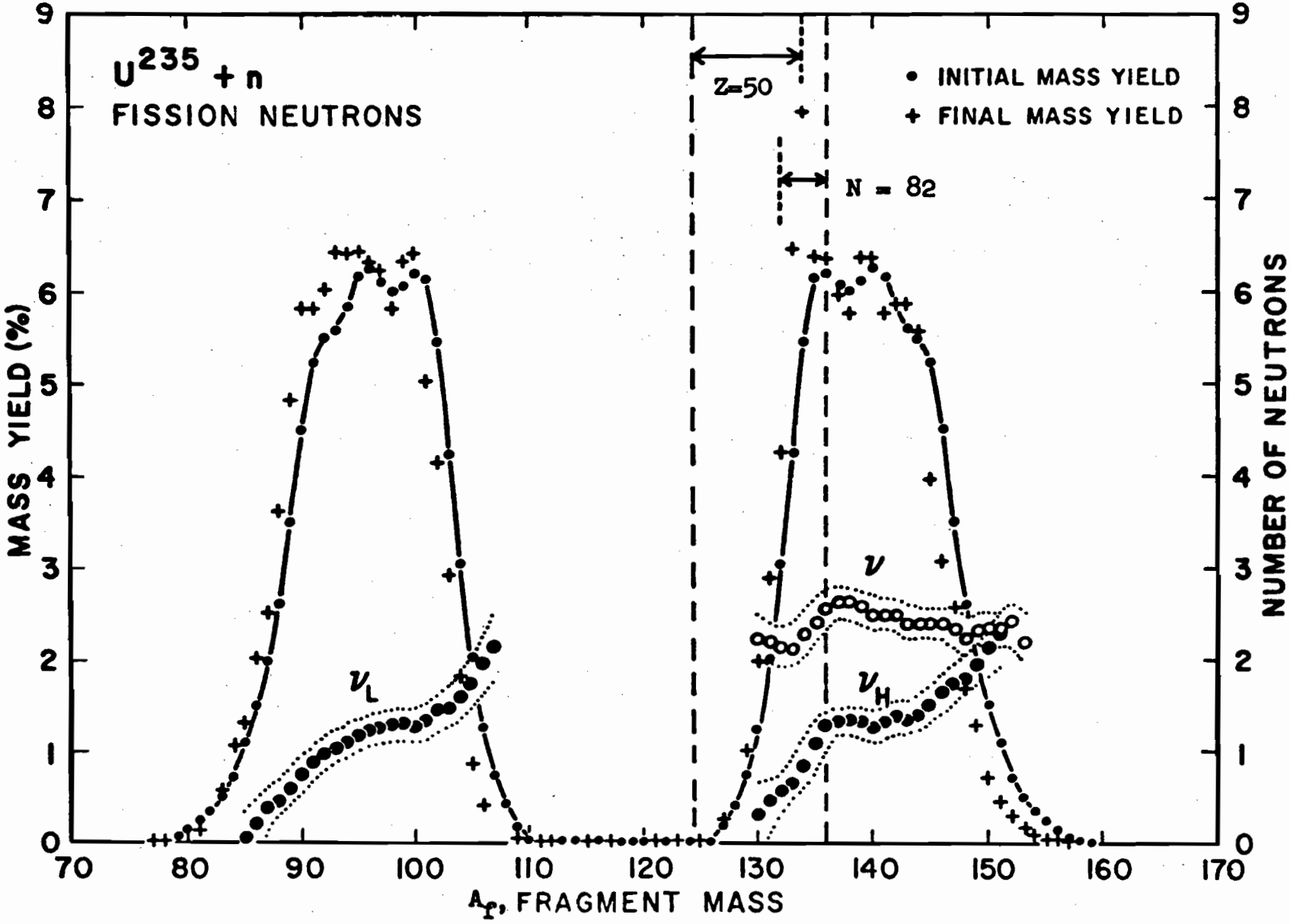
$U^{235} + n$
FISSION NEUTRONS
Z=50
N = 82
• INITIAL MASS YIELD
+ FINAL MASS YIELD
ν_L
ν
ν_H
MASS YIELD (%)
NUMBER OF NEUTRONS
A_f, FRAGMENT MASS
0
1
2
3
4
5
6
7
8
9
70
80
90
100
110
120
130
140
150
160
170

neutrons emitted from individual fragment mass chains. The latter function, (ν_f/A), has the well known saw-tooth shape. No neutron data could be obtained for the symmetric and very asymmetric fission fragments formed in very low yield. Whetstone et al. (BRI 64) in the studies described above for medium-energy fission obtained no such structure in the function, (ν_f/A), when they compared their purely physical data for initial and final mass distributions. However, a rather erratic structure was obtained when the same initial mass distribution measured by the double-velocity method was compared (WHE 64) with a final mass distribution measured radiochemically. The cause of this contradiction cannot be decided until more reliable radiochemical data become available. It is important to know if the structure does persist to higher energies in order to decide the importance of shell effects at these energies. Unfortunately Terrell's method to obtain the number of prompt neutrons as a function of fragment mass becomes less accurate when the light and heavy peaks of the mass distribution curve are not well separated.

Results from the new physical techniques have been precise enough to reveal a fine structure in the mass and kinetic energy distributions which suggest that particular

fragment masses and charges may be strongly favoured in fission. Similar structure in the mass distribution was observed mass-spectrometrically (FAR 62, FAR 64), but this was interpreted to be caused mainly by structure in the number of prompt neutrons as a function of mass. Fine structure near masses 133 and 135 was suggested from a radiochemical study by James et al. (JAM 64). However, their conclusions may need revision (see Appendix B), because of the results from the present work on ^{133}Xe.

The physical techniques have allowed a re-examination of the so called energy deficit. This describes a decrease (FRA 65, ARA 65) of total released kinetic energy for near symmetric fission, at low and medium energies (WHE 64), below the expected energy calculated from the Coulombic repulsion at the time of scission. This deficit is probably associated with an increase in fragment excitation energy which appears to be reflected in the increase of neutron emission for the symmetric mass region.

Most of the trends in mass distribution data have been explained at least qualitatively in terms of two different hypotheses about the mechanism of fission,

(1) The fragment-shell or fragment deformation theory (TER 62, TER 65),

(2) The two-mode hypothesis (BRI 64, FOR 65)

These hypotheses are now discussed and compared.

(1) The simple fragment-shell or fragment-deformation theory was suggested by the very low neutron yields in low-energy fission for fragments corresponding to magic numbers, in particular N = 50, Z = 50. The theory has been developed by Terrell (TER 62) and essentially the same ideas have been arrived at by many workers (TER 65).

The theory assumes that magic nuclides prefer spherical shapes and therefore have a resistance to deformation. A mechanism of low-energy fission is assumed in which the fragments are deformed but cold at scission. Their excitation energy after scission is therefore due mainly to the deformation energy at scission (FRA 65). Then, if near-magic nuclides have little deformation at scission they can have little excitation energy after scission and will therefore emit almost no neutrons. Conversely non-magic fragments will have considerable deformation, and a relatively large excitation energy and neutron yield. The stiffness of fragments with N = 50 or Z = 50 has been shown to increase the fission barrier thus decreasing their yield. This accounts for phenomena such as the presence of three mass peaks for the fission of radium, and the single mass

peak for the fission of bismuth. However, this reasoning cannot be applied to fragments with N = 82. The shaded areas in Fig. 2 show approximately the fragment masses that are influenced by the closed shells, Z = 50 and N = 82. The remarkable constancy of the heavy peak with different targets is obviously connected with these shells, and the fragments with N = 82 appear to be strongly favoured in low-energy fission. At higher energies insufficient evidence is available to evaluate this hypothesis conclusively. The changes in neutron and fragment yields can be explained qualitatively by assuming a decrease in the importance of shell effects at higher energies. Although the theory suggests that the deformation will be about the same at low and high energies the fragments will be hot at scission because of the extra excitation energy of the fissioning nucleus. In this case there will be two sources of the post-scission excitation energy of the fragments, and therefore the effect of the stiffness of magic fragments would be less important.

(2) The two-mode hypothesis was also suggested to explain the mass distribution at low energy (TUR 51). The hypothesis in its present form (LEV 61, HIC 62, EIS 63, WHE 64, BRI 64, FOR 65) assumes that there are two distinct

modes of fission, one producing predominantly asymmetric mass divisions and higher kinetic energy releases, and the other producing predominantly symmetric mass divisions and lower kinetic energy releases. The second mode becomes increasingly important at higher energies (SCH 54, PAP 61). Ford and Leachman (FOR 65) have recently surveyed the reasonably successful applications of this hypothesis to analyze (FOR 60, LEV 61) mass and kinetic energy distributions from low- and medium-energy fission (WHE 64, BRI 64).

Although the two hypotheses suggest basically different fission mechanisms they predict qualitatively similar mass and kinetic energy distributions. It has been suggested (WHE 64) that more detailed measurements of prompt neutrons may help decide between the two mechanisms. However the two hypotheses are not really independent (BRI 64). Although the fragment-shell theory does not assume two distinct modes, the asymmetric mode does show the characteristics predicted by the fragment-shell theory. The symmetric mode shows the characteristics predicted for a homogeneous charged liquid drop (BOH 39, NIX 65) with no shell effects.

It will be seen in the next section that reliable absolute total chain yields facilitate the correlation of independent yields of fission products.

1A.3.2 CHARGE DISTRIBUTION

Numerous studies have been made of this distribution, but it has not been defined as well as the mass distribution, because of inherent theoretical and experimental difficulties.

The charge distribution for a specific fission system may be conveniently described in terms of two functions.

FUNCTION (1), in an isobaric chain of mass A, represents the nuclear charge frequency-distribution function, or in the terms of nuclear chemistry it represents the independent yield as a function of the isobaric charge. This function gives the shape of the isobaric charge distribution curve about a most probable value, Z_p, which is a statistical value and therefore not necessarily an integer.

FUNCTION (2) represents Z_p as a function of A, the mass of the isobaric chain.

Changes in the shape of FUNCTION (1) with A must also be considered.

A complete picture of charge distribution requires a knowledge of FUNCTIONS (1) and (2) for many fission systems, so that their dependence on both excitation energy and target composition may be understood.

Definitions have already been given (Section 1A.1) to distinguish between the initial and the apparent charge distribution. The latter distribution is that given by radiochemical yield data, and there is at present no satisfactory method to convert this to the initial charge distribution. The complex nature of neutron emission from the fragments would make it very difficult to perform this conversion, even if the exact neutron parentage of every fission product were known (GOR 65). However, it is the division of nuclear charge in scission which is of major theoretical interest in studies of charge distribution. Since this is described by the initial charge distribution, only its general characteristics can be obtained from the apparent charge distribution measured experimentally. Even the latter cannot be defined easily or directly because it is very difficult to measure the independent yields of several fission products in one isobaric chain. In fact, this has only been done fairly recently and then only for a few suitable mass chains. Most studies of charge distribution have had only very limited data, for a few different isobaric chains, which were correlated by various methods.

These studies are quickly surveyed. Then the

methods used to correlate their data are discussed in order to introduce the method that will be used in this work, and also to indicate the present state of knowledge on charge distribution.

Table 1 summarizes the charge distribution studies for medium-energy fission which is of main interest in this thesis. However, a few studies at high energy and many at low energy have been very important in the slow, but steady, elucidation of charge distribution. A representative selection of these studies is given in the Bibliography for low-energy fission (GLE 51, PAP 53, PAP 55, STE 55, GRU 57, WAH 58, APA 60, COR 61, MIL 62, WAH 62, FIE 63, WAH 65, STR 65), and high-energy fission (GOE 49, HIC 55, PORS 57, BLA 60, FRI 63, KAU 63, HAG 64, FRI 65). At all energies only a few fission products could be measured in each study. Many mass chains have not been investigated.

In order to describe the complicated development of the numerous methods used to correlate the data from these studies, the methods will be divided into two main types.

(A) POSTULATE CORRELATION METHOD. This uses a postulated FUNCTION (2) to correlate the data and produces a semi-empirical FUNCTION (1).

(B) EMPIRICAL CORRELATION METHOD. This uses an

TABLE 1

Survey of Charge Distribution Studies at Medium Energy

Target	Projectile and Energy (MeV)	Fission Products Studied	Authors	References
^{238}U	d 19-190 p 70-340 50-380		Hicks and Gilbert	HIC 55
^{235}U	n 14	$(131\text{-}134)_I$, 131, ^{132}Te	Wahl	WAH 55
^{237}Np	α 20-40		Gibson	GIB 56
^{238}U	d 13.6	^{82}Br, ^{86}Rb, ^{136}Cs, ^{134}Te, 132, ^{134}I	Alexander and Coryell	ALE 57
^{232}Th	n 14			
^{232}Th	α 14-45		Foreman	FOR 58
^{232}Th	p 8-87	$(130\text{-}135)_I$, 131, ^{132}Te	Pate, Foster and Yaffe	PAT 58a,b
^{238}U	α 46	84, ^{86}Rb, ^{150}Pm, ^{154}Eu, $(131\text{-}136)_{Cs}$	Chu	CHU 59
^{235}U	α 46			

TABLE 1 (Continued)

Target	Projectile and Energy (MeV)	Fission Products Studied	Authors	References
^{232}Th	p 13-82	^{72}Ga, ^{82}Br, ^{112}Ag, ^{140}La	Kjelberg, Taniguchi and Yaffe	KJE 61
^{238}U, ^{235}U, ^{233}U	∝ 20-40	^{82}Br, 130, ^{135}I, ^{140}La, ^{142}Pr	Colby and Cobble	COL 61
^{232}Th, ^{235}U, ^{238}U	∝;d 24,14	^{133}I, ^{135}I, ^{135}Xe, ^{133}Xe	Storms	STO 62
^{237}Np,	∝ 20-41	about 20 "isotopes" A = (83-115)	Powers	POW 62
^{239}Pu	∝ 22-32	and A = (131-159)		
^{238}U	p 10-85	$(130-138)_{Cs}$, ^{86}Rb, $(95-97)_{Nb}$	Davies and Yaffe	DAV 63

TABLE 1 (Continued)

Target	Projectile and Energy (MeV)	Fission Products Studied	Authors	References
^{232}Th, ^{235}U	α 15-57	about 12 nuclides A = (80-86), and A = (128-150)	McHugh	MCH 63
^{232}Th	p 10-85	$(130\text{-}138)_{Cs}$, ^{86}Rb	Benjamin	BEN 65
^{232}Th	α 20-40	^{90}Y, ^{96}Nb, ^{136}Cs, ^{140}La	Nethaway and Levy	NET 65
^{235}U	n 15			
^{235}U, ^{238}U	n 14	$(89\text{-}95)_{Kr}$, $(137\text{-}144)_{Xe}$	Wolfsberg	WOL 65
^{238}U	p 20-85	isotopes of Ba, Cs, Ce, La of A = (139-143)	Parikh	PAR 66
^{232}Th, ^{235}U, ^{238}U, ^{233}U	p 20-85	^{133}I, ^{135}I, ^{133}Xe, ^{135}Xe	Forster	This work

empirical FUNCTION (1) to correlate the data and produces an empirical FUNCTION (2).

More importance will be given to the method (B), because it is essentially the method to be used for correlating the data in this thesis and for obtaining empirical values of Z_p.

(A) Postulate Correlation Method

This method was used exclusively until Wahl introduced method (B) in 1958 (WAH 58). It has not been used in the majority of more recent studies.

This method assumes that every isobaric chain has the same smooth symmetrical distribution curve, about the Z_p value characteristic of each A. Then, using an abscissa $(Z - Z_p)$, the FUNCTION (1) for any A can be exactly superimposed and the fractional independent yields, f_i, for fission products of any A can be plotted on the same curve. Thus, to plot the independent yield for a fission product it is necessary to know its value of Z_p. This value was taken from a postulated FUNCTION (2). The postulate was then assessed by its ability to correlate the data into a smooth approximately Gaussian FUNCTION (1).

The main postulates and prescriptions will be discussed only briefly since they have been exhaustively

reviewed and assessed elsewhere, and because little use can be made of them in this thesis. The postulates should ideally be based on a mechanism of fission and neutron emission, but it is disappointing that for the low-energy data the most successful postulated FUNCTION (2) came from the so called Equal Charge Displacement, ECD, prescription which was first introduced by Glendenin, Coryell and Edwards (GLE 51). This rule had no physical basis, but was an idealization of the observation that the most probable chain lengths, $(Z_A - Z_p)$, of complementary light, L, and heavy, H, fission products were about the same. The ECD rule is simply expressed,

$$(Z_A - Z_P)_L = (Z_A - Z_P)_H \quad ,$$

where Z_A is the hypothetically most stable charge of mass chain A, and like Z_P is not necessarily an integer. Chu (CHU 59) has shown how critically dependent the value of Z_P is upon the choice of many possible Z_A-functions, particularly near shell edges. In order to improve the correlation of the low energy data,refinements were made to this arbitrary ECD rule, (PAP 55, STE 55, GRU 57, CHU 59, COR 61, FIE 63) but these modifications added little to the theoretical understanding of charge distribution. The FUNCTION (1) that was

obtained did prove useful (WAH 58, COR 61) to initiate the first empirical correlation methods, type (B), described later.

Pate, Foster and Yaffe (PAT 58) used the postulate correlation method indirectly, by plotting their yield data for iodine and tellurium isotopes in the mass region 130-135 against the abscissa $(Z_A - Z)$. This plot is equivalent to the $(Z - Z_p)$-plot if it is assumed that in their small mass region there is an equal rate of change of Z_A and of Z_p, with respect to A. They chose a discontinuous Z_A-function (PAP 53) which gives ambiguous results in this mass region. Correlated in this way, their data were best fitted by a Gaussian FUNCTION (1) which is discussed later in other parts of this thesis.

Other postulates with a physical basis have been devised and were first tested by using their FUNCTION (2) in this Postulate Correlation Method. A brief survey is now given of important existing postulates. Further understanding of charge distribution can only come from improved nuclear data together with improved postulates. The postulates can be classified into two types, depending on which fission mechanism they assume, (i) Rapid Division, or (ii) Slow Division (HIC 55).

(i) Rapid Division Type of Postulate

It is assumed here that scission is too rapid for the fragments, during their deformation, to undergo nucleon rearrangement, or more specifically nuclear charge polarization. The most probable initial fragments will therefore have the same composition, (N/Z)-ratio, as the fissioning nucleus. Thus, this postulate has been described by the names Constant Charge Ratio, CCR, or Unchanged Charge Distribution, UCD. As the fission energy is increased the Z_P-FUNCTION (2) moves towards higher charge values because more neutrons, but few charged particles, are emitted. By this postulate, FUNCTION (2) for fission products, FP, would be given precisely by the formula,

$$(Z_P)_{FP} = (A_{FP} + \overline{\nu}_f) \frac{(Z_T + Z_{PROJ})}{(A_T + A_{PROJ} - \overline{\nu}_{pF})} , \quad (1A.1)$$

for fission of a target, T, induced by a projectile, PROJ, where $\overline{\nu}_{pF}$ is the average number of prefission neutrons and $\overline{\nu}_f$ is the average number of neutron emissions leading to the fission product, FP. Goeckermann and Perlman (GOE 49) first used this early (SUG 44) idea to correlate their data, for the fission of bismuth with 190-MeV protons. However, they employed a simplified approximate formula,

$$(Z_P)_{FP} = (A_{FP}) \frac{(Z_T + Z_{PROJ})}{(A_T + A_{PROJ} - \bar{\nu}_{Total})}, \qquad (1A.2)$$

where $\bar{\nu}_{Total}$ is the average total number of neutrons emitted in fission. Numerically formulae (1A.1) and (1A.2) give very similar results but it is often forgotten that they represent different assumptions. It has been stated above that (1A.1) assumes that the ratio (Z/A) is the same for complementary fragments, of mass $(A_{FP} + \bar{\nu}_f)_H$ and $(A_T + A_{PROJ} - \bar{\nu}_{pF} - (A_{FP} + \bar{\nu}_f)_H)$. However, formula (1A.2) assumes that (Z/A) is the same for complementary fission products, of mass $(A_{FP})_H$ and $(A_T + A_{PROJ} - \bar{\nu}_{Total} - (A_{FP})_H)$. Formulae (1A.1) and (1A.2) become identical if it is assumed (GOE 49) that $\bar{\nu}_{pF} \gg \bar{\nu}_f$, but this should not be assumed in many studies, where formula (1A.2) has been used without a clear statement that it is only an approximation to the CCR postulate. In fact the exact formula (1A.1) can rarely be used because the values of $\bar{\nu}_f$ and $\bar{\nu}_{pF}$ are not well defined, whereas there is a fairly good body of data for $\bar{\nu}_{Total}$ which makes it convenient to use formula (1A.2). The latter postulates a Z_P-FUNCTION (2) for fission products which is a straight line and this simple function will be used for a semiquantitative discussion of the results from the present work.

The CCR postulate has been widely tested and used (COL 61, GOE 49, HIC 55, CHU 59, POW 62, MCH 63, BEN 65) and has met with limited success for medium- and high-energy fission. It is obvious however from the above discussion that the result of these tests is dependent on the prompt neutron emission in fission, which is poorly understood in many fission systems. The CCR postulate gives a very simple mechanism for fission and can only account for shell effects that influence prompt neutron emission, but cannot account for shell effects on the charge division itself. For low-energy (WAH 65, WOL 65) and medium-energy (MCH 63) fission, it has been observed to predict too low values of Z_p for light fission products, but too high values for heavy fission products.

(ii) Slow Division Type of Postulate

It is assumed here that fission is an equilibrium type of process in which the nucleons have enough time to rearrange before scission. There is no simple method to determine the most probable initial fragment resulting from such an equilibrium configuration in the fissioning nucleus.

The Minimum Potential Energy, MPE, postulate has been the most successful of these Slow Division postulates.

It proposes that the sum of the nuclear potential energy and Coulombic repulsion energy is minimized by the above nucleonic rearrangement. Present (PRE 47) first introduced the MPE postulate and modifications have been used by several workers (FON 56, BLA 60, COR 61, MIL 62, MCH 63, ARM 65). The Z_p-FUNCTION (2) from this postulate is strongly dependent on the mass formula used. Coryell et al. (COR 61) have gone so far as to suggest that a good empirical Z_p-FUNCTION (2), obtained by methods described later, may be used to judge the reliability of a semi-empirical mass formula by use of the MPE postulate. The MPE postulate is not used in this thesis but in the future will probably provide a good picture of charge distribution when better data and nuclear parameters become available (MCH 63). It is interesting that the ECD rule has been given a degree of physical significance by its agreement in certain cases (HAL 59, BLA 60, COR 61) with the MPE rule.

(B) Empirical Correlation Method

This is a more powerful method than method (A) and is used to correlate the data in this thesis and in most recent studies.

It is assumed, as in method (A), that every isobaric chain has the same smooth symmetrical distribution

curve, FUNCTION (1). Two types of abscissa have been used for this function, $(Z - Z_p)$ and (N/Z). According to which of these two plots was used, these methods are now discussed and are further compared in the Discussion.

(i) The $(Z - Z_p)$-Plot of Empirical FUNCTION (1)

Although there was considerable uncertainty in the values of Z_p from the postulates used in correlation method (A) the various interpretations of the ECD postulate did give essentially the same FUNCTION (1). This curve was used by Wahl (WAH 58), and later by Coryell et al., (COR 61), to determine Z_p empirically, for short-lived krypton and xenon isotopes and other fission products whose fractional yields were available. The method involves simply reading the value of $(Z - Z_p)$ corresponding to a measured fractional independent or cumulative yield from the assumed curve for FUNCTION (1). The first empirical FUNCTION (2) which was obtained in this way suggested a smooth function, and not a discontinuous one as had been suggested by earlier workers (PAP 55). Much work has since been done to improve this empirical Z_p-FUNCTION (2).

The first development was the use of a more precise FUNCTION (1). This was determined from data alone

for more than one fractional yield in a given isobaric chain (WAH 62) and not from the Postulate Correlation Method (A). Wahl and coworkers used the emanation method already described (Section 1A.2.1) for the measurement of these fractional yields for thermal neutron fission. Up to 1965, they had determined three fractional yields in the mass chains 92, 93, 140, 141 and in addition had determined two fractional yields in the chains 91, 94, 95, 139, 142 and 143. These data were best fitted by a Gaussian FUNCTION (1), where an isobaric independent fractional yield,

$$f(Z) = \frac{1}{\sqrt{C\pi}} \exp\left(-(Z - Z_p)^2 / C\right) . \qquad (1A.3)$$

Here C defines the width of the curve and normalizes the area under the curve to approximately unity. From the evidence for the ten mass chains given above, the precise mean value of C was 0.86 $\pm$ 0.04 (WAH 65). Fig. 4 compares Gaussian curves, with C = 0.94 (WAH 62) and C = 1.20 (STO 62), with the FUNCTION (1) obtained in the early ECD studies (GLE 51, PAP 55). It had been suggested for many years that the FUNCTION (1) should be Gaussian. The ECD curve is approximately Gaussian (C 1.43) except when $|Z - Z_p| > 2$, when it falls off more steeply.

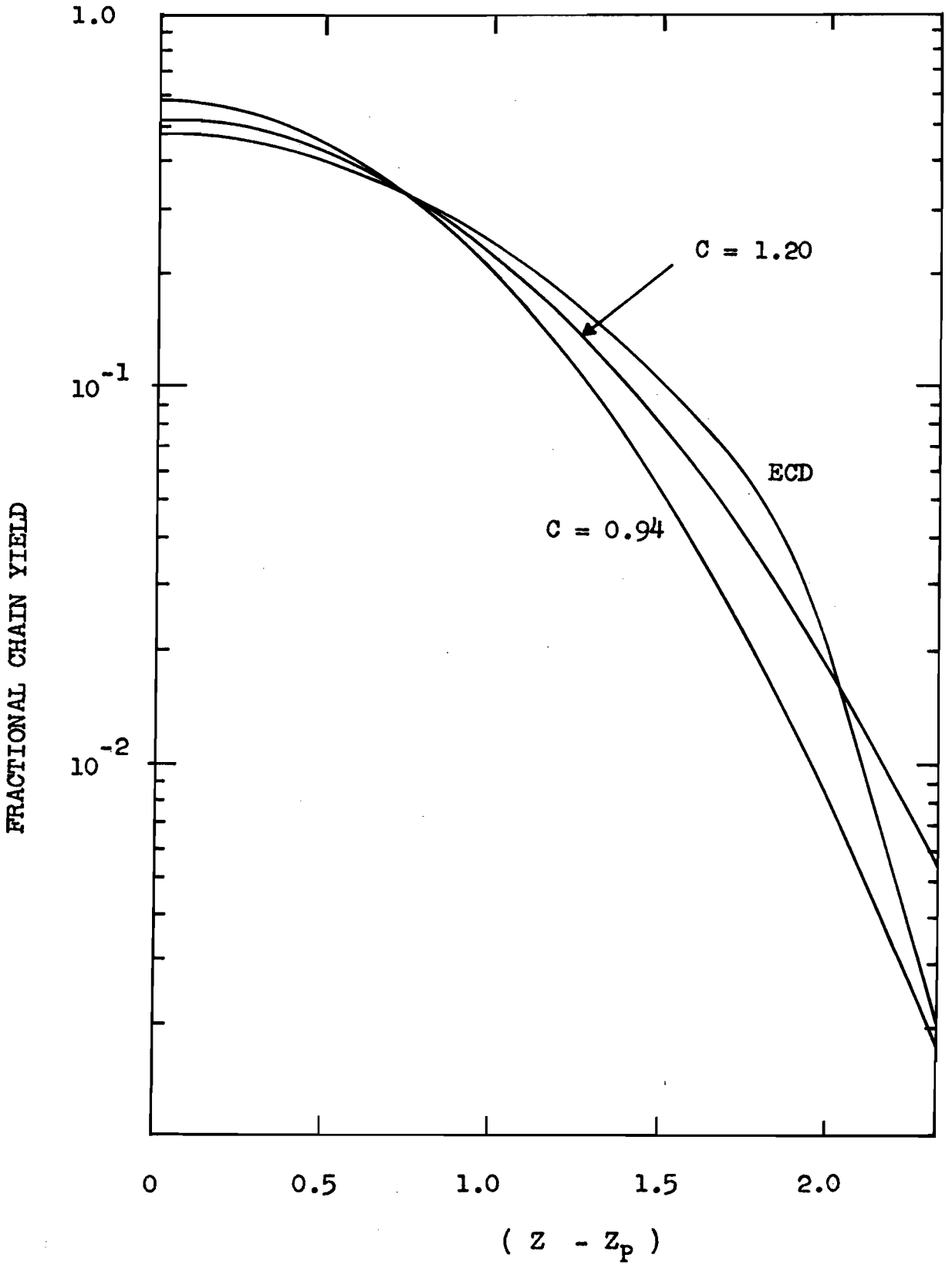

FIG.4 (STO 62) FUNCTION (1) from ECD Compared with Two Gaussian Functions (Equation (1A.3), with C = 0.94 and 1.20).

Using the more precise Gaussian FUNCTION (1), new curves for empirical Z_p-FUNCTION (2) have been recently discussed for thermal neutron fission of ^{235}U (WAH 65, STRO 65) and of ^{233}U and ^{239}Pu (WOL 65).

For fission induced by 14-MeV neutrons, Wolfsberg (WOL 65) obtained similarly a Gaussian FUNCTION (1) with $C = 0.86 \pm 0.15$. It therefore appears that this function can be assumed for many low-energy fission systems.

This thesis is concerned with fission excitation energies above 20 MeV. McHugh (MCH 63) has made a most precise analysis of charge distribution in medium-energy fission, for the initial "compound nucleus" ^{236}U, by measuring the relative abundances of a number of nuclides (Table 1), with high-sensitivity mass spectrometry. For the isobaric chain 135 he was able to measure the yield of iodine, xenon and cesium. These data allowed him to construct an empirical FUNCTION (1). Fig. 5 shows the Gaussian curves he fitted to some of his fractional yield data. The iodine fractional cumulative yields were fitted to an integrated Gaussian curve (Fig. 5). Identical curves fitted his yield data for chain 136 in which he measured the fractional yields of only xenon and cesium. Blann (BLA 60) reported essentially the same Gaussian FUNCTION (1) for

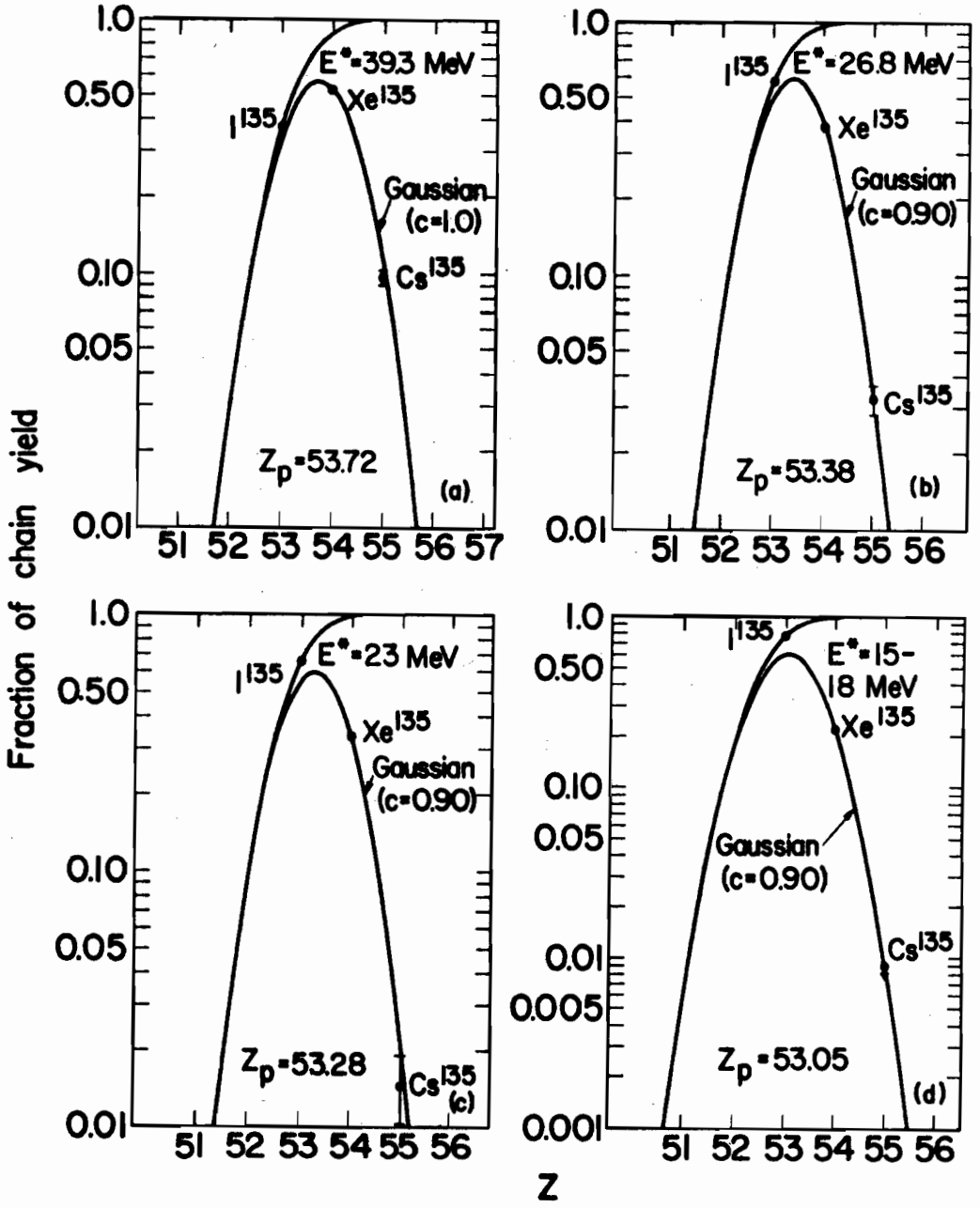

FIGURE 5. (MCH 63) The Gaussian charge distribution curves which were fitted by McHugh to his fractional yield data for the chain 135. The iodine fractional cumulative yields were fitted to an integrated curve.

fission of ^{197}Au with ^{12}C ions of 112 MeV.

All these results indicate that the same FUNCTION (1) is applicable through a rather wide range of excitation energies (at least from 6 - 40 MeV). Earlier work in this laboratory (PAT 58a, DAV 63, BEN 65) has shown a similar invariance of this function up to excitation energies of about 35 MeV for proton-induced fission of ^{232}Th and ^{238}U. However, the widths of FUNCTION (1) could not be very precisely determined in these radiochemical studies. It now appears from McHugh's results that they were probably too wide. There is an interesting parallel here with the history of charge distribution at low energy, in which the earlier curves for FUNCTION (1) were also shown to be too wide, as more precise data evolved. More recent radiochemical work in this laboratory by Parikh (PAR 66) (Table 1) has given further evidence for a narrower curve.

In this thesis and in the work of Storms (STO 62) and of Nethaway and Levy (NET 65) not enough radiochemical yield data were available to construct an empirical FUNCTION (1). This function was therefore assumed to be Gaussian and represented by formula (1A.3). Although in these studies not enough mass chains were investigated to construct a Z_p-FUNCTION (2), the data were useful to show

interesting trends with excitation energy and, in the present work, also to compare charge distributions for different targets. Nethaway and Levy used a curve with C = 0.86. Their data were in good agreement to those for identical fission systems (Table 1) studied by McHugh. Storms made a study closely parallel to the present work (Table 1). His data like those in this thesis consisted of one independent yield for xenon and one cumulative yield for iodine in the chains 133 and 135. The empirical method he used to obtain the value of Z_p for these chains is very similar to that used in this thesis. He used a curve with C = 1.20 as suggested by Coryell for medium-energy fission systems. However a serious error in his measurements for the chain 133, which was revealed by the present work, demands that his conclusions be revised (see Appendix B).

(ii) The (N/Z)-Plot of Empirical FUNCTION (1)

This method was first used for the correlation of high energy data (FRI 63). The methods described above could not be used at these energies because of the wide mass and energy spectra for the fissioning nuclei (FRI 65), which make it very unlikely that FUNCTION (1) can be represented

by a Gaussian or any other symmetric function. Above about 50 MeV this argument favours the (N/Z)-plot method, but below this energy it now appears that where applicable the $(Z - Z_p)$-plot method, assuming a Gaussian function, is more systematic and precise. Only the latter method has been used in this thesis.

Three previous studies of charge distribution in this laboratory (DAV 63, BEN 65, PAR 66) (Table 1) have correlated their data with an empirical FUNCTION (1) on an (N/Z)-plot. Their absolute cross sections were plotted against the (N/Z) of the fission product and a symmetric curve was manually adjusted to pass through the points representing the independent yields, while the area under the curve fitted the cumulative yield data. The following two assumptions in this method restrict it (HAG 64) to the relatively small mass range used in the above three studies (Table 1).

The first assumption is necessary because the absolute cross sections are plotted, and not the fractional yields as in other charge distribution studies. Therefore, to be able to superimpose the curves representing FUNCTION (1) for any value of A, the total chain yield must be assumed to be the same for these values of A. This can only be true

when the masses of the fission products are very close and if the total chain yields fall on a truly flat part of the mass distribution curve. Although the fission products in these studies were near the apparently flat heavy wing of the mass distribution curve no precise information is available on this curve for proton-induced fission. For the fission of ^{232}Th with alpha-particles of 44 MeV a precise mass yield curve in this mass region (MCH 63) has a fairly steep drop above about A = 136. However, the change in total chain yield for the small mass ranges in the three previous studies is probably within the experimental error of 20-30% in their cross sections. The (N/Z)-plot method could be more reliable if it could use fractional yields, obtained from absolute cross sections by using absolute mass distributions which are more precise than those presently available.

The second assumption like the first is necessary because fission products of different mass chains are plotted on the same curve. It is assumed in most correlation methods that the shape of FUNCTION (1) is the same for different values of A, but here it must also be assumed that $(N/Z)_p$, the most probable value of (N/Z) for a given mass chain, has the same value for different mass chains. The latter

assumption is a good approximation for a narrow range of A values (HAG 64).

All the empirical methods to obtain FUNCTION (2) do not require a Z_A-function and therefore avoid difficulties with possible discontinuities in this function at shell edges.

Before summarizing the present state of knowledge on Charge Distribution, which has been largely a result of the correlations outlined above under methods (A) and (B), some new physical methods to study this subject are considered.

Charge Distribution Studied by New Physical Methods

Physical methods to obtain information on charge distribution are only referred to briefly here, because they are still at an early stage of their development and so far have been applied only to spontaneous and thermal neutron fission. They involve the resolution of the fission fragments with respect to both their A and Z.

One basic method involves separation of the fission product with a mass separator (EWA 65) and then determination of the average length of the beta-chain, $(Z_A - Z_P)$. This determination is made either indirectly by measuring the energy of the beta particles, (ARM 64, ARM 65)

or directly by counting the number of beta particles from specific fragments. The counting has been done electronically (ARM 64, SPE 65) and even directly by laboriously counting under a microscope the number of beta tracks (KON 65) in a nuclear emulsion.

The other basic method is more complex but has proved fairly reliable (GLE 65) and will probably become a powerful tool in collecting data on charge division in fission. It involves the measurement of the energy of K x-rays in coincidence with fission fragment pairs. The masses of the fragments are determined, as described earlier, from their kinetic energies obtained using a pair of semiconductor detectors. Careful investigation (GLE 65, THOGP 65, BOW 65) of these K x-rays has shown that they originate from K-vacancies resulting from internal conversion after fission. This origin introduces uncertainties (THOGP 65) into the interpretation of the yields of K x-rays. However, these x-rays have been found (GLE 65) to characterize the atomic number, Z, of the fission products and therefore to give a reliable representation of the charge distribution.

For spontaneous and low-energy fission, these physical methods have given preliminary results (ARM 65,

ARM 64, BOW 65, GLE 65, KON 65, WAH 65) different to the FUNCTION (2) obtained by empirical methods or with existing postulates.

Summary of Present Knowledge on Charge Distribution

Slow progress has been made in the studies surveyed above, but charge distribution has still not been generally defined and explained satisfactorily.

FUNCTION (1) has been well established in only a few mass chains for low- and medium-energy fission. It is possible that the shape of this curve is a function (GOR 65, STR 65) of the mass of the isobaric chain, but because of the lack of experimental evidence it is usually assumed that the shape is the same for all masses.

In many correlations the yields of certain fission products indicated that there are perturbations to the smooth symmetrical FUNCTION (1) for certain mass chains. There are still insufficient precise data to confirm these perturbations. Explanations have been given (GRU 57, PAP 53, PAP 55, COL 61, WAH 65) in terms of the shell effects on charge division and on neutron emission. For medium-energy fission, the precise data of McHugh (MCH 63) for the chains 135 and 136 gave no evidence for such effects though the formation of these chains involves the nuclides ^{136}Xe and

^{135}I, both with the closed shell of 82 neutrons. It has also been suggested that perturbations may be caused by a preference in the charge division for fragments with even Z and even N (THOV 64, FRA 65, FER 65). A lack of information about nuclear isomers and the ratio of isomeric yields in fission, to be discussed in detail later in this thesis, has contributed to some apparent perturbations.

Above about 50 MeV, as the excitation energy increases FUNCTION (1) broadens, loses its symmetry (PAT 58, HAG 64, KAU 63, FRI 65), and is probably more dependent on A (HAG 64). Qualitatively this may be understood by the wider distributions of the number of neutrons emitted before and after the fission process, which gives rise to a greater variety of fissioning nuclides and fragment parents.

There have been numerous comparisons of FUNCTION (2) obtained from postulates, from the empirical correlation method, and from new physical methods. All these comparisons are strongly dependent on the reliability of data describing neutron emission and fission yields. They do not therefore provide a good test of the postulated mechanisms for charge division in fission (MCH 63). For thermal neutron fission of ^{235}U, Fig. 6 (WAH 65) compares the Z_p-FUNCTION (2) obtained empirically, for the mass chains indicated by the

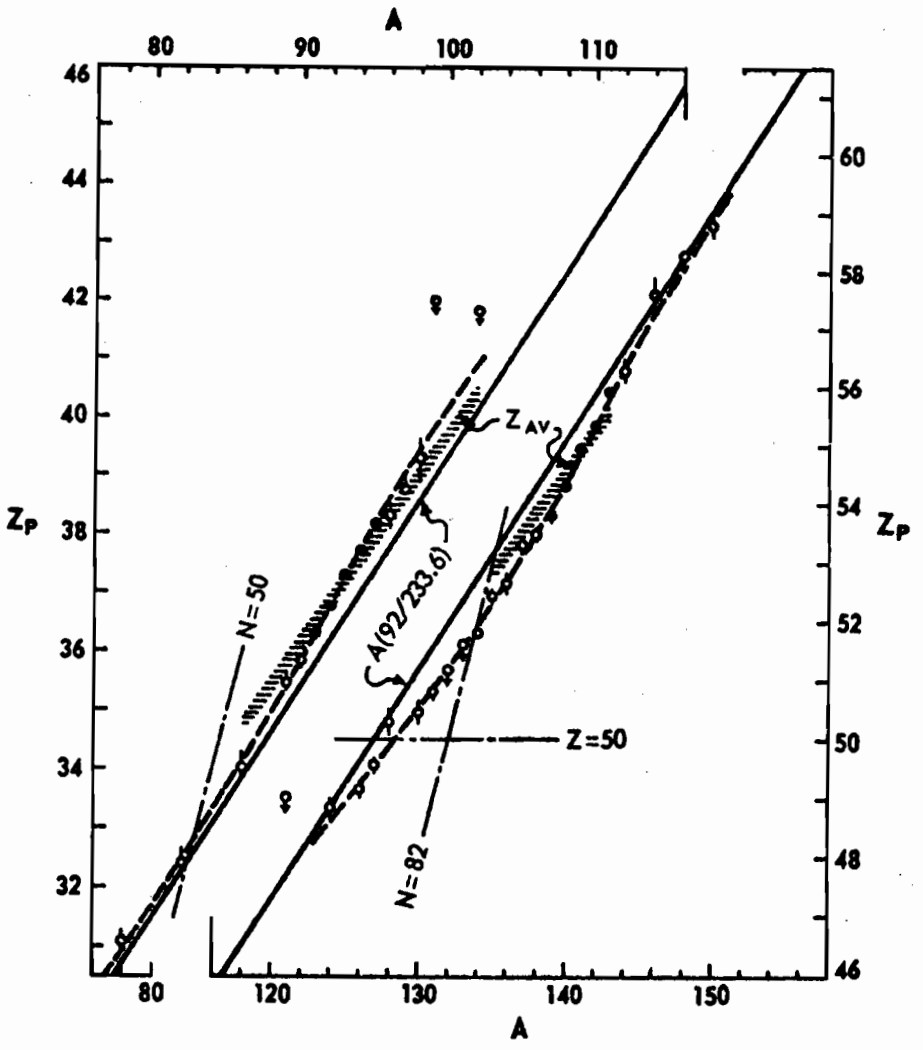

FIGURE 6. (WAH 65) Comparison of empirical and postulated Z_P-FUNCTION (2) for products from thermal neutron fission of ^{235}U. The broken lines represent an empirical function derived from the data points of Wahl et al. The continuous lines are for the simple CCR postulate. The average charge bands, Z_{AV}, are from a physical method (ARM 64).

points, and the function obtained by the simplified CCR rule represented by equation (1A.2) with $\bar{\nu}_{Total} = 2.4$. Results from a physical method (ARM 64) are also included in this figure. These physical data are averaged over a few mass chains because of the poor mass resolution of the method.

Fig. 7 replots the same empirical FUNCTION (2) of Wahl et al. on an expanded charge scale (Z_p - 0.4A) and compares it with the empirical function (MCH 63), for the same initial "compound nucleus" ^{236}U, but at an excitation energy of about 40 MeV. The function (Z_p - 0.4A) (COR 61) changes little with A, because $(dZ_p/dA) \approx 0.4$, and it clearly indicates any structure in FUNCTION (2). These two figures illustrate most of the following important features known about FUNCTION (2).

(i) There are no data for symmetric and very asymmetric fission. These fission products have extremely low yields at low energy, but could be measured at medium energy and this should be one of the purposes of future research.

(ii) The value of $(Z_p)_{FP}$ postulated by the approximate CCR rule (1A.2) is too low for light fragments and too high for heavy fragments. This shows that the value of $(N/Z)_p$ is not the same for complementary fragments

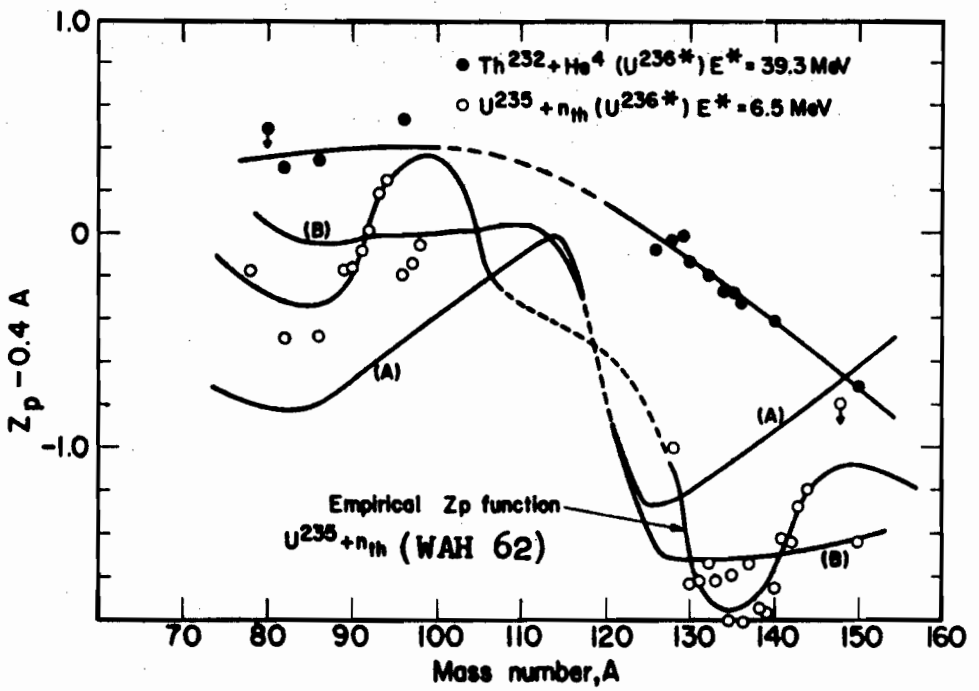

FIGURE 7. (MCH 63) Two empirical Z_p-FUNCTION (2)'s, for the "compound nucleus" $^{236}U^*$ at two energies, E^*. Also, two calculated functions for $^{235}U(n_{th},F)$

(A) with the CCR Postulate,

(B) with the MPE Postulate.

(HAG 64), and that it is higher for the heavy fragments.

(iii) Recent work (STR 65, TRO 64) has shown that the closed shell, Z = 50, does not have as strong an influence on FUNCTION (2) for low-energy fission as was earlier suggested, by Wahl et al. (WAH 58, WAH 62). Strom et al. have therefore revised the empirical plot of Wahl in this mass region. In these plots different coordinates were used from those in Figs. 6 and 7, in an attempt to represent FUNCTION (2) for the fission fragments though using data for the fission products. This approximate conversion had short-comings but the plot conveniently showed shell edges and predicted where they could probably affect the initial charge division. Their expanded charge ordinate was $(Z_P - A_f(Z_F/A_F))$, where F referred to the fissioning nucleus and A_f, which was used also as the abscissa, represented the approximate average mass of the fission fragment, assumed equal to $(A_{FP} + \nu_f)$. They used Terrell's (TER 62) sawtooth function for ν_f.

(iv) The structure in FUNCTION (2) between A = 128-136 for low-energy fission apparently disappears at medium energy (Fig. 7).

(v) Fig. 8 (MCH 63) shows the increase of Z_P with excitation energy of the initial "compound nucleus" ^{236}U, for

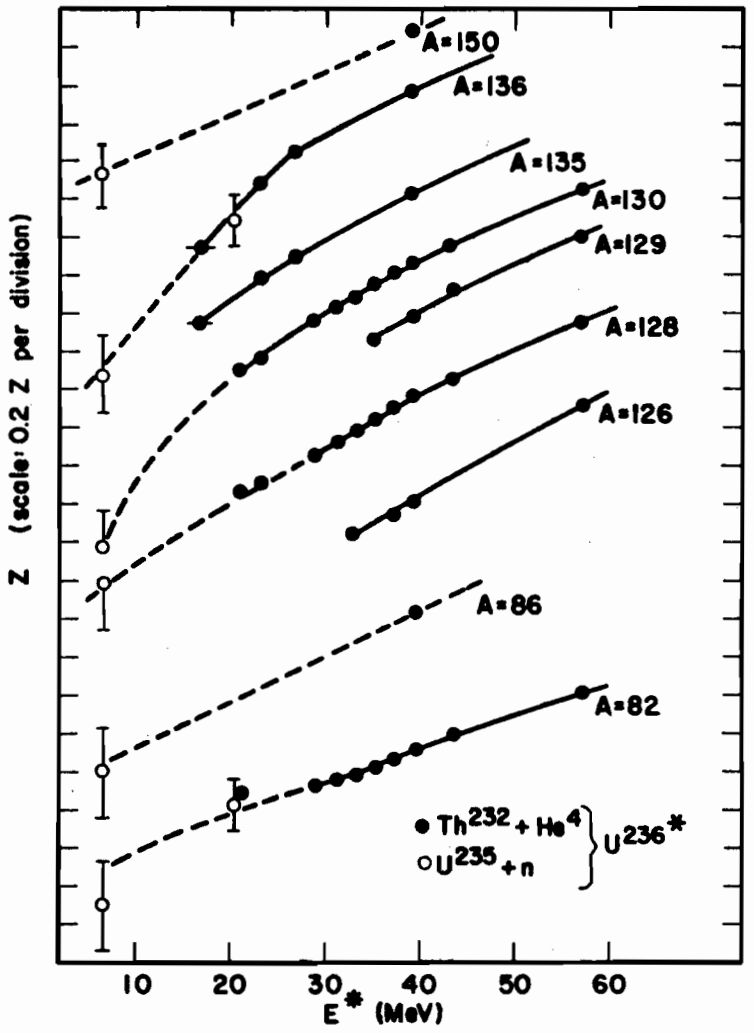

FIGURE 8. (MCH 63) Empirical Z_p's, for the fission of the "compound nucleus" $^{236}U^*$, as a function of excitation energy, E^*.

many mass chains. Similar results have been obtained by other workers (NET 65). Fig. 9 shows another method of plotting similar data (PAT 58a, DAV 63, BEN 65, PAR 66) previously obtained in this laboratory. In these studies the value of the most probable chain length ($Z_A - Z_P$) was obtained by using an early (COR 53, PAP 53) Z_A-function. Above about 20 MeV the steady rate of change of Z_P with energy has been assumed by McHugh to be due not to any change in the charge division itself, but to a steady increase in the total number of neutrons emitted.

The data from the present work will be plotted similarly and compared with the data in Figs. 8 and 9.

(vi) Attempts have been made to predict FUNCTION (2) for different types of fission from the function established for thermal neutron fission of ^{235}U, by accounting for the effect of changing the charge, mass and excitation energy of the fission system from the reference values 92, 236 and 6.5 MeV, respectively (KAP 61, COR 61, STO 62, WOL 65). The success of these methods was limited by the difficulty, now familiar in studies of charge distribution, that there are insufficient data for neutron emission and fission yields. This is particularly true in the energy region from about 8-18 MeV which is most important

FIGURE 9.

The most probable chain length, i.e. the displacement of the most probable charge Z_P from beta stability Z_A, as a function of the energy of protons inducing fission in

(a) ^{232}Th

—▲— Pate, Foster and Yaffe (PAT 58a)

—△— Benjamin (BEN 65)

(b) ^{238}U

—○— Parikh (PAR 66)

—●— Davies and Yaffe (DAV 63)

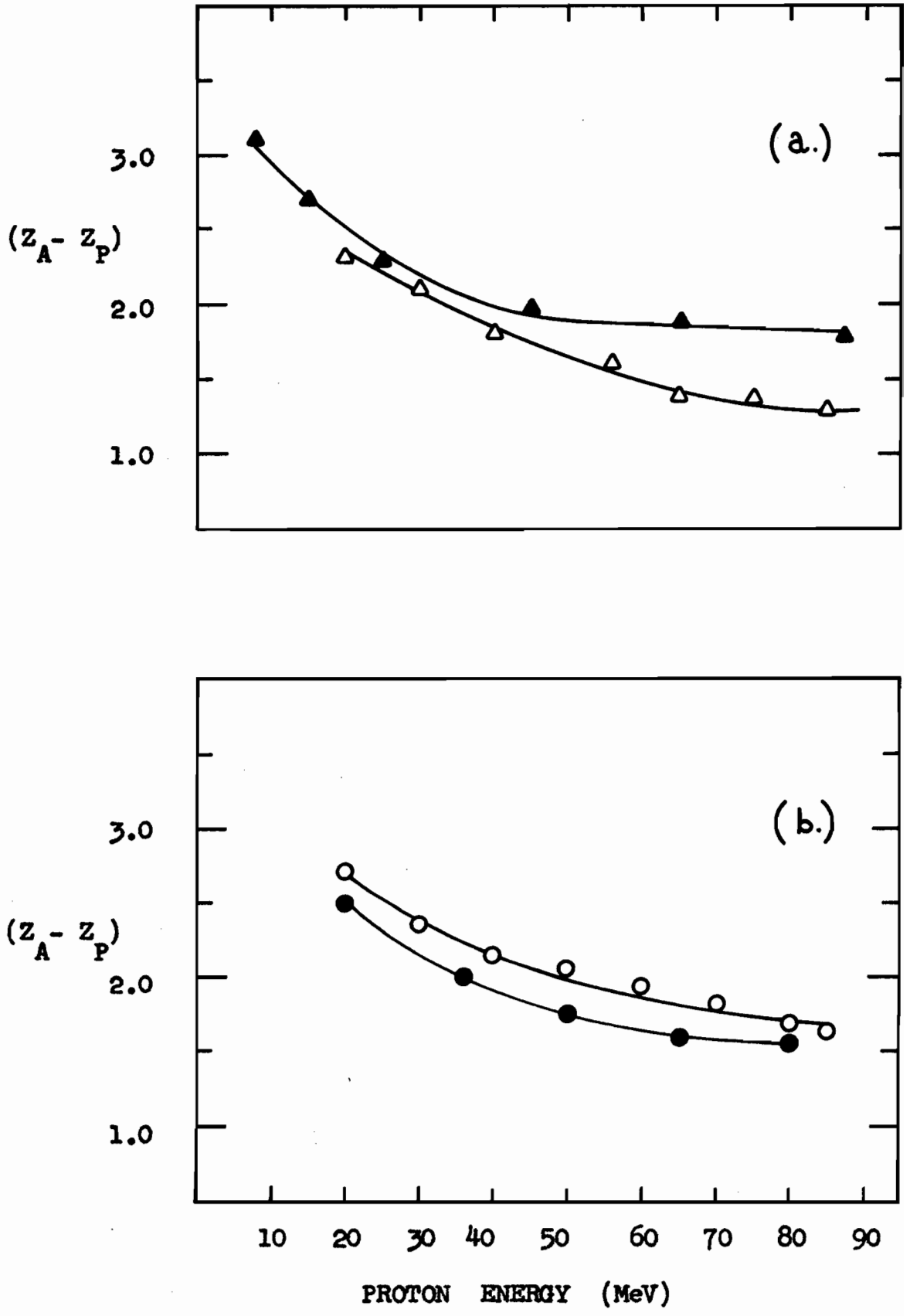
(a.)
3.0
2.0
1.0
$(Z_A - Z_P)$
(b.)
3.0
2.0
1.0
$(Z_A - Z_P)$
10
20
30
40
50
60
70
80
90
PROTON ENERGY (MeV)

in the construction and testing of these methods. A further weakness of these simple calculations is that they cannot account for the unsystematic differences that now appear to exist between low- and medium-energy fission (STO 62, MCH 63, NET 65). The assumptions in these formulae have been shown to be increasingly less successful as the excitation energy increases (STO 62, NET 65). It was unfortunate that although a small error due to an incorrect sign in the formula of Coryell et al. (COR 61) was found and reported in 1962 (STO 62), the uncorrected formula was still used in later work (HIC 62, WEA 63, WOL 65).

There are at present no very reliable methods to predict the majority of unmeasured independent fission yields in other than thermal neutron fission. Perhaps the more detailed empirical models devised recently (GOR 65, FER 65) to predict independent yields of fission products for thermal neutron fission ^{235}U will provide the basis of more successful methods to correlate FUNCTION (2) for various types of fission and to predict their fission yields. The data from this research contribute to the knowledge on charge distribution. In particular they show the effect on Z_p of different fission targets and energies. The present data alone are not extensive enough to improve FUNCTIONS

(1) and (2). The purpose of the present work is outlined later in Section 1AB.

Finally it is recalled here that all the above data were for the apparent charge distribution. Little reliable information is yet available on the initial charge distribution.

1A.4 DISTRIBUTIONS OF ISOTOPIC MASS AND OF ISOTONIC CHARGE

Another interesting method of correlating fission product yields has been used (TAL 63, MCH 63, BLA 60). The independent yields of the isotopes of one element are plotted against the isotopic masses. This has been called an element excitation function, but a more descriptive name is isotopic mass distribution. The wide Gaussian nature of this distribution for the elements Y, Cs, Xe and I for medium energy (MCH 63) has been shown to be a consequence of the Gaussian charge distribution and the total chain yields which are approximately constant over the mass ranges of the isotopes of these elements. This type of distribution is difficult to obtain and is at present not very useful except perhaps to check (WAH 65) that elements with complementary values of Z should have equal total isotopic "chain" yields, if charged particle emission in fission is neglected.

A rarely used method of correlating fission yields is the isotonic charge distribution (TAL 63).

1B. INTRODUCTION

SECTION B

ISOMERIC YIELD RATIOS IN FISSION

1B.1 GENERAL

This section of the Introduction surveys in some detail the relative formation of isomers in fission, and introduces the simple theoretical methods to be used in this thesis to discuss the isomeric yield ratios from this and other fission studies.

At present only crude theoretical calculations can be made to interpret the experimental ratios of independent yields of the two isomers of a fission product. These calculations are based on the moderately successful statistical model formalism introduced by Vandenbosch and Huizenga (HUI 60, VAN 60), and used with only minor modifications (VON 64, DUD 65, VAN 65) by numerous other workers (BIS 64a, BIS 64b, SAC 66), to study the angular momentum disposition in many spallation reactions with isomeric products. Studies of fission isomer ratios are limited by the very small number of isomeric fission products whose independent yield ratios can be measured precisely with existing techniques. Nevertheless the measurement of these

isomeric fission yield ratios does provide one of the few methods of obtaining information on the angular momentum of the fission fragments. These studies also make it possible to predict unknown, and often unmeasureable fission isomer ratios, which are frequently needed to interpret radiochemical fission data.

1B.2 FACTORS DETERMINING THE FISSION ISOMER RATIO

The formation of isomers is an even more complex process in fission than in spallation. The factors that determine the fission isomer ratio are :

(1) The spin distribution of the compound nucleus

(2) The spin changes following the emission of pre-fission neutrons

(3) The orbital angular momentum between the two fragments

(4) The disposition of angular momentum between the two fragments immediately after scission

(5) The orientation of the spins of complementary fragments

(6) The modification of the initial spin distribution of the fragments by the neutron- and gamma ray- de-excitation process

(7) The effective spin-pair for the isomeric species.

Calculations can be made for factors (1) and (2) since the formation of the compound nucleus and the emission of neutrons can be considered as part of a spallation reaction. However these results do not help in the calculation of the isomer ratio because factors (3), (4) and (5) are not understood. The theoretical interpretations of fission isomer ratios therefore have not attempted to deal with all of the above factors but have started by giving the initial fragments an assumed spin distribution and then treating factor (6) in a similar way to the de-excitation of a compound nucleus in a spallation isomer ratio calculation. These simple theoretical interpretations are discussed during the following systematic review of the factors listed above.

1B.2.Factor (1) THE SPIN DISTRIBUTION OF THE COMPOUND NUCLEUS

The normalized initial distribution of the compound nucleus spin, J_C, can be computed with Part 1 of the FORTRAN program of Hafner, Huizenga and Vandenbosch (HAF 62), which will be referred to as the HHV program. The latter was based (VAN 60) on the statistical model and took the vectorial sum of the target spin, the intrinsic spin of the projectile, and the orbital angular momentum brought in by the projectile.

The summation results in a variety of compound nucleus spin states whose statistical distribution was computed. The input data required for this program include a set of transmission coefficients for the projectile of a particular energy. These coefficients have not been given extensively for heavy nuclides. However, Feshbach et al. (FES 53, BLA 52) used a square-well nuclear potential for calculating some of these transmission coefficients for protons of energy up to about 25 MeV. With these coefficients, the spin distribution of the initial compound nucleus has been computed for the cases in Table 20(a). In this table the distributions are characterized by their root mean square angular momentum, $\sqrt{\overline{J_c^2}}$, and these will be discussed in Section 4B.

As the proton energy is increased above 25 MeV the spin of the compound nucleus is expected to increase. However, as the compound nucleus mechanism (BOD 62) becomes less important and as more direct reaction occurs with individual nucleons (SER 47, TOB 61) less angular momentum is transferred to the target by the proton. At the higher energies considerable angular momentum will be removed by a pre-fission cascade of particles. In spallation studies many isomer ratios (SAH 65) remain almost constant above

about 50 MeV. It was concluded that direct interactions predominate above this energy, and that the spin distribution of the residual nuclei resulting from the cascade process is nearly independent of bombarding energy above about 50 MeV.

Although an increase in the angular momentum of the compound nucleus is produced by an increase in the energy of the projectile or an increase in the spin of the target, the spin of the initial fragment may not increase very much, because of changes in other factors in the complex fission mechanism. Very few isomer ratio data previously measured are reliable enough and cover a wide enough energy range to test the energy dependence of the fission isomer ratio.

1B.2.Factor (2) THE SPIN CHANGES FOLLOWING EMISSION OF PRE-FISSION NEUTRONS

The modifications to the compound nucleus spin distribution by evaporation of pre-fission neutrons has been computed by Benjamin (BEN 65) using Part 2 of the same HHV program (HAF 62). This part of the program is used also for the neutron emission calculations for the fission fragments, to be described later. He showed that the change of spin per neutron-emission was very small for compound nuclei with mean spin of about 5. Table 2o(a) shows that this spin corresponds to a compound nucleus excitation energy of about 20 MeV.

It is still not clear how, as the fission energy is increased, the increased total neutron yield is divided between pre-fission and post-fission emission. It is difficult to estimate the number of neutrons in a pre-fission cascade at higher energies. There is evidence that the number of pre-fission neutrons evaporated (VAN 58, BRI 64, HUI 62) for a particular target should be about the same in medium-energy fission over a range of energies. The ratio of widths, Γ_n / Γ_F, has been found to be nearly independent of energy up to about 85 MeV (LIN 60, BRU 62).

1B.2.Factor (3) THE ORBITAL ANGULAR MOMENTUM BETWEEN COMPLEMENTARY FRAGMENTS

The orbital angular momentum between complementary fragments appears to be small in low- and medium-energy fission. A measure of this orbital angular momentum is given by the anisotropy of fission fragments (HUI 62, BLU 65) which has been measured in many angular distribution studies (HAL 58, CHA 62, VIO 65). The anisotropy was found to be very small for 22-MeV proton-induced fission of ^{232}Th, ^{233}U, ^{235}U and ^{238}U (COH 55). However when the fissioning nucleus has a very high spin, (20-40 units) as in heavy-ion-induced fission, Sikkeland and Choppin (SIK 65) concluded that a large fraction of this spin is carried off as orbital angular momentum of the fragments.

1B.2.Factor (4) THE DISPOSITION OF ANGULAR MOMENTUM BETWEEN COMPLEMENTARY FRAGMENTS

It is not known how the angular momentum is disposed between complementary fragments in the act of scission. However, estimates of the mean fragment spins have been made both experimentally, from studies of the prompt gamma rays from fission, and theoretically in calculations with simple electrostatic and mechanical models, and recently in more detail using a simplified liquid-drop theory of fission (NIX 65). Very little was known about the distribution function for this spin until Nix and Swiatecki (NIX 65) recently predicted not only the most probable value of the fragment angular momentum but also the distribution of the spin about this value.

Warhanek and Vandenbosch (WAR 64) had no information available on the distribution of the initial fragment spin, J_i. They tentatively suggested a distribution given by the formula,

$$N(J_i) = (2J_i + 1) \exp\left(- J_i(J_i + 1)/B^2 \right) , \qquad (1B.1)$$

where B is a free parameter which characterizes the distribution and has a physical significance which is given below. This distribution has the same functional form as the angular momentum distribution of the nuclear level density.

The procedure in previous fission isomer ratio calculations has been to use formula (1B.1) and to vary B until the experimental isomer ratio was reproduced by the detailed calculations of the de-excitation process described later in Section 1B.2.6. The value of B obtained was then taken to approximate closely the root mean square angular momentum, $\sqrt{\overline{J_f^2}}$, of the initial fragment spin distribution. This estimate of the mean spin of a few specific initial fragments is probably the most useful information that has come from isomer ratio studies (Section 4B, Table 21). Neither these studies nor any other known experimental method can yet determine the shape of the distribution function of the fragment spin.

The fragment spins estimated by the isomer ratio method contain large uncertainties, but so do the spins estimated by the other experimental and theoretical methods outlined below.

The anisotropy observed in angular distribution studies of gamma rays in low-energy fission (STR 60, BLI 63, HOF 64, KAP 64, PET 65, GRA 65, SKA 65) has been interpreted to indicate that the initial fragments contain about 8 units of angular momentum preferentially oriented perpendicular to the fission axis. This orientation of spin is consistent

with the mechanism where electrostatic forces induce a torque between the deformed scissioning fragments. Hoffman (HOF 64) used this electrostatic model to perform simple torque calculations and found that 5-6 units of angular momentum could reasonably be induced in a fragment. Strutinski (STR 60) had performed similar calculations but obtained higher spins. Lower spins were calculated by Sikkeland and Choppin (SIK 65) from a simple mechanical model (COH 63), but they neglected the repulsive Coulomb forces.

Maier-Leibnitz, Armbruster, and Specht (LEI 65a) have recently surveyed prompt gamma ray studies from low-energy fission. They concluded that the fragments have a spin of about 8-10. Johansson (JOH 64, JOH 65) arrived at the same conclusion from the multiplicity of the gamma cascade.

Whereas the gamma ray studies give an estimate of the spin averaged for all the fragments, the isomer ratio studies give the spin of a specific initial fragment. The latter studies can therefore be used to investigate the dependence of the initial spin on the fragment mass. There are only limited data available for this investigation and these will be discussed with the ^{133}Xe data from the present study, in Section 4B. The fragment spin has been predicted

to be appreciably lower for symmetric fission than for asymmetric fission (POR 57, HOF 64, SIK 65). This prediction was not restricted to low-energy fission. A similar mass dependence of the fragment spin was suggested by Johansson (JOH 64) to explain the measured mass dependence of the total gamma-cascade energy, but these measurements have been made only at low energies (LEI 65a, LEI 65b).

Nix and Swiatecki have suggested that it may be possible to obtain the degree of nuclear viscosity from accurate information about fragment spins. For only one example, have they calculated their formulae predicting the fragment spin distribution (NIX 65). They used the "compound nucleus" $^{213}_{85}At$, which would be formed in the fission of ^{209}Bi by 65-MeV alpha particles. For this system they plotted the probability distribution of the angular momentum of an individual fragment for the three cases:

(i) If the torque from Coulomb repulsion were zero,

(ii) If the fragments were non-viscous,

(iii) If the fragments were infinitely viscous.

The maximum of these three distributions corresponded to the spins 8.5, 10 and 15 respectively. The relatively large difference between cases (ii) and (iii) suggest that it may be possible to decide between them if accurate spin data can be obtained.

Their model is particularly useful for discussing fission of elements lighter than Rn. No attempt has yet been made by us or by other workers to use their spin distribution formula for the assumed initial fragment spin distribution. Their distribution could be used to interpret the isomer ratio data for fission of ^{209}Bi (HAG 63, HAG 65), but it is unlikely that the existing data are reliable enough to give any information on the nuclear viscosity.

1B.2.Factor (5) THE ORIENTATION OF COMPLEMENTARY FRAGMENT SPINS

Very little is known about the orientation between the spins of complementary initial fragments. Although this orientation is given by the formulae of Nix and Swiatecki they have not yet given examples of their results. An indication of this orientation may be obtained from isomer ratio studies by the construction of a simple spin vector triangle with sides equal to the calculated mean spin of the fissioning nucleus, the fragment spin estimated from the experimental isomer ratio, and the assumed spin of the complementary fragment. This simple treatment neglects the small fraction of the spin that appears as orbital angular momentum between the fragments (see Section 1B.2 above). Sarantites (SAR 65) used this method with his data for the isomers of ^{131}Te for the following two fission systems.

Fission system	Estimated mean spin of the ^{236}U "compound nucleus"	Estimated mean spin of the Te fission fragment	Assumed spin of the complementary fragment
(a) $^{235}U+n_{thermal}$	3.5	5 ± 1.5	5
(b) $^{232}Th+\alpha_{33\ MeV}$	~ 13	7 ± 2	7

A pair of complementary fragments was assumed to have about the same mean spins. Despite the fairly large uncertainties in the estimated fragment spins he was able to conclude that the spins of the two fragments in system (b) do not line up as nearly antiparallel as in the case of system (a).

It has been shown that a fissioning system of low angular momentum can give rise to fragments of high spin; and this has been explained simply by assuming a suitable orientation of the complementary fragment spins in the simple vector triangle (WAR 64, SAR 65).

1B.2.Factor (6) MODIFICATION OF THE SPIN DISTRIBUTION OF INITIAL FRAGMENTS

In fission isomer ratio studies most attention has been given to the process of de-excitation of the initial fission fragment. The spin distributions throughout the process have been calculated with the widely used statistical

model formalism of Huizenga and Vandenbosch. This process is even more complex than the de-excitation of the compound nucleus in a spallation reaction, and there are many uncertainties in the input data.

There are three stages in the detailed calculations. The first two account for the modification of an assumed initial fragment spin distribution by N_n neutron emissions followed by $(N_\gamma - 1)$ gamma ray emissions. The final stage splits the last spin distribution calculated in stage two, between the two isomeric states. This third stage is based on the rather poor assumption that the last gamma ray emitted may have any multipolarity so that a state can decay to the isomer with the nearest spin.

A full description of the theory has been given elsewhere (HUI 60, VAN 60, BIS 61, VON 64, DUD 65), and FORTRAN programs (HAF 62) for the computation of the first two stages are contained in Parts 2 and 3 of the report on the HHV program (HAF 62). The third stage is relatively simple and is described later in Section 4B.

1B.2.6.1 Stage 1, Neutron Emission from the Fission Fragment

Part 2 of the above FORTRAN program was used N_n times with a different set of input data for each of the N_n neutron emissions. The following data were used.

(a) The input spin distribution for the first neutron emission was the assumed spin distribution of the initial fragment, represented by equation (1B.1), but for the subsequent stages was the output distribution from the previous step.

(b) The set of transmission coefficients, $T_{\ell'}(\bar{E}_n)$, for neutrons of average kinetic energy, $\bar{E}_n$, and with angular momentum ℓ', have been taken from the curves of Feld et al. (FEL 51), using a nuclear radius parameter, $r_o = 1.5$fm. The calculations have been shown to be insensitive to small changes in $\bar{E}_n$ (VAN 60, BIS 61, BIS 64b, SAR 65) and it has been found satisfactory to use an average value, rather than to use a more complex treatment to account for the energy spectra of emitted neutrons (TER 65).

(c) The spin cutoff factor, σ, characterizes the spin distribution of the density of nuclear levels available in the residual fragment for each de-excitation step. This density of levels $\rho(J)$ is given by the formula, (ERI 60, BOD 62)

$$\rho(J) \propto (2J + 1) \exp\left(- (J + \tfrac{1}{2})^2 / 2\sigma^2 \right) . \qquad (1B.2)$$

In the de-excitation calculations this density is sampled by each neutron and each gamma ray emission. There is very little experimental information on the value of σ, especially for nuclides of mass $A > 60$, but spallation isomer ratio

studies (VAN 60, BIS 64a, VAN 65) have given a value of 4 ± 1 for medium weight elements up to $A \approx 200$. These values were used in most fission isomer ratio calculations, but, Warhanek and Vandenbosch used an energy dependent σ given by the formula (ERI 59),

$$\sigma^2 = \mathcal{I}_R t / \hbar^2 \quad , \qquad (1B.3)$$

where t represents the thermodynamic temperature, and $\mathcal{I}_R$ represents the rigid-body moment of inertia. They have pointed out that the σ values were too high (VON 64, BIS 64a, VAN 65) when the rigid-body moment of inertia was used. They partly corrected for this using the so called Shifted Fermi Gas model (VON 64). A pairing energy was subtracted from the excitation energy, U, equal to 2.2 MeV for even-even fragments and 1.1 MeV for odd-even fragments. This corrected excitation energy, U", above the shifted ground state, was introduced into formula (1B.3) through the definition, $U'' = at^2 - t$. Unfortunately they gave no details of the σ values they obtained nor the fragment excitation energies they used to calculate them. We estimate that, with a level density parameter, a, equal to A/8 and a nuclear radius parameter, r_o, equal to 1.2 fm, the values of σ are about 6, 7 and 8 for fragments of mass about 135 with excitation energies of 10, 20 and 30 MeV, respectively. For these

energies the simple formula, $U = at^2$, with no pairing correction gives nearly the same values.

1B.2.6.2 Stage 2, The Gamma Ray Cascade from the Fission Fragment

The spin distribution after N_n neutron emissions was then modified by a cascade of N_γ gamma rays. Part 3 of the HHV program was used $(N_\gamma - 1)$ times with the following input data.

(a) The input spin distribution for the first gamma ray emission was the output spin distribution following N_n neutron emissions, but for the subsequent stages was the output distribution from the previous step.

(b) The spin cutoff factor, σ, has been discussed above.

(c) The multipolarity of the gamma ray, ℓ, was usually assumed to be one, but quadrupole radiation has been introduced in some spallation studies (VAN 65, SAC 66), and Hagebo (HAG 65) has used one quadrupole gamma ray in the gamma cascade calculation for the fission fragment ^{120}In. Petrov (PET 65) has questioned Hoffman's (HOF 64) conclusion, from studies of gamma ray angular distribution, that a fraction of the prompt gamma ray transitions in fission are quadrupole. Warhanek and Vandenbosch argued that this

fraction of the gamma rays consists of forced quadrupole transitions, from only those fragments with the highest spins which cannot be dissipated by dipole radiation. However, Maier-Leibnitz et al. (LEI 65a) interpreted several experiments, including those of Hoffman, by assuming quadrupole gamma-transitions from fission fragments with a high spin of about 10. Johansson (JOH 64) concluded that a cascade of E2-transitions de-excites the fragment after neutron emission; only vibrational states of the quadrupole type have life-times short enough to explain the results of his experiments in which most of the gamma-quanta were found to be emitted within 10^{-11} seconds after fission.

1B.2.6.3 Choice of Input Parameters for stages (1) and (2)

Table 2 summarizes the input parameters used in previous fission isomer calculations.

Since the values of the parameters N_n, σ, E_n, $T_{\ell'}(\bar{E}_n)$, N_γ, and ℓ all contain uncertainties, even for low-energy fission, and, since these parameters change with energy, the question arises as to whether the calculations can still be useful. Sarantites (SAR 65) has claimed that despite the complexities and uncertainties of the calculations a meaningful estimate of the average spin of the primary

TABLE 2 Input Parameters Used in Previous Fission Fragment De-excitation Calculations

Isomeric Species	Fission Reaction			Input Parameters				Comments	Ref.
	Target	Proj.	$E_{Proj.}$ (MeV)	N_n	σ_n	N_γ	σ_γ		
^{95}Nb	^{238}U, ^{232}Th Pb, Bi	p	20-160	1	3,4,∞	4	3,4,	$\bar{J}$, not formula (1B.1), assumed for initial fragment	HAG 63
^{117}In	^{238}U, ^{232}Th Bi	p	20-160	3	3	4[a]	3	a. one quadrupole transition used	HAG 65
^{131}Te (^{133}Te)	^{235}U	n	thermal	0,1,2,3[b]	4	3	3,4	b. neutron-parentage calculated by Monte Carlo method	SAR 65
	^{232}Th	∝	33	2	4	3	3,4		
^{134}Cs	^{233}U	γ	≤16	2,(1)	-[c]	2,(3)	-[c]	c. Used formula (1B.3). High σ values	WAR 64
	^{232}Th	p	20-85	1,2	4,5	3,4	4,5		BEN 65

fragment may be obtained. His conclusions, however, were based on calculations for the fission of ^{235}U with thermal neutrons. For this system,more theoretical and experimental information is available than for any other fission system (HYD 62, HUI 62, GOR 65, FER 65, FRA 65), and his fission isomer ratio calculations were the most detailed that have yet been attempted. Unfortunately, only one suitable isomer pair, $^{131m}Te/^{131g}Te$, has been studied successfully in thermal neutron fission. There were uncertainties even in the input parameters for Sarantites' calculations, but these uncertainties are magnified at higher energies for which most of the fission isomer ratio data have been obtained. The difficulties in estimating N_n and N_γ in fission are made obvious by the following considerations.

(i) The energetics of the de-excitation of fission fragments are not well defined experimentally nor theoretically. Sarantites was able to estimate N_n, $\bar{E}_n$ and N_γ from the results of the Monte Carlo calculations on prompt neutron emission and the calculation of the energy balance in thermal neutron fission, recently described by Gordon and Aras (GOR 65). He performed calculations for three N_n values (0, 1 and 2) and, using the calculated neutron parentage of his isomeric fission product, took a

weighted average of these three results to obtain a final value for the isomer ratio. Gordon and Aras, however, expressed doubts concerning their assumptions in the calculation of individual fragment excitation energies.

As the fission energy increases, an estimation of how the energy of the fissioning nucleus is divided between complementary fragments is even more difficult and is complicated by the energy removed in pre-fission neutron emission (BRI 64). It is known that the average kinetic energy of the fission fragments does not change appreciably with increase of fission energy (HUI 62, HYD 62).

(ii) Even if the fragment excitation energies (HYD 62) were known, the values of N_n and N_γ cannot be calculated satisfactorily from energy considerations alone without a knowledge of the angular momentum dependent competition between neutron and gamma ray emissions (GRO 61, GRO 62, MOL 62, CHO 63, WAR 64, JOH 64, THO 64). This is briefly discussed below.

(iii) The recent survey by Maier-Leibnitz et al. (LEI 65a) showed that prompt gamma ray emission from fission fragments is more complex than had been predicted, and differs from gamma ray emission in spallation product de-excitation. A fission fragment de-excites by a larger number

of smaller energy steps than does a nucleus after neutron capture. It is therefore doubtful whether formulae used to calculate the multiplicity of the gamma cascade in spallation (DUD 65) are applicable to fission fragments. However, Sarantites did use such a relationship, given by Strutinski et al. (GRO 60), to calculate the average number of gamma rays emitted,

$$\bar{N}_\gamma = \sqrt{a E_\gamma} / (\ell + 1) \quad . \qquad (1B.4)$$

Here the level density parameter, a, was taken to be $A/13\ MeV^{-1}$, and E_γ was taken to be the residual excitation energy after the maximum number of energetically possible neutron emissions. Formula (1B.4) gave an $\bar{N}_\gamma$ value of about 3, for an $E \approx 4$ MeV and multipolarity $\ell = 1$. The statistical model predictions of N_γ are lower than the measured average values of 4-5, for low-energy fission. The competition between gamma and neutron emission provides an explanation (JOH 64, WAR 64) for the discrepancy in the predicted and measured N_γ. The high spin of the fragments and the low E_γ available for gamma emission allow this process to compete successfully with neutron emission. The effective E_γ is therefore higher than would be expected if neutron emission always took place when energetically possible. The increase in E_γ has been estimated to be about

1.5 MeV for a fragment of spin 8 (WAR 64), and about 2.0 MeV for a fragment of spin 10 (JOH 64). Warhanek and Vandenbosch argued that the fragments of very high spin are responsible for the high observed multiplicities, since they probably emit a very large number of quanta. For this reason they used a value of N_γ lower than the experimental value.

(iv) In low-energy fission, fragment shell-effects are well known in prompt neutron studies (TER 65, APA 62, APA 64) (cf. Section 1A.3.1 and Fig. 3) and more recently have been found in prompt gamma ray studies (MIL 58, LEI 65a, LEI 65b, JOH 64). The curves for both N_n and N_γ, as a function of the mass of the fragment, have a saw-tooth shape.

The total gamma ray energy was found to be at a minimum in the fragment mass region A = 128-134; these fragments involving closed shells have been found to emit a smaller number of quanta of higher energy than average. There is no evidence available to decide whether shell effects on N_γ are as important at higher fission energies. At medium energies, there is evidence (MCH 63, BRI 64) that the value of N_n for the fragments from symmetric fission is no longer lower than that for the asymmetric fragments, but there is some evidence to the contrary. Hagebo assumed that shell effects are still present in medium-energy proton

fission. For one such fission system, he used $N_n = 3$ for the fragment ^{120}In (HAG 65), but $N_n = 1$ for the fragment ^{96}Nb (HAG 63). However, he used $N_\gamma = 4$ in both cases.

The best method to estimate N_n and N_γ is to use the available experimental values, but to take into account the above considerations. Terrell (TER 65) recently reviewed the many experimental data for N_n at low energy. There are fewer data for N_n for medium-energy fission (MCH 63, BRI 64, WHE 64), and they are for fission induced by medium-energy helium-ions. It is not known how the number of neutrons emitted from individual fragments increases with increasing fission energy, but reasonable assumptions can be made (WOL 65) up to about 40 MeV. Below this energy, it has been established that the total average number of prompt neutrons, $\bar{\nu}_T$, (FRA 65, BAT 65) and its rate of increase with energy, were similar for a wide range of fissioning systems (POW 62, MAT 65). The rate of increase was nearly constant and had a value of about 0.13-0.16 neutrons per MeV. From these studies it is reasonable to assume that on the average only about one neutron is emitted from a low-energy fission fragment, and that a change in fission energy of at least 15 MeV is needed to change N_n by one unit. Only an approximate estimate of an average N_n can be obtained because of many unknown factors

in the de-excitation process leading to a specific isomeric nuclide, and because even at low energies this nuclide has several neutron parents (SAR 65).

The data for N_γ, which are for low-energy fission only, have been surveyed recently (LEI 65a). From the observed value of N_γ, it is difficult to estimate a meaningful N_γ for the gamma cascade model because of the possibility, discussed above, that the fragments of highest spin may have gamma cascades with a higher multiplicity than the average. There are no available data for N_γ for medium-energy fission and it has been assumed that $N_\gamma = 3 \pm 1$.

The effect of the uncertainties in the input data on the results of the isomer ratio calculations is assessed in Section 4B.

1B.2.Factor (7) THE EFFECTIVE SPIN-PAIR OF THE ISOMERIC SPECIES

Generally, two nuclear isomers have spins separated by several units (up to 5) of angular momentum, but have a difference in energy of only a few hundred kev. The shell model of the nucleus gives a good explanation of nuclear isomerism and the spins of isomer pairs. The comprehensive review of nuclear isomerism by Alburger (ALB 57) contains an account of this explanation.

Segrè and Helmholz (SEG 49) suggested the first method of predicting the isomer ratio in nuclear reactions, but this method has proved incorrect. They suggested that, if the excitation energy were high enough to allow population of many levels, the isomeric yield ratio would reach a limiting value equal to the ratio of the statistical weights of the isomeric states, $(2J_{high} + 1)/(2J_{low} + 1)$. It has been shown (LEV 53, VAN 65) that no such limit exists. The process of isomer formation is too complex, particularly in fission, to beexplained by the spins of the isomeric states alone. However, the isomer-pair spins are very important in the final stage (cf. Section 4B) of the fragment de-excitation calculation. Qualitatively it may be predicted that an isomeric pair with low spins will have a higher isomer ratio than a pair with higher spins. The fission studies of independent isomeric yield ratios surveyed in Table 3 have therefore been divided into classes of isomer-pair spins, or spin-pair classes. Table 3 shows that the best available studies fall into only three spin-pair classes:
Class 1 (9/2, 1/2); Class 2 (11/2, 3/2); Class 3 (8, (5), 4).
During this thesis isomer pairs will be discussed with reference to these three classes. The number of fission isomer data is very small compared to the numerous data that

TABLE 3 Classification and Summary of the Main Studies of Fission Isomer Ratios

Spin-Pair Class	Isomer Spin-Pair H,L	Isomeric Species		Half-Life	Target (I = 0)	Target (I ≠ 0)	Projectile, Energy (MeV)	Isobaric Parent	Half-Life	Ref.
1	9/2,1/2	^{95}Nb g	H	35d.	^{238}U, ^{232}Th	^{208}Pb, ^{209}Bi	p 20-160	^{95}Zr	65d.	HAG 63
		m	L	90h.						
		^{117}In g	H	38m.	^{238}U, ^{232}Th	^{209}Bi	p 20-160	^{117}Cd (m)	3.1h	HAG 65
		m	L	1.9h.				(g)	2.7h	
2	11/2,3/2	^{131}Te m	H	30h.	^{238}U, ^{232}Th	^{235}U	α 33 d 18 n Thermal	^{131}Sb	19.4m.	SAR 65
		g	L	25m.		^{233,235}U, ^{239}Pu	n Thermal			ERB 63
		^{133}Te m	H	53m.	^{238}U, ^{232}Th		α 33 d 18	^{133}Sb	3m.	SAR 65
		g	L	12.5m.						
		^{133}Xe m	H	2.3d.	^{238}U, ^{232}Th	^{233}U, ^{235}U	p 20-85	^{133}I	20.8h.	This work
		g	L	5.3d.						
3	8,(5),4	^{134}Cs m	8	2.9h.	^{238}U	^{233}U, ^{235}U ^{237}Np ^{233}U	α 27,42 d 21 δ 16	both isobaric neighbours are stable		WAR 64
		g	4	2.1y.	^{238}U		p 25-80			DAV 63
					^{232}Th		p 20-85			BEN 65

have been obtained from isomeric spallation products (WIN 62, SAC 66). A few other fission data are available, as well as those referred to in Table 3.

Many studies have been made on the isomer pair ^{115m}Cd and ^{115g}Cd with the spins 11/2 and 1/2 but these isomer ratios are not for independent yields, because of the short-lived beta parents ^{115m}Ag (21 seconds) and ^{115g}Ag (21 minutes). The relative yield of ^{115}Ag to ^{115}Cd decreases with increasing fission energy and the measured ratios for moderately high energy fission are mainly for independently-formed ^{115}Cd (HIC 55, POR 57, BAI 59, TIL 63b, SIK 65). Nevertheless, over the range of medium energies considered in this thesis the ^{115}Cd data probably reflect the change of the isobaric charge dispersion with energy as well as any change in the isomer ratio. Häller and Andersson (HAL 61) measured independent isomer ratios for ^{80m}Br (I = 5) and ^{80g}Br (I = 1,(2)), but these isomers have very low fission yields and could only be measured for fission induced by protons above 70 MeV in energy.

The effective isomer-pair spins to be used in stage 3 of the isomer ratio calculation are not always the spins of the isomeric states. If between the two isomeric states an energy level exists, usually with an intermediate

spin, then the effective isomer-pair spins for the calculation are those of the metastable state and this intermediate level (HUI 60, VAN 60, STR 65). More difficult situations could arise. For example (HUI 60), if a state of intermediate spin had an energy just above the metastable state and decayed by a crossover transition to the ground state the isomer ratio would be low and the calculations could not easily account for this type of decay scheme. It is important in isomer ratio calculations that the decay scheme for an isomeric nuclide be well known because of the large perturbations that may be caused by unknown levels.

1B.3 SUITABILITY OF THE ISOMERS OF ^{133}Xe FOR THIS STUDY

The xenon isotopes of odd mass number, A, are situated in the so called "island" of isomeric nuclides with odd A, just before the closed neutron shell, N = 82 (BER 52, ALB 57). The isomeric pair ^{133m}Xe and ^{133g}Xe is very suitable for medium-energy proton-induced fission studies, for the following reasons.

(a) ^{133}Xe is formed in good yield, though the gamma ray activity of ^{133m}Xe is fairly low.

(b) The beta parent, ^{133}I, has a reasonably long half-life, 20.8 hours, so that only small corrections are

needed to account for the decay of ^{133}I by a 98% branching (NDS) to ^{133g}Xe.

(c) The half-lives of ^{133m}Xe (2.3 days) and ^{133g}Xe (5.3 days) are very convenient.

(d) Xenon can be easily and quickly isolated from the fission target and other products. The only impurity is krypton which gives no long-lived activities, and can be separated almost quantitatively from xenon.

(e) The spins of ^{133m}Xe ($I = 11/2$) and ^{133g}Xe ($I = 3/2$) are known and no other interfering levels have been reported for ^{133}Xe.

Unfortunately the absolute values of the experimental isomer ratios depend strongly upon the internal conversion coefficient of the M4 transition between the isomers of ^{133}Xe (cf. Section 4B). However, the results for the isomeric yields of ^{133}Xe are very suitable for relative studies of the isomer ratio over a fairly wide range of fission energy, for four targets of three different spins.

1AB. INTRODUCTION

PURPOSE OF THE PRESENT WORK

In the present work the independent yields of ^{135}Xe, ^{133m}Xe and ^{133g}Xe and the cumulative yields of ^{135}I and ^{133}I have been measured from fission of ^{232}Th, ^{233}U, ^{235}U and ^{238}U induced by protons of 20-85 MeV. A radiochemical gas-sweeping technique was used and the activity of the separated xenon samples was measured by a gamma spectrometer calibrated with a gas-phase beta proportional counter.

The relative independent yields of the ^{133}Xe isomer-pair, the isomer ratio, of spin-pair class 2, were obtained. Simple statistical model calculations have been made of the type described above in Section 1B. The compound nucleus spin distribution has been computed up to 30 MeV. Most of the calculations have been for the de-excitation of the fragments leading to three spin-pair classes of isomers. The results of these calculations have been used as a framework for the discussion of the data from this and other studies of the isomer ratio in fission, and in an assessment of the theoretical and experimental aspects of these studies.

Up to about 50 MeV, the relative yields of iodine

and xenon have been used to obtain empirically fractional yields and values of Z_p for the mass chains 133 and 135. These data have been used to investigate the effect of target composition and excitation energy on the value of Z_p for the apparent charge distribution of these mass chains. The Z_p data for different fission systems were compared semi-quantitatively using the simplified CCR rule.

Except for the fission of ^{233}U, absolute cross sections were obtained from most of the irradiations, by measuring the proton flux with the monitor reaction $^{65}Cu(p,pn)^{64}Cu$. These data gave excitation functions and total chain yields. The present results were compared to related medium-energy studies of fission yields.

2. EXPERIMENTAL

2.0 OUTLINE OF EXPERIMENTAL PROCEDURE

Twenty-eight experiments are reported in this thesis. Four different types of heavy metal targets were used, ^{232}Th, ^{238}U, ^{235}U and ^{233}U. The procedure in an individual experiment is briefly summarized in the following paragraph and is described in detail in subsequent sections.

A heavy metal target was bombarded with protons and then quickly removed to the Chemistry laboratory. There it was dissolved and a gas-sweeping technique and subsequent adsorption gas chromatography were used to extract the xenon fission products from the target material and other fission products. After about thirty hours, a similar extraction and separation produced a second sample of xenon which was formed purely by precursor decay. The activity of the xenon samples was measured with a gamma spectrometer. The efficiencies of these measurements were determined relative to a gas-phase beta proportional counter which was calibrated in this work. In most of the experiments the proton beam was monitored by simultaneously irradiating a similar copper target. The copper was dissolved, about one day after a bombardment, was separated on an ion-exchange resin, and its activity measured on the gamma spectrometer.

2.1 IRRADIATIONS AND TARGET ASSEMBLY

The internal circulating beam of protons in the McGill Synchrocyclotron was used for the irradiations. The target was held in a simple aluminium clamp which was screwed to the end of a probe and inserted to a certain distance from the centre of the cyclotron. The revised curve of Kirkaldy (KIR 54) gave the distance for a required proton energy. For the targets and energies used in this work the degradation in the proton energy (STE 59) was within the energy spread ($\pm$ 2 MeV.) of the proton beam, and was therefore neglected. The intensity of the beam was 0.5-1.0 micro amp. It was monitored with the reaction $^{65}Cu(p,pn)\ ^{64}Cu$ for the entire energy range, 20-85 MeV. (cf. Appendix A.2). Table 6 summarizes the 28 irradiations in this work and shows that the times of bombardment, t_o, were from 5-25 minutes.

The target material for all of the irradiations of ^{233}U (and for one of ^{238}U, R16) was finely powdered uranium oxide (5-12 mg) wrapped in aluminium foil of surface density 5.5 mg/cm^2. These runs were not monitored.

Table 4 describes the target foils used for ^{232}Th, ^{235}U and ^{238}U and the monitor foil of "spec-pure" copper.

TABLE 4. Description of Target and Monitor Foils
(cf. Table A2, Appendix A)

Target Isotope	Surface Density (SD) (mg/cm^2)	Isotopic abundance %
^{232}Th	80.8	100
^{238}U	46.4	99
^{235}U	104.0	94
^{65}Cu	45.9	31.9

The target was assembled as follows.

(a) Fig. 10(a) shows the target foil contained in an aluminium foil (5.5 mg/cm^2) envelope placed beside a copper monitor foil of similar size.

(b) Fig. 10(b) shows these metals clamped in the aluminium target holder. They were pressed between two aluminium plates in a vise, cut with scissors along dotted line AB, and again pressed. This ensured that the leading edges of the monitor and target foils were aligned and close together.

(c) Fig. 10(c) shows a plan view of the target assembly screwed on to the probe. The proton beam first strikes the copper foil.

FIGURE 10.

Target assembly

(a) and (b) before irradiation,

(c) during irradiation,

(d) after irradiation.

10 (a)

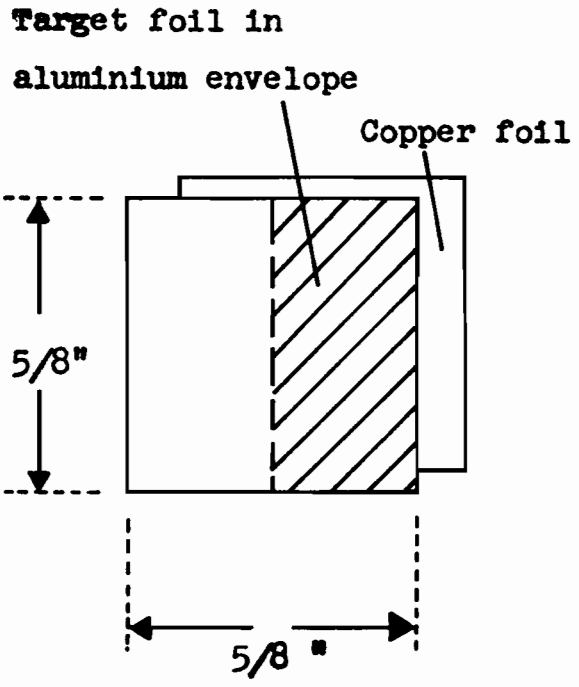

10 (b)

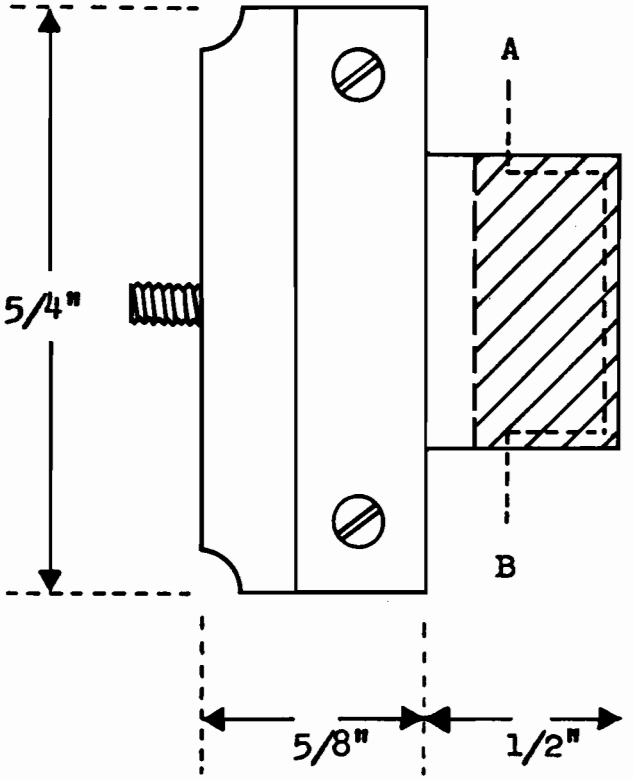

10 (c)

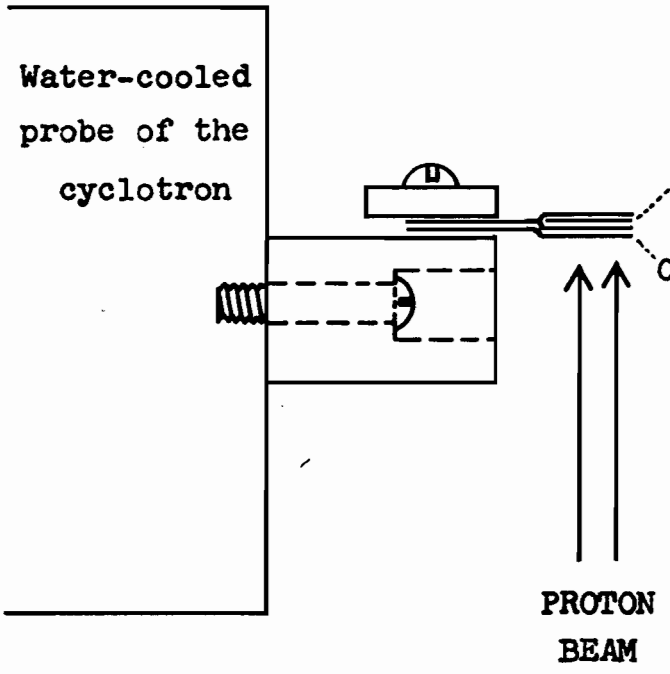

10 (d)

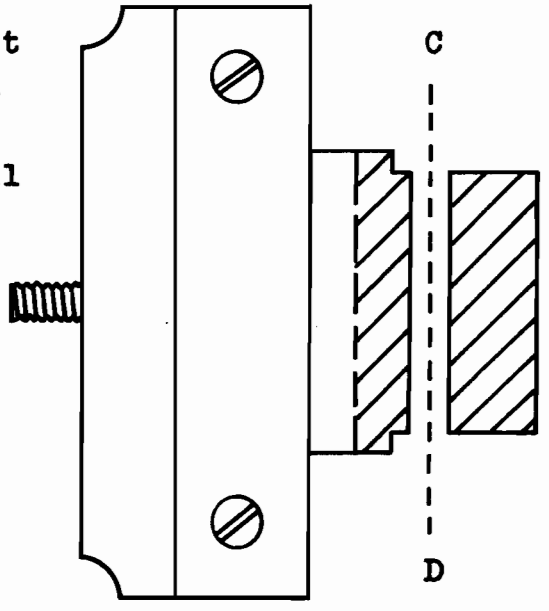

(d) Fig. 10(d) shows where the irradiated foils were sheared, along CD. This was done as soon as possible after a hurried journey from the cyclotron to the Chemistry laboratory. The cut target and aluminium catcher foil were immediately introduced into the gas-sweeping apparatus as described later. The copper foil was put aside for one day.

The products of nuclear reactions could be lost from the target material by recoil, by diffusion and by further nuclear reaction. The last-mentioned may be neglected in the present work. The recoil losses for the spallation reaction of copper may also be neglected here. Recoiling fission products were held in the aluminium catcher foil which was thicker than the range (~ 3 mg/cm^2) (ARA 65) of the fission products, xenon and iodine, in aluminium.

Diffusion losses of xenon from the target material have been examined elsewhere (GRA 60, STO 62, MCH 63) and found to be very small for foil targets but significant for powder targets. No absolute measurements of cross section were made with powdered targets of uranium oxide, and the measured isomeric yield ratio of ^{133}Xe would not be affected by a diffusion loss. This loss may have a small effect on the relative yields of iodine and xenon. This effect should be apparent in the two results for the fission of ^{238}U with

75-MeV protons, which was studied with a target of uranium foil (irradiation number R11) and uranium oxide (R16).

Tables 9 and 17 give the ratios $R_{c/i}^{133}$ and $R_{c/i}^{135}$ for these two experiments which give no evidence for a significantly larger diffusion loss from the powdered oxide target.

Diffusion losses could have been completely avoided by sealing the wrapped target in a quartz tube (KAT 53). This technique was not used here because it would introduce monitoring difficulties and probably lengthen the first separation time, t_1.

The method of using the aluminium envelope for the target foil was chosen for several reasons given below. This method was preferred to a method previously used in which three similar target foils were irradiated, but only the central foil was used.

(i) Obviously the present method saved valuable target material (particularly important for foils of ^{235}U) and also reduced the level of radiation during the early stages of an experiment.

(ii) The monitor and target foils could more conveniently be pressed together for cutting and be kept close together during the bombardment. This was extremely

important if the two foils were to receive the same number of protons, because most of the protons hit the foils over a small area close to the leading edge of the target (Fig. 10(c).).

(iii) The aluminium envelope delayed the initial release of xenon from the target foil when acid was first introduced into the dissolver, and therefore avoided loss of rare gas before the dissolver was resealed.

2.2 CHEMICAL SEPARATIONS AND YIELDS

2.2.1 COPPER

After about twenty-four hours the copper foil was weighed and then dissolved in a mixture (1:1) of hydrogen peroxide and concentrated hydrochloric acid, evaporated to dryness and redissolved in a minimum of conc. HCl. This solution was then passed through an anion-exchange resin (Dowex-1X8, mesh size 100-200) in a column of length 10 cm and diameter 1 cm. The copper was separated (KRA 53) from other spallation products by preferentially eluting nickel, manganese and cobalt with 4M HCl until the colour band of copper reached the bottom of the column. The copper was then eluted with 1.5M HCl while iron and zinc remained on the column. All but the head and tail of the copper eluate was collected, evaporated to dryness and made up to

approximately 2 ml in a glass vial, of standard dimensions and with a screw top, for measurement of gamma radiation. The fraction of the copper foil in the gamma sample, the chemical yield Y_{Cu}, was determined after the activity had decayed. The 2 ml counting solution was made up to 10 ml and aliquots were titrated with EDTA (the disodium salt of ethylene-diamine tetra-acetic acid), using a murexide indicator (WEL 58).

2.2.2 XENON

The techniques in this radiochemical study of xenon were essentially those used by Dostrovsky and Stoenner (DOS 62) and have been briefly outlined in the Introduction. Fig. 11 schematically summarizes the techniques used and shows that they fall into three parts. It will be convenient to give the details of the apparatus during a systematic description of these three parts of the experiment. Two gas-sweeps were made, sweeps (a) and (b).

2.2.2.1 Gas-Sweep (a)

Part 1. Extraction of Xenon and Krypton

In order to minimize the growth of xenon from iodine precursors the rare gases were separated from the target and other fission products as quickly as possible after the bombardment, while still permitting a complete

FIGURE 11.

The Experimental Study of Fission Product Xenon,

Divided into Three Parts.

PART 1. QUICK SEPARATION OF Xe+Kr FROM TARGET

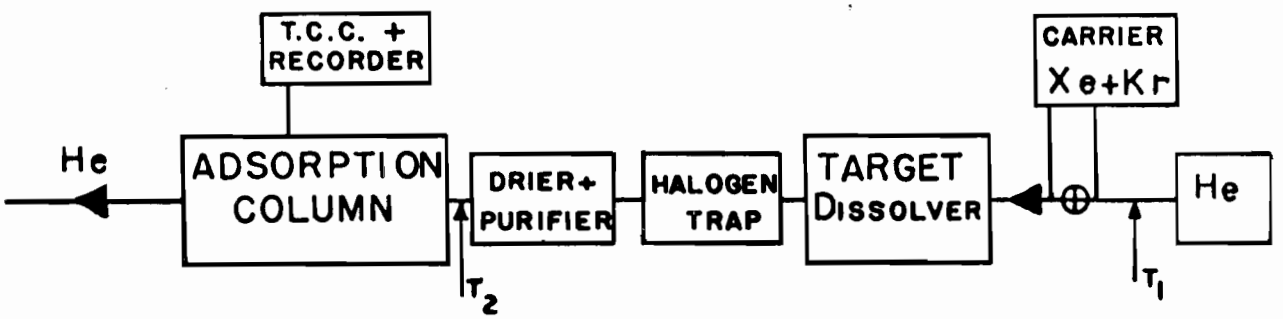

PART 2. SEPARATION OF Xe BY FRACTIONAL DESORPTION

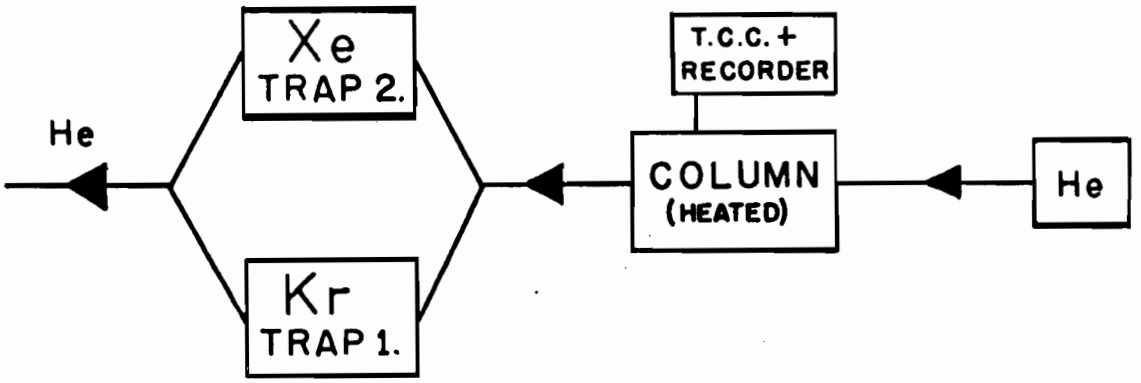

PART 3. PREPARATION OF Xe SAMPLE (OF MEASURED YIELD) FOR GAMMA- (OR BETA-) COUNTING

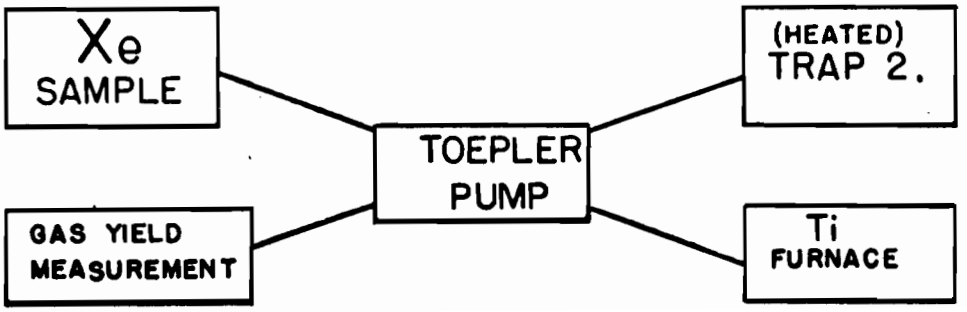

extraction from the target and catcher foils. Fig. 11, part 1, is a simplification of Fig. 12 which schematically describes part 1 of the experiment in detail. Most of the apparatus was constructed from simple pyrex glass components common to any vacuum apparatus and will not be described in detail here.

Helium (MATH) from a cylinder was passed at a controlled rate through the following components (from right to left in the figures).

(i) Flow-rate meter. A commercial (MANO) flowmeter consisting of a glass tube with a spherical stainless steel float measured flow rates up to about 100 c.c. per min.

(ii) Carrier gas injection system. The flow of helium could be diverted through a standard volume (12.2 $\pm$ 0.1 c.c.) which could be connected to a manometer and a reservoir containing a carrier gas mixture of spec-pure (MATH) xenon and krypton (73:27). The standard volume was calibrated with mercury.

In order to inject carrier gas into the helium stream, the standard volume was evacuated and filled with carrier gas at a pressure of a few centimeters of mercury measured with a mercury manometer. The manometer and reservoir were sealed off and then the helium was allowed

FIGURE 12

PART 1. Extraction of Xenon and Krypton from the Target

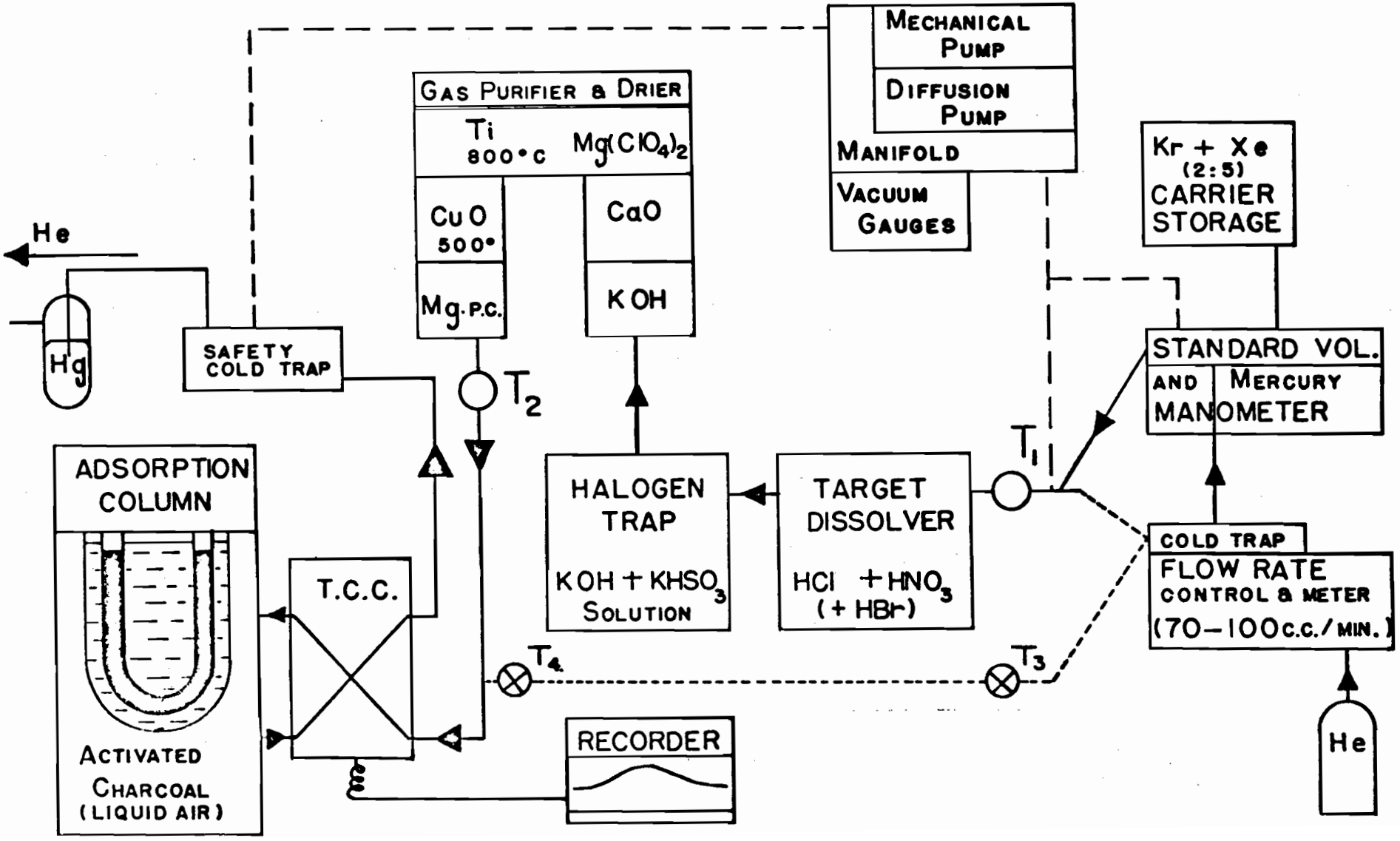

to sweep the known amount of carrier gas through the dissolver. The carrier gas facilitated the handling of the unmeasurably small volume of radioactive xenon and krypton formed in the irradiation.

The present technique could be used (DOS 62) with no carrier gas, but then recovery yields cannot be measured and the separation of xenon from krypton cannot be easily controlled.

(iii) Dissolver and halogen trap. The helium flowed through tap T_1 into this unit consisting of two simple bubblers, each attached to a small (100 ml) flask with a ground glass joint at the neck, and to a funnel for introducing liquids.

Before an irradiation the vacuum in this unit was tested and then a few pellets of KOH with about half its weight of $KHSO_3$ were put into the flask of the halogen trap. After the irradiation the cut foils of the target and aluminium catcher were quickly put into the dissolver flask, and the unit evacuated before helium was passed through the system. Water was then introduced into the halogen trap and the funnel closed. A cold acid mixture (about 20 ml of a (1:2) mixture of conc. HNO_3 and conc. HCl, with about 1 c.c. of 6M HBr) was then quickly added to the dissolver and the

funnel closed. During the addition of the acid the loss of rare gas must have been very small because the initial attack of the foils was slow. Storms (STO 62) suggested that in his work this loss was an important source of error. However, this was not the case in the present work, because of the fast introduction of cold acid, and because the aluminium wrapping initially inhibited the release of xenon. As soon as the acid had been introduced and the funnel closed the dissolution was accelerated by heating the dissolver with an air-blower. At the same time the carrier gas was injected into the helium stream. With a helium flow rate of about 80 c.c./minute, all the metal dissolved in less than five minutes. Halogens that were swept out of the dissolver were held in the alkaline reducing solution in the halogen trap, or in the next unit.

The dissolver flask was surrounded by lead sheeting to reduce the radiation hazard during the early stages of the separation.

(iv) Drier and purifier. Acid fumes and halogens remaining in the helium stream were retained in this unit by solid KOH and CaO, and water vapour was removed by anhydrous magnesium perchlorate. Other non-inert gases were removed from the stream by passing the gases through

a quartz tube containing oil-free titanium sponge at 800°C and copper oxide powder at 500°C. The dried and purified inert gases left this unit through tap T_2.

(v) Adsorption column and thermal conductivity cell. The xenon and krypton were now loaded on to the adsorption column cooled in liquid air. The column was a U-tube of pyrex glass tubing (diameter 0.5 cm and length 12 cm) containing activated charcoal (Columbia, grade L, 40-60 mesh) held in position between two sintered glass discs. A stainless steel thermal conductivity cell, T.C.C., (GOW) in a simple bridge circuit, indicated on a recorder (TEX) the loading of the xenon and krypton on to the column. A cold trap similar to that used for the adsorption column was used to purify the helium at the beginning of the flow system, and another was used as a safety trap at the end of the system. The time, t_1, from the end of bombardment to the end of this sweep (a) was usually less than half an hour (Table 6). At the end of sweep (a) the taps T_1 and T_2 were closed and the helium stream diverted through taps T_3 and T_4 during part 2 of the experiment.

Part 2. Separation of Xenon from Krypton

There was no further need for fast procedures in parts 2 and 3 which took about one hour each.

Fig. 11, part 2, is a simplification of Fig. 13 which schematically describes part 2 of the experiment in detail. This figure also includes a table giving the temperatures and helium flow rates used for the fractional desorption of first the krypton and then the xenon from the column. The separate fractions were collected on activated charcoal in cold traps 1 and 2, and the unloading was indicated on the recorder. A water bath was used to heat the column to 40°C and a small electric furnace was used to heat it to 120°C. The desorption of krypton was continued for 10-15 minutes and the xenon desorption was continued for a further 45 minutes. Then, trap 2 was maintained at liquid air temperature and evacuated for ten minutes to remove helium. This evacuation was shown to cause no measurable loss of xenon.

A mechanical forepump (WELC) and a mercury diffusion pump were used in the vacuum apparatus. A tilting McLeod gauge was used to check the vacuum which could be held at less than one micron in most parts of the apparatus. The stainless steel thermal conductivity cell was not designed for high vacuum work and this part of the system could be reduced to only about five microns, but was quite suitable for working with helium at a pressure just above

FIGURE 13

PART 2. Separation of Xenon from Krypton

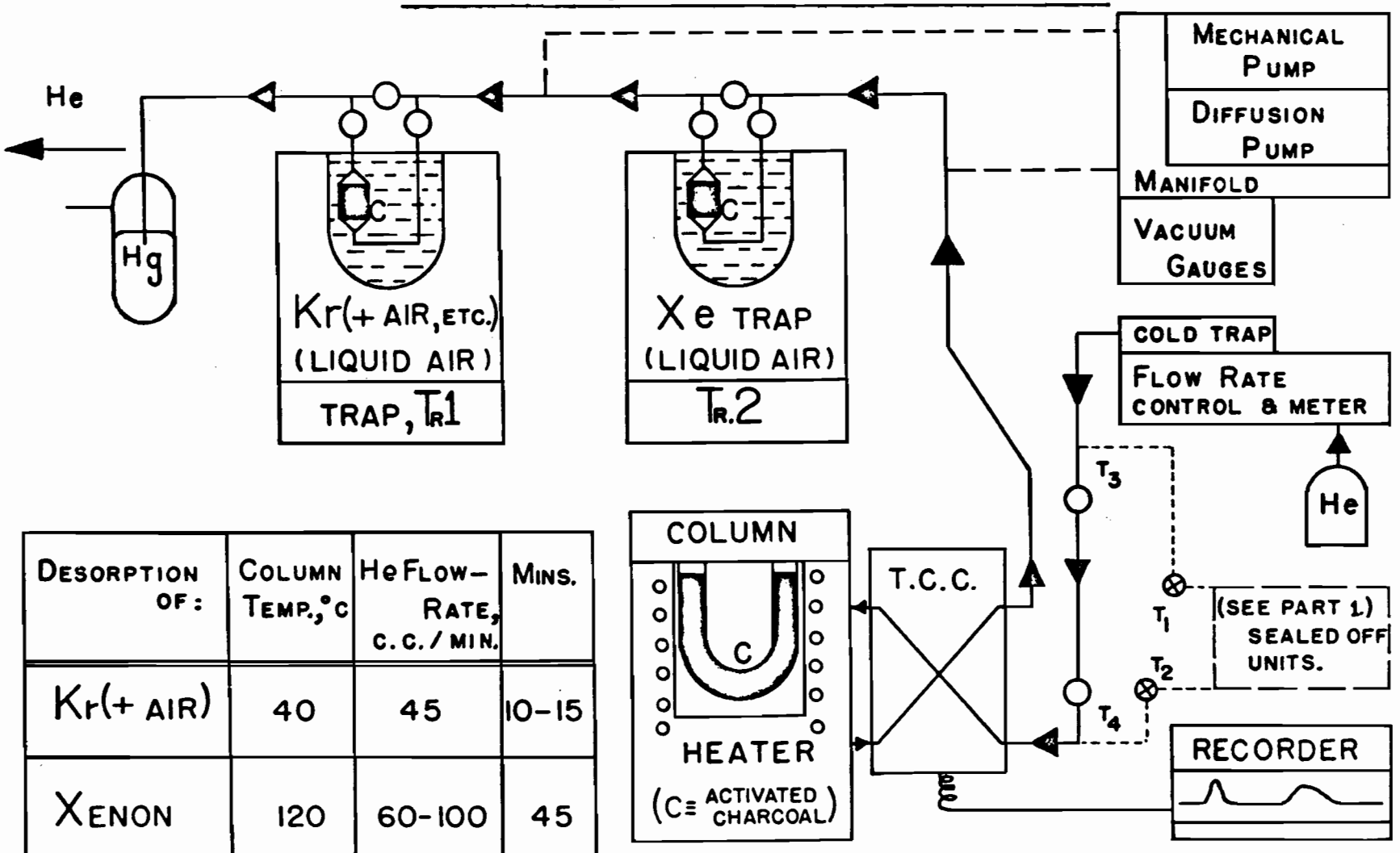

DESORPTION OF:	COLUMN TEMP., °C	He FLOW-RATE, C.C./MIN.	MINS.
Kr(+ AIR)	40	45	10-15
XENON	120	60-100	45

one atmosphere. This slight excess of pressure (2-3 cm of mercury) in the helium carrier gas was maintained by a manostat at the beginning of the flow system. A safety valve at the end of the flow system contained a minimum of mercury. Pressure-stopcocks (SCIE) were used in the flow system, because of the excess pressure.

Part 3. Preparation of Xenon Sample

Fig. 11, part 3, gives a simple description of this part of the experiment. Trap 2 was heated to 120-150°C and the desorbed xenon was pumped with an automatic Toepler mercury-pump (DELM) to a quartz furnace for purification over oil-free titanium sponge at 800-900°C. The pumping was continued for 45 minutes and the gas kept in the hot furnace for about 15 minutes. After the xenon had cooled it was transferred with a Toepler pump to a gas burette for measurement of its fractional recovery, or chemical yield, which was usually about 95%. To prepare a xenon sample for gamma spectrometry the xenon was condensed into a pyrex glass vial cooled in liquid air. These vials were of standard dimensions (cf. Fig. B1(b), in Appendix B). The cooled vial was sealed and removed with a blow torch. The pressure of the residual gas was always found to be very small.

Appendix B describes the preparation of xenon samples for beta activity measurements in a gas-phase proportional counter.

2.2.2.2 Gas-sweep (b)

After about thirty hours a similar experiment was made in which a second sweep (b) was taken to prepare a sample of xenon formed purely from decay of iodine precursors. Part 1 was repeated with the exception of the dissolving procedure. Taps T_1 and T_2 were reopened and for about 45 minutes helium was bubbled at 80 c.c./minute through the dissolver and halogen traps, both warmed with the air blower. The time, t_2, was taken from the end of sweep (a) to the end of sweep (b). Parts 2 and 3 were then repeated as in sweep (a).

2.2.2.3 Miscellaneous Experimental Details

Some further particulars of the experiment are now described. When the apparatus was not in use the four traps containing activated charcoal were kept under vacuum and at a temperature of about 120°C in order to avoid any adsorption of gas on the charcoal. Before a gas-sweep the apparatus was preconditioned as follows. The vacuum in the apparatus was tested and helium passed through the flow system for about

one hour with the initial and final traps cooled in liquid air, and with the electric furnaces in the purifier unit turned on. After a complete experiment, at the end of a sweep (b), the dissolver, halogen trap, purifier and drier units were dismantled, and thoroughly cleaned and de-contaminated with conc. HNO_3. The chemicals in the drier and purifier were replaced, the taps and joints were regreased, and the units were then refitted into the main apparatus.

The gas techniques were tested previously by Dostrovsky and Stoenner (DOS 62). In the present work the high efficiency of the xenon separation was confirmed by two methods.

(i) Two xenon fractions were found by mass spectrometric analysis to contain only 1-2% of krypton.

(ii) No xenon activity was detected in a krypton fraction from sweep (a). This sample was prepared in a sealed vial and gamma-counted only a few hours after bombardment. The 249-kev gamma ray of ^{135g}Xe was not detected though this had a very intense activity in the xenon fractions from sweep (a).

2.3 RADIATION MEASUREMENT

The activity of the xenon and copper samples was measured by scintillation spectrometry. The phosphor was a crystal (3" x 3") (HARS) of sodium iodide activated with thallium iodide (0.1%), hermetically sealed in an aluminium can. This crystal had a resolution of about 12% for gamma rays with an energy of 0.5 MeV. Optically coupled to the crystal was a photomultiplier tube whose output was passed through a pre-amplifier (HAMN) to a multichannel analyser (RIDL). The stored data were printed in digital form (HEWL), and also obtained graphically on an X-Y plotter (MOSE). The latter had its Y-axis related to the count rate and its X-axis related to the channel number, or energy of the incident gamma ray. Lead, lined with iron and lucite, shielded the crystal and photomultiplier in order to reduce the natural background. Although the dead-time of the analyser was relatively high no correction was necessary for this because the samples were always measured on "live-time".

The above method of measuring gamma radiation is in common use and therefore its principles are only briefly described here, with reference to the type of gamma spectra obtained in this study. By the Photoelectric Effect a photon of gamma radiation may be completely absorbed by an atomic

electron in the NaI(Tl). This electron causes ionization in the phosphor, with accompanying flashes of light which have an intensity proportional to the energy of the initial electron. If this were the only effect occurring a gamma spectra would contain a simple photopeak with some statistical broadening caused in the photomultiplier tube, where the light flashes are converted proportionally into electrical pulses. However, other well-known phenomena, Compton Scattering and "Back-scattering", produce in the spectra an irregular tail at energies below the photopeak energy. Pair Production need not be considered here since the spectra in this work contained no gamma rays with energy greater than 1.02 MeV. These complex phenomena often cause considerable difficulty in the analysis of gamma spectra. Fortunately in the present work the photopeaks, characteristic of xenon and copper, were fairly simple and the background could rather easily be drawn intuitively (cf. Section 3.1).

Appendix B describes the equipment and method used to measure rare gas activities by beta proportional counting. In this research, measurement of beta activities was useful only to calibrate the gamma spectrometric method, described above, used to measure the activity of xenon produced in

fission. Appendix B explains why the gamma and not the beta activity of this xenon was measured and considers probable errors in some previous fission studies of xenon where the beta activity was measured.

3. TREATMENT OF DATA FROM THE ACTIVITY MEASUREMENTS

3.1 ANALYSIS OF SPECTRA AND DECAY CURVES

The spectra observed for the copper samples and for the xenon samples from sweeps (a) and (b) are now described with the methods used to analyse them. The photopeaks were identified with an energy-calibration curve which was obtained from photopeaks of known energies in the spectra of several long-lived standard sources. The decay curves obtained from these spectra are described.

3.1.1 COPPER

Fig. 14 shows an example of the simple gamma ray spectrum of ^{64}Cu with the dotted curved line intuitively drawn as the background. The area of the 511-kev photopeak, above the dotted line, was divided by the time of measurement to give a counting rate. This rate was divided by two to account for the two 511-kev gamma rays resulting from each positron annihilation. A semi-logarithmic plot of this rate against time gave a decay curve with a half-life of 12.8 $\pm$ 0.1 hours. The count rate at the end of bombardment, $C^{o}_{(^{64}Cu)}$, was obtained by back-extrapolation of this curve. At medium energies the reaction ^{63}Cu (p,p2n) produced ^{61}Cu (3.3 hours)

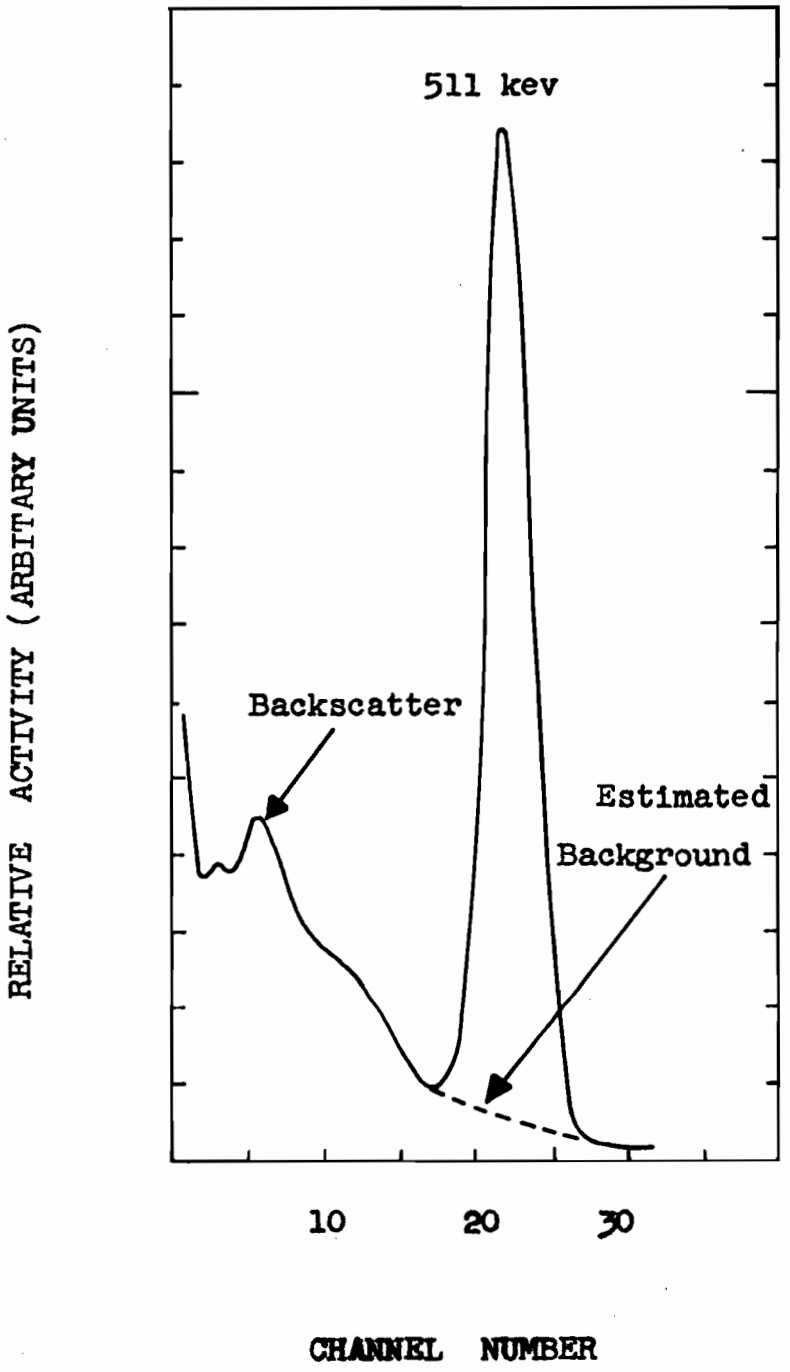

FIG. 14 Typical Spectra for a Copper Sample, the 511-kev Peak is due to ^{64}Cu.

which also gives a 511-kev annihilation-gamma ray. This activity was therefore allowed to decay for about 30 hours before the activity of ^{64}Cu was measured.

3.1.2 XENON

Sample from Sweep (a)

Table 5 gives the xenon isotopes that contributed to the gamma spectra in the present study. Fig. 17 shows simplified decay schemes for ^{133}Xe and ^{135g}Xe, which were the two most important isotopes of xenon in this study. Fig. 15 describes typical spectra for a xenon gas sample from sweep (a). Counting rates and decay curves were obtained from these spectra. The intensity of the gamma rays of ^{135}Xe was so much higher than that of the highly converted gamma rays of ^{133m}Xe that the sample from sweep (a) was placed on a high shelf, (shelf 7) above the NaI(Tl) crystal, during the first day in which measurements were taken every two hours, but was placed on the lowest shelf (shelf 0) for the remaining measurements. These were taken twice a day for seven days and then daily for a further four weeks. Fig. 16 shows a typical decay curve for the first several days taken from spectra of the type shown in Fig. 15(i) and (ii). In this decay curve the ordinate, C', is the count rate divided by the efficiency of the shelf used. The components with half-lives of 9.2 hours

TABLE 5

XENON SPECIES CONTRIBUTING TO THE GAMMA SPECTRA IN THE PRESENT STUDY (NDS)

Xenon species	Half-life	Gamma ray energy (MeV)	α_K	$\frac{\alpha_K}{\alpha_{LM}}$	An approx. estimate of chain yield (%)* for 30-MeV protons	
					+ ^{233}U	+ ^{238}U
^{133m}Xe	2.3d	.233	4.4 ± 1.4**	2.2	45	15
^{133g}Xe	5.3d	.080	1.5 ± 0.2	5		
^{135g}Xe	9.2h	.250	.054	6.5	50	45
		(.610)	-	-		
^{131m}Xe	12.0d	.164	29	2	(20)	(3)
^{129m}Xe	8.0d	.196	10	2	(5)	(0.1)
^{127g}Xe	36.0d	.173	.13	-	(0.6)	-
		.205	.09	-		
		(.378)	.01	-		

* the sum of the yields of both isomers are given

** experimental value which may be too low (cf. Section 4)

FIG. 15 Typical gamma ray spectra for a xenon sample from sweep (a). Dashed lines indicate estimated background.

(i) 10 hours after bombardment, the 249-kev peak is due to ^{135g}Xe, with a small contribution from ^{133m}Xe.

(ii) 6 days after bombardment, the 233-kev peak is due to ^{133m}Xe.

(iii) 20 days after bombardment, the 80-kev peak is due to ^{133g}Xe.

There is a 30-kev x-ray peak in all these spectra. These three spectra were taken from experiment R11 (^{238}U + 75-MeV protons).

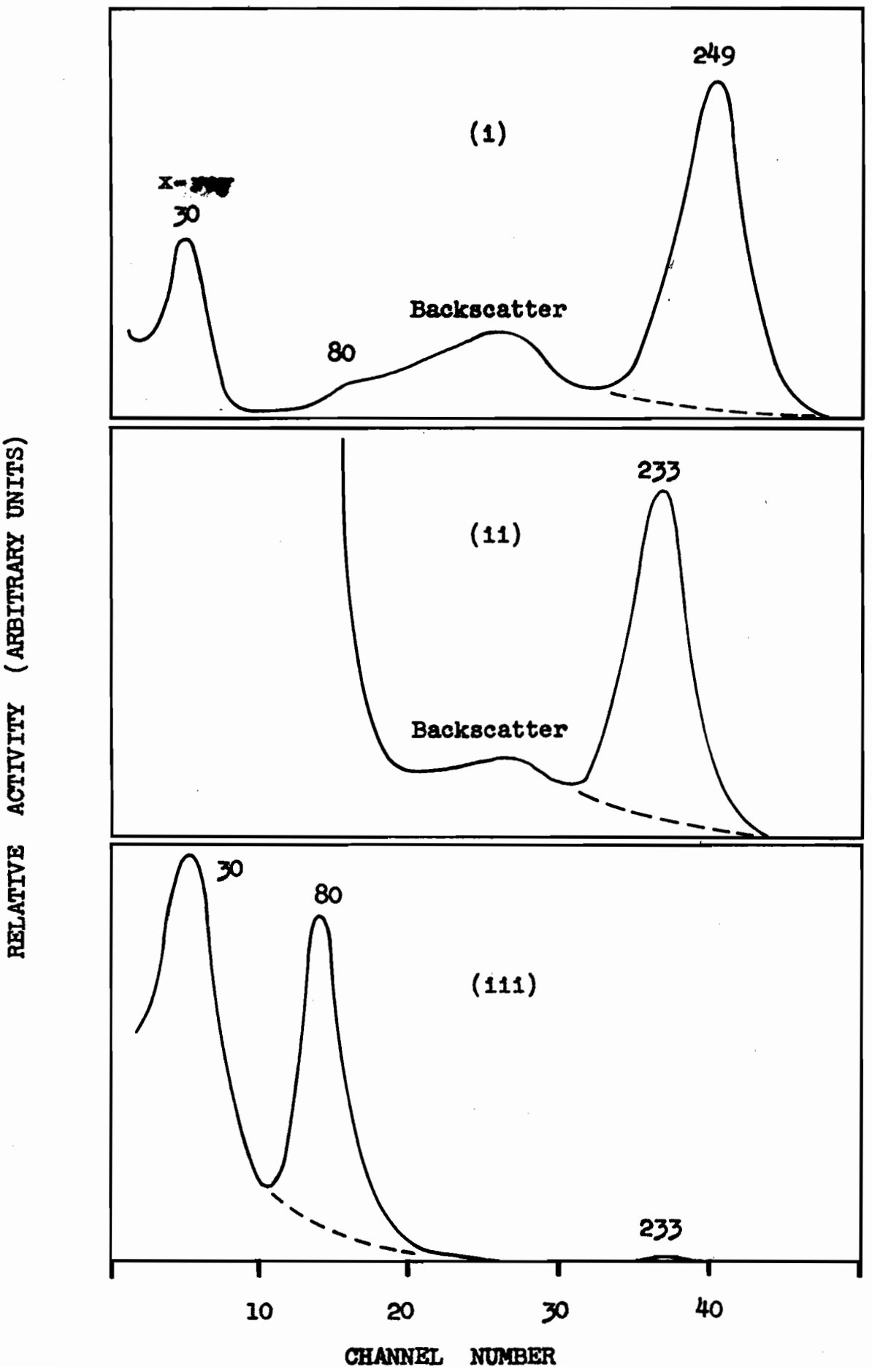
249
(1)
X-[redacted]
30
Backscatter
80
233
(11)
Backscatter
30
80
(111)
233
10
20
30
40
CHANNEL NUMBER
RELATIVE ACTIVITY (ARBITRARY UNITS)

FIGURE 16.

A typical two-component decay curve, for a xenon sample from sweep (a). It was obtained from the composite photopeak due to the 233- and 249-kev gamma rays, shown in Figs. 15(i) and (ii).

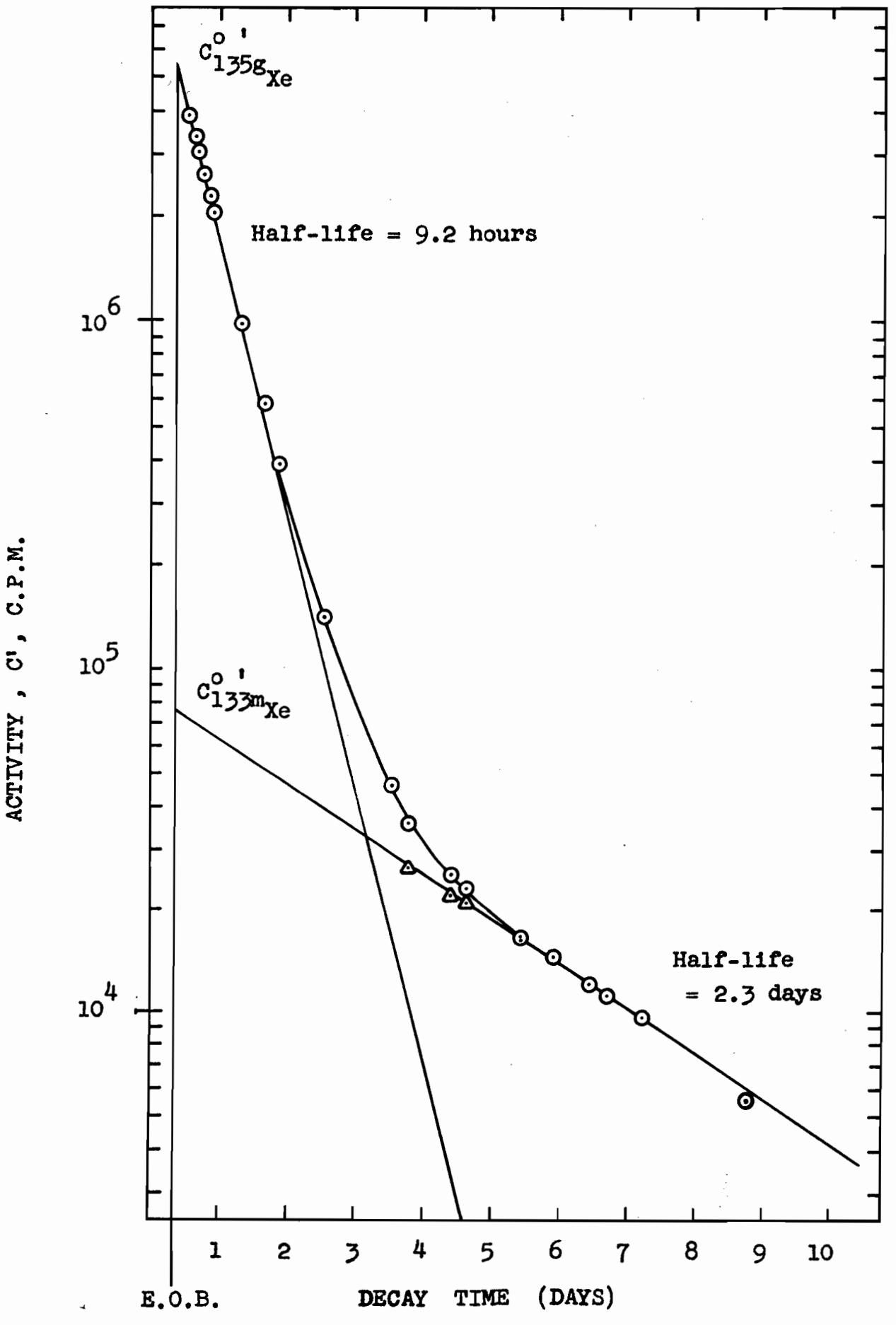
$C^{o\,'}_{135g_{Xe}}$
Half-life = 9.2 hours
10^6
10^5
$C^{o\,'}_{133m_{Xe}}$
10^4
Half-life
= 2.3 days
ACTIVITY , C' , C.P.M.
1
2
3
4
5
6
7
8
9
10
E.O.B.
DECAY TIME (DAYS)

and 2.3 days were resolved by hand. The resolution becomes increasingly difficult at low energies where the activity of the 2.3 day-component is very weak because of the rapid decrease of the fission yield of ^{133}Xe below about 35 MeV. It was therefore necessary to use counting periods of a few hours and to subtract large natural backgrounds from the spectra. The activity of ^{133m}Xe could have been increased by longer bombardments for low energies, but this would also increase the growth error in ^{133g}Xe.

Table 7 gives the counting rate at the end of bombardment, C^o, for ^{133m}Xe and Table 6 gives the C^a, at the end of sweep (a), for ^{135}Xe.

When most of the ^{133m}Xe (2.3 days) had decayed to the ground state after 12-15 days, spectra of the type shown in Fig. 15(iii) gave a simple decay curve with a half-life of 5.3 days. Table 7 gives the counting rates C^o for ^{133g}Xe.

The yield of more neutron-deficient xenon isotopes increases as the ratio (N/Z) of the target decreases and as the energy of the protons increases. Table 5 contains a rough estimate of the relative yields of these isotopes for 30-MeV protons with ^{233}U and ^{238}U. This estimate was made with the results for charge distribution at 30 MeV described later and with the assumption that Z_p changes linearly with

A, in the mass region 127-135. The gamma rays of ^{131m}Xe and ^{129m}Xe are highly converted and ^{127}Xe is formed in relatively low yield. These activities interfere significantly only above about 70 MeV for ^{235}U, and above about 30 MeV for ^{233}U. Where necessary, a correction was made for this interfering activity by an approximate graphical extrapolation of the long-lived tail in the decay curve. This method was considered satisfactory, even for the worst case of ^{233}U with 70-MeV protons, in which the correction to the peak of the gamma ray of ^{133m}Xe was as much as 25%. No such interference occurred in the samples of decay-product xenon from the second gas-sweep (b).

Sample from Sweep (b)

As expected from the isobaric charge distribution and the decay chains in Fig. 17 a considerable amount of ^{135}Xe and ^{133g}Xe, formed from decay of their iodine parents, was found in the xenon sample from sweep (b), but a negligible amount of ^{133m}Xe was detected. The lack of ^{133m}Xe confirmed that the extraction of xenon was essentially complete in sweep (a). The spectra were similar to those in Fig. 15(i) for the first few days and the 249-kev photopeak gave a one-component decay curve with a half-life of 9.2 hours. The 80-kev peak gave a decay curve with a half-life of 5.3 days

FIGURE 17.

Simplified Decay Schemes of ^{133}Xe and ^{135g}Xe,

and

Decay Chains for A = 133 and A = 135 (NDS).

A = 133

DECAY CHAIN

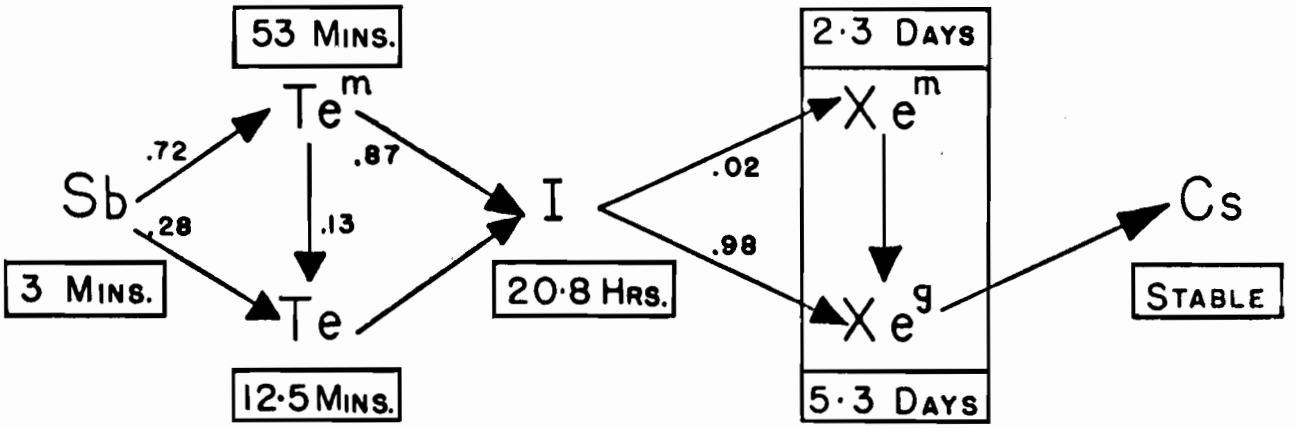

DECAY SCHEME

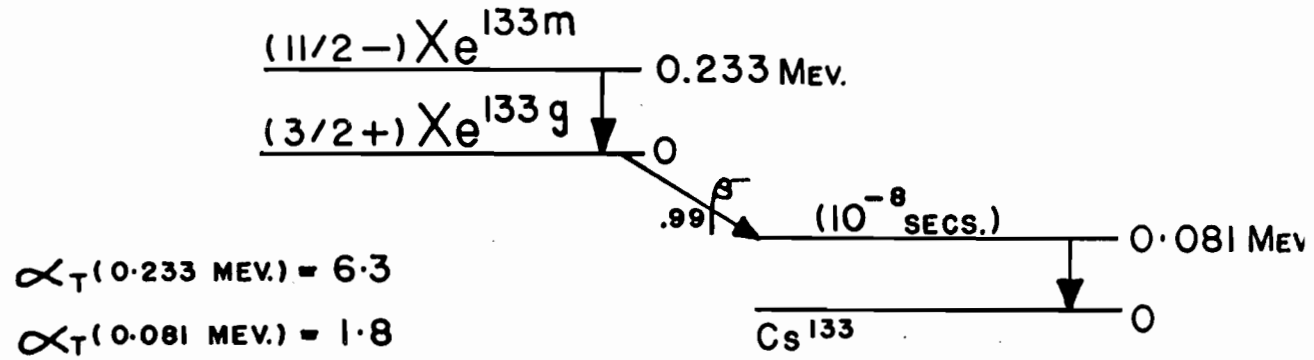

A = 135

DECAY SCHEME

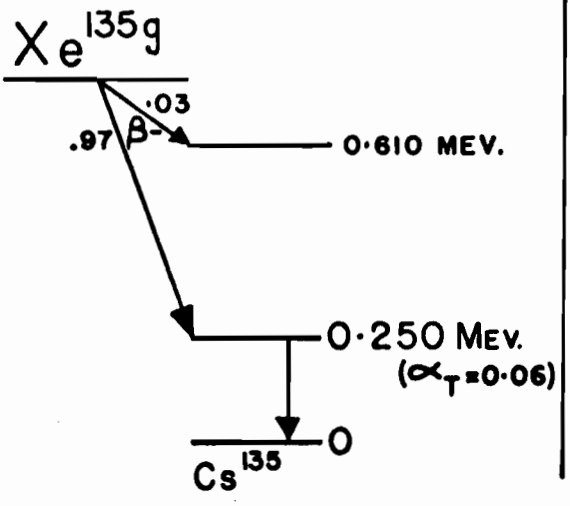

DECAY CHAIN

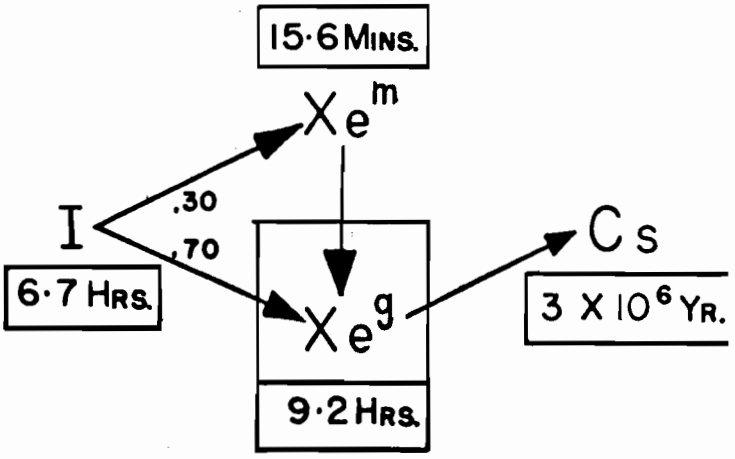

without any perturbation due to growth from ^{133m}Xe. Tables 6 and 7 give the count rates, C^b, obtained at the end of sweep (b) from these simple decay curves.

3.2 CALCULATION OF RELATIVE AND ABSOLUTE CROSS SECTIONS

Appendix A describes the procedures and equations to calculate cross sections from the counting rates obtained from the above spectra. All the cross sections reported were computed with a simple FORTRAN program based on the equations in Appendix A. The input parameters for this program are contained in various tables. The symbols representing the input parameters are redefined here.

C^o, C^a, C^b = gamma activities at the end of bombardment, sweep (a) and sweep (b), respectively.

Y^a, Y^b = recovered fraction of xenon carrier gas in sample from sweeps (a) and (b).

Y_{Cu} = fraction of copper monitor foil in the 2-ml sample.

t_o = time of bombardment.

t_1 = time from end of bombardment to the end of sweep (a).

t_2 = time between the ends of sweeps (a) and (b).

Table 6 gives the parameters for the computation of the independent cross section of ^{135}Xe, and of the cumulative cross section of ^{135}I. It gives C^a and C^b together with values for t_o, t_1, t_2, Y^a and Y^b for the 28 irradiations performed. Table 7 gives the parameters for the computation of the independent cross sections of ^{133m}Xe and ^{133g}Xe, and of the cumulative yield of ^{133}I. It gives C^o for ^{133m}Xe, and C^a and C^b for ^{133g}Xe. Table 8 gives the values used for the monitor cross section; Y_{Cu}, and $(C^o)/(eff)$ for ^{64}Cu. Tables A1 and A2 and Fig. 17 contain other necessary constants for the input data.

3.3 ERRORS

The determination of the formation cross sections of ^{135}Xe, ^{135}I, ^{133m}Xe, ^{133g}Xe ^{133}I involved many errors either originating in this research or existing in published material used in the calculations. These errors are discussed, as far as possible in the order in which they were introduced during an experiment and its interpretation. A serious source of error could result from poor alignment of the leading edges of the foils of copper and the heavy metal. Although precautions were taken an uncertainty as high as 10-15% could be introduced in unfavourable experiments. The error in the

measurement of surface density, (SD), of the foils was of the order of ± 1%. For the monitor cross sections (MEG 62) it was difficult to estimate the error beyond that given in Meghir's measurements, ± 10%. The uncertainty in the mean energy of the proton beam probably introduced little error, but the energy spread of the beam, ± 2 MeV, would lead to errors where the slopes of the excitation functions were not similar for the monitor reaction and the reaction investigated.

The extraction of xenon from the target and catcher foils was assumed to be quantitative and the loss of decay product xenon in sweep (b) was assumed to be very small.

The error in the chemical yield of copper was only ± 3%. The xenon yields were estimated to have an error of ± 7% due to errors in the composition, volumes and pressures of the carrier gas. In some early experiments with ^{238}U (R8-R10) the xenon sample was not well purified and the yield errors here were probably as high as ± 12%.

The error in the photopeak area, due to uncertainty in drawing the background, should not be large for the well-defined photopeaks due to ^{64}Cu and the xenon isotopes. For the xenon peaks this error was largely eliminated during the determination of their efficiency (Appendix B). For ^{64}Cu

and ^{135}Xe this error was estimated to be $\pm$ 3%, and for ^{133g}Xe and ^{133m}Xe to be $\pm$ 6%. The photopeak efficiency, (eff), for ^{64}Cu had an error of $\pm$ 10% (GRA 61). For the xenon isotopes the same error, $\pm$ 10%, was given to the efficiencies determined here.

The decay curve analysis introduced errors of $\pm$ 3% for ^{64}Cu and ^{135}Xe, of $\pm$ 5% for ^{133g}Xe, and as high as 12% for ^{133m}Xe when this activity was very low.

The above random errors were combined by taking the square root of the sum of their squares. This total random error in the absolute cross sections was estimated to be from 20-30%.

In this thesis, Z_P values and isomer ratios were obtained from relative cross sections in which many of the above errors were eliminated. These yield ratios were estimated to have a total random error of 10-20%.

A few other sources of error summarized briefly below are discussed further in appropriate sections of the thesis.

The growth correction for ^{133g}Xe and ^{135}Xe caused various errors depending on the fission system studied (Section 4A.1).

In a few experiments there was an additional error

in the analysis of the photopeak due to ^{133m}Xe, caused by interference from activities due to more neutron-deficient isotopes of xenon (Section 3.1.2).

The most important systematic error in this research was due to the large uncertainty in the value of α_T for the internal transition between the isomers of ^{133}Xe. This affects the reported cross sections (Section 4A.1) and has a large effect on the isomer ratios (Section 4B.1).

TABLE 6. Summary of Irradiations and Data for Activities of ^{135}Xe

Exp. No.	E_p (MeV)	t_o hr.	t_1 hr.	t_2 hr.	Xenon Yields Y^a	Xenon Yields Y^b	Counting Rates at End of Sweep (a) ($C^a \times 10^{-3}$) c.p.m.	Counting Rates at End of Sweep (b) ($C^b \times 10^{-3}$) c.p.m.
^{232}Th								
T6	30	.20	.50	26.87	0.97	0.97	4400	1225
T3	40	.20	.50	26.27	0.90	0.97	3840	770
T4	52	.18	.45	30.50	0.97	0.90	3560	377
T1	65	.17	.50	29.83	0.73	0.97	1820	341
T5	75	.17	.50	26.70	0.82	0.97	1690	370
T2	85	.20	.50	31.50	0.96	0.93	2310	282
^{238}U								
R10	15	.42	.62	30.00	0.93	0.72	400.0	207.0
R15	17	.42	.55	28.55	0.84	0.70	1763	776.1
R14	20	.33	.50	28.97	0.97	0.86	1333	382.1
R18	30	.17	.37	29.68	0.97	0.97	3300	700.0
R8	42	.17	.73	26.25	0.73	0.97	1462	248.8
R17	57	.12	.50	30.50	0.62	0.97	598.0	86.0
R9	65	.17	.55	28.92	0.97	0.84	1806	234.8
R11	75	.17	.62	28.30	0.92	0.94	1103	209.0
*R16	75	.25	.40	35.25	0.97	0.97	3225	441.8
R12	85	.20	.63	30.30	0.95	0.97	1129	197.0
^{235}U								
E10	20	.17	.33	51.93	0.98	0.98	5450	151
E9	25	.17	.33	25.85	0.97	0.98	6810	824
E7	35	.17	.50	27.95	0.95	0.95	3000	325
E5	45	.13	.50	28.85	0.97	0.70	2705	225
E3	55	.08	.60	27.03	0.88	0.97	1343	250
E8	70	.13	.50	26.13	0.95	0.97	2280	417
E4	85	.13	.57	55.00	0.95	0.93	2340	60.0
^{233}U								
*U5	20	.17	.34	55.03	0.97	0.84	2070	16.9
*U4	30	.17	.37	49.43	0.97	0.97	3010	62.2
*U3	42	.15	.42	51.88	0.97	0.97	545.0	10.7
*U1	55	.22	.55	-	0.97	-	1600	-
*U2	70	.18	.50	50.78	0.97	0.97	990.0	20.7

* The target material was powdered uranium oxide

TABLE 7. Data for Activities of ^{133m}Xe and ^{133g}Xe

(Table 6 gives t_o, t_1, t_2, Y^a, Y^b)

Exp. No.	E_p (MeV)	^{133m}Xe $(C^a x 10^{-2})$ c.p.m.	^{133g}Xe $(C^a x 10^{-2})$ c.p.m.	^{133g}Xe $(C^b x 10^{-2})$ c.p.m.
^{232}Th				
T6	30	148	575	1520
T3	40	247	962	1290
T4	52	382	1440	940
T1	65	252	940	760
T5	75	258	940	622
T2	85	360	1300	640
^{238}U				
R10	15	6.60	29.46	269.1
R15	17	35.0	146.2	935.0
R14	20	31.0	141.5	547.5
R18	30	152	575.0	1310
R8	42	110	438.5	464.0
R17	57	75.7	273.0	182.0
R9	65	230	881.6	440.8
R11	75	153	545.2	366.6
*R16	75	444	1578	1260
R12	85	158	598.6	399.0
^{235}U				
E10	20	355	1430	1980
E9	25	615	2400	1710
E7	35	425	1550	770
E5	45	439	1660	517
E3	55	240	860	460
E8	70	404	1450	710
E4	85	390	1440	780
^{233}U				
*U5	20	287	1095	450
*U4	30	530	2060	965
*U3	42	116	425	157
*U1	55	310	1165	-
*U2	70	180	685	260

* The target material was powdered uranium oxide

TABLE 8. Monitoring Data, Including Activities of ^{64}Cu

Exp. No.	E_p (MeV)	t_o Hr.	σ_M* mb.	Y_{Cu}	(C°)/(eff) c.p.m.	Approx.wt. of Cu Target mg
^{232}Th						
T6	30	.20	390	.46	33330	59
T3	40	.20	270	.57	23080	16
T4	52	.18	205	.70	19490	17
T1	65	.17	173	.90	18970	13
T5	75	.17	150	.50	8205	17
T2	85	.20	140	.94	19490	11
^{238}U						
R15	17	.42	(100)	.32	16300	9
R14	20	.33	(240)	.93	36100	19
R8	42	.17	250	.33	9100	21
R17	57	.12	190	.86	6666	3
R9	65	.17	170	.27	4700	23
R11	75	.17	150	.27	3800	28
R12	85	.20	140	.59	6800	13
^{235}U						
E10	20	.17	(240)	.70	29610	17
E9	25	.17	488	.29	18720	14
E7	35	.17	310	.59	14100	4
E5	45	.13	235	.91	12560	6
E3	55	.08	195	.89	6564	11
E8	70	.13	160	.63	9359	5
E4	85	.13	140	.95	10510	9

* The cross sections σ_M, for the formation of ^{64}Cu, were taken from the work of Meghir (MEG 63).

4. RESULTS AND DISCUSSION

In the Introduction it was indicated that this research gave information mainly about the isomeric yield ratios of ^{133}Xe, but that the same experiments enabled one to obtain fission yields and to study their variations in the mass chains 133 and 135.

It is convenient to divide the rest of this thesis into two sections,

SECTION A. FISSION YIELDS AND THEIR VARIATIONS,

SECTION B. ISOMERIC YIELD RATIOS IN FISSION.

Inevitably this division gives rise to some duplication, but provides a clearer picture of these topics.

4A. SECTION A

FISSION YIELDS AND THEIR VARIATIONS

4A.1 ABSOLUTE AND RELATIVE CROSS SECTIONS

Table 9 gives the cross sections for the 135 chain computed from the data for the fission of ^{232}Th, ^{238}U, ^{235}U and ^{233}U. For the irradiations which were not monitored the cross sections are given relative to the cumulative formation cross section of ^{135}I, $Y^{(\text{experiment number})}$. In

TABLE 9. Cross Sections for the Independent Formation of ^{135}Xe and the cumulative formation of ^{135}I

Exp. No.	E_p (MeV)	Independent σ(mb), ^{135}Xe Uncorrected	Independent σ(mb), ^{135}Xe Corrected	Cumulative σ(mb), ^{135}I	R^{135} c/i
^{232}Th					
T6	30	21.1	20.3	23.3	1.15
T3	40	24.9	24.0	17.9	0.75
T4	52.5	23.6	23.0	12.9	0.56
T1	65	17.9	17.3	11.7	0.68
T5	75	16.5	15.9	12.0	0.75
T2	85	14.2	13.7	9.1	0.66
^{238}U					
R10	15	0.32 Y^{R10}	.25 Y^{R10}	1.0 Y^{R10}	3.94
R15	17.5	6.5	(5.6)*	(14.8)*	2.64
R14	20	13.3	(12.3)*	(19.1)*	1.55
R18	30	1.03 Y^{R18}	0.99 Y^{R18}	1.0 Y^{R18}	1.01
R8	42	28.9	27.8	14.4	0.52
R17	57.5	37.0	36.2	16.4	0.45
R9	65	28.6	27.5	19.0	0.69
R11	75	20.2	19.2	16.1	0.84
R16	75	1.16 Y^{R16}	1.12 Y^{R16}	1.0 Y^{R16}	0.89
R12	85	22.8	21.6	18.6	0.86
^{235}U					
E10	20	21.5	21.1	10.7	0.51
E9	25	36.6	36.0	16.7	0.46
E7	35	28.2	27.5	12.8	0.47
E5	45	32.7	31.9	16.6	0.52
E3	55	28.0	26.8	19.0	0.71
E8	70	17.8	17.2	12.2	0.71
E4	85	21.6	20.8	12.6	0.61
^{233}U					
U5	20	4.77 Y^{U5}	4.74 Y^{U5}	1.0 Y^{U5}	0.21
U4	30	3.16 Y^{U4}	3.13 Y^{U4}	1.0 Y^{U4}	0.32
U3	42.5	2.83 Y^{U3}	2.79 Y^{U3}	1.0 Y^{U3}	0.36
U1	55	5.01 Y^{U1}	no sweep b.	(1.0 Y^{U1})	-
U2	70	2.86 Y^{U2}	2.81 Y^{U2}	1.0 Y^{U2}	0.36

* Very large uncertainty in $\sigma(^{64}Cu)$ at this energy

order to obtain independent yields for ^{135}Xe, corrections were made for the decay of ^{135}I during the times t_o and t_1, as discussed in Appendix A. This correction was always relatively small, as is shown in Table 9 which gives both the corrected and uncorrected independent cross sections of ^{135}Xe. Fig. 18 shows the cumulative cross sections of ^{135}I and the corrected independent cross sections of ^{135}Xe, plotted as excitation functions. Obviously the results for the unmonitored irradiations could not be plotted in this form.

For all four targets, Fig. 19 shows the ratio, $R^{135}_{c/i}$ of the cumulative yield of ^{135}I to the corrected independent yield of ^{135}Xe. This ratio was used to obtain empirical values of Z_p by a method developed in this research and to be discussed later. In the calculations for the 135 chain, the isomer ^{135m}Xe (15 minutes) was not considered.

Table 10 gives the cross sections computed from the data for the more complex 133 chain. As in Table 9 the cross sections for the unmonitored irradiations are given relative to the cumulative yield of ^{135}I, $Y^{(\text{experiment number})}$. The independent cross section for ^{133m}Xe required no growth correction for the very small fraction (branching ratio $\approx .02$) of the ^{133}I which decayed to ^{133m}Xe. The ^{133g}Xe yield had to

FIGURE 18.

Excitation functions for the cumulative formation of ^{135}I, and the independent formation of ^{135}Xe (corrected for growth from the decay of ^{135}I). These were obtained in the present work on the proton-induced fission of,

(a) ^{232}Th

(b) ^{238}U

(c) ^{235}U

Included in (a), the filled triangles are the cumulative cross sections of ^{135}I reported previously by Pate, Foster and Yaffe (PAT 58a).

18 (a) ^{232}Th

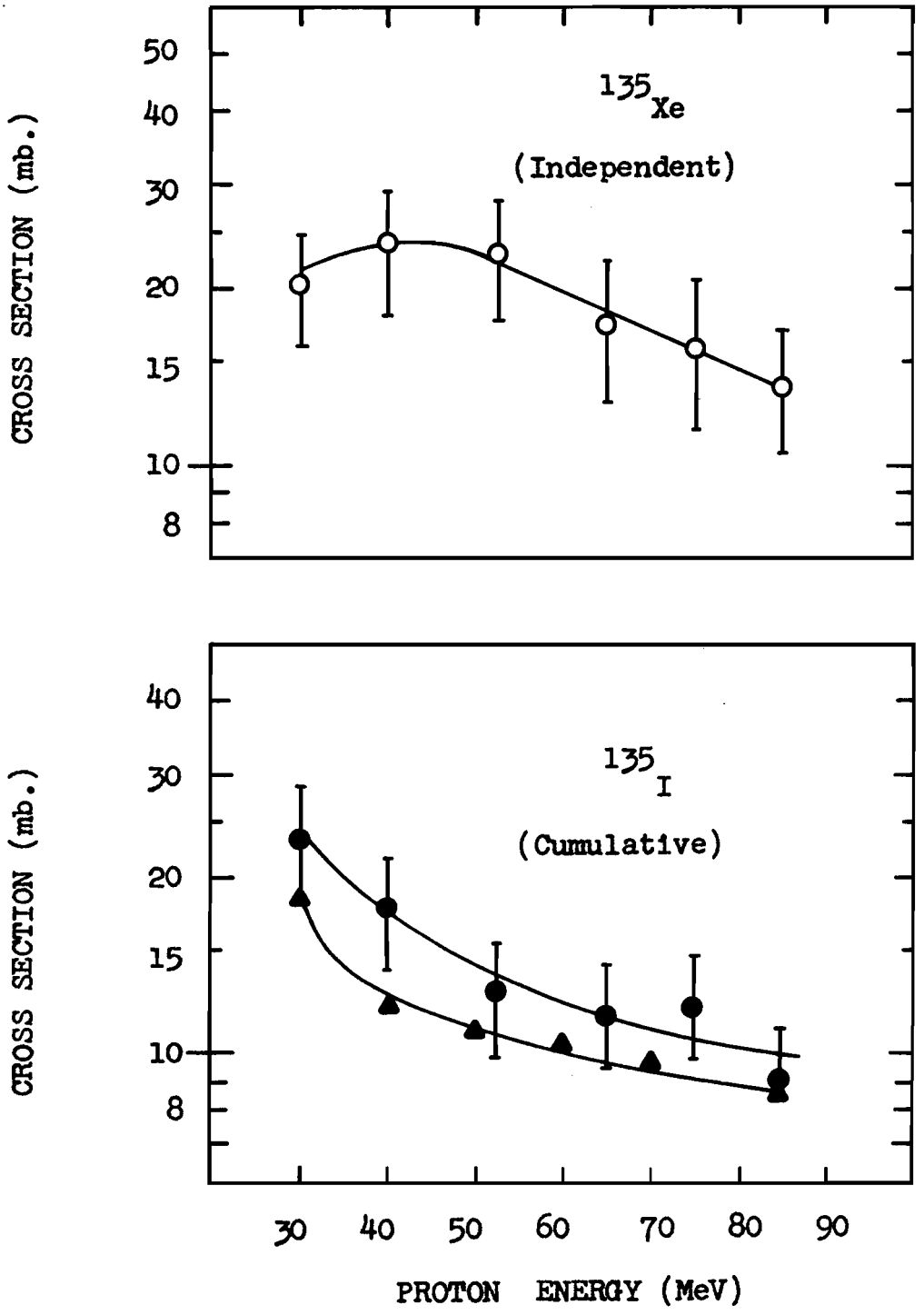
CROSS SECTION (mb.)
50
40
30
20
15
10
8
^{135}Xe
(Independent)
CROSS SECTION (mb.)
40
30
20
15
10
8
^{135}I
(Cumulative)
30
40
50
60
70
80
90
PROTON ENERGY (MeV)

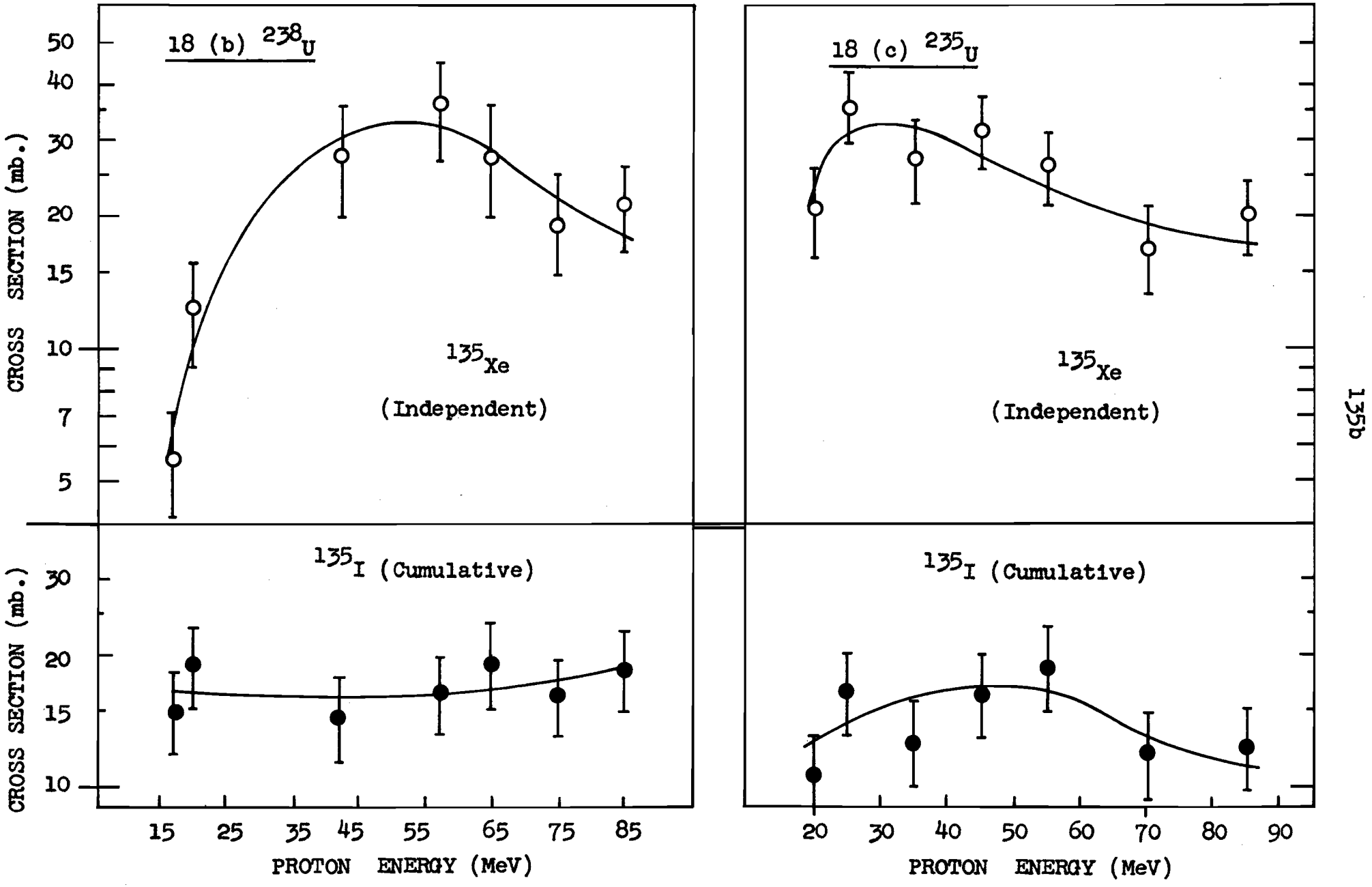
18 (b) ^{238}U
18 (c) ^{235}U
^{135}Xe
(Independent)
^{135}I (Cumulative)
CROSS SECTION (mb.)
50
40
30
20
15
10
7
5
30
20
15
10
15 25 35 45 55 65 75 85
20 30 40 50 60 70 80 90
PROTON ENERGY (MeV)

135b

FIGURE 19.

The dependence of the relative formation of ^{135}I and ^{135}Xe upon proton energy. This is expressed in the form,

$$R^{135}_{c/i} = \frac{\text{(cumulative yield of } ^{135}I)}{\text{(independent yield of } ^{135}Xe\text{, corrected)}}$$

These ratios were measured in the present work on the proton-induced fission of,

(a) ^{232}Th

(b) ^{238}U

(c) ^{235}U

(d) ^{233}U

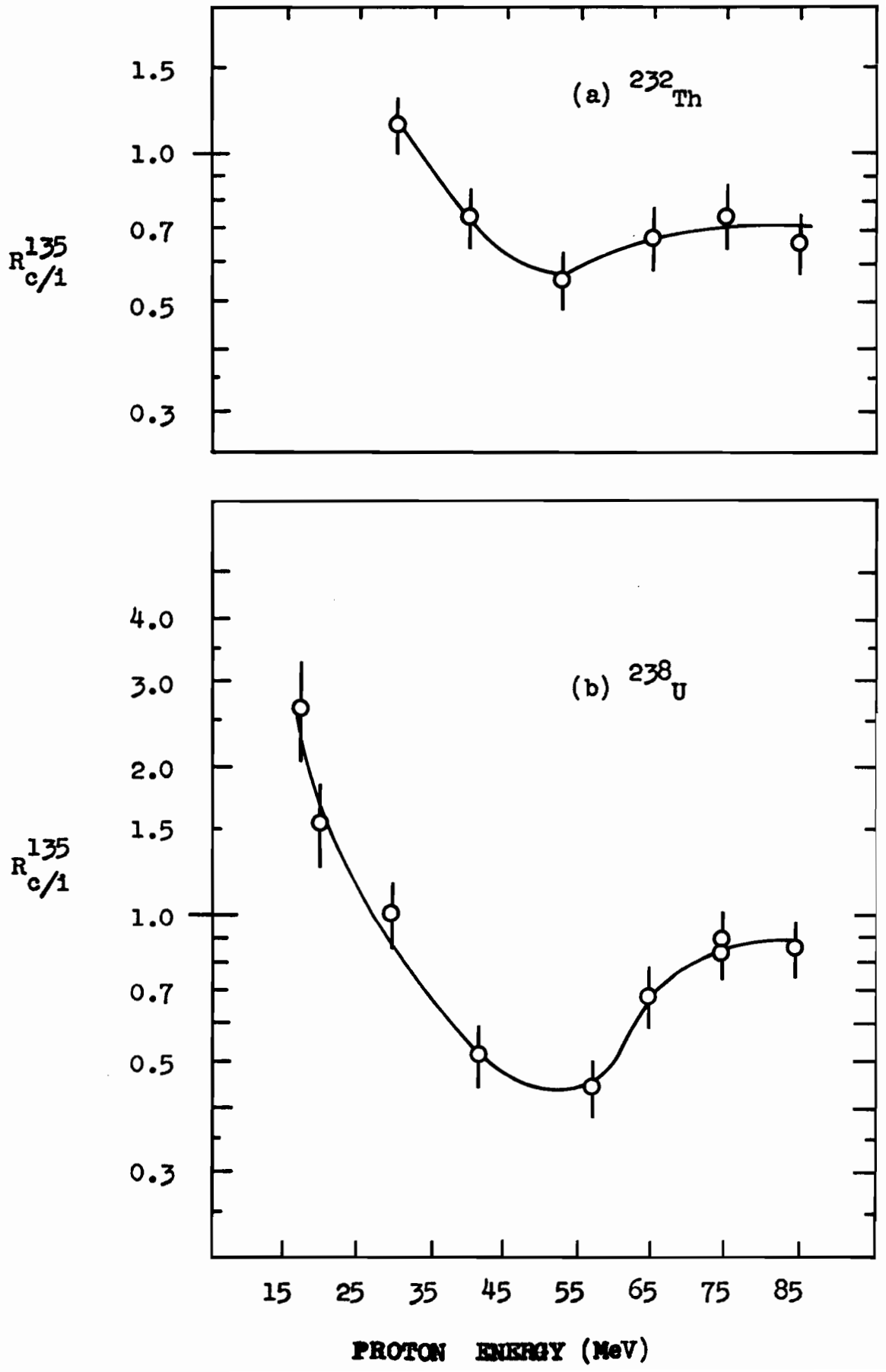
(a) ^{232}Th
(b) ^{238}U
$R^{135}_{c/i}$
$R^{135}_{c/i}$
1.5
1.0
0.7
0.5
0.3
4.0
3.0
2.0
1.5
1.0
0.7
0.5
0.3
15
25
35
45
55
65
75
85
PROTON ENERGY (MeV)

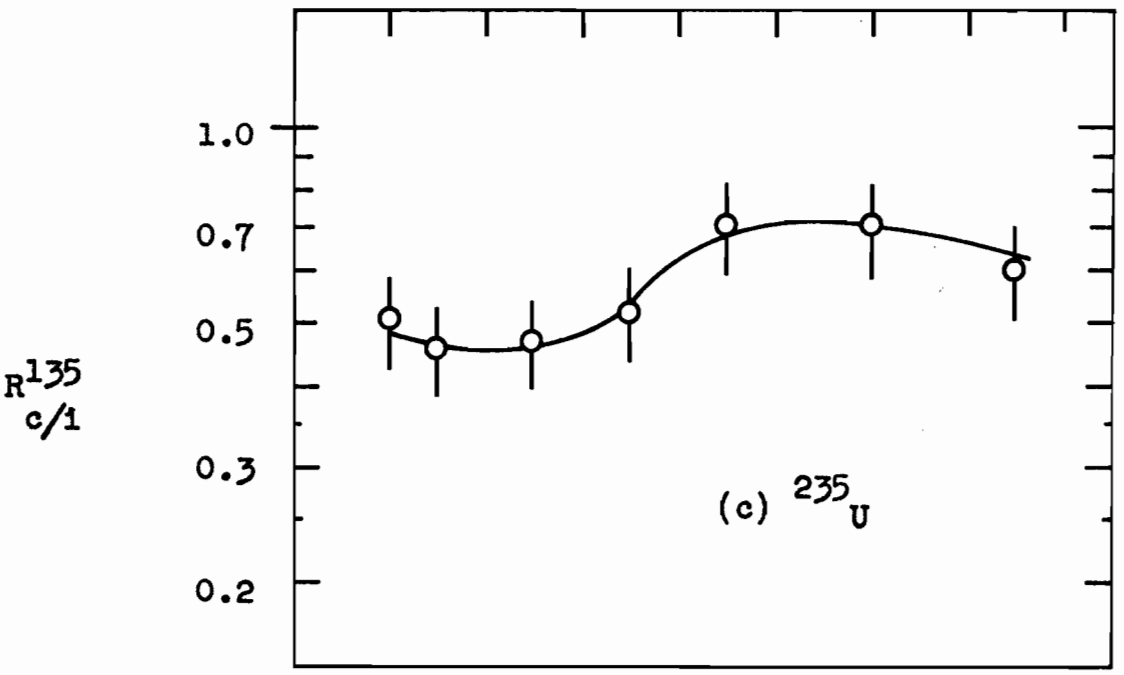
1.0
0.7
0.5
0.3
0.2
$R^{135}_{c/i}$
(c) ^{235}U

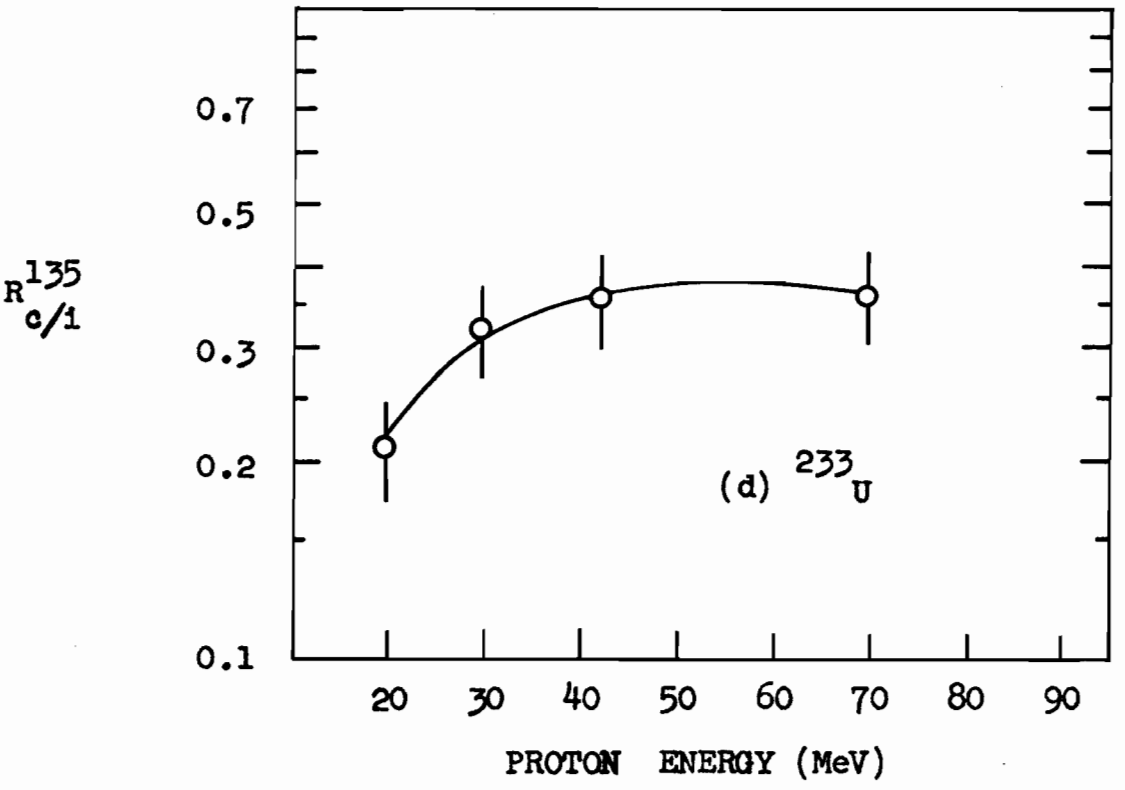
0.7
0.5
0.3
0.2
0.1
$R^{135}_{c/i}$
(d) ^{233}U
20
30
40
50
60
70
80
90
PROTON ENERGY (MeV)

TABLE 10. Cross Sections for the Cumulative Formation of ^{133}I and independent formation of ^{133m}Xe and ^{133g}Xe

Exp. No.	E_p (MeV)	Cum. σ(mb), ^{133}I	Indep. σ(mb), ^{133m}Xe	"Independent" σ (mb), Uncorr. ^{133g}Xe	"Independent" σ (mb), "Over-corr." ^{133g}Xe	"Independent" σ (mb), Uncorr. $^{133m+g}Xe$	"Independent" σ (mb), "Over-corr." $^{133m+g}Xe$
^{232}Th							
T6	30	38.9	2.7	3.1	2.7	5.8	5.4
T3	40	41.6	6.1	6.9	6.2	13.0	12.3
T4	52	33.4	9.7	10.1	9.6	19.7	19.2
T1	65	28.3	9.4	9.6	9.1	19.0	18.5
T5	75	27.2	9.6	9.1	8.6	18.7	18.2
T2	85	19.9	8.4	7.8	7.5	16.2	15.9
^{238}U							
R10	15	1.38 Y^{R10}	.020 Y^{R10}	.031 Y^{R10}	(.003 Y^{R10})*	.051 Y	(.023 Y^{R10})*
R15	17	(21.1)*	0.5	0.7	0.3	1.2	(0.8)*
R14	20	(31.4)*	1.2	1.9	1.4	3.1	(2.6)*
R18	30	2.07 Y^{R18}	0.182 Y^{R18}	.191 Y^{R18}	.166 Y^{R18}	.373 Y^{R18}	.348 Y^{R18}
R8	42	36.6	8.1	9.8	8.9	17.9	17.1
R17	57	35.8	17.8	16.4	15.8	34.2	33.6
R9	65	40.9	13.8	15.0	14.3	28.8	28.1
R11	75	33.6	10.6	9.4	8.7	19.9	19.2
R16	75	2.13 Y^{R16}	0.613 Y^{R16}	0.540 Y^{R16}	0.513 Y^{R16}	1.15 Y^{R16}	1.12 Y^{R16}
R12	85	39.1	12.0	12.7	11.9	24.7	23.9

TABLE 10. (Continued)

Exp. No.	E_p (MeV)	Cum. σ(mb), ^{133}I	Indep. σ(mb), ^{133m}Xe	"Independent" σ (mb), Uncorr. ^{133g}Xe	"Over-corr." ^{133g}Xe	Uncorr. $^{133m+g}Xe$	"Over-corr." $^{133m+g}Xe$
^{235}U							
E10	20	32.8	5.4	6.6	6.3	12.0	11.7
E9	25	49.5	12.8	14.5	14.0	27.2	26.7
E7	35	37.5	15.2	14.5	13.8	29.7	29.0
E5	45	44.2	20.2	21.2	20.5	41.4	40.7
E3	55	45.7	18.9	17.1	16.2	36.0	35.1
E8	70	29.2	12.0	10.9	10.4	22.9	22.4
E4	85	30.4	13.6	13.4	12.8	27.0	26.5
^{233}U							
U5	20	5.00 Y^{U5}	2.55 Y^{U5}	2.74 Y^{U5}	2.68 Y^{U5}	5.29 Y^{U5}	5.23 Y^{U5}
U4	30	4.30 Y^{U4}	2.14 Y^{U4}	2.42 Y^{U4}	2.36 Y^{U4}	4.56 Y^{U4}	4.50 Y^{U4}
U3	42	3.42 Y^{U3}	2.31 Y^{U3}	2.22 Y^{U3}	2.17 Y^{U3}	4.52 Y^{U3}	4.47 Y^{U3}
U1	55	6.57 Y^{U1}	3.68 Y^{U1}	3.80 Y^{U1}	no sweep b.	7.48 Y^{U1}	-
U2	70	3.15 Y^{U2}	1.98 Y^{U2}	2.11 Y^{U2}	2.06 Y^{U2}	4.09 Y^{U2}	4.04 Y^{U2}

** The simple growth correction is not satisfactory at this energy

* Very large uncertainty in $\sigma(^{64}Cu)$ at this energy

be corrected for growth from the decay of iodine during the time t_o and t_1, as discussed in Appendix A. Tables 10 and 11 give the cross sections for ^{133g}Xe and $^{133total}Xe$ both uncorrected and corrected by the simplified method which is shown in Appendix A to overcorrect slightly for the precursor decay. Figs. 20 and 21 show these results for ^{133}Xe, but only for $^{133total}Xe$ are both the uncorrected and over-corrected yields shown. The latter results show that the growth corrections were within the experimental error for the energy range 20-85 MeV. Therefore, a more complex correction method was not considered necessary here. However, a complex treatment of the 133 chain was developed for use in a rather exact reiteration method to obtain empirical values of Z_P (cf. Section 4A.2.3). Possibly it will be of use in future work at lower energies.

The cross sections of ^{133m}Xe, and therefore of ^{133g}Xe and $^{133total}Xe$, were very dependent upon the value of α_K used in treating the data from measurements of the gamma activity of ^{133m}Xe. For the internal conversion coefficient, α_K, of the M4 transition of energy 233 kev between the isomers of ^{133}Xe, Rose's (ROS 58) theoretical value of 6.7 is much higher than the only reported (BER 54) experimental value of 4.4 ± 1.4. The cross section of $^{133total}Xe$ was

FIGURE 20.

Excitation functions for the cumulative formation of ^{133}I and the independent formation of ^{133m}Xe, ^{133g}Xe, and $^{133total}Xe$. These were obtained from the proton-induced fission of ^{232}Th. The cross sections were plotted as follows,

—△— "over-corrected" independent, ^{133g}Xe

—■— independent, ^{133m}Xe

—○— uncorrected

—●— "over-corrected" independent, $^{133total}Xe$

The above data were obtained with $\alpha_K=4.4$ ($\alpha_T=6.3$).

--⊕--- "over-corrected" independent $^{133total}Xe$, with $\alpha_K=6.4$ ($\alpha_T=9.3$).

—●— cumulative cross sections of ^{133}I (this did not involve the value of α_K).

Included in this figure the filled triangles are the cumulative cross sections of ^{133}I reported previously by Pate, Foster and Yaffe (PAT 58a).

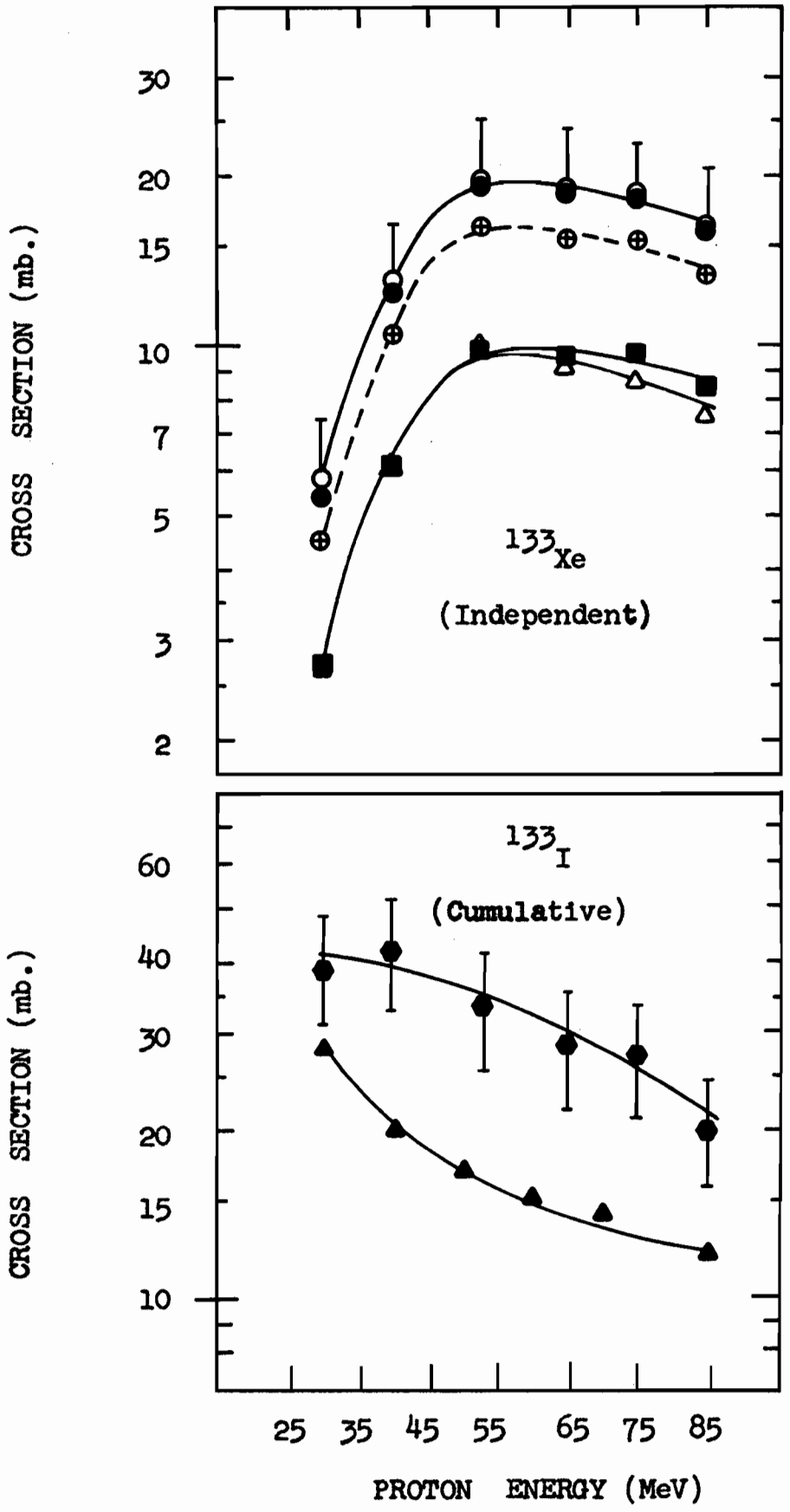
CROSS SECTION (mb.)
30
20
15
10
7
5
3
2
^{133}Xe
(Independent)
CROSS SECTION (mb.)
60
40
30
20
15
10
^{133}I
(Cumulative)
25 35 45 55 65 75 85
PROTON ENERGY (MeV)

FIGURE 21.

Excitation functions for the cumulative formation of ^{133}I and the independent formation of ^{133m}Xe, ^{133g}Xe and $^{133total}Xe$. These were obtained from the proton-induced fission of,

(a) ^{238}U

(b) ^{235}U

The cross sections for ^{133}Xe were obtained with $\alpha_K = 4.4$ ($\alpha_T = 6.3$), and were plotted as follows,

—△— "over-corrected" independent, ^{133g}Xe

—■— independent, ^{133m}Xe

—○— uncorrected independent, $^{133total}Xe$

—●— "over-corrected"

Fig.21 (a) ^{238}U

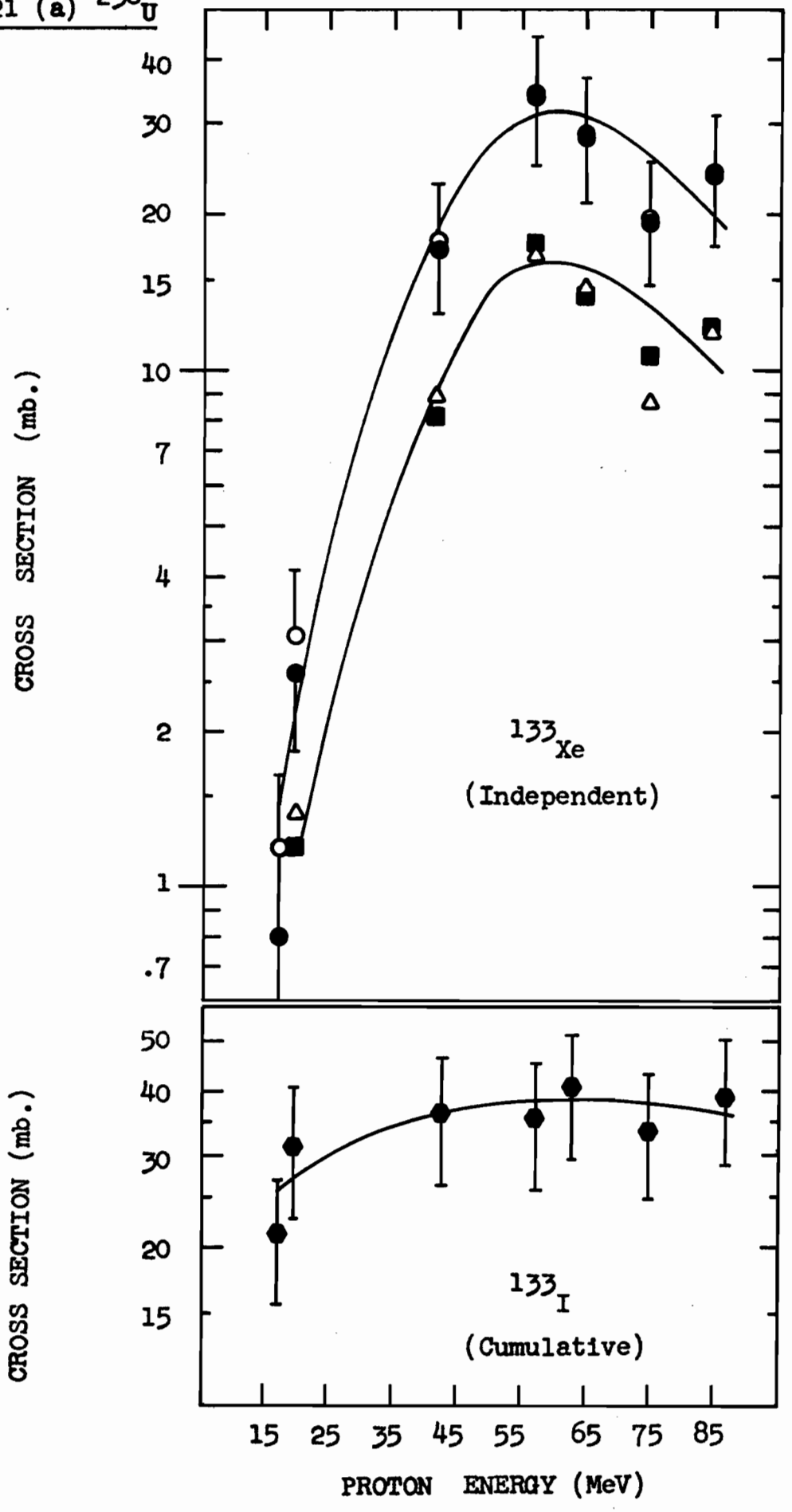
CROSS SECTION (mb.)
40
30
20
15
10
7
4
2
1
.7
^{133}Xe
(Independent)
CROSS SECTION (mb.)
50
40
30
20
15
^{133}I
(Cumulative)
15 25 35 45 55 65 75 85
PROTON ENERGY (MeV)

Fig.21 (b) ^{235}U

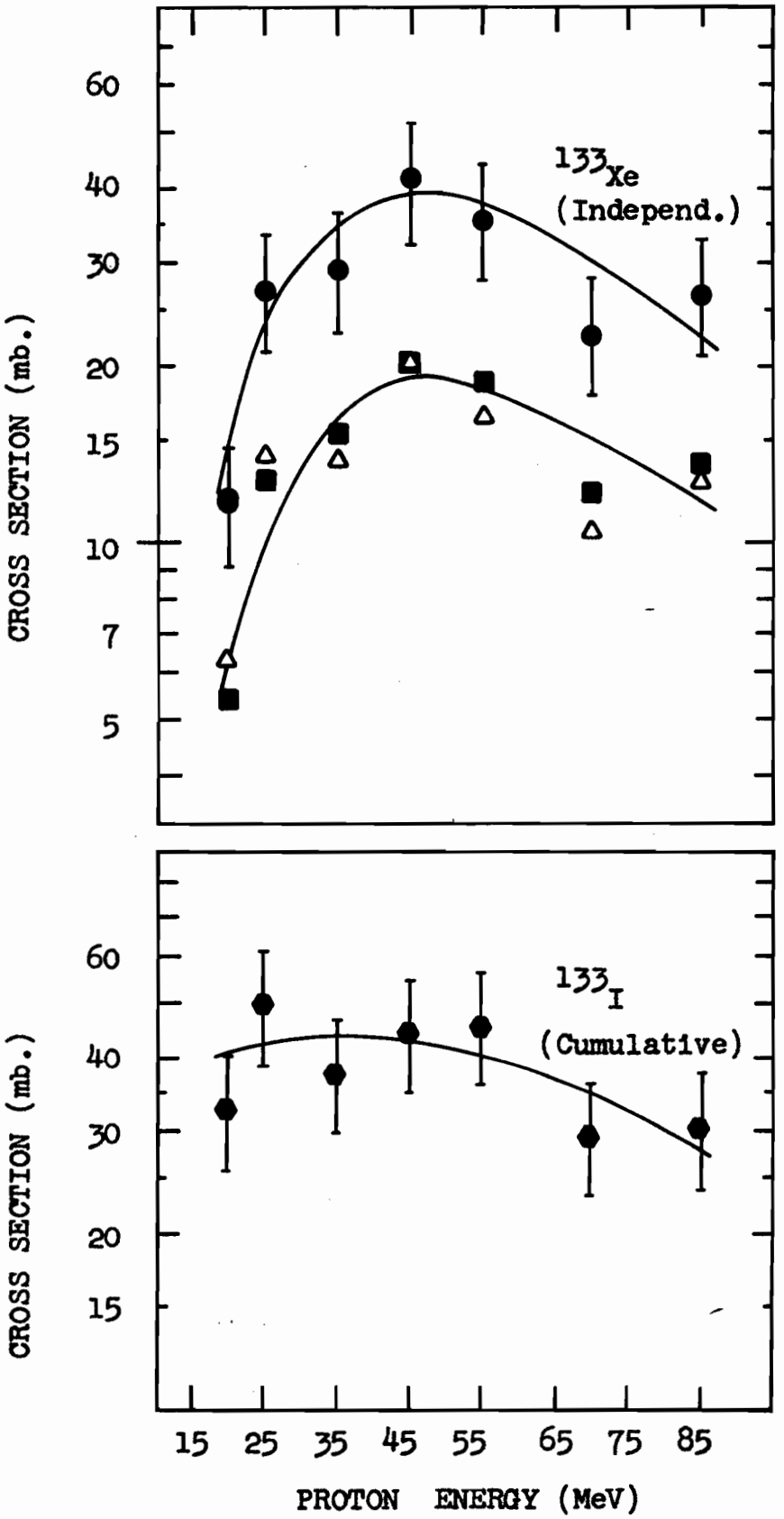
60
40
30
20
15
10
7
5
CROSS SECTION (mb.)
^{133}Xe
(Independ.)
60
40
30
20
15
CROSS SECTION (mb.)
^{133}I
(Cumulative)
15 25 35 45 55 65 75 85
PROTON ENERGY (MeV)

therefore computed for $\alpha_K = 4.4$, and also for three other possible higher values, 5.0, 5.7, and 6.4. Using the value of (α_K/α_{LM}) in Table 5, these values of α_K corresponded to values of $\alpha_T = 6.3$, 7.3, 8.3 and 9.3, respectively. Table 11 gives these cross sections and, for fission of ^{232}Th, Fig. 20 shows the extreme values for $\alpha_K = 4.4$ and 6.4. The correct value of the cross section for ^{133}Xe probably falls between these extremes. The uncertainty in α_K introduced only a fairly small error in the absolute cross sections and this error was smaller than the experimental error of 20-30% (cf. Section 3.3). Similarly this uncertainty introduced only fairly small errors in the ratio $R^{133}_{c/i}$. Fig. 22 shows these ratios. All the solid lines are for $\alpha_K = 4.4$ and, for ^{232}Th, the dotted line is for $\alpha_K = 6.4$.

A brief discussion of the excitation functions is now given. The positions of the maximum in the xenon excitation functions will be discussed further with respect to the empirical Z_P values in Section 4A.4.

Only two of the fifteen excitation functions presented here have been previously reported. By a totally different measurement method, using solid iodide sources, Pate, Foster and Yaffe (PAT 58) determined the cumulative yields of ^{133}I and ^{135}I for the fission of ^{232}Th with

TABLE 11. Dependence of the Independent Cross Section of ^{133}Xe on the Value of α_K for the .233-MeV Gamma Ray

Exp. No.	E_p (MeV)	σ (mb), $^{133m+g}Xe$ using α_K, (α_T): 5.0, (7.3) Uncorr.	5.0, (7.3) "Over-corr."	5.7, (8.3) Uncorr.	5.7, (8.3) "Over-corr."	6.4, (9.3) Uncorr.	6.4, (9.3) "Over-corr."
^{232}Th							
T6	30	5.5	5.1	5.2	4.8	5.0	4.5
T3	40	12.4	11.7	11.7	11.0	11.1	10.4
T4	52	18.7	18.2	17.7	17.2	16.7	16.2
T1	65	18.0	17.5	17.0	16.5	16.0	15.5
T5	75	17.7	17.2	16.6	16.2	15.6	15.2
T2	85	15.3	15.0	14.4	14.1	13.6	13.2
^{238}U							
R10	15	-	-	-	-	-	-
R15	17	1.1	0.7	1.0	0.7	1.0	0.6
R14	20	3.0	2.5	2.9	2.3	2.7	2.2
R18	30	0.354 Y^{R18}	0.329 Y^{R18}	0.335 Y^{R18}	0.310 Y^{R18}	0.316 Y^{R18}	0.290 Y^{R18}
R8	42	17.1	16.2	16.2	15.3	15.4	14.5
R17	57	32.3	31.8	30.5	29.9	28.6	28.0
R9	65	27.4	26.6	25.9	25.2	24.4	23.7
R11	75	18.8	18.1	17.7	17.0	16.6	15.9
R16	75	1.09 Y^{R16}	1.06 Y^{R16}	1.02 Y^{R16}	1.00 Y^{R16}	0.96 Y^{R16}	0.93 Y^{R16}
R12	85	23.5	22.7	22.2	21.4	20.9	20.1

TABLE 11. (Continued)

Exp. No.	E_p (MeV)	σ (mb), $^{133m+g}Xe$ using α_K, (α_T): 5.0, (7.3) Uncorr.	5.0, (7.3) "Over-corr."	5.7, (8.3) Uncorr.	5.7, (8.3) "Over-corr."	6.4, (9.3) Uncorr.	6.4, (9.3) "Over-corr."
^{235}U							
E10	20	11.5	11.1	10.9	10.5	10.3	10.0
E9	25	66.1	64.7	62.7	61.3	59.3	57.9
E7	35	28.1	27.4	26.5	25.8	24.8	24.2
E5	45	39.3	38.6	37.2	36.4	35.0	34.3
E3	55	34.0	33.1	32.0	31.0	30.0	29.1
E8	70	21.6	21.1	20.4	19.9	19.1	18.6
E4	85	25.6	25.0	24.1	23.6	22.7	22.1
^{233}U							
U5	20	5.02 Y^{U5}	4.96 Y^{U5}	4.75 Y^{U5}	4.69 Y^{U5}	4.48 Y^{U5}	4.42 Y^{U5}
U4	30	4.33 Y^{U4}	4.28 Y^{U4}	4.11 Y^{U4}	4.05 Y^{U4}	3.88 Y^{U4}	3.83 Y^{U4}
U3	42	4.27 Y^{U3}	4.23 Y^{U3}	4.04 Y^{U3}	3.98 Y^{U3}	3.79 Y^{U3}	3.74 Y^{U3}
U1	55	7.08 Y^{U1}	(6.97 Y^{U1})	6.71 Y^{U1}	(6.58 Y^{U1})	6.31 Y^{U1}	(5.12 Y^{U1})
U2	70	3.88 Y^{U2}	3.82 Y^{U2}	3.67 Y^{U2}	3.62 Y^{U2}	3.46 Y^{U2}	3.41 Y^{U2}

FIGURE 22.

The dependence of the relative formation of ^{133}I and ^{133}Xe upon proton energy. This is expressed in the form,

$$R^{133}_{c/i} = \frac{\text{(cumulative yield of } ^{133}I)}{\text{(independent yield of } ^{133}Xe, \text{"overcorrected"})}$$

These ratios were obtained from the proton-induced fission of,

(a) ^{232}Th

(b) ^{238}U

(c) ^{235}U

(d) ^{233}U

The data for ^{133}Xe were obtained using $\alpha_K = 4.4$ ($\alpha_T = 6.3$). In Fig.22(a), the data were plotted also for $\alpha_K = 6.4$ ($\alpha_T = 9.3$),

—o— for $\alpha_K = 4.4$

--⊕-- for $\alpha_K = 6.4$

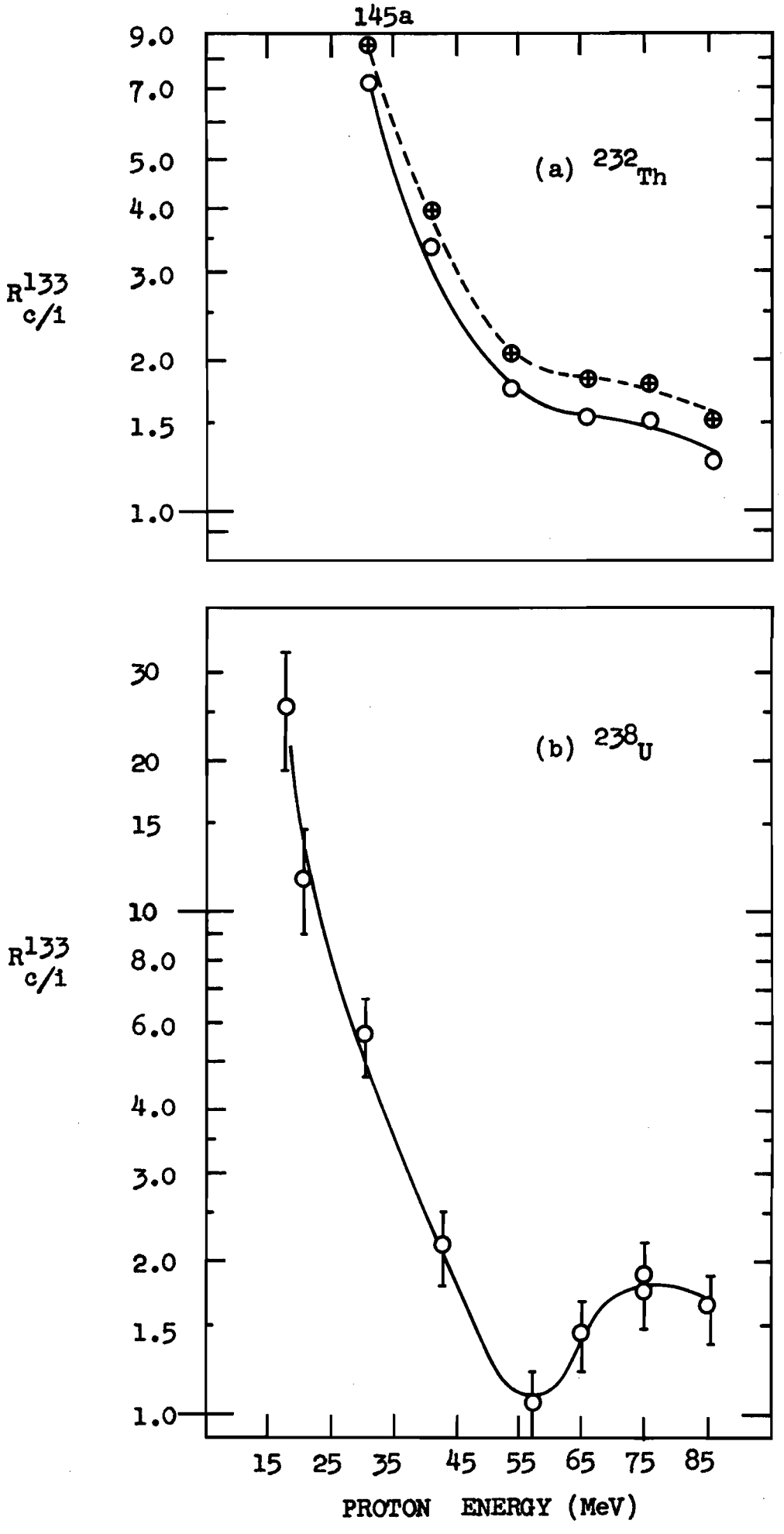
9.0
7.0
5.0
4.0
3.0
2.0
1.5
1.0
(a) 232Th
R133 c/i
30
20
15
10
8.0
6.0
4.0
3.0
2.0
1.5
1.0
(b) 238U
R133 c/i
15
25
35
45
55
65
75
85
PROTON ENERGY (MeV)

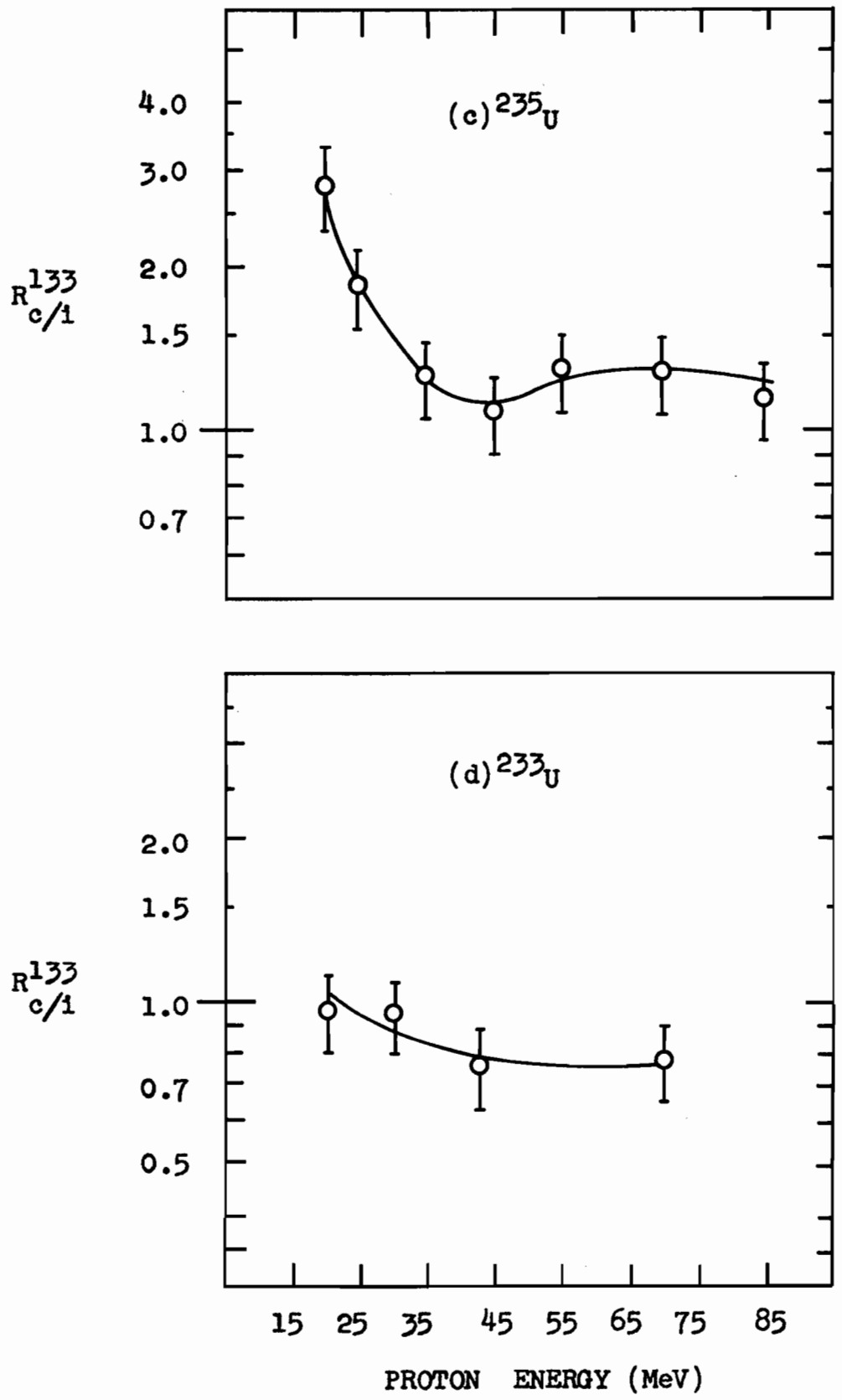
(c) ^{235}U
(d) ^{233}U
$R^{133}_{c/i}$
4.0
3.0
2.0
1.5
1.0
0.7
0.5
15
25
35
45
55
65
75
85
PROTON ENERGY (MeV)

10-85-MeV protons. Their excitation functions are plotted as the dashed lines in Figs. 18(a) and 21(a). Meghir (MEG 62) has related the monitor reactions used by Pate et al. and in the present work. He showed that at proton energies of 26 MeV and between 55-85 MeV there was little systematic error between the monitor cross section used in these two studies. Therefore, for these energies the excitation functions can be directly compared for ^{135}I, in Fig. 18(a), and for ^{133}I, in Fig. 21(a). The present values were slightly higher for ^{135}I and considerably higher for ^{133}I. The compared excitation functions show a similar decrease with energy. The previous results were obtained after a difficult resolution of beta decay curves. The present results for ^{133}I were obtained from a simple decay curve of half-life 5.3 days measured for the xenon sample from sweep (b). Probably the present results are therefore more reliable. Indirect confirmation of the relative accuracy of the ^{133}I and ^{135}I yields in this work will be demonstrated later in this thesis by the internal consistency of the empirical Z_p values for the chains 133 and 135.

The main conclusions in this thesis were drawn from the relative yields which were obtained with better accuracy than the above absolute yields.

4A.2 DETERMINATION OF EMPIRICAL Z_P VALUES

The data available for this study of charge distribution were independent yields of xenon and cumulative yields of iodine for two different chains, 133 and 135. Sets of these four yields were available for fission of four targets with protons of energy 20-85 MeV.

These data were insufficient to construct an empirical FUNCTION (1), which in Section 1A.3.2 was defined as the isobaric charge distribution curve about a most probable charge, Z_p. However, the Introduction showed that the function is fairly well defined for medium-energy fission products in this mass region. Assuming a suitable FUNCTION (1), empirical Z_p values and corresponding fractional chain yields were obtained from the above data.

The empirical FUNCTION (1) from previous studies using the (N/Z)-plot method might have been used for ^{238}U (DAV 63, PAR 66) and ^{232}Th (BEN 65). However, these functions were plotted for absolute cross sections, and systematic errors in the present and previous studies would seriously influence the determined values for Z_p. There is still uncertainty about the width of these curves, and no curves exist for the fission of ^{233}U and ^{235}U with protons.

The Gaussian FUNCTION (1) from the $(Z - Z_p)$-plot

method (Section 1A.3.2) was chosen here because it allowed a more systematic analysis of the data for all four targets. The method also allowed a systematic study of the effect of the width of FUNCTION (1) on the empirical Z_p values.

The present data could not be put directly in the form of fractional yields which must be used in the method of Wahl (WAH 62) and others (WOL 65). Therefore two modifications of their method were used here. Method (1) has been developed in this thesis, but the more complex method (2) is similar to that used by Storms (STO 62). Both of these methods used a Gaussian FUNCTION (1) given by equation (1A.3).

4A.2.1 USE OF A GAUSSIAN FUNCTION (1)

FUNCTION (1) is a narrow discrete frequency distribution with only a few grouping units, each separated by one charge unit. Statistically it is only a crude approximation to represent such a distribution with a continuous function, as given by equation (1A.3). Wahl et al. (WAH 62) and Wolfsberg (WOL 65) have obtained fractional cumulative yields for a fission product of charge Z' by integrating this continuous function between $Z = (Z' + 0.5)$ and $Z = -\infty$. In this work and that of Storms it was considered a good enough approximation simply to add the

discrete fractional yields calculated for $Z = Z'$, $(Z' - 1)$, $(Z' - 2)$, $(Z' - 3)$ and $(Z' - 4)$ in order to obtain this fractional cumulative yield. When the latter yield was added to the fractional yields calculated for $Z = (Z' + 1)$ to $(Z' + 4)$ the sum was always found to approximate unity, within less than 0.001, for the C values used in the present computations.

The choice of C in equation (1A.3) was made from the functions previously used. These have been introduced in Section 1A.3.2 and are further discussed here.

Figs. 23(b) and (c) show the full width at half maximum, FWHM, of FUNCTION (1) obtained empirically in previous studies. When the functions that were plotted originally on an (N/Z)-plot (DAV 63, BEN 65, PAR 66) were replotted on a $(Z - Z_p)$-plot they closely approximated Gaussian functions, as represented by equation (1A.3). Their values of C in this equation can be readily obtained from their FWHM, in charge units, by using Fig. 23(a). This figure shows the FWHM of FUNCTION (1) (equation (1A.3)) with values of C from 0.8 to 1.9. Using Fig. 23(a), an ordinate (C) corresponding to the ordinate (FWHM) was constructed in Figs. 23(b) and (c). This ordinate shows directly the C values for empirical FUNCTION (1) used in previous studies.

FIGURE 23

(a) Full width at half maximum, FWHM, of the Gaussian function given by equation (1A.3), for various C values.

(b) FWHM of FUNCTION (1) from previous studies of charge distribution in the fission of ^{238}U with protons,

—△— Davies and Yaffe (DAV 63)

—○— Parikh (PAR 66)

(c) FWHM of FUNCTION (1) from previous studies of the fission of ^{232}Th with protons,

—△— Pate, Foster and Yaffe (PAT 58a)

—○— Benjamin (BEN 65)

Shown for comparison in (b) and (c) are the FWHM used in other medium-energy fission systems (cf. Table 1, Section 1A.3.2),

———— Storms (STO 62)

---------- McHugh (MCH 63)

In (b) and (c), the alternative ordinates, FWHM and C, were related through the function shown in (a).

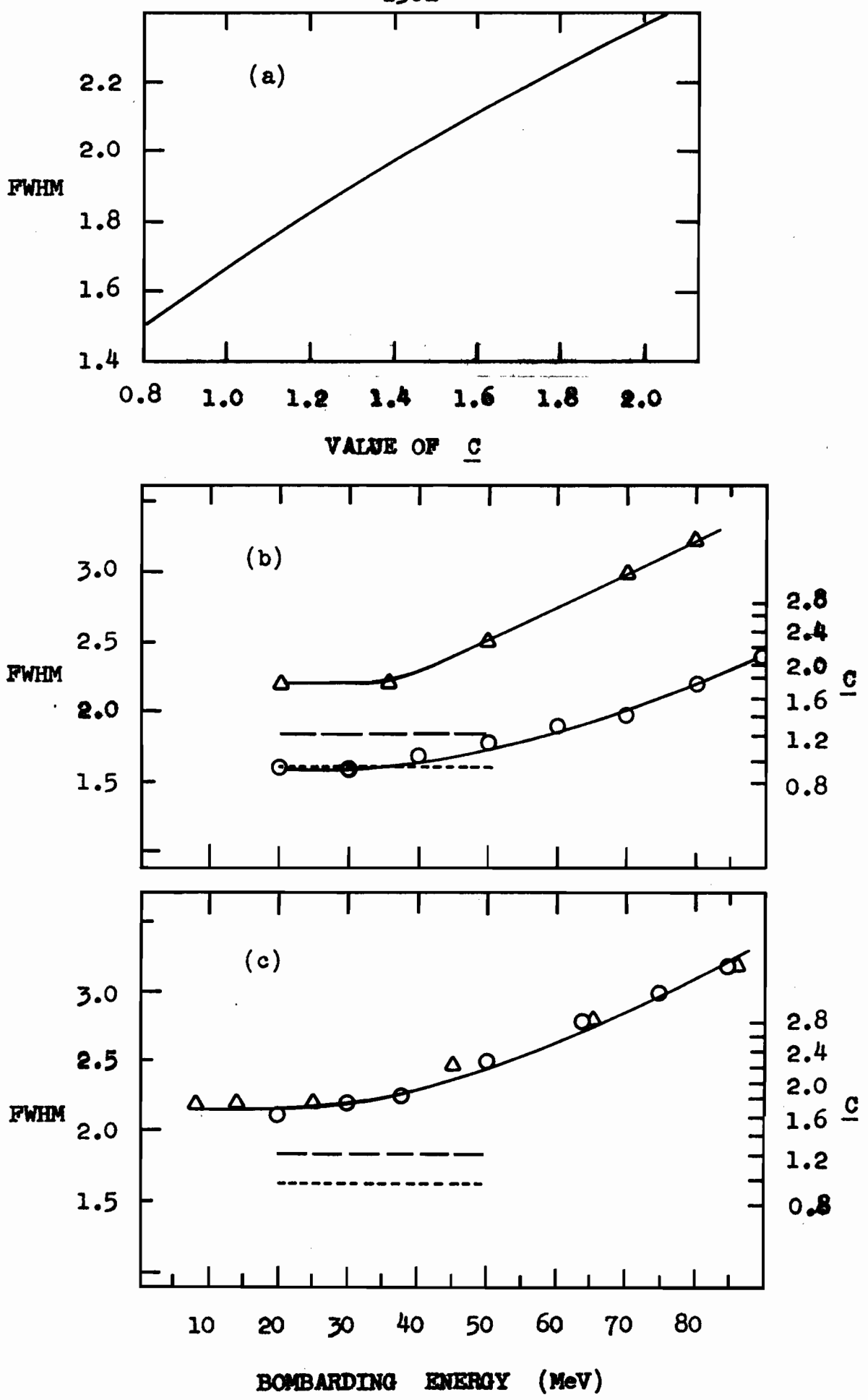
(a)
FWHM
2.2
2.0
1.8
1.6
1.4
0.8
1.0
1.2
1.4
1.6
1.8
2.0
VALUE OF C
(b)
FWHM
3.0
2.5
2.0
1.5
2.8
2.4
2.0
1.6
1.2
0.8
C
(c)
FWHM
3.0
2.5
2.0
1.5
2.8
2.4
2.0
1.6
1.2
0.8
C
10
20
30
40
50
60
70
80
BOMBARDING ENERGY (MeV)

Between 20-50 MeV the width of FUNCTION (1) does not change appreciably and probably the best estimate of C is 1.20 ± 0.25. Above 50 MeV, FUNCTION (1) broadens and possibly loses its symmetry. These poorly defined changes would introduce large uncertainties in the empirical value of Z_p. Therefore no attempt was made to extract Z_p values from the present data for those experiments with bombarding energy greater than about 50 MeV.

4A.2.2 METHOD (1). TO DETERMINE EMPIRICAL VALUES OF Z_p

It was shown in the Introduction (Section 1A.3.2) that generally the value of Z_p for an isobaric chain increases as the fission energy increases. This means that with increase in energy the charge distribution shifts towards more stable isobars. Consequently there will be a decrease in the ratio, represented as $R^A_{c/i}$, of the cumulative yield of a negative-beta parent to the independent yield of its daughter, in a chain of mass A. For example, the independent yield of ^{133}Xe is very low for thermal fission, while the cumulative yield of its beta parent ^{133}I is approximately equal to the total yield of chain 133. However for medium-energy fission the independent yield of ^{133}Xe is a considerable fraction of the chain yield and of

course the fractional cumulative yield of ^{133}I is correspondingly lower. In this example the value of $R^{133}_{c/i}$ would be of the order of 10^2 at low energy, but at medium energy would be of the order of 10^0.

In this work the quantitative relationship between the yield ratio $R^A_{c/i}$ and Z_p was investigated and used as the basis of this empirical method, method (1), to determine the value of Z_p for chain A, and the fractional yields of the chain members. Assuming that the charge distribution curve, FUNCTION (1), is a Gaussian function represented by equation (1A.3) it was possible to construct the following expression for $R^A_{c/i}$ as a function of $(Z' - Z_p)$, where Z' was the charge of the daughter isobar, and therefore $(Z' - 1)$ was the charge of the beta parent.

$$R^A_{c/i} = \frac{\text{(cumulative yield of beta parent)}}{\text{(independent yield of daughter)}} = \frac{\left[\sum_{Z_i=(Z'-1)}^{Z_i=(Z'-6)} \exp\left(-(Z_i - Z_p)^2 / C\right)\right]}{\exp\left(-(Z' - Z_p)^2 / C\right)} \quad . \qquad (4A.1)$$

Using this equation, a simple FORTRAN program computed the theoretical ratio $R^A_{c/i}$ for values of $(Z' - Z_p)$ from + 3.00

to - 3.00, in steps of 0.05 charge units. The whole computation was made for thirteen C values from 0.7 to 1.9.

Fig. 24 shows some of these computed functions. Now, if $R^{A}_{c/i}$ is known experimentally for a pair of adjacent isobars (e.g. $^{133}I/^{133}Xe$), the corresponding value of $(Z' - Z_p)$, for the daughter isobar, may be read from one of the functions for a particular C value.

Fig. 24 also demonstrates the dependence of Z_p on the value of C which is used to define FUNCTION (1). When the daughter nuclide has $(Z' - Z_p) \approx + 0.7$ the empirical value of Z_p is shown to be almost independent of C.

For the isobaric pairs $^{133}I/^{133}Xe$ and $^{135}I/^{135}Xe$, the yield ratios $R^{133}_{c/i}$ and $R^{135}_{c/i}$ were obtained in this work with less experimental error than the absolute yields which would be used in an (N/Z)-plot method to determine empirical Z_p values. Only at energies below 20 MeV would the ratio $R^{133}_{c/i}$ contain large errors and require a more complex growth correction. Although method (1) was satisfactory for nearly all the data a more complex method (2) was developed and is reported here for possible use in later work at lower energy. Method (2) also served to check the results from method (1).

FIGURE 24.

Theoretical $R^{A}_{c/i}$ versus $(Z' - Z_p)$, from equation (4A.1) with values of C = 0.7, 0.9, 1.2, 1.5 and 1.9.

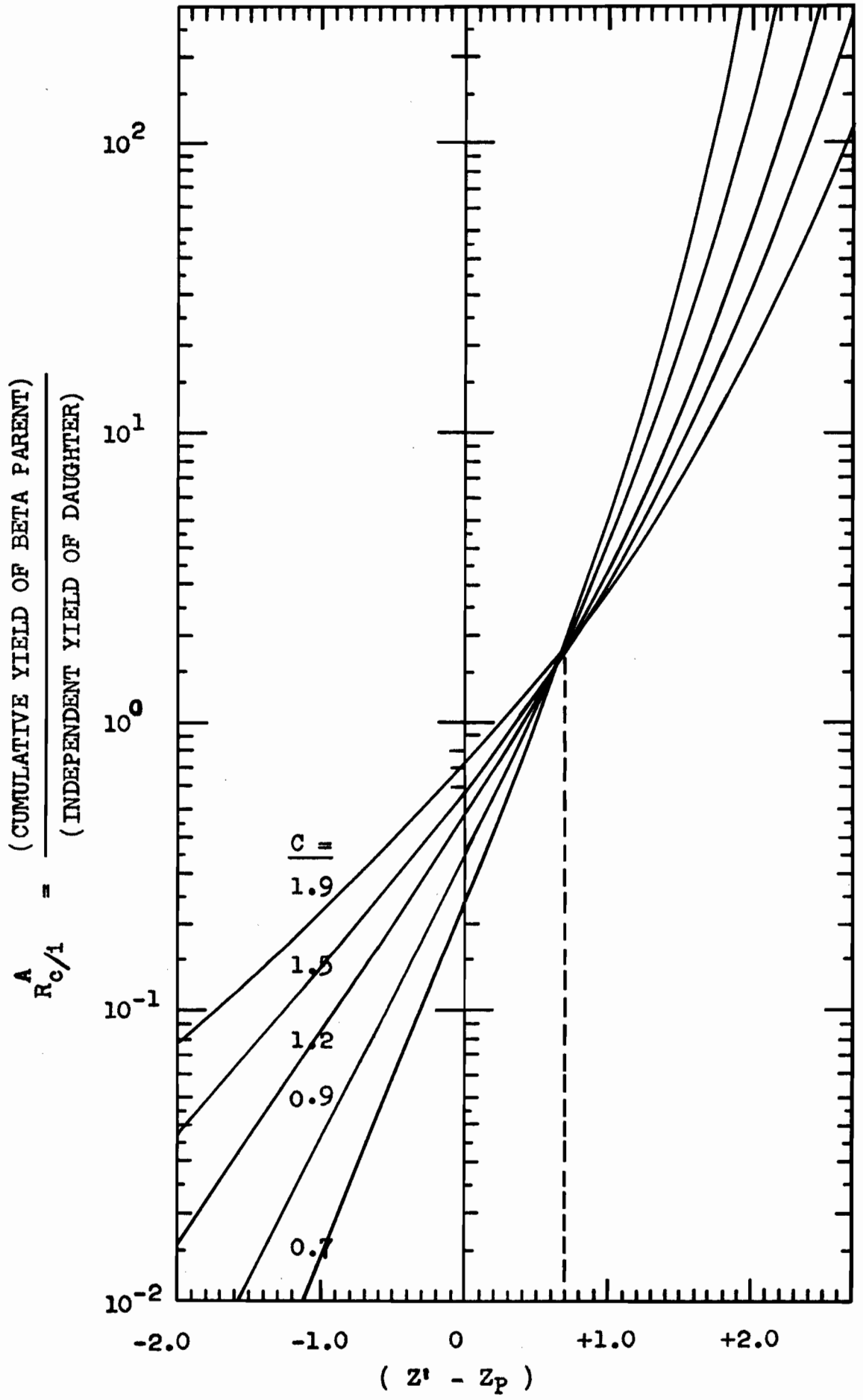
$A_{R_{c/1}}$ = (CUMULATIVE YIELD OF BETA PARENT) / (INDEPENDENT YIELD OF DAUGHTER)
10^2
10^1
10^0
10^{-1}
10^{-2}
C =
1.9
1.5
1.2
0.9
0.7
-2.0
-1.0
0
+1.0
+2.0
(Z' - Z_P)

4A.2.3 METHOD (2). TO DETERMINE EMPIRICAL Z_P VALUES FOR CHAINS 133 AND 135

This method also assumed a Gaussian FUNCTION (1). The measured gamma activities for ^{133}Xe or ^{135}Xe, from sweeps (a) and (b), were used as the input data for a FORTRAN program which fitted these directly with a value of Z_P. The program was based essentially on a method used by Storms (STO 62). Appendix C gives further details of the FORTRAN program which was based on a simple reiteration method outlined here, for A = 133.

Bateman equations were used to give a lengthy expression (cf. Appendix C, equation C.3) for the activity, $C^{b}_{133g_{Xe}}$, from sweep (b) and another expression (cf. Appendix C, equation C.2) for $C^{o}_{133g_{Xe}}$ from sweep (a). A Gaussian FUNCTION (1) was assumed to relate the fractional yields of the isobars of mass 133, so that the above two simultaneous equations had only two unknowns. These unknowns were Z_P and Y which was proportional to the total chain yield. To solve for Z_P, the value of $(Z - Z_P)$ for ^{133}Xe was first set equal to + 2.0 and the value of Y calculated from the first expression (C.3). This value of Y was substituted in the second expression (C.2) to give a fractional yield, XENEW, for ^{133}Xe. XENEW was lower than the fractional yield, XEOLD, obtained by substituting the originally assumed $(Z - Z_P)$ in

the Gaussian FUNCTION (1). Therefore stepwise iterations were made with $(Z - Z_p)$ decreasing in steps of 0.1, and finally in steps of 0.01, until a value of Z_p was obtained which produced nearly the same values for XENEW and XEOLD. This was taken to be the best empirical Z_p value for chain 133. The procedure was repeated for a Gaussian FUNCTION (1) with C = 0.95, 1.20 and 1.45.

Although this method was designed for chain 133 it was tested by writing a similar FORTRAN program for the simpler chain 135. The Z_p values obtained were checked with those determined by method (1) for A = 135, and showed excellent agreement.

4A.3 EMPIRICAL Z_p VALUES FOR CHAINS 133 AND 135

Table 12 gives the values of $(Z - Z_p)$ obtained from the data for chains 133 and 135, from method (2) with the three values of C, 0.95, 1.20 and 1.45. For C = 1.20, the table also gives the corresponding values obtained from method (1). The latter values were read from Fig. 24 using the experimental values of $R^A_{c/i}$ given in Table 12 (cf. Tables 9 and 17).

For proton energies of 20-57 MeV, there was very good agreement between Z_p values obtained by the two independent methods. The simple direct method (1) was

TABLE 12. Empirical Values of $(Z-Z_p)$ for Chains 133 and 135, from Methods (2) and (1)

Exp. No.	E_p (MeV)	$(Z - Z_p)$ from METHOD 2 for ^{135}Xe C=0.95	C=1.20	C=1.45	for ^{133}Xe * C=0.95	C=1.20	C=1.45	$R^{133}_{c/i}$	$R^{135}_{c/i}$	$(Z-Z_p)$ from METHOD 1 ^{135}Xe C=1.20	^{135}Xe C=1.20
^{232}Th											
T6	30	0.51	0.48	0.44	1.22	1.32	1.40	7.21	1.15	1.32	0.48
T3	40	0.32	0.25	0.18	0.95	1.00	1.04	3.37	0.75	1.00	0.25
(T4)	(52)	0.20	0.10	-0.01	0.69	0.69	0.69	1.74	0.56	0.69	0.10
^{238}U											
R10	15	1.07	1.15	1.21	1.75	1.92	2.07	(61)	3.94	2.03	1.08
R15	17	0.91	0.96	0.99	1.60	1.75	1.88	(28)	2.64	1.80	0.90
R14	20	0.68	0.68	0.68	1.39	1.51	1.61	12.2	1.55	1.51	0.65
R18	30	0.46	0.41	0.36	1.15	1.24	1.31	5.93	1.01	1.24	0.41
R8	42	0.19	0.10	-0.01	0.77	0.79	0.80	2.15	0.52	0.79	0.05
(R17)	(57)	0.10	-0.02	-0.15	0.48	0.44	0.40	1.06	0.45	0.44	-0.02
^{235}U											
E10	20	0.15	0.04	-0.07	0.88	0.92	0.95	2.81	0.51	0.92	0.03
E9	25	0.10	-0.02	-0.14	0.71	0.72	0.72	1.85	0.46	0.72	-0.02
E7	35	0.11	-0.01	-0.13	0.56	0.54	0.52	1.27	0.47	0.54	0.00
E5	45	0.16	0.05	-0.06	0.49	0.45	0.41	1.09	0.52	0.45	0.05
(E3)	(55)	0.30	0.23	0.15	0.57	0.55	0.52	1.30	0.71	0.55	0.22
^{233}U											
U5	20	-0.26	-0.46	-0.57	0.43	0.39	0.33	0.96	0.21	0.39	-0.46
U4	30	-0.06	-0.22	-0.39	0.43	0.39	0.33	0.95	0.32	0.38	-0.22
U3	43	-0.01	-0.16	-0.31	0.34	0.27	0.19	0.76	0.36	0.27	-0.15

* Using $\alpha_K = 4.4$ ($\alpha_T = 6.3$)

therefore proved to be reliable and should be useful in other work, since accurate values of $R^{A}_{c/i}$ can fairly easily be obtained for many pairs of adjacent isobars formed in fission.

4A.3.1 VARIATIONS IN Z_P

For the 135 chain for the fission of ^{238}U, Fig. 25 conveniently illustrates the above results on the three Gaussian curves used for FUNCTION (1). This figure is similar to Fig. 5 (Section 1A.3.2) for the chain 135. However, an additional fractional chain yield, that of ^{135}Cs, was available for McHugh's determination of the empirical value of Z_P. Fig. 25 and Figs. 26(a)-(d) show the variation of Z_P with energy. The values of Z_P used for chains 133 and 135 were readily calculated from the values of $(Z - Z_P)$ for the xenon isotopes which have $Z = 54$. In Fig. 26 the solid lines were obtained with $C = 1.20$ and the dashed lines with $C = 0.95$ and 1.45. As was noted from Fig. 24, the variation of C had least effect on the empirical Z_P when, for the xenon isotopes, $Z_P \approx 53.3$ (i.e. $(Z - Z_P) \approx + 0.7$). Depending on the value of $(Z - Z_P)$ its uncertainty was estimated to be from 0.1 to 0.2 charge units.

For the fission of ^{232}Th and ^{238}U, Fig. 27 shows the present results (obtained for $C = 1.20$) on a plot

FIGURE 25.

Gaussian charge distribution curves, FUNCTION (1), obtained using equation (1A.3),

with C = 0.95, 1.20 and 1.45.

Fitted on these curves are a sample set of results from Table 12. These data were for chain 135, from the fission of ^{238}U with protons of energy E_p MeV. Values of E_p are given beside the points in this figure.

For C = 1.20, the fractional cumulative yields for ^{135}I are fitted to an "integrated" curve.

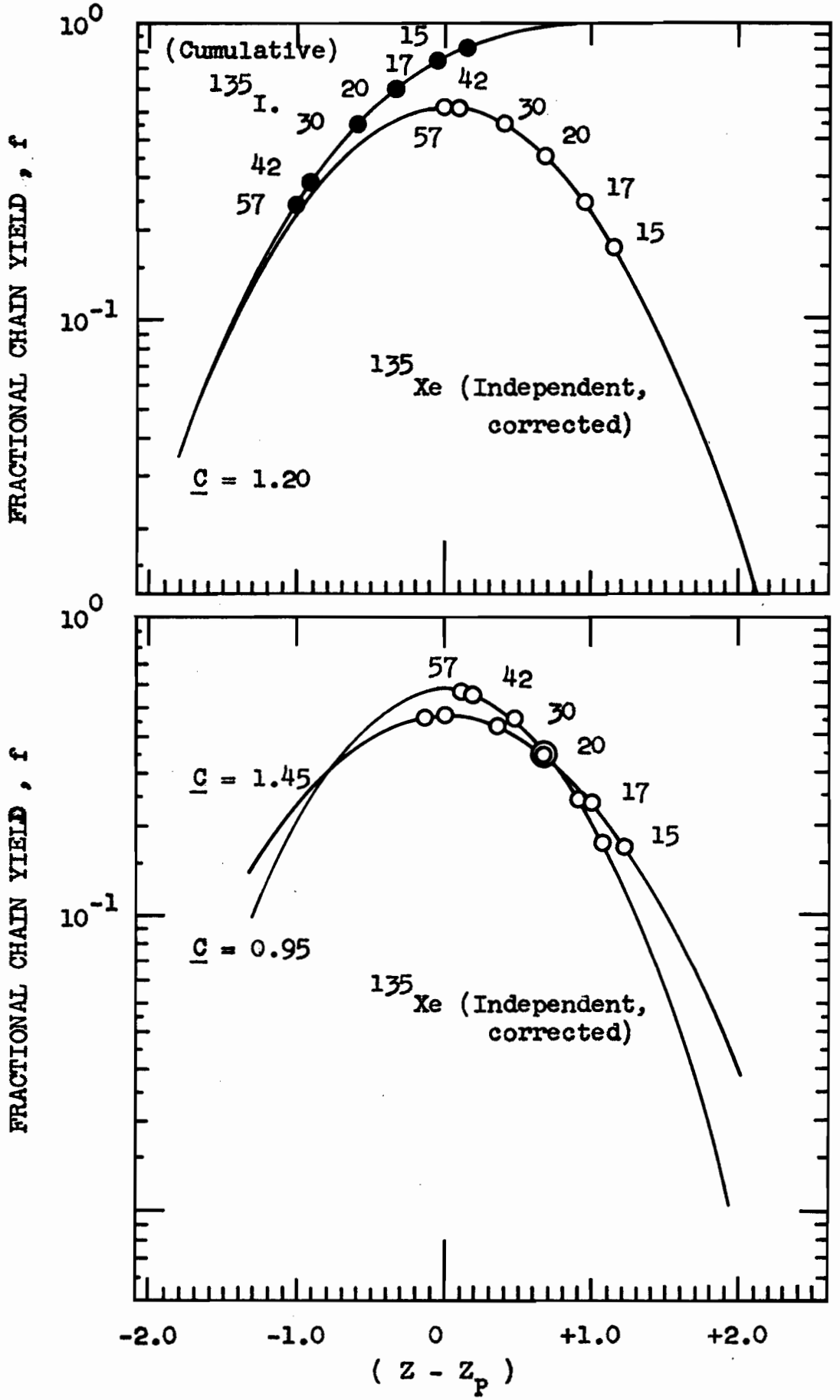
(Cumulative)
135 I.
15
17
20
30
42
57
135 Xe (Independent, corrected)
C = 1.20
C = 1.45
C = 0.95
FRACTIONAL CHAIN YIELD , f
10^0
10^{-1}
-2.0
-1.0
0
+1.0
+2.0
(Z - Z_p)

FIGURE 26.

The variation of the empirical value of Z_P with the energy of protons inducing fission in

(a) ^{232}Th

(b) ^{238}U

(c) ^{235}U

(d) ^{233}U

The Z_P values were obtained by method (2) using the Gaussian FUNCTION (1) from equation (1A.3), with

– – – •– – – C = 0.95

———•——— C = 1.20

-------•------ C = 1.45

The divisions on the vertical lines, to the right of the figure, show Z_P values postulated for chains 133 and 135 from the simplified CCR equation (1A.2). The numbers given beside these lines are the total number of fission neutrons, ν_T, used in postulating the corresponding Z_P values.

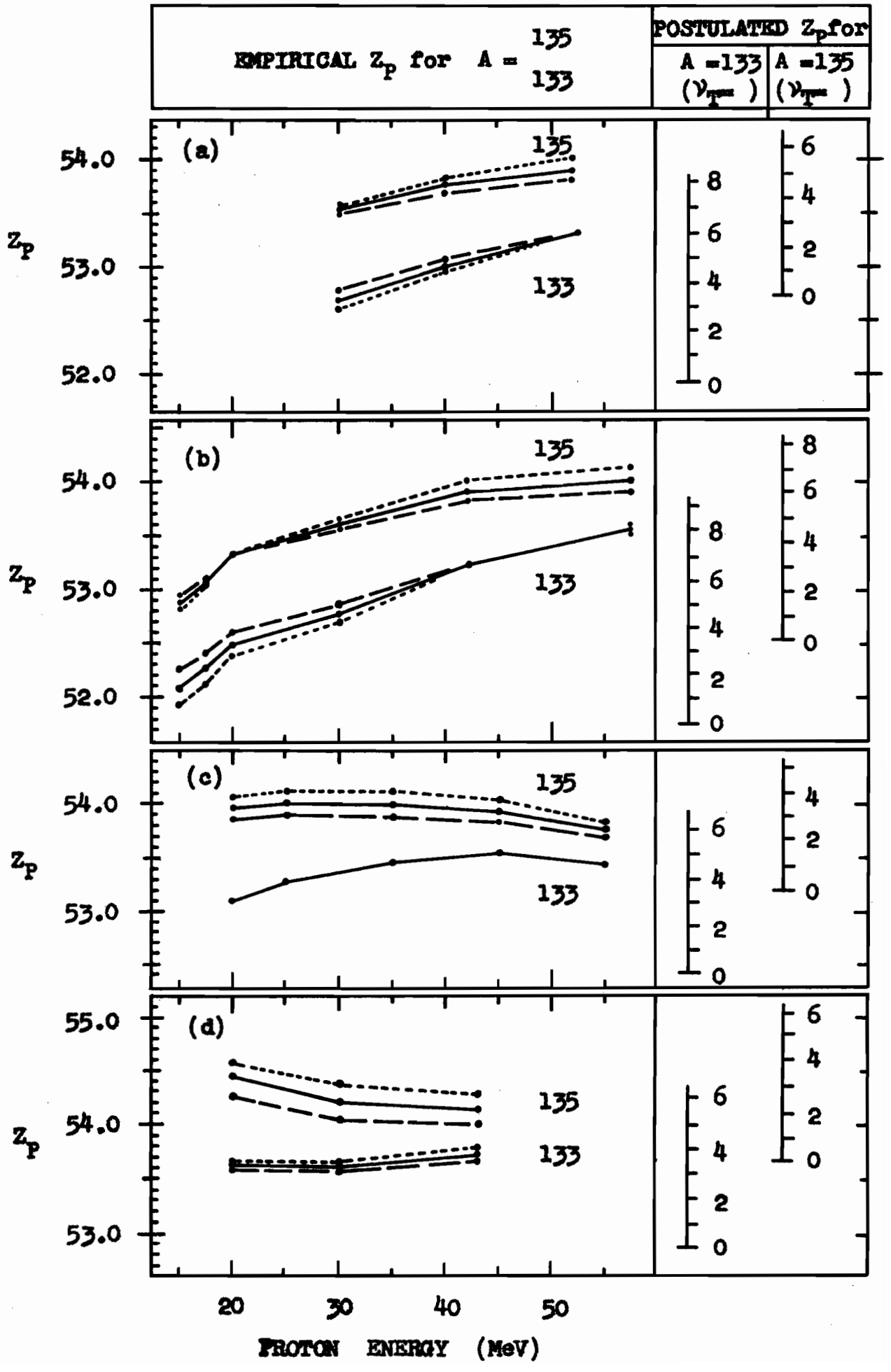
EMPIRICAL Z_p for A = 135 / 133
POSTULATED Z_p for
A =133 (ν_T=)
A =135 (ν_T=)
(a)
(b)
(c)
(d)
135
133
Z_p
54.0
53.0
52.0
55.0
20
30
40
50
PROTON ENERGY (MeV)

FIGURE 27.

The displacement of the empirical value of Z_P from beta stability, Z_A, and the effect of variations in the energy of protons inducing fission in,

(a) ^{232}Th (cf. Fig. 9(a), p.59)

(b) ^{238}U (cf. Fig. 9(b))

(c) ^{235}U

(d) ^{233}U

For the chains,

—△— A = 133

—○— A = 135

(Table 13 contains these data).

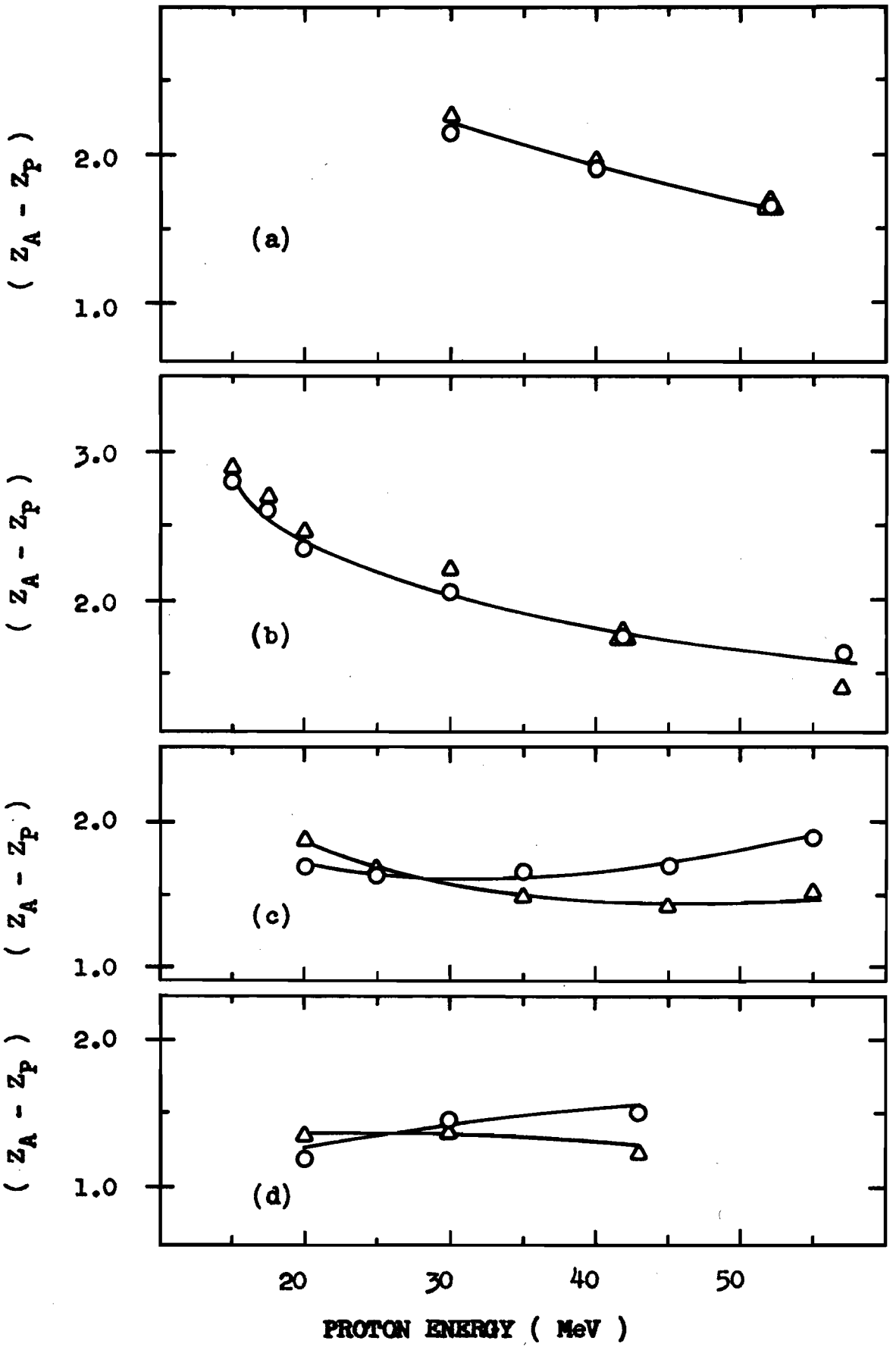
($Z_A - Z_P$)
2.0
1.0
(a)
3.0
2.0
(b)
2.0
1.0
(c)
2.0
1.0
(d)
20
30
40
50
PROTON ENERGY (MeV)

similar to that used in Fig. 9 which presented the results of previous work in this laboratory. The same early Z_A-function (COR 53, CHU 59) was used which gave 54.95 and 55.65 for Z_{133} and Z_{135}, respectively. Table 13 gives the present values of $(Z_A - Z_P)$ for the chains 133 and 135. For ^{238}U and ^{232}Th, the good agreement between these values for the two chains suggested that the change in Z_P for the mass change, A = 133 to 135, is approximately equal to the corresponding change of Z_A with mass. The latter change was (55.65 - 54.95) = 0.70. These results support the assumption made in the work on the fission of ^{232}Th with protons, by Pate, Foster and Yaffe (PAT 58). Section 1A.3.2 showed that in order to plot FUNCTION (1) with their abscissa $(Z_A - Z)$, rather than $(Z - Z_P)$, it was essential to assume that, for a particular energy, $(Z_A - Z_P)$ was constant for the mass region 130-135. For ^{235}U and ^{233}U, it will be shown later that no simple conclusions could be made.

4A.3.2 CONCLUSIONS ON THE VARIATION OF EMPIRICAL Z_P VALUES WITH TARGET AND PROJECTILE ENERGY

For ^{232}Th and ^{238}U, the variation of Z_P with energy presented in Figs. 26 and 27 agreed well with the previous data for the same mass region, presented in Figs. 8 (MCH 63) and 9 (PAT 58, DAV 63, BEN 65, PAR 66).

TABLE 13. The Empirical Z_P Values from Method 2 with C=1.20, in the Form $(Z_A - Z_P)$ for Chains 133 and 135

Exp. No.	E_p (MeV)	^{135}Xe $(Z - Z_P)$	A = 135 $(Z_A - Z_P)$	^{133}Xe $(Z - Z_P)$	A = 133 $(Z_A - Z_P)$
^{238}U					
R10	15	1.15	2.80	1.92	2.87
R15	17	0.96	2.61	1.75	2.70
R14	20	0.68	2.33	1.51	2.46
R18	30	0.41	2.06	1.24	2.19
R8	42	0.10	1.75	0.79	1.74
(R17	57)	-0.02	1.63	0.44	1.39
^{232}Th					
T6	30	0.48	2.13	1.32	2.27
T3	40	0.25	1.90	1.00	1.95
(T4	52)	0.10	1.64	0.69	1.64
^{235}U					
E10	20	0.04	1.69	0.92	1.87
E9	25	-0.02	1.63	0.72	1.67
E7	35	-0.01	1.64	0.54	1.49
E5	45	0.05	1.70	0.45	1.40
(E3	55)	0.23	1.88	0.55	1.50
^{233}U					
U5	20	-0.46	1.19	0.39	1.34
U4	30	-0.22	1.43	0.39	1.34
U3	43	-0.16	1.49	0.27	1.22

No previous Z_P data exist for the fission of ^{235}U and ^{233}U with protons. The reliability of the present results for ^{238}U and ^{232}Th suggested that interesting preliminary conclusions could be made from the limited data in the present work on ^{233}U and ^{235}U. For the proton-induced fission of ^{235}U and ^{233}U, Fig. 26 shows that the variations of Z_P with energy are significantly different from the changes, which are now fairly well established, for the proton-induced fission of ^{238}U and ^{232}Th.

The Introduction showed the difficulties and uncertainties still existing in a theoretical interpretation of charge distribution. However, in order to make a convenient semi-quantitative comparison of the present empirical values of Z_P for different targets and energies a very simple model was used. The Z_P values were assumed to be given by the simplified CCR postulate (equation (1A.2)). Fig. 26 includes vertical lines for $A_{FP} = 133$ and $A_{FP} = 135$ with divisions corresponding to the postulated Z_P values for various values of ν_{Total}, shortened here to ν_T, the total number of fission neutrons. For a particular energy, the empirical Z_P was equated with a postulated Z_P in order to estimate the corresponding value of ν_T. Figs. 28(a) and (b) show the estimated total neutron yields, ν_T, as a

FIGURE 28.

Total neutron yields, ν_T, in the fission of (Δ,○,●,□) ^{232}Th, ^{238}U, ^{235}U, and ^{233}U induced by protons with a range of energies.

These rough estimates of ν_T were obtained from Fig. 27. The estimated value of ν_T was that needed to fit an empirical value of Z_P with one postulated by the simplified CCR equation (1A.2).

Estimates were made for the independent sets of empirical Z_P values, for chains of mass,

(a) A = 135

(b) A = 133

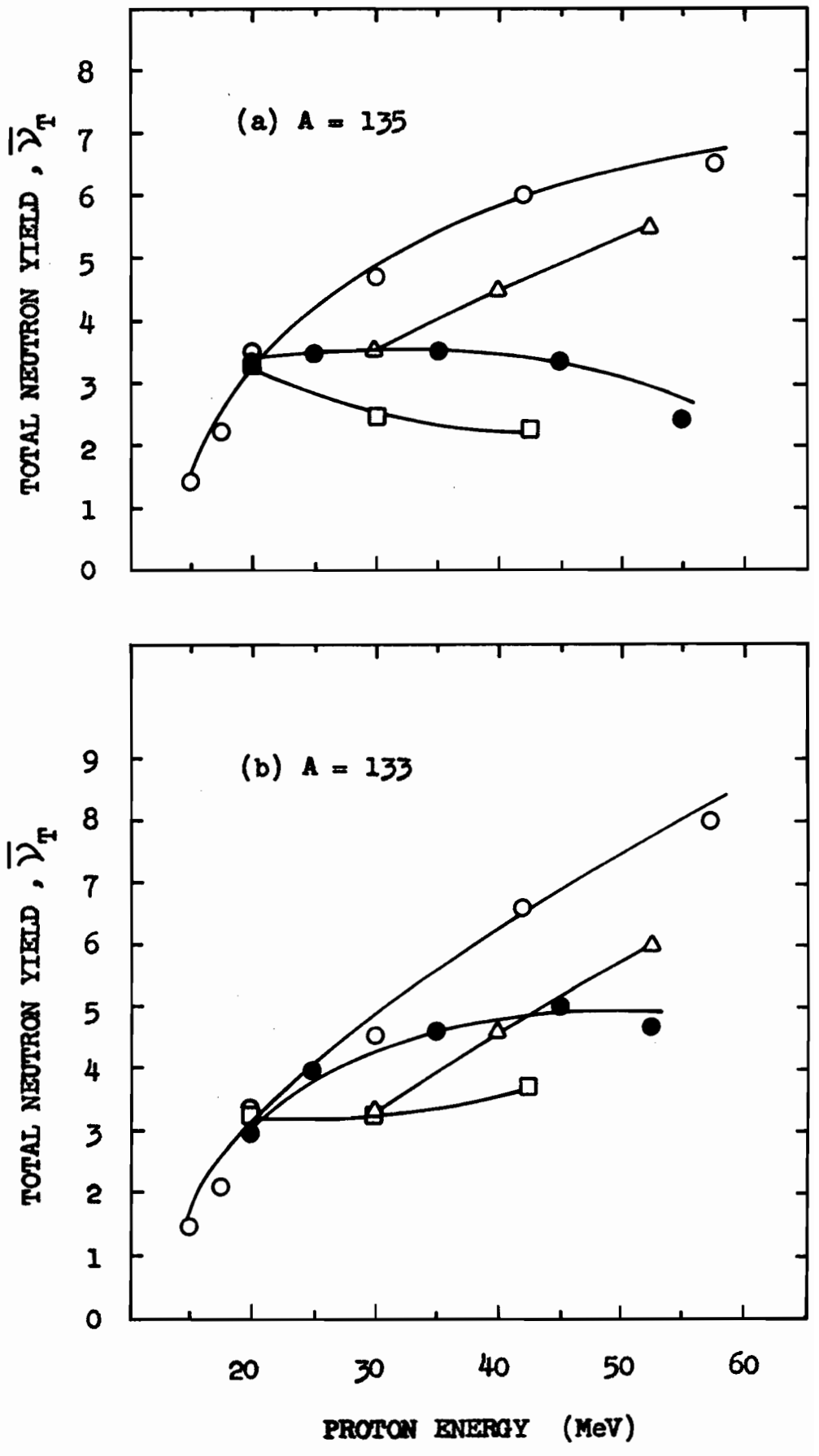
(a) A = 135
(b) A = 133
TOTAL NEUTRON YIELD , $\bar{\nu}_T$
PROTON ENERGY (MeV)
0
1
2
3
4
5
6
7
8
9
20
30
40
50
60

function of energy, from two independent sets of data for the chain 135, and the chain 133. No attempt has been made to set errors for these rough estimates of ν_T. Previously reported neutron yields suggest that the estimates here were generally too low. This discrepancy is explained qualitatively by the considerable evidence (Section 1A.3.2) that the CCR postulate predicts values of Z_P which are too high for heavy mass chains. The present method therefore would be expected to give lower limits for ν_T. The main use of Fig. 28 was to illustrate considerable differences in the fission of the different targets. Section 1B.2.6 discussed some previous more accurate data for $(d\nu_T/dE)$. The latter was suggested to have values from 0.13 - 0.16 for many fission systems with energies below about 40 MeV. For ^{238}U and ^{232}Th, Figs. 28(a) and (b) were consistent with this suggestion. However these figures suggested that, as the energy increased, the rate $(d\nu_T/dE)$ was less for the targets of lower (N/Z). These trends were reflected in the variations of Z_P in Figs. 27 and 26. Fig. 27 shows that at lower energies the targets of lower (N/Z) have Z_P values closest to beta stability, Z_A, but at 40-50 MeV the value of $(Z_A - Z_P)$ was almost equal for all four targets. Similarly, Fig. 26 shows that although at lower energies the Z_P values were higher

for the targets of lower (N/Z), at 40-50 MeV the Z_p values for a particular chain were almost equal for all four targets.

These rather surprising differences in the charge division and neutron emission in the fission of different targets cannot be confirmed with the limited data in this research, which was not primarily designed as a study of charge distribution.

A most interesting research project would be an extension of the work that has been done in this laboratory on the charge distribution, in the fission of ^{232}Th and ^{238}U, to the targets ^{233}U and ^{235}U. This would provide a more complete picture of charge distribution and should confirm and extend the present preliminary conclusions on the comparison of charge distribution in the fission of different targets.

4A.4 Z_p VALUES AND THE MAXIMUM IN EXCITATION FUNCTIONS

In an excitation function for the independent formation of a fission product, the exact position of the maximum cannot yet be explained satisfactorily. For a fission product, N(Z',A), of charge Z' and mass A, this maximum is related to the energy dependence of the value of Z_p in chain A. The value of Z_p corresponds of course to the

maximum isobaric yield in the charge distribution. If at low energy $Z' > Z_p$, then as the fission energy is increased Z_p generally increases and approaches Z'. Hicks and Gilbert (HIC 55) made the simple suggestion that the excitation function for the fission product $N(Z',A)$ would have a maximum at the energy for which $Z' = Z_p$ for chain A. For example, in the chain 135 the excitation function of ^{135}Xe should therefore show a maximum for the energy at which ^{135}Xe ($Z' = 54$) is the most probable isobar formed in chain 135.

No simple hypothesis can be expected to relate the maxima in excitation functions and in charge distribution curves because of the complexities of charge distribution, especially above medium energies, and because of the difficulty in defining the position of the broad maxima in excitation functions. However, the very simple suggestion outlined above serves as a useful guide to predict qualitatively from Z_p data the relative positions of the maxima for different fission products and different fission targets.

Fig. 26 shows that the chain 135 would have a value of $Z_p = 54$ at lower energies than chain 133. Therefore the maximum in the excitation function of ^{135}Xe should occur at

lower energy than that for ^{133}Xe. Comparing the targets ^{235}U and ^{238}U, Figs. 26(c) and (b) show that for the chain 135 the value of Z_p approaches 54 at lower energies for the former target. It might therefore be expected that for a target of lower (N/Z) the maximum in an excitation function occurs at lower energy than for a target of higher (N/Z).

The present experiments were not designed to obtain very accurate excitation functions and therefore the position of the rather flat maximum in the excitation functions of ^{135}Xe and ^{133}Xe could not be well defined. However, rough estimates of these maxima were made from the functions drawn in Figs. 18, 20 and 21 and the corresponding energies are shown in Table 14.

TABLE 14

Rough Estimates (from Figs. 18, 20 and 21) of the Proton Energy, E_p^{max}, at which the Maximum Occurred in the Excitation Function of ^{133}Xe and ^{135}Xe.

Target	E_p^{max}	
	^{133}Xe(N/Z=1.46) (MeV)	^{135}Xe(N/Z=1.50) (MeV)
^{238}U	55	47
^{232}Th	(48)[a]	42
^{235}U	45	28

(a) this maximum in Fig. 20 was particularly flat and ill-defined.

These values are now qualitatively compared with the above simple predictions, from the empirical Z_P values. As expected above, the maximum for ^{135}Xe did occur at lower energy than that for ^{133}Xe. Also as expected above, the excitation functions of ^{133}Xe and ^{135}Xe had their maxima for ^{238}U at about the same energies as for ^{232}Th, but for ^{235}U these maxima occurred at lower energies. No excitation functions were obtained for ^{233}U.

For ^{238}U, a more quantitative prediction of the maxima for ^{133}Xe and ^{135}Xe may be made from the data of Friedlander et al. (FRI 63) and of Davies and Yaffe (DAV 63). For the fission of ^{238}U, curve I in Fig. 29 shows their plot of the proton energies at which excitation functions reached a maximum for many nuclides characterized by their value of (N/Z). If curve I were extended for fission products with $(N/Z) > 1.50$, the latter would most probably have a maximum in their excitation functions at an energy < 30 MeV. The position of these maxima would be influenced not only by the variations in Z_P, but also by the rapid decrease in the total fission cross section with decreasing proton energy below about 30 MeV.

Curve I predicted that, for the fission of ^{238}U, the maxima for ^{133}Xe $(N/Z = 1.46)$ and ^{135}Xe $(N/Z = 1.50)$ should

FIGURE 29.

The axes, proton energy, E_p, versus (N/Z), are used for two different types of function,

CURVE I

CURVES II and III.

CURVE I This was taken from the work of Davies and Yaffe (DAV 63) and of Friedlander et al. (FRI 63) on the fission of ^{238}U. It shows their plot of the proton energies at which excitation functions reached their maximum for many nuclides characterized by their value of (N/Z).

CURVE II With the data for ^{238}U from the same work by Davies and Yaffe, this curve was first plotted here. It shows the empirical values of $(N/Z)_p$ from their charge distribution curves at various proton energies, E_p.

CURVE III Taken from the data in the present work on ^{238}U, this curve, similar to CURVE II, shows the function E_p versus $((A - Z_p)/Z_p)$. The two empirical functions for A = 133 and 135 were almost identical (Table 15).

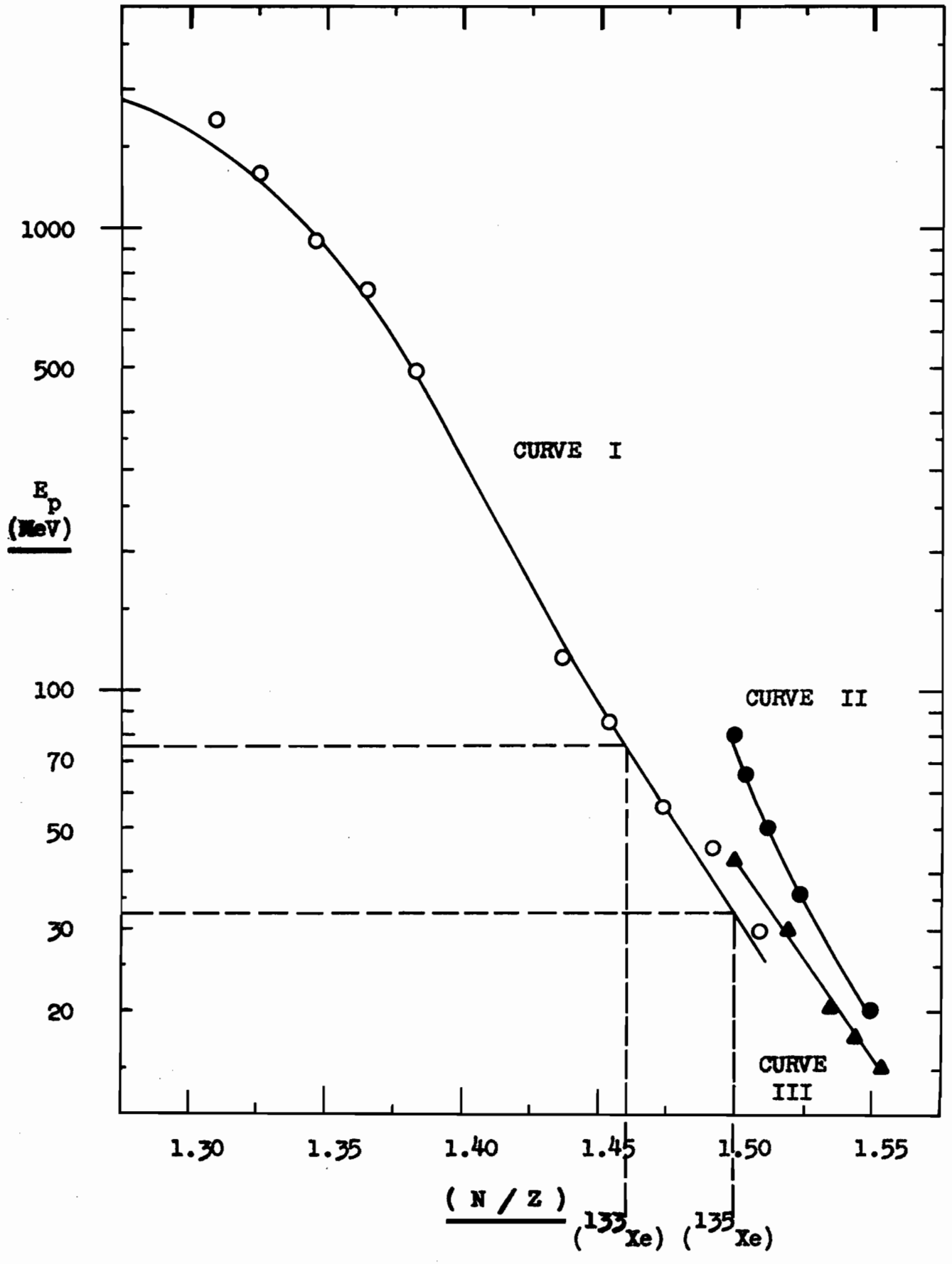
1000
500
100
70
50
30
20
E_p (MeV)
CURVE I
CURVE II
CURVE III
1.30
1.35
1.40
1.45
1.50
1.55
(N / Z)
(^{133}Xe)
(^{135}Xe)

occur at energies of 75 ± 10 MeV and 35 ± 10 MeV, respectively. These predicted energies are in reasonable agreement with those, in Table 14, which were estimated roughly from the present excitation functions.

Curve I has not yet been explained satisfactorily. It is therefore of interest to discuss it here, relative to the empirical values of Z_p. For the purpose of this simple discussion, let the curve I be applied to one isobaric chain A, with isobars of charge Z', Z' + 1, Z' + 2, etc. As the fission energy is increased Z_p increases and successively reaches values of Z', Z' + 1, Z' + 2, etc. By the simple suggestion of Hicks and Gilbert the excitation functions of these successive isobars should reach their maximum at energies when their charge equals the value of Z_p of chain A. Therefore the curve I should coincide with a function, energy versus $((A - Z_p)/Z_p)$. Curve II in Fig. 29 is the latter function, E_p versus $(N/Z)_p$, taken from the same data used by Davies et al. to plot curve I.

These two curves I and II have similar slopes, but curve II is displaced to higher values of (N/Z). The significance of this may be shown by the following example. At 35 MeV, curve I indicates that the excitation function of ^{135}Xe (N/Z = 1.50) reaches a maximum, but at this energy

curve II shows that the Z_p value of chain 135 is about 0.5 charge units lower than 54, the charge of ^{135}Xe.

The present data were insufficient to construct functions similar to curve I. The present empirical Z_p values for chains 133 and 135 were used to construct the function, E_p versus $((A - Z_p)/Z_p)$, for the limited energy range 15 to 57 MeV. Table 15 gives the values used to plot this function for ^{238}U, as curve III in Fig. 29. The two functions for chains 133 and 135 were almost identical and were plotted as the single curve III.

The two curves I and III have similar slopes, and for the limited energy range over which they can be compared they do coincide, as predicted by the simple suggestion discussed above. Therefore the excitation function of ^{135}Xe has a maximum at about the same energy at which ^{135}Xe is the most probable isobar formed in chain 135 (i.e. when $Z_p = 54$ for chain 135). There is a small discrepancy between this conclusion and that from the comparison of curves I and II above. With the limited data available the only conclusion that can be made here is that at present the maximum in excitation functions can be predicted only very approximately from empirical Z_p data. The latter data are however useful to predict the relative positions of the maximum for

TABLE 15. The Empirical $(Z-Z_p)$ Values for ^{238}U (cf. Table 12), from Method 2 with C = 1.20, in the form $((A-Z_p)/Z_p)$ for Chains 133 and 135

^{238}U Exp. No.	E_p (MeV)	^{135}Xe $(Z - Z_p)$	A = 135 $((135/Z_p) - 1)$	^{133}Xe $(Z - Z_p)$	A = 133 $((133/Z_p) - 1)$
R10	15	1.15	1.556	1.92	1.555
R15	17	0.96	1.545	1.75	1.545
R14	20	0.68	1.530	1.51	1.535
R18	30	0.41	1.520	1.24	1.520
R8	42	0.10	1.505	0.79	1.500
(R17)	57	(-0.02)	(1.500)	(0.44)	(1.485)

different fission products in different fission systems.

For ^{232}Th and particularly for ^{235}U and ^{233}U, it would be interesting to obtain a function like the curve I which was determined for ^{238}U. The curve for ^{232}Th should be very similar to curve I, because the (N/Z) of the two targets are nearly equal and the empirical Z_p values vary with energy in a similar way. For ^{235}U and ^{233}U, the differences in the function, Z_p versus energy, suggested by this work, may produce a rather different shaped function to curve I, and it would be expected to be displaced towards lower values of (N/Z) corresponding to the lower value of (N/Z) for these two targets.

4A.5 FRACTIONAL AND TOTAL CHAIN YIELDS FOR A = 133 AND 135

The Introduction showed that there are still large uncertainties involved in predicting fission yields for various fission systems, and more yield data are therefore required. From the present research many absolute and relative yields have been reported elsewhere in this thesis. The following fractional chain yields and total chain yields could also be obtained.

For those irradiations for which $(Z - Z_p)$ values were obtained (Table 12) the corresponding fractional yields

can be obtained from equation (1A.3) or read from the appropriate FUNCTION (1) in Fig. 25.

Table 16 lists those results from which total chain yields could be obtained for A = 133 and 135. For C = 1.20 and 1.45 this table gives the fractional yields, f_N, and absolute cross sections, σ_N, (Tables 9 and 10) for the independent formation of ^{135}Xe, and cumulative formation of ^{133}I. The absolute total chain yields, σ_T, were calculated with the simple expression, $\sigma_T = (\sigma_N/f_N)$. Table 16 gives these yields, which were estimated to have an uncertainty of about 30%.

For proton-induced fission very few chain yields have been reported previously (cf. Section 1A.3.1). For the proton-induced fission of ^{238}U, the present total chain yields were in agreement with those for the same mass region determined previously in this laboratory (DAV 63, PAR 66), and by Stevenson et al. (STE 58) (cf. Fig. 1). This agreement suggested that there were no serious systematic errors in the present results.

For fission of ^{232}Th and ^{238}U for a particular energy, the chain yields for A = 133 and 135 were about the same. These results support the assumption, made in previous studies of charge distribution made in this

TABLE 16. Total Chain Yields for A = 133 and 135

Exp. No.	E_p (MeV)	Indep. yields of ^{135}Xe			Cum.	yields of ^{133}I		$\left(\frac{\sigma}{f}=\right)$ Total Chain Yields (mb)			
		σ (mb)	f (from method 2) C=1.20	f (from method 2) C=1.45	σ (mb)	f (from method 2) C=1.20	f (from method 2) C=1.45	A = 135 C=1.20	A = 135 C=1.45	A = 133 C=1.20	A = 133 C=1.45
^{238}U											
R15	17	6.5*	0.24	0.24	21.1*	0.96	0.96	27.1	27.1	22.0	22.0
R14	20	13.3*	0.35	0.34	31.4*	0.92	0.92	38.0	39.1	34.1	34.1
R8	42	28.9	0.51	0.47	36.6	0.66	0.65	56.6	61.4	55.4	56.3
**(R17)	57	37.0	0.52	0.46	35.8	0.47	0.45	71.1	80.4	76.2	79.5
^{232}Th											
T6	30	21.1	0.42	0.41	38.9	0.87	0.87	50.2	51.4	44.7	44.7
T3	40	24.9	0.49	0.46	41.6	0.76	0.75	50.8	54.2	54.7	55.4
**(T4)	52	23.6	0.51	0.47	33.4	0.60	0.59	46.3	50.3	55.6	56.7
^{235}U											
E10	20	21.5	0.51	0.47	32.8	0.72	0.71	42.2	45.7	45.6	46.2
E9	25	36.6	0.51	0.46	49.5	0.62	0.61	71.7	79.5	79.8	81.1
E7	35	28.2	0.51	0.46	37.5	0.52	0.51	55.3	61.3	72.1	73.5
E5	45	32.7	0.51	0.47	44.2	0.47	0.46	64.1	69.5	94.0	96.0
**(E3)	55	28.0	0.49	0.46	45.7	0.53	0.51	57.2	60.9	84.3	87.6

* Large uncertainty in monitor cross section at this energy

** At this energy, charge distribution curves probably have $C \geq 1.45$

laboratory, that the mass yield curve has a flat peak in this mass region for these fission systems. However, for the fission of ^{238}U with 14.7-MeV neutrons, James et al. (JAM 64) found that the chain yield for A = 133 was much higher than for A = 135. They therefore suggested that fine structure existed in the mass distribution. In Appendix B these results have been discussed and a possible error suggested in the measured yields for chain 133.

4B. RESULTS AND DISCUSSION

SECTION B

ISOMERIC YIELD RATIOS IN FISSION

4B.1 EXPERIMENTAL ISOMER RATIOS OF ^{133}Xe

In Section 4A.1 are found the independent cross sections for ^{133m}Xe and ^{133g}Xe, which were used here to give the isomeric yield ratios for ^{133}Xe. Table **17** and Figs. 30(a)-(d) give these ratios, with the yield of ^{133g}Xe, uncorrected and also with the simplified growth correction discussed previously. These results were obtained with $\alpha_K = 4.4$ ($\alpha_T = 6.3$), but the results with other coefficients will be given below.

The experiments were designed primarily to determine precise isomer ratios for several fission targets with a range of proton energies. The precision and extent of these measurements were determined by the uncertainties discussed in Section 3.3 and by the further considerations given below.

(i) The growth correction for ^{133g}Xe was minimized by a fast sweep (a). This correction could still be considerable if there were a high ratio, $R^{133}_{c/i}$, of the cumulative yield of ^{133}I to the independent yield of ^{133}Xe. Fig. 22 showed that this was true only for proton energies

TABLE 17. Isomeric Yield Ratios for ^{133}Xe Obtained with $\alpha_K = 4.4$ ($\alpha_T = 6.3$)

Exp. No.	E_p (MeV)	Yield Ratios $\frac{\sigma_m}{\sigma_g}'$ Uncorr.	Yield Ratios $\frac{\sigma_m}{\sigma_g}''$ "Over-corr."	$R_{c/i}^{133}$
^{232}Th				
T6	30	0.89	(1.03)	7.21
T3	40	0.88	0.98	3.37
T4	52	0.96	1.01	1.74
T1	65	0.99	1.04	1.53
T5	75	1.05	1.11	1.50
T2	85	1.08	1.13	1.25
^{238}U				
R10	15	0.64	(7.45)	61
R15	17	0.74	(1.79)	28
R14	20	0.61	0.84	12.2
R18	30	0.95	1.10	5.93
R8	42	0.83	0.91	2.15
R17	57	1.09	1.13	1.06
R9	65	0.92	0.97	1.46
R11	75	1.13	1.21	1.75
R16	75	1.14	1.20	1.89
R12	85	0.95	1.01	1.64
^{235}U				
E10	20	0.81	0.86	2.81
E9	25	0.88	0.91	1.85
E7	35	1.05	1.10	1.27
E5	45	0.95	0.99	1.09
E3	55	1.11	1.17	1.30
E8	70	1.10	1.15	1.29
E4	85	1.02	1.06	1.13
^{233}U				
U5	20	0.93	0.95	0.96
U4	30	0.89	0.91	0.95
U3	42	1.04	1.06	0.76
U1	55	0.97	—no sweep (b)—	
U2	70	0.94	0.96	0.78

FIGURE 30.

The energy dependence of the experimental isomeric yield ratios for ^{133}Xe, from the proton-induced fission of,

(a) ^{232}Th

(b) ^{238}U

(c) ^{235}U

(d) ^{233}U

The values are shown for $\alpha_K = 4.4$ ($\alpha_T = 6.3$),

o uncorrected,

—●— "overcorrected".

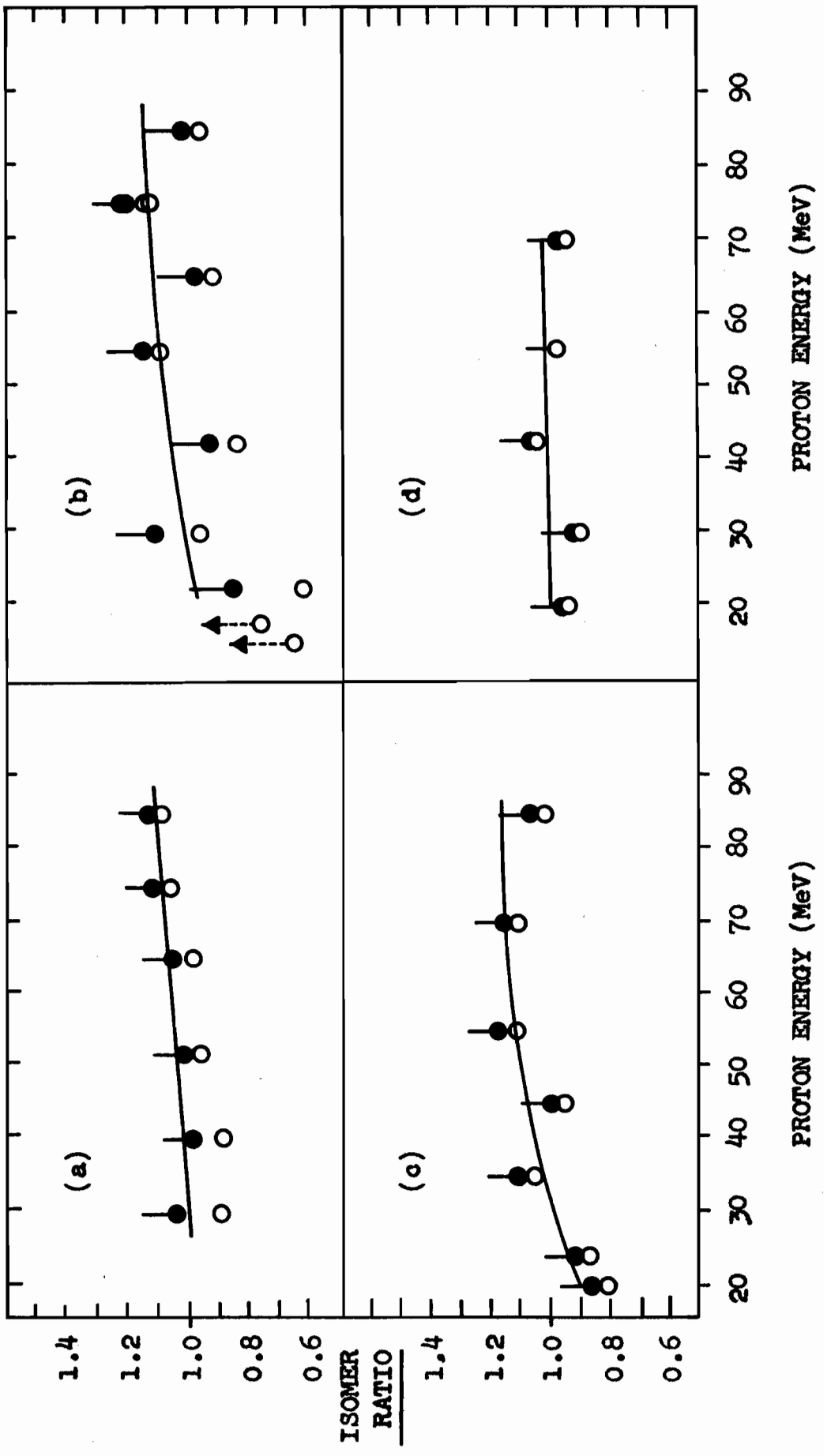
ISOMER RATIO
1.4
1.2
1.0
0.8
0.6
(a)
(b)
(c)
(d)
20
30
40
50
60
70
80
90
PROTON ENERGY (MeV)

below about 35 MeV with ^{232}Th and ^{238}U, and below about 20 MeV with ^{235}U. The growth corrections were small in most of the present isomer ratios and were within the estimated experimental error of 10-20% (cf. Section 3.3). These ratios do not therefore reflect the change of charge distribution with energy, as do the data for several other fission isomer ratio studies (POL 60, TIL 63b, SIK 65).

(ii) There were only small relative errors in measuring the gamma peaks for the two isomers. The same xenon sample was used and the two peaks, taken with the same amplifier gain, were obtained on the same spectrum. The calibration with the beta proportional gas counter (Appendix B) minimized the relative errors in the subtraction of gamma background activities and in the efficiencies of the two peaks.

(iii) Section 4A.1 explained that the yields of ^{133m}Xe, ^{133g}Xe and $^{133m+g}Xe$ were computed with four values of α_T (6.3, 7.3, 8.3 and 9.3), because of the uncertainty in this coefficient. It was shown in Section 4A.1 that changes in α_T did not cause a very serious error in the cross section of $^{133m+g}Xe$ nor in the yield ratio $R^{133}_{c/i}$. However, the isomer ratio was strongly dependent on the value of α_T. Table 18 compares the isomer ratios for the four values of

TABLE 18. Effect of α_T for ^{133m}Xe on the Isomer Ratios of ^{133}Xe

(where σ_g' = Uncorrected yield of ^{133g}Xe
σ_g'' = "Over-corrected" yield of ^{133g}Xe)

Exp. No.	$\alpha_T = 6.3$		$\alpha_T = 7.3$		$\alpha_T = 8.3$		$\alpha_T = 9.3$	
	$\frac{\sigma_m}{\sigma_g'}$	$\frac{\sigma_m}{\sigma_g''}$	$\frac{\sigma_m}{\sigma_g'}$	$\frac{\sigma_m}{\sigma_g''}$	$\frac{\sigma_m}{\sigma_g'}$	$\frac{\sigma_m}{\sigma_g''}$	$\frac{\sigma_m}{\sigma_g'}$	$\frac{\sigma_m}{\sigma_g''}$
^{232}Th								
T6	0.89	1.03	1.28	1.56	1.98	2.62	3.53	5.80
T3	0.88	.98	1.27	1.46	1.96	2.37	3.46	4.79
T4	0.96	1.01	1.42	1.52	2.29	2.52	4.49	5.37
T1	0.99	1.04	1.48	1.58	2.41	2.67	4.95	6.00
T5	1.05	1.11	1.61	1.73	2.75	3.06	6.41	8.16
T2	1.08	1.13	1.67	1.77	2.90	3.19	7.20	9.00
^{238}U								
R10	0.64	-	0.86	-	1.18	-	1.69	-
R15	0.74	-	1.03	-	1.48	-	2.28	-
R14	0.61	0.84	0.82	1.19	1.11	1.80	1.55	3.03
R18	0.95	1.10	1.41	1.70	2.25	2.97	4.36	7.60
R8	0.83	0.91	1.18	1.33	1.77	2.09	2.96	3.84
R17	1.09	1.13	1.68	1.76	2.93	3.17	7.33	8.86
R9	0.92	0.97	1.34	1.43	2.11	2.31	3.90	4.59
R11	1.12	1.21	1.76	1.96	3.16	3.77	8.79	14.83
R16	1.14	1.20	1.78	1.92	3.22	3.65	9.24	13.24
R12	0.95	1.01	1.40	1.52	2.23	2.53	4.29	5.41
^{235}U								
E10	0.81	0.86	1.15	1.23	1.70	1.87	2.78	3.21
E9	0.88	0.91	1.27	1.33	1.94	2.08	3.42	3.81
E7	1.05	1.10	1.61	1.70	2.74	3.00	6.33	7.75
E5	0.95	0.99	1.41	1.47	2.25	2.41	4.37	4.92
E3	1.11	1.17	1.72	1.85	3.05	3.44	8.05	11.08
E8	1.10	1.15	1.71	1.82	3.02	3.33	7.86	10.12
E4	1.02	1.06	1.53	1.62	2.55	2.79	5.50	6.57
^{233}U								
U5	0.93	0.95	1.36	1.40	2.16	2.24	4.05	4.33
U4	0.89	0.91	1.28	1.32	1.98	2.06	3.51	3.74
U3	1.04	1.06	1.58	1.62	2.27	2.79	6.00	6.58
U1	0.97	-	1.44	-	2.32	-	4.61	-
U2	0.94	0.96	1.38	1.42	2.18	2.29	4.14	4.48

α_T. The ratios are given uncorrected and "overcorrected", and Fig. 31 shows the latter set of isomer ratios.

The uncertainties in the isomer ratios, discussed above and in Section 3,3, are briefly summarized in this paragraph. Uncertainties of 10% were estimated for most of the results in Table 17, calculated for $\alpha_T = 6.3$. A higher value of 15% was given for most of the ^{238}U results which were obtained at the beginning of this work when the experimental technique had not been fully developed. Uncertainties of up to 20% were estimated for the lowest energy results for ^{238}U and ^{232}Th. These had larger growth corrections and larger graphical errors particularly in the ^{133m}Xe yields.

The large uncertainty in the value of α_T was not included in these estimated errors.

4B.2 THEORETICAL CALCULATIONS OF THE SPIN DISTRIBUTIONS DURING FRAGMENT DE-EXCITATION

The computations that have been made, their input data and their results are discussed and then used to consider the experimental isomer ratios from this and other fission studies. The calculations were introduced in Section 1B.2. Most of them were made for the spin distributions during the de-excitation of the fragments.

FIGURE 31.

The experimental isomeric yield ratios for ^{133}Xe, from proton-induced fission of

(a) ^{232}Th

(b) ^{238}U

(c) ^{235}U

(d) ^{233}U

The "overcorrected" values are shown for four values of the total internal conversion coefficient.

● $\alpha_T = 6.3$

▲ $\alpha_T = 7.3$

■ $\alpha_T = 8.3$

⊖ $\alpha_T = 9.3$

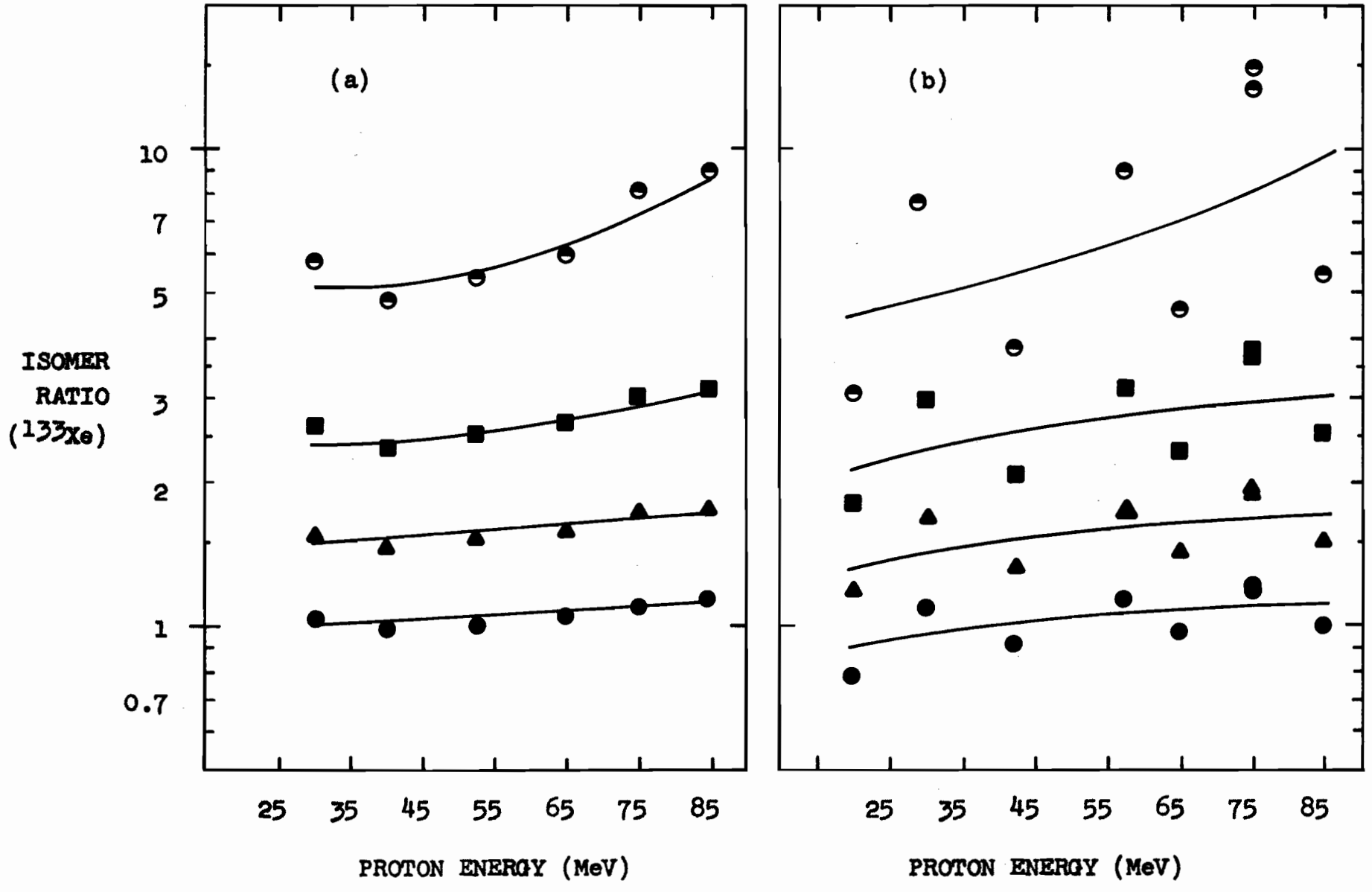
(a)
(b)
ISOMER RATIO (^{133}Xe)
10
7
5
3
2
1
0.7
25
35
45
55
65
75
85
PROTON ENERGY (MeV)
PROTON ENERGY (MeV)

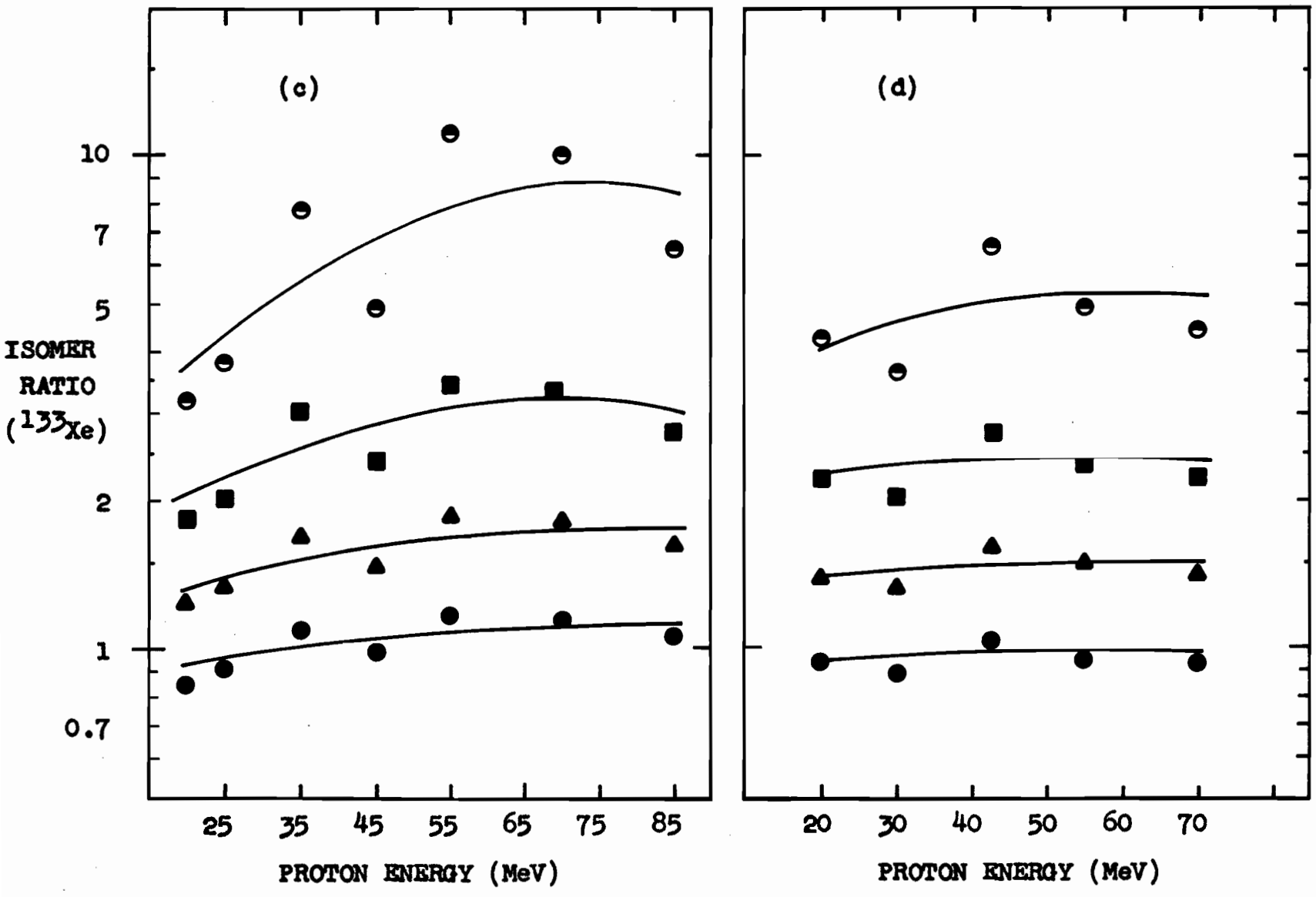
(c)
(d)
10
7
5
2
1
0.7
ISOMER RATIO (^{133}Xe)
25 35 45 55 65 75 85
20 30 40 50 60 70
PROTON ENERGY (MeV)
PROTON ENERGY (MeV)

185b

4B.2.1 INPUT DATA FOR STAGES 1 AND 2

Stage One, Neutron Emission from the Fragments

Table 19(a) summarizes the input data for this stage of the calculation. The value of N_n was fixed at three in all calculations; it is estimated that about three neutrons are emitted from a ^{136}Xe fragment from fission induced by 30-MeV protons.

The HHV program was slightly modified to allow equation (1B.1) to define the input spin distribution for the first neutron emission.

Values of $\overline{E}_{n_i}$ were approximated using the simple assumption that the average neutron kinetic energy is equal to twice the maximum nuclear temperature of the residual fragment, t_{max} (ERI 60). Here t_{max} was related to the maximum excitation energy of the residual fragment, U_{max}, by the equation $U_{max} = at^2$, with $a = A/8$. The neutron transmission coefficients for a nucleus with A = 136 were read from the curves of Feld et al. (FEL 51), for a nuclear radius parameter $r_o = 1.5$fm.

The spin cutoff factor, σ, was assumed to decrease as the fragment excitation energy decreases with successive neutron emissions. Very little information is

TABLE 19(a) and (b). Input Data for Stages 1 and 2 of the Fragment De-excitation Computations

(a) For Part 2 of HHV FORTRAN program (HAF 62)

Input Parameters \ Neutron Emission Step		1st.	2nd.	3rd.
Spin Distribution		Assumed; formula (1) B=3,4.6,7,9,11	Output from 1st step	Output from 2nd step
$\overline{E}_{n_i}$ (MeV)		2.0	1.5	1.0
$T_{\ell'}(\overline{E}_{n_i})$ / ℓ'				
0		0.73	0.70	0.60
1		0.66	0.60	0.50
2		0.51	0.40	0.25
3		0.25	0.14	0.05
4		0.04	0.01	-
$\sigma_{(n)}$	Trial i	6	5	4
	Trial ii	7	6	5

(b) For Part 3 of HHV FORTRAN program

Input Parameters \ Gamma-cascade Step		1st.	2nd to 5th.
Spin Distribution		Output following 3rd neutron emission	Output from previous step
$\sigma_{(\gamma)}$	Trial i	3	3
	Trial ii	4	4
ℓ	Trial I	1	1
	Trial II	2	(2nd,3rd-, =2 : 4th,5th-, =1)

available to estimate the values of σ. Values were chosen intermediate to those used in most spallation studies ($\sigma = 4 \pm 1$) and to the higher values calculated from formula (1B.3). Two sets of cutoff factors were tried in trial (i) and trial (ii).

Stage Two, the Gamma Ray Cascade from the Fragments

Table 19(b) summarizes the input data for this stage of the calculation. The value of N_γ was fixed at six in all calculations (i.e. Part 3 of the HHV program was used five times). A cascade of six gamma rays is larger than has been observed experimentally, but the distribution of spin following any smaller number of emissions was also contained in the output for the corresponding step of the computation. It is estimated that $N_\gamma = 4 \pm 1$, for medium-energy fission.

The spin cutoff factor was assumed to be constant throughout the gamma cascade since the energy change in the fragment for each gamma ray emission is only about 1 MeV.

Calculations have been made for both dipole radiation, $\ell = 1$, and quadrupole radiation, $\ell = 2$.

Fixed values of N_n and N_γ were chosen in order to limit the large number of possible combinations of input parameters. However, the effect of other N_n and N_γ values could be estimated from the results. Stage One and Stage Two

were computed with Parts 2 and 3 of the HHV FORTRAN program on the IBM 7040 machine at the McGill University Computing Centre.

4B.2.2 RESULTS FOR STAGES ONE AND TWO

In Fig. 32 the calculated spin distributions, following each of the three neutrons and five gamma ray emissions, are conveniently characterized by their root mean square angular momentum, $\sqrt{\overline{J_f^2}}$. The number above the line in Fig. 32 is the value of the spin cutoff factor, σ, used for that step of the computation. To the right of the figure are given the B values used for the assumed initial fragment spin distribution, given by equation (1B.1). Computations were made for B = 3, 4,6, 7, 9 and 11. Fig. 33 shows an example of the frequency distribution curves, calculated for B = 7 and $\sigma_{(n)}$ = 6, 5, 4 and $\sigma_{(\gamma)}$ = 3.

4B.2.3 STAGE THREE, THE FINAL GAMMA RAY IN THE CASCADE

This stage predicts a value of the isomer ratio from the calculated distribution of spin following the last-but-one emission in the gamma cascade. The spin states in this distribution were divided between the two isomeric states by an over-simplified model which assumes that one final gamma ray with a suitable multipolarity allows these

FIGURE 32.

Values of $\sqrt{J_f^2}$ characterizing the spin distribution at each step of the fragment de-excitation. The numbers are the values of the spin cutoff factor, σ, used for particular steps of the computation. Only dipole gamma radiation was used here.

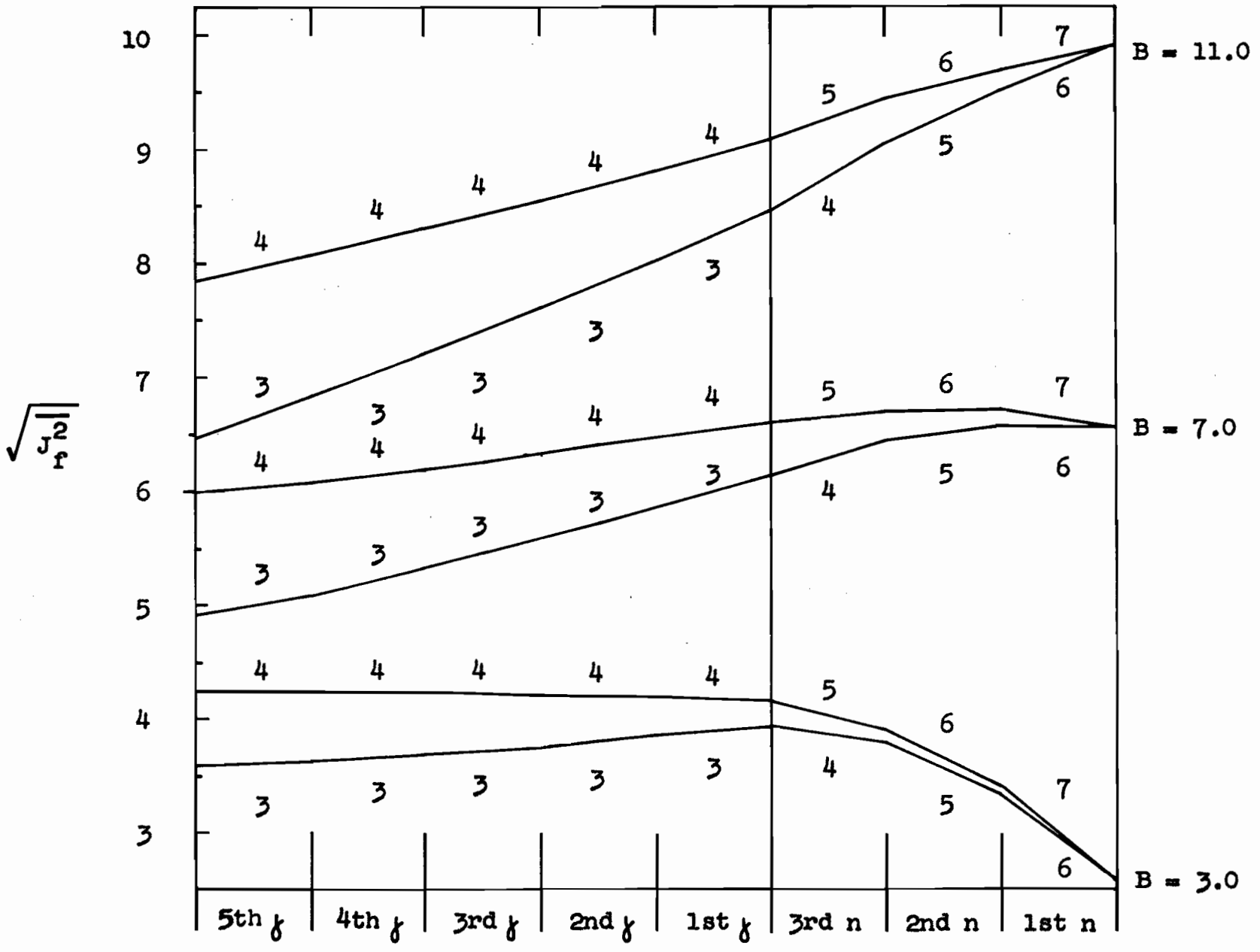
$\sqrt{\overline{J_f^2}}$
10
9
8
7
6
5
4
3
B = 11.0
B = 7.0
B = 3.0
5th γ
4th γ
3rd γ
2nd γ
1st γ
3rd n
2nd n
1st n
STAGES IN THE FRAGMENT DE-EXCITATION

FIGURE 33.

Theoretical Probability Distributions of the spin of fragments, during their de-excitation.

DISTRIBUTION A. is the initial distribution given by equation (1B.1), with B = 7.

DISTRIBUTION B. is the spin distribution after the emission of three neutrons and five dipole gamma rays.

The spin-dividing line, $J_f = 7/2$, is shown for Class 2 isomers (3/2, 11/2).

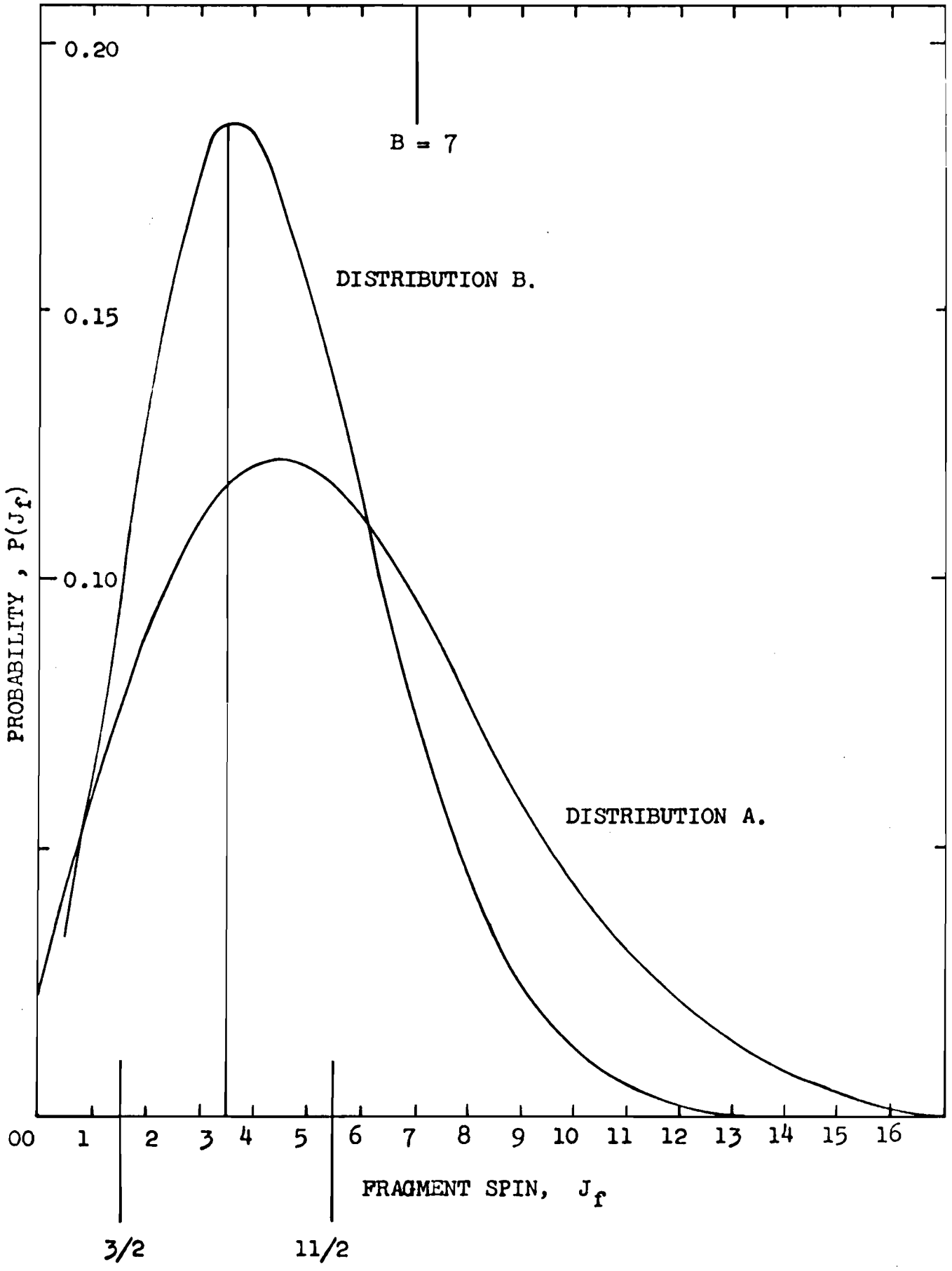
0.20
0.15
0.10
B = 7
DISTRIBUTION B.
DISTRIBUTION A.
PROBABILITY , P(J_f)
00 1 2 3 4 5 6 7 8 9 10 11 12 13 14 15 16
FRAGMENT SPIN, J_f
3/2
11/2

states to decay to the isomeric state with the nearest spin. If a state has a spin equally placed between the two isomeric spins, it is simply assumed that half of these states decay to each isomer. As an example, for spin-pair Class 1 isomers (9/2, 1/2), states in the final calculated spin distribution with spins less than 5/2 populate the low spin isomer; states with spins greater than 5/2 populate the high spin isomer; whereas states with a spin of 5/2 divide equally between the two isomers.

This stage of the isomer ratio calculation could have been performed by adding the calculated probabilities for individual spin states according to the simple prescription outlined above. We have employed a direct geometric method using the cumulative spin distribution function curves. Fig. 34 gives an example of these curves for the same output data used for the frequency distribution curves in Fig. 33. The geometric method is as follows, for the three spin-pair classes of isomers in Table 3.

Class 1 isomers (9/2, 1/2)

A vertical line at $\overline{J}_f = 2$ cuts the normalized cumulative spin distribution (Fig. 34) at ordinate Y_1 which by simple geometry represents the fractional population of the low spin isomer, thus the isomer ratio is simply $(1 - Y_1) / Y_1$.

FIGURE 34.

Theoretical normalized cumulative distributions of the spin of fragments, during their de-excitation. With the same initial spin distribution shown in Fig. 33 as DISTRIBUTION A, the following modified distributions are shown, after the emission of

a. one neutron,

b. three neutrons,

c. three neutrons and three dipole gamma rays

d. three neutrons and three quadrupole gamma rays.

The intersection points, Y_i, and the corresponding ordinate, on the right of the figure, are described in the text.

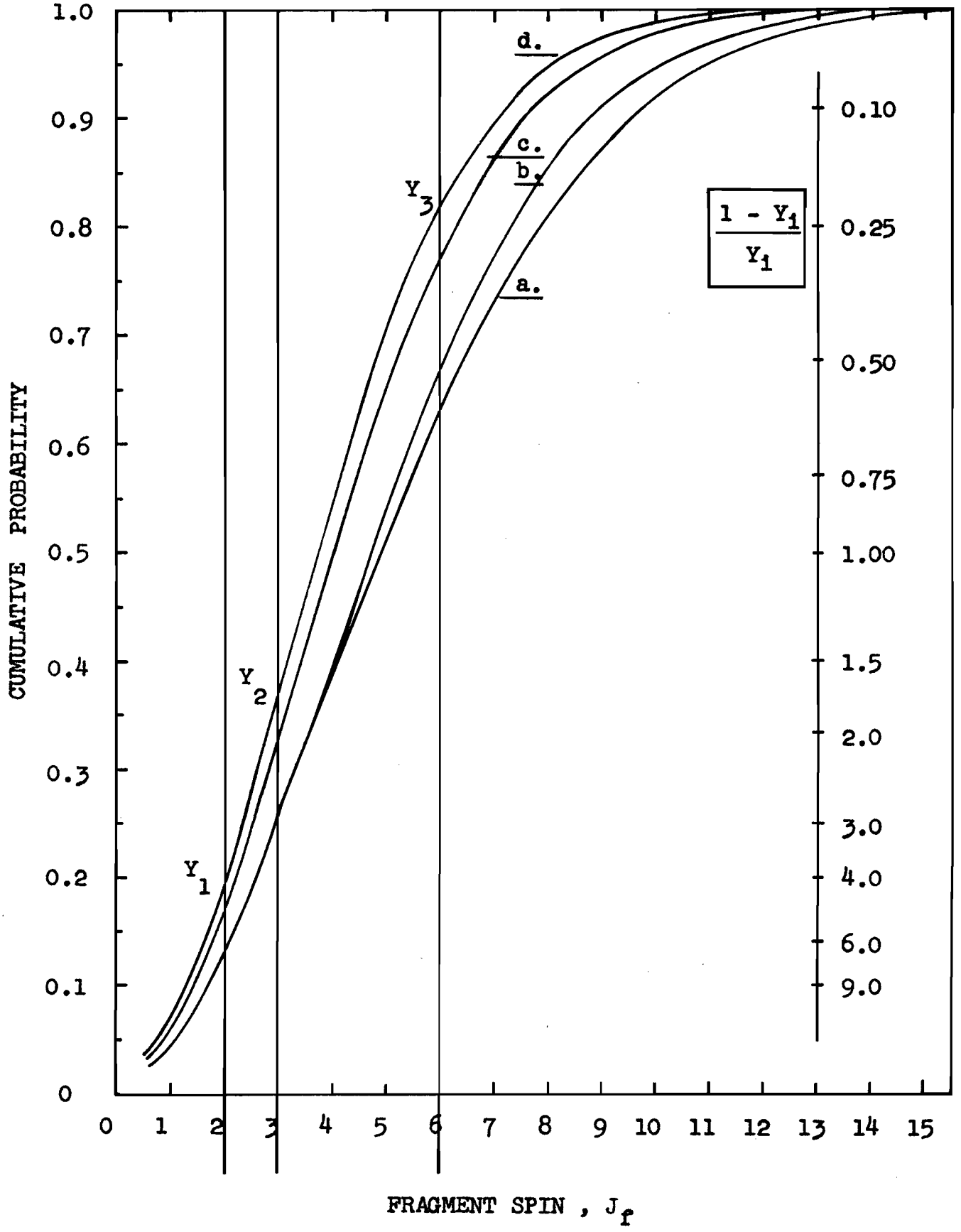
1.0
0.9
0.8
0.7
0.6
0.5
0.4
0.3
0.2
0.1
0
CUMULATIVE PROBABILITY
0 1 2 3 4 5 6 7 8 9 10 11 12 13 14 15
FRAGMENT SPIN , J_f
Y_1
Y_2
Y_3
d.
c.
b.
a.
$\frac{1 - Y_1}{Y_1}$
0.10
0.25
0.50
0.75
1.00
1.5
2.0
3.0
4.0
6.0
9.0

Class 2 isomers (11/2, 3/2)

By the same reasoning, a vertical line at $\bar{J}_f = 3$ cuts the cumulative distribution at the ordinate Y_2 so that the isomer ratio from this distribution is given by $(1 - Y_2) / Y_2$.

Class 3 isomers (8, (5), 4)

Although the ^{134}Cs isomers have spins of 4 and 8 the spin-pair to be considered in this stage of the calculation is (5,8) because of a state of intermediate energy with spin 5 which acts as the effective low spin isomer for our model. Therefore a vertical line at $\bar{J}_f = 6$ which cuts the cumulative distribution at the ordinate Y_3 gives the isomer ratio as $(1 - Y_3) / Y_3$.

The ordinate on the right of Fig. 34 gives the isomer yield ratio corresponding to the intersections of the cumulative spin distributions and the vertical dividing-spin lines ($\bar{J}_f = 2$, 3 or 6.). This type of figure gives a good direct representation of the isomer ratio for isomer pairs of different classes from the distributions calculated at each step of the fragment de-excitation, for a particular assumed B value.

4B.2.4 THEORETICAL ISOMER RATIOS

Figures, similar to Fig. 34, were constructed for

the five values of B in order to obtain functions of the type shown in Fig. 35. This figure shows the predicted isomer ratios for the three isomer classes as a function of B, or as a function of the alternative abscissa $\sqrt{\overline{J_f^2}}$. The value of B is nearly equal to $\sqrt{\overline{J_f^2}}$ at the higher values; and $\overline{J}_f$ has a slightly lower value. All the lines in Fig.35 are for the same set of σ values ($\sigma_{(n)}$ = 6, 5, 4 and $\sigma_{(\gamma)}$ = 3) and for the same N_n value equal to 3; the solid lines are for $(N_\gamma - 1) = 3$ and the dashed lines are for $(N_\gamma - 1) = 5$.

All the results discussed so far have assumed only dipole gamma ray transitions. The evidence already discussed for the existence of quadrupole transitions in fission made it necessary to consider the effect of using $\ell = 2$, in place of $\ell = 1$, in the gamma cascade calculation. Computations were made with N_γ still equal to 6, but the first three gamma rays were taken to have $\ell = 2$. Fig. 37 represents some of these results (cf. Fig. 32). Fig. 38 (cf. Fig. 35) shows the predicted isomer ratios for the three isomer classes, for three assumed B values. All the lines in Fig. 38 are for $N_n = 3$ and $(N_\gamma - 1) = 3$; only the long dashed lines are for three quadrupole transitions, the other lines are for three dipole transitions. The solid and long dashed

FIGURE 35.

The theoretical values of the isomer ratios for three spin pair classes of isomers (cf. Table 3, p. 87). The values were computed with initial fragment spin distributions given by equation (1B.1) and characterized by the value of B. The set of spin cutoff factors used in the computation was σ_n = 6, 5, 4 and σ_γ = 3. The number of neutrons emitted, N_n, was 3 and two different gamma cascades were used.

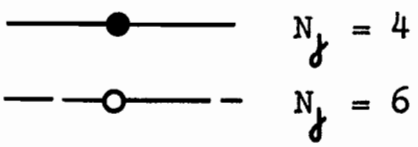

Only dipole gamma radiation was used. The lower abscissa shows the corresponding $\sqrt{\overline{J_f^2}}$ of the initial spin distributions.

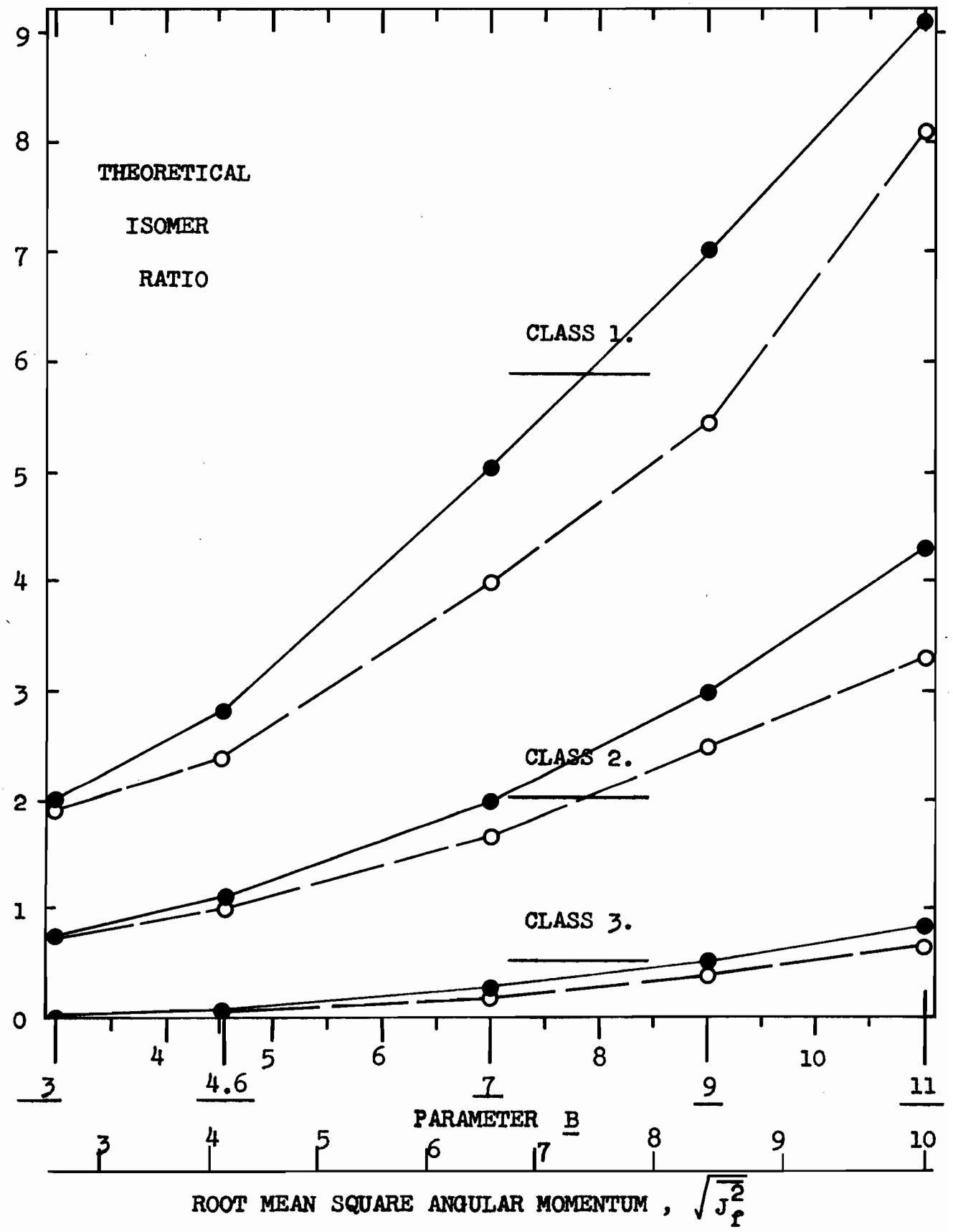
THEORETICAL
ISOMER
RATIO
CLASS 1.
CLASS 2.
CLASS 3.
0
1
2
3
4
5
6
7
8
9
3
4
4.6
5
6
7
8
9
10
11
PARAMETER B
ROOT MEAN SQUARE ANGULAR MOMENTUM , $\sqrt{J_f^2}$

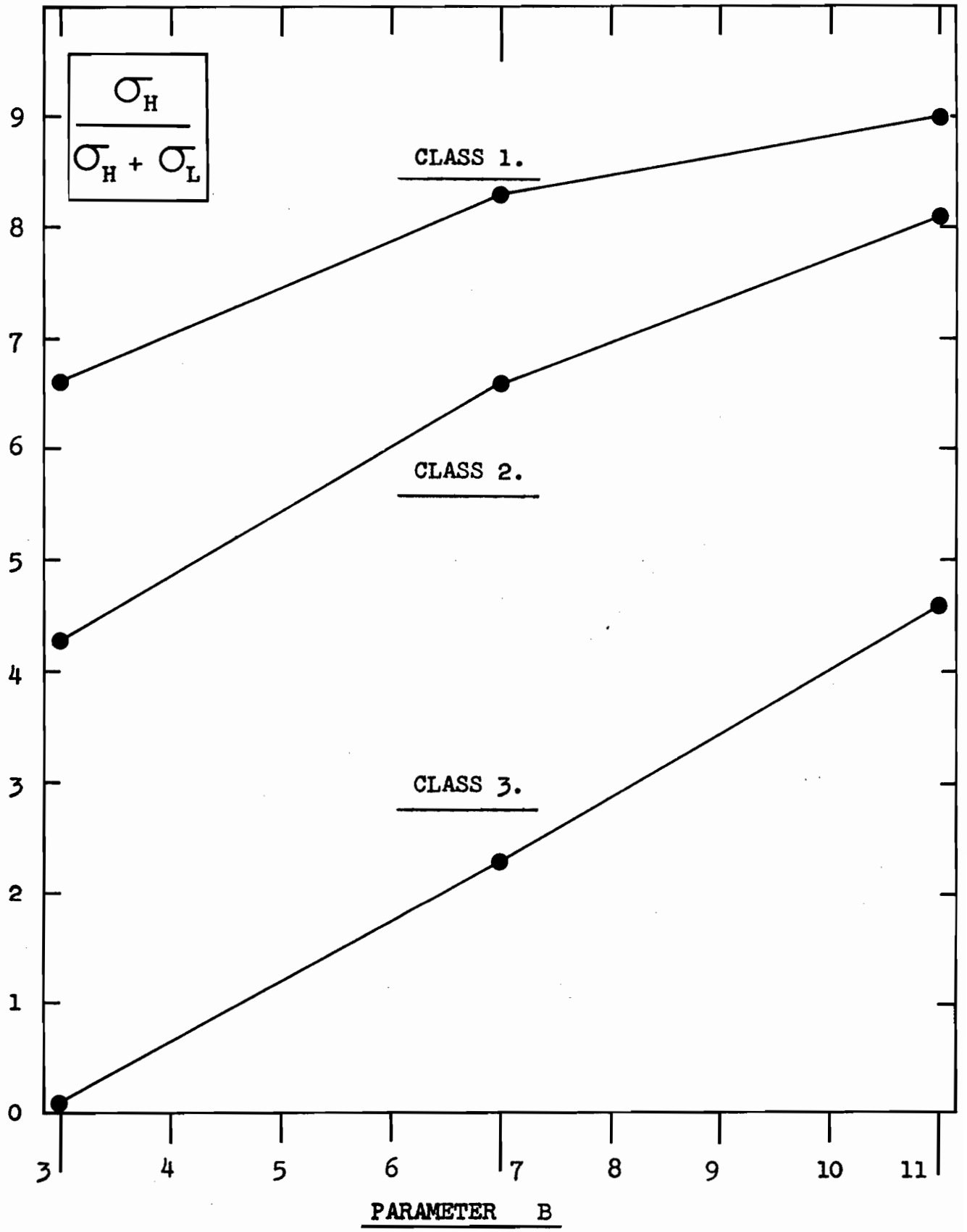

FIGURE 36. Solid Lines from Fig.35 Replotted with a Different Ordinate.

FIGURE 37.

Values of $\sqrt{\overline{J_f^2}}$ for successive steps in the fragment de-excitation. This is similar to Fig. 32, except that here the first three gamma rays in the cascade had $\ell = 2$.

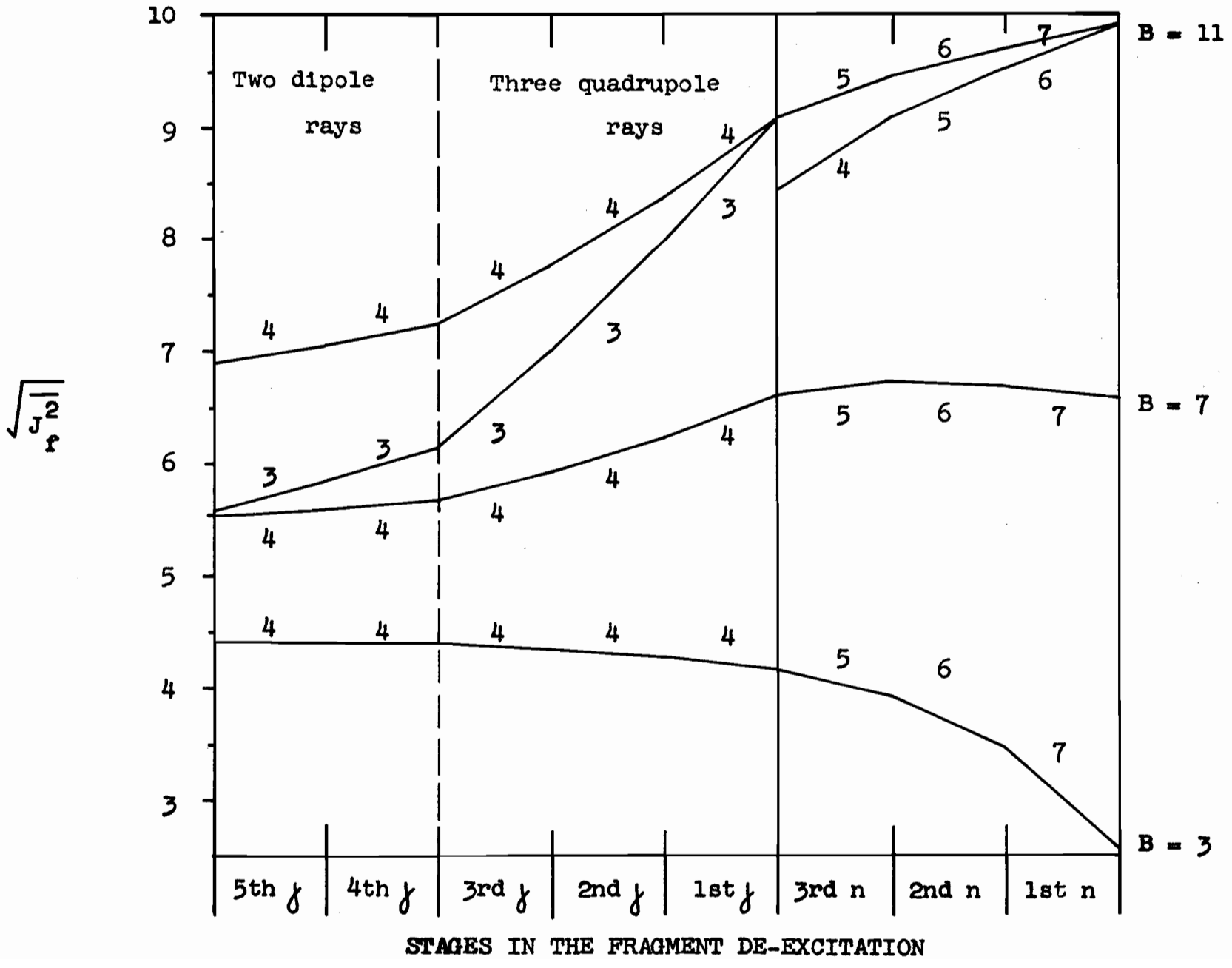
10
9
8
7
6
5
4
3
$\sqrt{J_f^2}$
Two dipole rays
Three quadrupole rays
B = 11
B = 7
B = 3
5th γ
4th γ
3rd γ
2nd γ
1st γ
3rd n
2nd n
1st n
STAGES IN THE FRAGMENT DE-EXCITATION

FIGURE 38.

Theoretical values of the isomer ratio for three spin-pair classes of isomers. This is similar to Fig. 35, except that it shows the effect of the multipolarity and the spin cutoff factor upon the theoretical ratios.

All computations had $N_n = 3$ and $(N_\gamma - 1) = 3$.

Dipole gamma radiation was used except for the long dashed lines which were computed for three quadrupole gamma rays.

Different sets of spin cutoff factors were used.

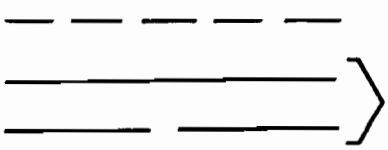

$\sigma_n = 6, 5, 4$ and $\sigma_\gamma = 3$

$\sigma_n = 7, 6, 5$ and $\sigma_\gamma = 4$.

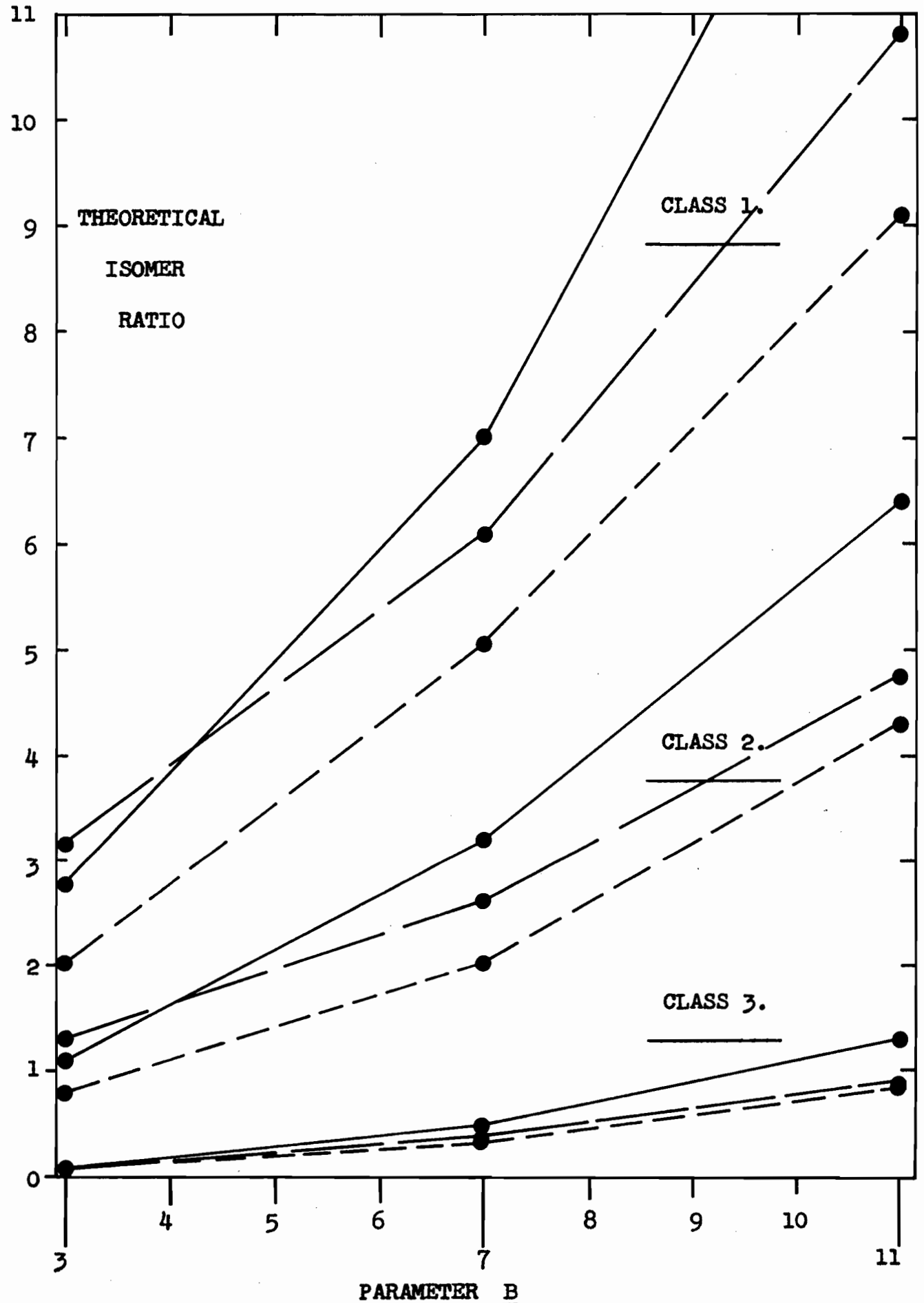
THEORETICAL
ISOMER
RATIO
CLASS 1.
CLASS 2.
CLASS 3.
0
1
2
3
4
5
6
7
8
9
10
11
3
4
5
6
7
8
9
10
11
PARAMETER B

lines are for the same set of σ values ($\sigma_{(n)} = 7, 6, 5$ and $\sigma_{(\gamma)} = 4$). In order to show the effect of using a lower set of σ values the solid lines from Fig. 35 have been replotted as the short dashed lines in Fig. 38.

4B.2.5 CONCLUSIONS FROM THE FRAGMENT DE-EXCITATION CALCULATIONS

Figures 32 and 37 show the following changes of mean spin of a fragment during the de-excitation process.

(i) For initial fragment distribution with B≈6-7 there are only small changes in $\sqrt{\overline{J_f^2}}$ of the distributions

(ii) For higher B values $\sqrt{\overline{J_f^2}}$ decreases, and these changes become larger per step as B is increased

(iii) For lower B values $\sqrt{\overline{J_f^2}}$ increases.

There is a simple explanation for these results which depends on the fact that the spin-dependent part of the level density formula, given by formula (1B.2), is sampled by each neutron and gamma ray emission, during the computation. The distribution which suffers the smallest change of mean spin has $B \approx (\sigma - 1/2)$ which is the spin, $J_{f(max)}$, at which the density function (1B.2) has its maximum value. If a distribution has a B value lower than $J_{f(max)}$ its states decay preferentially towards higher spins; and conversely

if a distribution has a B value higher than $J_{f(max)}$ it moves towards lower spins during the de-excitation process. From this argument it is seen that raising the input σ raises $J_{f(max)}$ so that high spin states decrease their spins less but low spin states increase their spins more; the effect here is to increase the predicted isomer ratios of all classes of spin-pairs (cf. Fig. 38, the solid and short dashed lines). The opposite trends occur when the input σ is decreased. The estimated amount of angular momentum carried away by either neutrons or gamma rays is strongly dependent on the value of σ, particularly in the de-excitation from fragment states of high spin. During the gamma cascade these spin changes are larger for quadrupole than for dipole transitions, again particularly for the higher spin states. The effect of quadrupole radiation therefore is to reduce the predicted isomer ratios for B values above about 4.

The effective converging of spin states during the de-excitation process will reduce the sensitivity of the isomer ratio to the angular momentum of the initial fragment (HUI 62, SAR 65). The rate of change of the isomer ratio with B is greatest for Class 1 isomers. This can be misleading and should not be interpreted to mean that for a

pair of isomers with a low spin-pair a change in the initial fragment spin is more easily detected in the experimental isomer ratios. This misunderstanding can be avoided when the solid lines in Fig. 35 are represented in another form in Fig. 36, where $\sigma_H/(\sigma_L + \sigma_H)$ is plotted against B. For all three classes, these functions show a similar rate of change with respect to B. Comparison of Figs. 35 and 36 shows that, when one isomer is formed in much greater yield than the other, a small change in the higher yield or in $\sigma_H/(\sigma_L + \sigma_H)$ changes the isomer ratio considerably. This explains why the spread of experimental isomer ratios for ^{133}Xe in Figs. 31(a)-(d) increases for the higher isomer ratios obtained using higher α_K values. Huizenga and Vandenbosch (HUI 60) have stated that the experimental isomer ratios are in least agreement with the calculations when one isomer has a relatively low yield. This can be illustrated by the cumulative spin distributions in Fig. 34 which would give the most unreliable prediction of isomer ratios at either end of the distribution, where the ratio would be very high or very low.

Before discussing the experimental data and comparing them with the above theoretical results, a few calculations that have been made for the compound nucleus are described.

4B.3 CALCULATION OF THE SPIN DISTRIBUTION OF THE COMPOUND NUCLEUS

These calculations were introduced in Section 1B.2.1. In this laboratory Sachdev (SAC 66) has written a FORTRAN program to compute transmission coefficients with an optical model potential of the type used by Perey (PER 63, BJO 58). Although the model has only been tested for nuclides with mass up to about 200 it was thought worthwhile to use Sachdev's program with the parameters of Perey for 10- and 20- MeV, and of Hodgson (HOD 65) up to 30 MeV in order to compute proton transmission coefficients for ^{232}Th. It was reasonable to use these coefficients also for ^{233}U, ^{235}U and ^{238}U, since the parameters for these heavy nuclides contained large uncertainties. Table 20(b) shows the $\sqrt{\overline{J_c^2}}$ characterizing the spin distributions which were obtained using Part 1 of the HHV FORTRAN program with these computed transmission coefficients. These spin values are in good agreement with those in Table 20(a) which were computed with the same program but with transmission coefficients obtained for a square-well nuclear potential. Since the transmission coefficients were considerably higher when calculated with the optical model nuclear potential, the agreement between values in Tables 20(a) and (b) illustrates the insensitivity

TABLES 20(a) and (b)

Root Mean Square Angular Momentum, $\sqrt{\overline{J_C^2}}$ of the Compound Nucleus Spin Distribution

(a) Computed with the proton transmission coefficients of Feshbach et al. (FES 53) (with a square-well potential)

Proton Energy MeV.	Target	Target Spin	$\sqrt{\overline{J_C^2}}$	Ref.
24.2	^{209}Bi	9/2	7.3	HAG 65
25.7	^{238}U	0	5.9	
19	^{232}Th	0	4.5	BEN 65
24			5.5	

(b) Computed with the proton transmission coefficients obtained with the FORTRAN program of Sachdev (SAC 66) (with an optical-model potential). (The coefficients for ^{232}Th were used also for ^{238}U, ^{235}U and ^{233}U).

	$\sqrt{\overline{J_C^2}}$		
Target (Spin) / Proton Energy (MeV)	^{232}Th, ^{238}U (0)	^{233}U (5/2)	^{235}U (7/2)
10	2.3	3.6	4.4
20	4.5	5.4	5.9
30	6.3	7.0	7.4

(DUD 65) of the calculated spin distributions to the values for the transmission coefficients.

The conclusions that were drawn in Section 4B.2.5, about the changes in the spin distribution of the excited fragments apply also to the excited compound nuclei. Therefore it may be predicted that a compound nucleus distribution with a mean spin of about 7 will suffer very little change of spin per prefission neutron emission. A spin value of 7 corresponds to the case of fission energies of about 30 MeV (Table 20(b)), but for higher energies and correspondingly higher spins of the compound nucleus a larger spin change will be caused per evaporated neutron. During the compound nucleus de-excitation by prefission neutron emission, as in the fragment de-excitation process, there is an effective converging of higher spin states towards lower spins. This effect will further reduce the sensitivity of the isomer ratio to an increase in the angular momentum of the initial compound nucleus.

We are now in a position to discuss the effect of the target spin and projectile energy on the spin of an initial fragment, and consequently their effect on the isomer ratio in fission.

4B.4 EFFECT OF TARGET SPIN ON THE FISSION ISOMER RATIO

Table 20(b) shows that at 30 MeV an increase of target spin from 0 to 7/2 changes the mean spin of the compound nucleus by only about one unit. Similarly from Table 20(a), at 25 MeV the compound nucleus spin changes by less than two units for the targets ^{238}U (I = 0) and ^{209}Bi (I = 9/2). If other factors in fission are assumed to be unchanged by this change, of one or two units, in the spin of the compound nucleus, and if this small angular momentum change were completely disposed between the two fragments the change in their spin would still be less than could be detected by a change in the experimental isomer ratio. In order to see a change in this ratio, a change in the initial fragment spin of at least two units is necessary; this was estimated from Figs. 35, 36 and 37 for a probable range of initial fragment spins (6 - 10).

For the targets ^{232}Th and ^{238}U which have I = 0, and for ^{233}U (I = 5/2) and ^{235}U (I = 7/2), the experimental ^{133}Xe isomer ratios in this study have the same absolute values, and behave in the same way with energy.

From these experimental results and from the theoretical considerations it can only be concluded that the spin and type of the fission target do not affect the isomer

ratio. This is in agreement with most of the limited data previously reported though some of these have been inconclusive and in certain cases contradictory. These data are now summarized and, for convenience, they are divided into the three spin-pair classes in Table 3 which summarizes the fission systems leading to these data and their references.

The data for Class 1 isomers have been obtained by Hagebo. For proton energies up to 115 MeV, his ^{117}In isomer ratios for the target ^{232}Th were the same as those for ^{238}U and for the considerably different target ^{209}Bi. However in his earlier work on the isomers of ^{95}Nb the ratios were lower for ^{238}U than for thorium, bismuth and lead. Although there were very large experimental uncertainties in the ^{95}Nb work these do not appear large enough to be able to explain the low results for ^{238}U. No explanation can be offered at present.

The data for Class 2 isomers, previous to our ^{133}Xe results, gave confusing conclusions about the dependence of isomer ratios on various targets. The ^{131}Te isomer ratios from thermal neutron fission were about the same for ^{233}U and ^{235}U, but are higher for ^{239}Pu ($I = 1/2$). The ^{131}Te isomer ratios, for fission induced by medium-energy deuterons

and alpha-particles were about the same for ^{232}Th and ^{238}U, except for the rather high value from the fission of ^{238}U with 33 MeV alpha-particles. The ^{133}Te results had larger uncertainties and are not considered here.

The data for Class 3 have been obtained for the isomers of ^{134}Cs. Although the measurements involved large experimental errors the following conclusions can be made. These ratios, like those in this work for ^{133}Xe, were the same for ^{238}U and ^{232}Th with protons of energy 30-85 MeV. Davies and Yaffe (DAV 63) obtained a result, with 20-MeV protons, which had an astonishingly high value of about 20 for the isomer ratio. This result was obtained from only one experiment and should be confirmed because no similar trend has been found in this energy region for ^{232}Th (BEN 65), and because this result is inconsistent with all other data and cannot be explained by any present model. The values of the ^{134}Cs isomer ratios for proton-induced fission of ^{238}U and ^{232}Th were about the same as those for ^{134}Cs from fission of ^{233}U, ^{235}U and ^{238}U induced by medium-energy deuterons and alpha-particles.

4B.5 EFFECT OF PROJECTILE ENERGY ON THE FISSION ISOMER RATIO

Fig. 30 shows that the present experimental isomer

ratios do not change significantly with proton energy, from 20-85 MeV. However, if the value of α_K for ^{133m}Xe is taken to be 5.0 or greater, our results would be consistent with a very slight increase of isomer ratio with energy (Fig.31). It has been estimated above that, to cause a detectable change in the isomer ratio, a change in the spin of the initial fragment of about two units is necessary. It may therefore be concluded from our data that this spin is different by less than two units in all of our fission systems though the compound nucleus spin goes from a lower limit (Table 20(b)) of about five to a probable value of greater than ten.

All other isomer ratio data that exist for a wide range of fission energies are also for proton-induced fission. The ^{134}Cs isomer ratios, like the ^{133}Xe ratios, have been shown to have very little energy dependence over the same proton energy range, with the exception of the one result at 20 MeV for ^{238}U which has been discussed above. The experimental isomer ratios for ^{117}In on the other hand show a strong energy dependence, up to about 115 MeV. For ^{95}Nb the data are less reliable but show the same trend, i.e. an increase of isomer ratio with energy. The isomer ratios of ^{117}In increase from about 2 to 10 over the proton

energy range 20 to 100 MeV. The corresponding change in the spin of the initial fragments may be estimated from the results of our calculation (Figs. 35 and 38). Thus, a low B value of three or less is needed to predict these ratios below about 40 MeV; the ratios at about 100 MeV correspond to a high initial fragment spin, with B equal to at least ten.

The above evidence that with increase of proton energy the fission isomer ratios of ^{95}Nb and ^{117}In increase considerably whereas those of ^{134}Cs and particularly of ^{133}Xe do not increase significantly, is not understood.

Some other evidence does exist on the energy dependence of fission isomer ratios, but is less conclusive. The independent isomer ratio of ^{80m,80g}Br increases slightly with proton energy from 70 to 100 MeV (HAL 61). The cumulative isomer ratio of ^{115}Cd increases rapidly with energy. Although the energy dependence of the isobaric charge dispersion explains part of this increase, particularly up to about 40 MeV, the independent isomer ratio also appeared to be energy dependent. It does seem that the near symmetric fission products ^{115}Cd and ^{117}In have isomer ratios with a greater energy dependence than those of the asymmetric fission products with mass about 133. However, there is the following limited contrary evidence which shows

that asymmetric fragments are not insensitive to the angular momentum of the fissioning system. The ^{134}Cs isomer ratios are slightly but significantly higher for medium-energy alpha particle and deuteron fission than for low-energy photo-fission (WAR 64); and the ^{131}Te ratios are similarly higher for this type of medium-energy fission than for thermal neutron fission (SAR 65).

4B.6 ESTIMATE OF FRAGMENT SPIN FROM THE ISOMER RATIO

The present data for ^{133}Xe were good for the relative studies so far discussed. These data cannot give a very accurate estimate of B because, as shown in Section 4B.1, the absolute values of the isomer ratios depend strongly upon the value of α_K for ^{133m}Xe. It is hoped that a value of α_K will soon be available with a smaller error than in the one previous measurement. Matuszek (MATU 65) has recently informed us that he is beginning a study of ^{133}Xe produced by the reaction ^{130}Te (α,n). If α_K is taken to have a value of 5.0, the corresponding isomer ratio is 1.6 ± 0.2 which gives an estimated value of B equal to 5 ± 2, from Figs. 35 and 38.

Storms (STO 62) has studied ^{133}Xe formed in medium-energy fission of thorium and uranium induced by charged particles, and has concluded that the yield of ^{133m}Xe was

negligible. The following considerations leave little doubt that this conclusion is erroneous. It is unlikely that there is a large difference between the ^{133}Xe isomer ratios for the different fission systems in his and the present work (cf. Table 1). However, his conclusion is very different to ours. The ratios reported in our work are consistent with those reported for the similar Class 2 isomeric pairs of ^{131}Te and ^{133}Te (ERB 63, SAR 65), and with the ratios predicted by the calculations for a reasonable initial fragment spin. Possible errors in Storms' work are discussed in more detail in Appendix B.

Table 21 gives the value of B estimated for three reasonable ^{133}Xe isomer ratio values of 1.0, 2.0 and 3.0 and summarizes the B values estimated in other fission isomer studies. The estimated spin values in Table 21 would be even higher if quadrupole radiation were assumed and a higher value of N_γ used. Most of these B values from the isomer ratio studies agree with the high spin values of 8-10 units obtained from the prompt gamma ray studies already discussed in Section 1B.2.6. However, just as in the discussion of the energy dependence of the isomer ratio, different conclusions can be drawn from the data for the Class 1 isomers. Below about 30 MeV, very low fragment spins are

TABLE 21

Values of B Estimated in Fission Isomer Ratio Calculations, with Initial Fragment Spin Distribution Given by Equation (1B.1)

Fission System			Estimated Spin of Compound Nucleus	Isomeric Nuclide	Expt. Isomer Ratio	Estimated $\underline{B}$ of Initial Fragment	Ref.
Target	Projectile	(MeV)					
^{238}U	p	30	5-8	^{117}In	~2.0	~3	HAG 65
^{232}Th	p	30	5-8	^{117}In	~2.0	~3	HAG 65
^{209}Bi	p	100	-		~10.0	10	HAG 65
^{235}U	n	thermal	3.5	^{131}Te	1.8±0.4	6±1.5	ERB 65 SAR 65
^{232}Th	α	33	~13	^{131}Te	3.3±0.5	~8	WAR 64
^{232}Th	p	20-85	cf. Table 20(b)	^{133}Xe	(i) 1.0 (ii) 2.0 (iii) 3.0	4±1.0 6±1.5 8±1.5	THIS WORK
^{238}U	p	20-85	cf. Table 20(b)	^{133}Xe	(i) 1.0 (ii) 2.0 (iii) 3.0	4±1.0 6±1.5 8±1.5	THIS WORK
^{235}U	p	20-85	cf. Table 20(b)	^{133}Xe	(i) 1.0 (ii) 2.0 (iii) 3.0	4±1.0 6±1.5 8±1.5	THIS WORK
^{233}U	p	20-85	cf. Table 20(b)	^{133}Xe	(i) 1.0 (ii) 2.0 (iii) 3.0	4±1.0 6±1.5 8±1.5	THIS WORK
^{233}U	γ	16	5/2	^{134}Cs	0.8±0.2	⩾7.5	WAR 64
^{232}Th	p	20	~5	^{134}Cs	1.2±0.6	~9	BEN 65

estimated from the isomer ratios of ^{117}In. Although large corrections were necessary in these data it can still be assumed that the isomer ratios are indeed very low.

In this low-energy region the experimental isomer ratios of ^{117}In and ^{134}Cs cannot be predicted from the same initial fragment spin distribution if the de-excitation processes are similar for both cases. Only if the de-excitation processes leading to ^{117}In and ^{134}Cs are very different (e.g. if the N_γ for a Class 1 isomer is much larger than for a Class 3 isomer) would it be possible to reconcile the data with the present model (i.e. be able to predict both of these isomer ratios from the same high B value). The very low experimental values for the cumulative isomer ratios of ^{115}Cd provide further evidence that symmetric fission fragments have a low initial spin. If the neutron parents of ^{115}Cd and of ^{117}In do have about the same low mean spin then it is obvious from the respective spin-pairs, (11/2, 1/2) and (9/2, 1/2), that the ^{115}Cd isomer ratios should be lower than those of ^{117}In. This prediction agrees with the data though the low values for ^{115}Cd are partly caused by precursor decay from ^{115}Ag to ^{115g}Cd.

Sikkeland et al. (SIK 65) observed that for the fission of ^{238}U induced by ^{12}C (73-120 MeV), the ^{115}Cd

isomer ratios were considerably lower than for the same type of fission of ^{197}Au. The centres of the mass-yield curves for these two fission systems are at A ≈ 118, and at A ≈ 98; they concluded that the asymmetry of the fission fragments strongly influences the isomer ratio. To further support this conclusion they made a comparison between the low ^{115}Cd ratio formed in 100-MeV proton-induced symmetric fission of ^{238}U and the higher ratios from 450-MeV proton fission of ^{209}Bi. However, the energies of these two systems are very different and the comparison is not meaningful. A more useful comparison can be made between the data for the ^{117}In isomer ratios formed in the fission of ^{238}U and ^{209}Bi induced by protons over the same energy range (40-160 MeV). No significant difference existed in these data (HAG 65). The isomer ratios in the fission of ^{238}U might have been expected to be lower than those for ^{209}Bi, because in the latter fission system the ^{117}In is formed in a more asymmetric fission mode, and ^{209}Bi has a high spin value of 9/2.

There was very poor evidence available from fission isomer ratio data when Croall and Willis (CRO 62) made the tentative conclusion that a difference may exist between the isomer yield ratios for nuclides near the trough of the fission mass yield curve and for those near the peaks. This

hypothesis is supported both by theoretical predictions (POR 57, HOF 64, JOH 64, SIK 65) that the angular momentum induced in the fragments is appreciably lower in symmetric than in asymmetric fission, and by many of the additional experimental data now available. The evidence is still not conclusive and it is not known up to what energy this phenomenon is important.

4B.7 COMPARISON OF YIELD RATIOS FOR AN ISOMER PAIR FORMED IN FISSION AND IN SPALLATION

There have been several interesting studies where the yield ratios for the isomer pairs of ^{115}Cd, ^{80}Br, ^{134}Cs and ^{83}Se have been obtained in both fission and in spallation reactions. It would be interesting to use the rather reliable ^{133}Xe isomer ratio data from this study to make a more quantitative comparison with data that could be collected in the energy range 10-25 MeV from the reaction ^{130}Te (α,n) ^{133}Xe. Similar (α,n) reactions have been studied by Bishop et al. (BIS 64) and Matsuo et al. (MATS 65). In the reaction of ^{130}Te the spin distributions of the initial compound nucleus, ^{134}Xe, and their modification during the de-excitation process could be obtained as in the calculation for the ^{107}Ag (α,n) reaction (BIS 64) or with the improved calculations performed for the (α,n) reactions of ^{41}K, ^{55}Mn

and ^{93}Nb by Dudey and Sugihara (DUD 65). It is estimated from the approximate formula of Halpern and Strutinski (HAL 58) that the spin of the ^{134}Xe compound nucleus formed by 20 MeV alpha particles is about seven units, which is a spin value similar to that expected in a fission fragment with this excitation energy. It may therefore be possible to obtain a better value of the spin cutoff parameter (DUD 65) for our fission calculations and to compare the de-excitation process in spallation- and fission- products leading to ^{133}Xe.

Sharp and Pappas (SHA 59) compared the ^{115}Cd isomer rations, in the energy range 10-25 MeV, obtained in fission and in five spallation reactions. Unfortunately this energy range is very unsuitable for a study of the independent isomer ratios for ^{115}Cd. Tilbury and Yaffe (TIL 63b) also studied the isomeric yields of ^{115}Cd from fission of ^{238}U by protons in the same energy range. They obtained results which contradicted those of Sharp et al. whose results were thought to be complicated by chemical separation problems. Therefore, there is only weak supporting evidence that the high spin isomer ^{115m}Cd is preferentially populated in low-energy fission. Sharp et al. had assumed this was true and proposed that it was caused by increased fission barrier

penetration for compound nuclei of high spin. This phenomenon might be important at low excitation energies when symmetric fission is highly improbable.

Häller et al. (HAL 61) compared the ^{80}Br isomer ratios, in the proton energy range 70-160 MeV, obtained in fission and in the reactions ^{81}Br(I=3/2) (p,pn) and ^{89}Y(I=1/2) (p,5p 5n). The fission isomer ratios were higher than the ratios from the simpler spallation reaction but lower than those from the (p,5p 5n) reaction. The large population of the high spin isomer ^{80m}Br, in the last reaction, was explained by assuming that although at these energies a wide spectrum of excited nuclei are formed in direct interactions, only those with high energy and correspondingly high angular momentum could lead to this reaction. Calculation of these spins would be very difficult, for such high excitation energies.

Table 22 shows two examples in which an isomer ratio was measured for an isomeric species formed in fission and in spallation. The much larger ratios obtained from fission provide striking evidence that the asymmetric fission fragments, leading to ^{83}Se and ^{134}Cs, have high spins.

TABLE 22. Two Comparisons of an Isomer Ratio Obtained in Fission and in a Thermal Neutron Capture Reaction

Isomeric Nuclide	Target for (n,γ) reaction (I=spin)	Ratio, $\sigma_H/(\sigma_H + \sigma_L)$	
		from (n,γ) reaction	from low-energy fission
^{134}Cs	^{133}Cs(I=7/2)	0.08 (BIS 64a)	0.43 (WAR 64)
^{83}Se	^{82}Se(I = 0)	0.08 (ARN 47)	0.8 (CRO 63)

4B.8 PREDICTION OF UNMEASURED FISSION ISOMER RATIOS

A fairly reliable prediction of yield ratios for isomeric fission products is now possible as a result of the experimental and theoretical studies reviewed in this thesis; it is of course necessary to know the effective spin-pair of the isomeric nuclide.

Strom, Grant, and Pappas (STR 65) have recently used the HHV program for computations, similar to those in this thesis, to predict the relative isomeric yields in the shielded nuclides ^{124}Sb and ^{126}Sb formed in thermal neutron fission of ^{235}U. With these predicted values and activity data for the ground states, they were able to estimate the total independent yields of these two nuclides. They used the following input data: B = 6.5; σ= 3; N_n = 1, with $\overline{E}_n$ = 1.0 MeV; and $(N_\gamma - 1)$ = 2, with ℓ = 1. We consider

that their B and N_γ values are too low and that at least one quadrupole gamma radiation should have been used. However, the effect of these changes would not significantly alter the predicted values, because a larger B value would have the opposite effect to the use of quadrupole radiation and a larger N_γ value. Table 23 gives the predicted populations that were obtained for the ground, g, and metastable, m, states of ^{124}Sb and ^{126}Sb.

TABLE 23. (STR 65, Table IV)

Spin of Isomeric State	Predicted Relative Population of Isomeric States			
	^{124}Sb, Isomeric State		^{126}Sb, Isomeric State	
3	0.28	g	-	-
5	0.57	m_1	0.85	m
8	0.15	m_2	0.15	g

In order to obtain the best possible predicted value of the isomer ratio it is not sufficient to use the calculations alone, because of the discrepancies between theory and experiment that have been discussed. The calculated results should be modified on the basis of these discrepancies. The isomeric nuclides in Table 23 have an effective spin-pair of (8, 5) which is that for the class 3 isomers. Although

there is no experimental evidence for class 3 isomers formed in thermal neutron fission the theory has been shown to predict too low values for this isomer class. The estimated relative population of high to low spin states is probably too low, in Table 23, and the values should be closer to those for the relative population of the similar spin states in ^{134}Cs (0.43/0.57 for states of spin 8 and 5, from photo-fission, and an even higher ratio for low-energy fission by protons).

Predicted fission isomer ratios could be useful to obtain other total independent fission yields of nuclides that have one isomer which is stable and one which can be measured radiochemically. As an example, total yields could be calculated for ^{83}Kr, ^{129}Xe and ^{131}Xe from partial yields measured in experiments similar to those in the present work.

4B.9 LIMITATIONS OF THE DE-EXCITATION MODEL

Even with input data which were well determined the calculations would be limited by weaknesses in the model for the fragment de-excitation. There are several weaknesses in the gamma cascade model. There is little physical significance to the arbitrary division of the cascade into $(N_\gamma - 1)$ gamma rays which decay statistically and a final gamma ray which has a peculiar range of values for its

multipolarity. This model is particularly unfeasible for class 1 and other low spin-pair isomers. There are still a large number of high spin states in a fragment spin distribution even after (N_γ - 1) quadrupole gamma transitions have modified an initial distribution with B = 8; if the final gamma ray is to allow these high spin states to decay to the isomer of higher spin (I = 9/2, for class 1), then final gamma rays with multipolarities of 1, 2, 3, 4 etc. must be assumed.

An even more serious fault is introduced into the model if the gamma cascade process cannot be treated statistically. The statistical description, depending as it does on the availability of many levels both in the initial and final nuclei, may be expected to break down for the high spins and low excitation energies in the gamma cascade process in fission, particularly towards the end of this cascade. Johansson (JOH 64) has concluded from his gamma decay curves and gamma energy spectra that the gamma cascade in fission is not a de-excitation via statistically distributed levels, as is assumed in isomer ratio calculations, but is an ordered quadrupole gamma de-excitation (from fragments of spin about 10). For the gamma cascade in neutron-capture de-excitation calculations (BIS 64b, VON 64) the

statistical description has been considered invalid particularly when the excitation energy becomes very low towards the end of the cascade. Even the minor adjustment that was made to the model in this case, cannot be made in fission calculations because of the poorly known energetics of the fragment de-excitation process.

The gamma cascade model might be improved by assuming that for a particular initial spin state the multiplicity and multipolarity (DUD 65) of the gamma rays are dependent on the difference of angular momentum between this state and the nearest isomeric state (WAR 64). This implies that it is wrong to use the same N_γ and ℓ for all of the spin states in an input spin distribution, in the gamma cascade calculation. It also implies that N_γ should be higher and that there should be more quadrupole radiation in a gamma cascade leading to class 1 isomers than for class 3 isomers. The latter implication could help to explain the discrepancies between the experimental and calculated isomer ratios of ^{117}In, and also of ^{134}Cs; the predicted ^{117}In ratios would be lower, and the predicted ^{134}Cs ratios would be higher.

Dudey and Sugihara (DUD 65) have introduced two modifications into their spallation isomer ratio calculations. The first modification depends on the interesting concept that a nuclide can become "saturated" with regard to spin and

that it has a limiting J value above which there are very few levels. Obviously the predicted isomer ratio for systems with high spin will be reduced by this modification. Secondly they have considered in some detail the effect of competitive emission of charged particles in the de-excitation process (THO 64, VAN 65). This second modification slightly lowers the predicted isomer ratio. In fission fragments of fairly high excitation energy it is feasible that a limiting J_f value and competing emission of particles could be important.

4B.10 CONCLUDING ASSESSMENT OF FISSION ISOMER RATIO STUDIES

There are still very few data available to assess the simple theoretical interpretations that have been made in fission isomer ratio studies.

The isomer ratio studies in fission have had a very different objective to those in spallation. For spallation there is considerable confidence in the theoretical model describing the disposition of angular momentum during the reaction. This model has been used with the large number of isomer ratio data from spallation studies in order to study the nuclear level density, and to estimate the energy where direct interactions begin to become more important than a compound nucleus mechanism. Conversely, in fission

the disposition of angular momentum is poorly understood. In similar calculations to those used in spallation the few isomer ratio data and an assumed level density can be used to study the angular momentum in the fragments. The results of these calculations are most sensitive to the assumed spin cutoff factor, σ, characterizing the level density, particularly if the fragment has a spin well above the value of σ. The results are fairly sensitive to the multiplicity and multipolarity of the gamma rays. There are limitations to the fragment de-excitation model which does not give a good representation of the process and could be modified in several ways. To make such changes would greatly increase the complexity of the calculations and probably would not be worthwhile until more information is available on the fragment de-excitation process.

Despite the many shortcomings in these fission studies they have been pursued because of the few other experimental methods that can give information about the angular momentum in the fragments. This information is interesting for the theoretical investigation of the configuration at scission and of the nuclear viscosity in the liquid drop theory of fission, though at present the data have not been accurate enough to allow these

investigations to be quantitative.

The fission isomer ratio studies have the advantage that they give an estimate of the spin of specific fragments. They have given some evidence for the theoretical prediction that the spin may be less for symmetric than for asymmetric fission fragments. Thus, although the main factor determining the value of the isomer ratio is the effective spin-pair of the isomeric fission product the ratio, particularly at lower energies, may also depend on the mode of fission in which it is formed (i.e. symmetric or asymmetric mode).

There is now considerable experimental evidence that the isomer ratio is almost independent of the spin and type of the fission target; except in an extreme case where the masses of the targets are so widely separated that an isomeric nuclide is formed in a symmetric mode in one system, but in an asymmetric mode in the other. This independence is to be expected from the small change in the mean spin of the calculated compound nucleus spin distributions for targets with the largest possible difference in spin, and also from the many factors in fission which may prevent changes in the compound nucleus spin from being reflected in the spin of the fragments.

Most of the experimental data suggest that the isomer ratio is only weakly dependent on fission energy, but the ratio appears to increase with energy for fragments formed in near symmetric fission. Only qualitative generalizations can be given to explain this behaviour. Many factors have been discussed that could contribute to the insensitivity of the isomer ratio to the projectile energy; and these are now summarized briefly.

Direct interactions become most important as the energy of the projectile increases above about 40 MeV; there is less transfer of energy and angular momentum to the target, and angular momentum is removed by the neutron cascade. It is possible that as the fissioning energy increases the orbital angular momentum between the fragments increases so that there is less spin available for the initial fragments. If the fragments have high spins considerable amounts of angular momentum will be removed by neutron and possibly by competing particle emission, and by a gamma cascade of quadrupole radiation of high multiplicity. If a limiting spin value exists in the fragments this would obviously help to maintain the isomer ratio constant at higher energies.

At lower projectile energies, below about 40 MeV,

where a compound nucleus mechanism predominates an increase of isomer ratio with energy may be expected. This increase has only been observed in the isomer ratio data for near symmetric fission fragments. It may be that these fragments have a low spin of about three at low energy and the spin increases with energy up to a value of about ten. Then the so called "converging" effect in the de-excitation process decreases the sensitivity of the isomer ratio to any increase of fragment spin with projectile energy. This effect, which is also present but is of less importance in the compound nucleus de-excitation, is caused by the increase in the amount of angular momentum removed per de-excitation step from the fragment as its spin increases. If the asymmetric fragments have high spin even at low energy then the converging effect will decrease the sensitivity of their final spin to increasing energy over the whole energy range. It was estimated that no change of isomer ratio could be observed if the fragment spin does not change by more than about two units.

It seems unlikely that much data for isomer ratios in fission will be obtained from isomer pairs outside the few that have already been studied. It may be possible to obtain better results for some of these isomer pairs from

the fission target ^{235}U, or even better ^{233}U. This may be possible, because of the large variation in isobaric charge distribution for different targets (cf. Section 4B). This difference can have a large effect on the chain yield of a nuclide, and, for a nuclide which is not shielded, can greatly decrease precursor decay. The use of beta spectrometry to count conversion electrons could improve the data in the present study (cf. Appendix B).

The present crude calculation for the fragment de-excitation process is very sensitive to the values for the spin cutoff factor and a better knowledge of this parameter will be difficult to obtain except perhaps from spallation isomer ratio studies. It may even become possible to construct a more complex model for the fragment de-excitation process. The most promising theoretical development has been made by Swiatecki and Nix (NIX 65) in their recent work on the simplified liquid-drop theory of fission, though at present their results apply only for targets lighter than $A \approx 220$. It will be interesting to see more results calculated from their formulae describing the disposition of angular momentum in the fission fragment. Their formulae could be used with the few isomer ratio data for fission of bismuth, but the existing data are probably not reliable enough to give information on the nuclear viscosity.

5. SUMMARY

This thesis has surveyed and given new information on two aspects of fission,

A. FISSION YIELDS AND THEIR VARIATIONS

B. ISOMERIC YIELD RATIOS IN FISSION.

Measurements were made of the activity of xenon isotopes formed directly and indirectly in the fission of the heavy nuclides ^{232}Th, ^{238}U, ^{235}U and ^{233}U with protons of energies from 20 to 85 MeV. The same experiments were used mainly to study the isomeric yield ratios of ^{133}Xe, but also to study fission yields and their variations in the mass chains 133 and 135. Much of the information in this thesis was obtained using relative yield data which had less uncertainty than the absolute yield data.

5A. SECTION A. FISSION YIELDS AND THEIR VARIATIONS

Relative fission yields and some absolute yields were measured for the independent formation of xenon and for the cumulative formation of iodine in the chains 133 and 135.

Relative yield data were used for a study of charge distribution in the above fission systems. Assuming a Gaussian charge distribution curve, FUNCTION (1), two methods

were used to obtain Z_P values empirically. Method (1) was developed in this research and was proved reliable by comparison with a more complex method (2) which was similar to one previously reported. Method (1) used the ratio of the cumulative yield of a beta parent to the independent yield of the daughter. This ratio, $R^A_{c/i}$, was found to be a good parameter for determining, in a chain A, the value of Z_P and also the fractional chain yields. Here the method was successfully used for fission energies below about 55 MeV for the pairs $^{135}I/^{135}Xe$ and $^{133}I/^{133}Xe$. The method should be useful in future work since accurate values of $R^A_{c/i}$ could fairly easily be measured for many pairs of adjacent isobars formed in fission.

For ^{238}U and ^{232}Th, the variation with energy of Z_P for chains 133 and 135 showed the trends now fairly well established for this mass region. However, the variation of Z_P with energy was shown to be considerably different for the proton-induced fission of ^{235}U and ^{233}U, which has not been studied in any detail. Although the present data for the latter systems were limited this interesting preliminary conclusion suggested that the work on ^{235}U and ^{233}U should be extended.

No attempt was made to develop the difficult and

poorly understood theory of charge division and neutron emission in fission. The simplified CCR postulate was used to estimate roughly the total neutron yield, from the present empirical Z_p values.

In order to obtain absolute cross sections, the flux of the proton beam was monitored in most of the experiments, except those with ^{233}U. For the whole proton energy range, 20-85 MeV, the monitor reaction was $^{65}Cu(p,pn)^{64}Cu$. The absolute yields were used to construct fifteen excitation functions. Only two of these had previously been reported. The present cumulative cross sections for proton-induced fission of ^{232}Th were slightly higher for ^{135}I, and considerably higher for ^{133}I, than those reported by Pate, Foster and Yaffe. It is suggested that the present results are more reliable because they were obtained from less complex activity data.

From the absolute data for energies below about 55 MeV, the total chain yields were calculated using fractional yields from the determined charge distribution curves. For a particular fission system, the total chain yield was about the same for chains 133 and 135. This was consistent with a flat mass distribution curve in this mass region.

5B. SECTION B. ISOMERIC YIELD RATIOS IN FISSION

Relative independent yields of the isomers of ^{133}Xe were measured for twenty-seven fission systems, consisting of the targets ^{232}Th, ^{238}U, ^{235}U and ^{233}U with protons of energies from 20 to 85 MeV.

The measured isomer ratios were reported with four possible values of α_T for the 233-kev gamma ray of ^{133m}Xe, because of the present uncertainty in this coefficient. The existing experimental value of α_T has a large error and is much lower than the theoretical value. A more accurate determination of this coefficient is urgently required in order to reduce the large uncertainty in the present absolute values of the isomer ratios of ^{133}Xe. However, the present data were suitable for a precise comparison of the isomer ratio for the different fission systems in this research.

Crude statistical computations were performed in order to improve our understanding of the relative formation of isomers in fission.

The summary of the present and related previous studies has already been presented in a "Concluding Assessment of Fission Isomer Ratio Studies" (Section 4B.10, p.224). Only the main conclusions from the present research are repeated here.

The present experimental and theoretical results leave little doubt that Storms made an erroneous conclusion in 1962. He concluded that there was a negligible yield of ^{133m}Xe in medium-energy fission. Possible errors have been considered in the measurements, made by him and other workers, of the beta activity of fission product xenon.

The present data, together with a few previous data, suggested that the isomer ratio is apparently independent of the spin and type of the fission target.

The present data gave substantial evidence that the isomer ratio is more weakly dependent on fission energy than was generally concluded in most previous studies. However, there are a few previous data which show that the isomer ratios increased more strongly with energy, particularly for fragments formed in near-symmetric fission.

APPENDIX A

EQUATIONS AND MONITORING USED TO OBTAIN CROSS SECTIONS

A.1 EQUATIONS USED IN CALCULATION OF CROSS SECTIONS

The probability that a nuclear reaction will occur under given conditions is usually given in terms of the cross section, σ, in units of barns (1 barn = 10^{-24} cm^2).

The first step in the calculation of cross sections is to obtain a disintegration rate, D_N^o, of a product nuclide, N, at the end of bombardment (of duration t_o). This was obtained from the corresponding gamma counting rate, C_N^o, in the expression,

$$D_N = C_N \times \frac{1}{(eff)} \times \frac{1}{Y} \times \frac{(1 + \alpha_T)}{(BR)} \quad . \qquad (A1)$$

Here Y = the fraction of the product nuclides that were counted,

(eff) = the photopeak efficiency for the particular gamma ray energy and source geometry,

α_T = the total internal conversion coefficient,

(BR) = the branching ratio.

Table 8 gives the values of Y_{Cu} for copper, and Table 6 gives values of Y^a for the xenon sample from sweep (a), and Y^b for sweep (b). Table A1 gives the values for

TABLE A1. (NDS) Values Used in Equation (A1)

Species	Gamma Ray Energy kev	(eff), Zero Shelf		(BR)	α_T
		2 ml Gas Vial	2 ml Liquid Source		
^{64}Cu	511[a]	-	.105[b]	0.19	0
^{133g}Xe	80	0.27±.02[c]	-	0.99	1.8
^{135g}Xe	249	0.22±.02[c]	-	0.97	0.06
^{133m}Xe	233	0.225±.02[c]	-	1.00	6.3[d]

a. The observed activity was divided by 2 to account for the production of two 511-kev γ rays emitted at 180° in each positron annihilation.

b. From the curves of Grant et al. (GRA 61).

c. From present work (cf. Appendix B).

d. Calculated also for α_T = 7.3, 8.3 and 9.3 (cf. Sections 4A.1, 4B.1).

TABLE A2. Values Used in Equations (A8) and (A9)

Target Nuclide	A_{Target}	$(Ab)_{Target}$ %	$(SD)_{Target}$ (mg/cm^2)
^{232}Th	232	100	80.8
^{238}U	238	100	46.4
^{235}U	235	(100)	104.0
^{65}Cu	65	31.9	45.9

(eff), (BR) and α_T. Appendix B discussed these values of (eff) and describes the method used in this work to determine (eff) for the xenon photopeaks.

The disintegration rate at the end of bombardment, D_N^o, was related to the formation cross section, σ_N, to the proton flux, F, and to the number, n_T, of target nuclei in the beam, by the expression,

$$D_N^o = Fn_T \sigma_N (1 - e^{-\lambda_N t_o}) \quad . \qquad (A2)$$

Here λ_N is the decay constant of N, and the term $(1 - e^{-\lambda_N t_o})$ accounts for the decay of N during the bombardment.

In order to obtain independent cross sections for unshielded fission products, decay corrections must be made. In the very simple beta-decay chain $N_1 \rightarrow N_2 \rightarrow$ the independent disintegration rate of N_2 may be obtained from the measured cumulative rate $D^o_{N_2 cum}$ by subtracting the disintegration rates, $D^o_{N_2(N_1,t_o)}$ and $D^o_{N_2(N_1,t_1)}$, caused respectively by decay of N_1, during the time of bombardment, t_o, and during the time, t_1. Here t_1 is the time from the end of bombardment to the end of the first separation of N_1 from N_2 (sweep (a) in this work). These corrections are given by the commonly used formulae given below, with N_1 and N_2

replaced by I and Xe respectively, because these corrections were used in the present calculations to obtain independent yields for ^{135}Xe and for ^{133g}Xe. These nuclides are both unshielded (Fig. 17).

$$D^{o}_{Xe(I,t_o)} = \frac{D^{o}_{Icum}}{(1 - e^{-\lambda_I t_o})}\left[1 - \frac{(\lambda_{Xe} e^{-\lambda_I t_o} - \lambda_I e^{-\lambda_{Xe} t_o})}{(\lambda_{Xe} - \lambda_I)}\right], \quad (A3)$$

$$D^{o}_{Xe(I,t_1)} = \frac{D^{o}_{Icum}}{(\lambda_{Xe} - \lambda_I)} \frac{\lambda_I (e^{-\lambda_I t_1} - e^{-\lambda_{Xe} t_1})}{e^{-\lambda_{Xe} t_1}}, \quad (A4)$$

where D^{o}_{Icum} is the disintegration rate of the parent iodine nuclide at the end of bombardment. This value was obtained from the D^{b}_{Xe} at the end of sweep (b) for ^{135}Xe and ^{133g}Xe, by using the formula,

$$D^{b}_{Xe} = \frac{\lambda_{Xe} D^{o}_{Icum}}{(\lambda_{Xe} - \lambda_I)} e^{-\lambda_I t_1} (e^{-\lambda_I t_2} - e^{-\lambda_{Xe} t_2}). \quad (A5)$$

The cumulative cross sections for ^{135}I and ^{133}I can be obtained by substituting the respective values of D^{o}_{Icum} in equation (A2). In order to use D^{o}_{Icum} from equation (A5) in equations (A3) and (A4), the assumption must be made that the decay precursors of iodine are very short-lived. This is a

reasonable assumption for the simple chain of mass 135, but this is not true for the more complex chain of mass 133 (Fig. 17). In the latter case, during the period t_1 a fraction of the cumulative yield of ^{133}I is held back by the relatively long-lived isomers of ^{133}Te. Therefore the above correction procedure uses a value of $D^o_{^{133}I_{cum}}$ in equations (A3) and (A4) which is too high. Therefore the independent yield of ^{133g}Xe will be too low, or is "over-corrected". This over-correction introduces significant errors only when there is a large growth of ^{133g}Xe; therefore the time t_1 was minimized in the present experiments. The above equations were satisfactory for the data considered in this work on fission induced by protons of energy 20-85 MeV. The use of more exact decay equations is discussed in Appendix C.

The experimental values of $C^o_{^{133g}Xe}$, after the above corrections for the decay of iodine, must also be corrected for the growth resulting from decay of ^{133m}Xe. This final correction to the disintegration rate of ^{133g}Xe is given by,

$$D^o_{^{133g}Xe(^{133m}Xe)} = (\lambda_{^{133g}Xe} / (\lambda_{^{133m}Xe} - \lambda_{^{133g}Xe})) D^o_{^{133m}Xe} . \quad (A6)$$

There is no separation of ^{133m}Xe from daughter ^{133g}Xe, as

there is for ^{133}I after a time t_1. Equation (A6) is similar to equation (A4) if "t_1" is long enough to allow the first exponential term to be neglected.

A.2 MONITORING THE PROTON BEAM

Without a value for F in equation (A2) only relative cross sections can be obtained. The main purpose of the present work was to obtain relative cross sections, either for the two isomers of ^{133}Xe or for the parent and daughter nuclides of iodine and xenon in the chains 133 and 135. However, it was considered worthwhile to obtain cross section values from the same irradiations by monitoring the proton flux, F, in the heavy metal foil target by simultaneously bombarding a similar copper foil. The monitor reaction ^{65}Cu (p,pn) ^{64}Cu was used in the present work over the whole energy range from 20-85 MeV. The revised excitation function of Meghir was used to obtain the monitor cross sections given in Table 8.

Substituting the data for copper in equation (A2) the proton flux, F, can be obtained from the expression,

$$F = \frac{D^{\circ}_{^{64}Cu}}{\sigma_{^{64}Cu}\, n_{^{65}Cu}\, (1 - \exp(-\lambda_{^{64}Cu}\, t_o))} \quad . \qquad (A7)$$

Assuming the same flux passes through the heavy metal target,

HMT, the cross section of a fission product nuclide, N, is given by substituting F from equation (A7) into equation (A2).

$$\sigma_N = \sigma_{64_{Cu}} \frac{D_N^o}{D_{64_{Cu}}^o} \frac{n_{65_{Cu}} (1 - \exp(-\lambda_{64_{Cu}} t_o))}{n_{HMT} (1 - \exp(-\lambda_N t_o))} . \qquad (A8)$$

It is convenient to express the relative number of monitor and heavy target nuclei in the beam by,

$$\frac{n_{65_{Cu}}}{n_{HMT}} = \frac{(SD)_{Cu}}{(SD)_{HMT}} \frac{(Ab)_{65_{Cu}}}{(Ab)_{HMT}} \frac{A_{HMT}}{A_{65_{Cu}}} . \qquad (A9)$$

Table (A2) lists the foils used and their surface densities, (SD), in mg/cm^2. In equation (A9), A is the mass number and of course $A_{65_{Cu}} = 65$; and (Ab) is the abundance of the target isotope. For all the heavy metal targets it was assumed that (Ab) = 100%. The error caused in the present results for ^{235}U by the presence of a small concentration ($\sim$5%) of ^{238}U was estimated to be negligible.

APPENDIX B

B.1 PHOTOPEAK EFFICIENCIES AND MEASUREMENT OF BETA ACTIVITY

The efficiency for detection of a gamma ray depends on its energy and the geometrical efficiency of the measurement equipment. The efficiencies used for the copper and xenon samples in this work are discussed below.

B.1.1 PHOTOPEAK DUE TO ^{64}Cu

The sample used to measure the 511-kev gamma ray of ^{64}Cu was contained in 2 ml of solution in a 5 ml standard vial. The efficiency used for this system, on different counter shelves above the crystal, was taken from the experimental calibration of Grant, May and Rayudu (GRA 61). They calibrated the equipment for the 511-kev gamma ray for a similar sample of ^{22}Na whose disintegration rate was obtained by measurement of its positron activity with a 4π-counter (PAT 55).

B.1.2 PHOTOPEAKS DUE TO XENON ISOTOPES

The xenon samples were sealed into a pyrex glass vial of approximately the same dimensions as the 2 ml liquid sample mentioned above. Fig. B1(b) shows one of these vials. Narang (NAR 63) used a similar vial to measure the 377-kev gamma ray due to ^{127}Xe (37 days). He used the efficiencies

referred to above for liquid samples. However, xenon samples are gaseous and their geometry not exactly that of the liquid samples. Therefore for the present work, efficiencies were determined for the photopeaks of energy 80 kev and 249 kev, due respectively to ^{133g}Xe and ^{135g}Xe (the latter being similar to the photopeak of 233 kev due to ^{133m}Xe). This determination also eliminated most of the error due to the method of drawing the background of the photopeaks (cf. Fig. 15). These efficiencies were measured by calibrating the gamma spectrometer for ^{133g}Xe and ^{135g}Xe, in samples from sweep (b), for which the disintegration rate was measured with a gas phase beta proportional counter. The absolute efficiency of this gas counter was determined with a standard beta source of ^{85}Kr (10.4 years) (NATL).

B.1.2.1 Equipment for Measurement of Beta Activity

First the equipment used in the measurement of beta activity is described and then the calibration of this counter and the determination of the two photopeak efficiencies is reported.

The beta proportional gas counter used in this work was similar to that described originally by Bernstein and Ballentine (BER 50) and later by several other workers (KAT 52, KAT 53, KAT 65, MEG 62, DOS 62). Fig. B1(a) shows

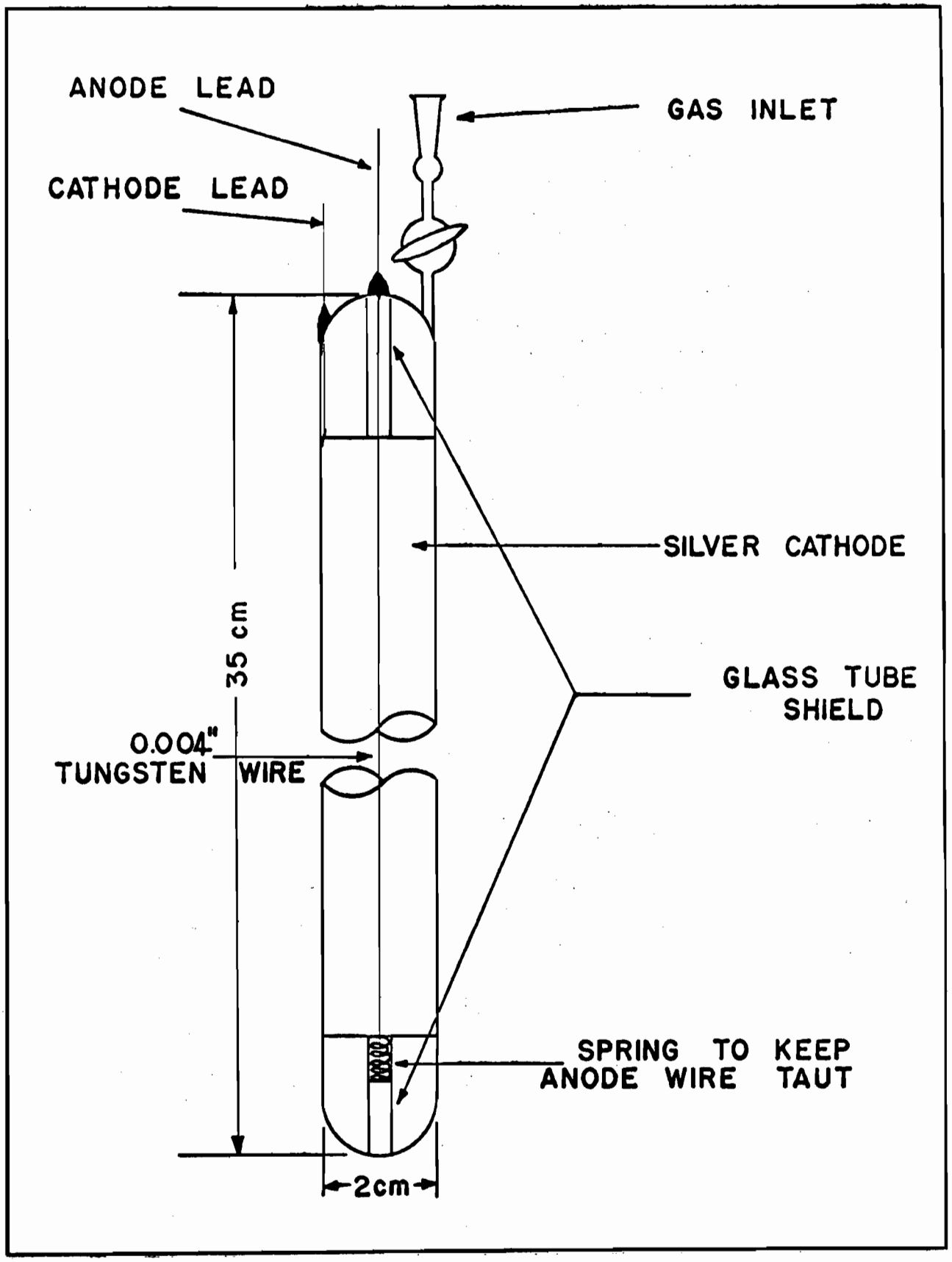

FIGURE B1. (a) The Gas-phase Beta Proportional Counter.

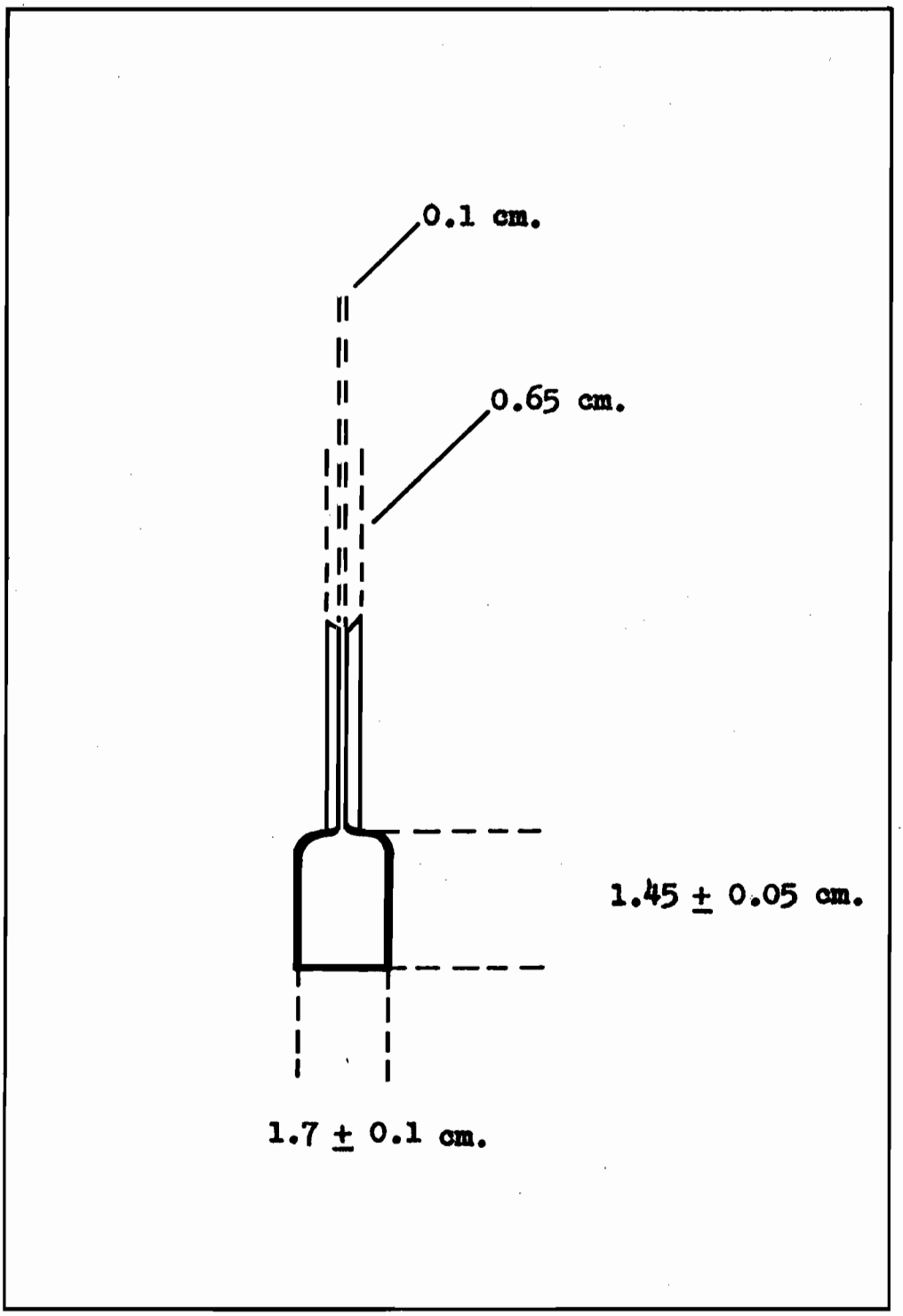

FIGURE B1. (b) Standard Vial of Pyrex Glass, used to contain a xenon sample for measurement of the gamma activity.

the cylindrical glass counter with its silver cathode on the inside walls of the tube. Fig. B2 shows schematically the counting assembly. The counter was placed vertically in a covered cylindrical lead castle. The cathode was grounded and the anode had a high positive potential from a 3 kilovolt power supply (NICH). The cathode was connected to a White 6AN8 cathode follower constructed in this laboratory by Drouin (DRO 61), which was preferred to the cathode follower used by Meghir (MEG 62). The output was fed into an amplifier-discriminator (AECL) with an overall gain of 4000. A scaler unit (MARC) recorded the counts.

The method to prepare samples in the beta counter was similar to that used to prepare the gamma samples. The rare gas sample was measured in the gas burette and transferred to the counter with the Toepler pump. The pressure of this sample in the counter was only a few millimeters of mercury. The pressure in the counter was brought up to one atmosphere with P-10 counting gas from a cylinder (MATH), with a simple filling arrangement attached to the vacuum apparatus. This arrangement was thoroughly tested to ensure that there was no loss of the active rare gas sample during the short filling period.

The counter characteristics and factors that

FIGURE B2. Schematic Diagram of the Beta Counting Assembly.

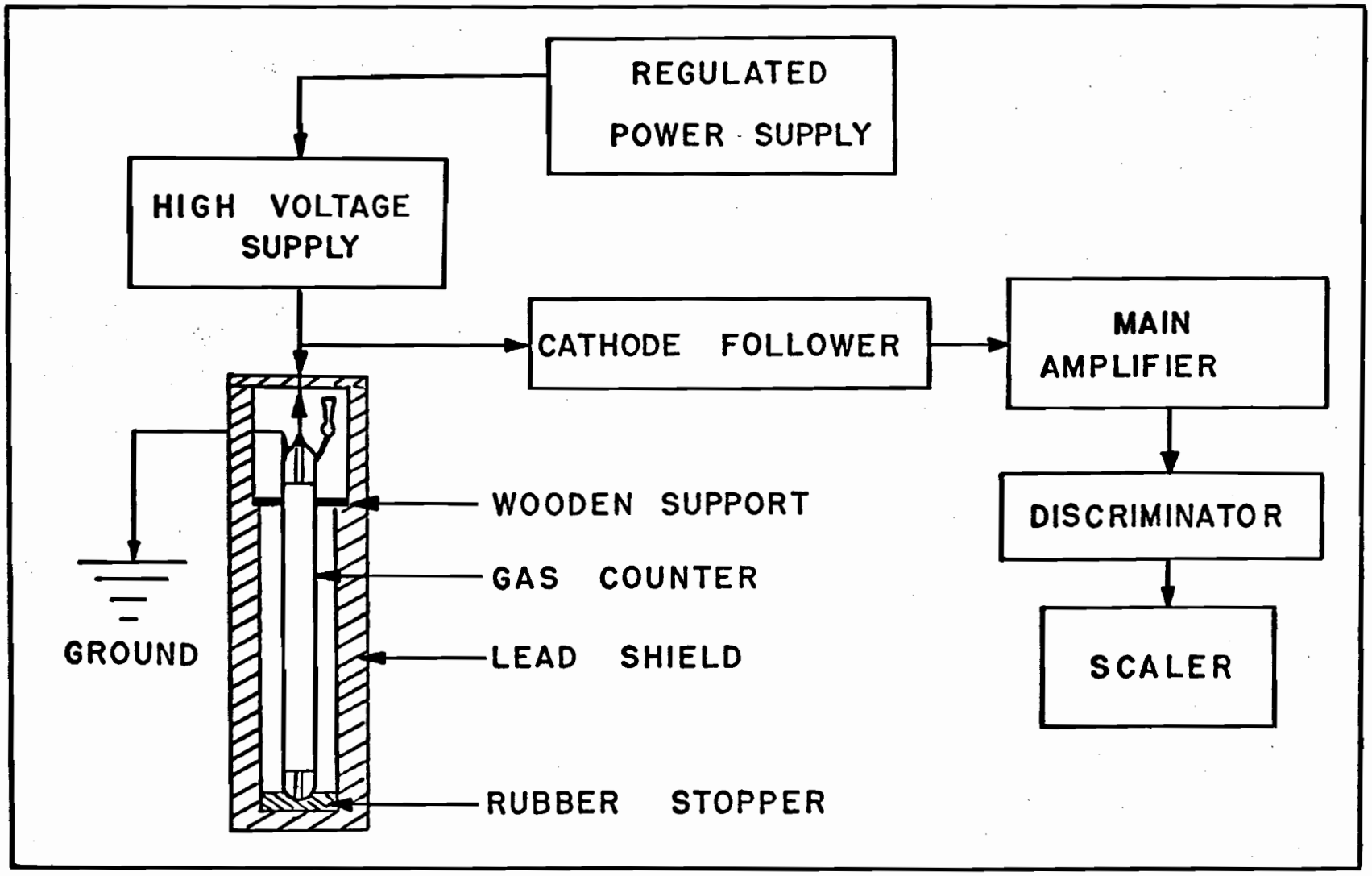

influence them have been thoroughly investigated elsewhere (BER 50, DRO 61, MEG 62). Plateau characteristics were checked in each experiment. The operating potential was about 2100 volts and the plateau length was always about 200 volts. The discriminator bias was maintained at 10 volts. Gas impurities, particularly electro-negative species, in a rare gas sample increase the threshold and shorten the plateau. Before preparation of beta samples the rare gases were therefore carefully purified over titanium sponge at 850°C. The P-10 counting gas was a mixture of very pure argon and methane (9:1).

Resolution losses were not very large for the samples that were measured, which had activities below 10^5 c.p.m. and much lower activities for the ^{133g}Xe. The dead time, 90 microseconds, reported by Meghir (MEG 62) using a different cathode follower was longer than expected (BER 50). He described the method to determine resolution loss using paired sources (PAT 55) of ^{32}P (14.3 days). This experiment was repeated for the present equipment and gave a dead time of about 20 microseconds. This necessitated a small correction of about 3×10^3 c.p.m. to be added to a measured beta counting rate of 10^5 c.p.m.

B.1.2.2 Efficiency of the Beta Counter

The efficiency of the counter was obtained by measuring the activity of a known amount of a standard beta source of ^{85}Kr (10.4 years) (NATL). This isotope emits a beta particle of energy 0.67 MeV which is intermediate to the energies, 0.347 MeV and 0.91 MeV, of the beta particles from ^{133g}Xe and ^{135g}Xe, respectively. It may therefore be assumed that the efficiency determined for ^{85}Kr would be the same as that for these two isotopes of xenon.

With the same apparatus used for handling the xenon samples, a krypton sample was prepared by transferring krypton with the Toepler pump from a reservoir to the gas burette from which a measured number of gram molecules were transferred to the beta counter. The disintegration rate of the sample was obtained from the known specific disintegration rate of the standard beta source of krypton (60.8×10^6 d.p.s./gm.mol. on October 9, 1962). The pressure in the counter was brought up to one atmosphere with P-10 gas and the plateau characteristics were determined to optimize the operating voltage. Only the fraction of the krypton sample in the "active volume" of the counter contributed to the measured activity. The electric field was restricted to this active volume enclosed by the cathode. Fig. B1(a) shows that

outside this region the anode wire was surrounded by glass tube shields. The active volume was determined simply by weighing the counter empty and then filled with appropriate amounts of toluene (MEG 62). The active volume of the tube was found to be 84.0 $\pm$ 0.5%.

For five different samples with activities from 40,000-100,000 c.p.m., the mean efficiency in the active volume was 97%. The low standard deviation of 3% in these measurements demonstrated indirectly the reliability of the gas handling and measuring techniques and the P-10 filling system and counting equipment. In previous work an efficiency of $\sim$99% was used by Dostrovsky and Stoenner (DOS 62) and for lower beta energies Meghir obtained an efficiency of about 80%, but Bernstein and Ballentine used an efficiency of 98%.

B.1.2.3 Efficiency of Xenon Photopeaks

For the determination of the photopeak efficiency xenon samples from sweep (b) were used. The activity of these samples was due to xenon which had come only from decay of iodine, and therefore contained only ^{135g}Xe (9.2 hours) and ^{133g}Xe (5.3 days), with no interfering activity from ^{133m}Xe (2.3 days) and from more neutron-deficient xenon

isotopes. Two types of calibration were made.

Method (i). A sample of xenon was divided, in a measured ratio, into a beta sample and a gamma sample. The disintegration rate of the gamma sample was then calculated from the beta counting data, and the efficiency of the photopeak area determined, for the sample on a particular counting shelf above the crystal.

Method (ii). The gamma activity of a xenon sample was first measured for about twelve days and then the vial was broken in the vacuum apparatus and a known fraction ($\approx 100\%$) of this sample then transferred to the beta counter. The beta counting provided a disintegration rate for the ^{133g}Xe in the sample. It proved difficult to break the vial, but one successful experiment was made.

Table B1 gives the measured efficiencies for the photopeaks of energy 80 kev and 249 kev, when the sample was on the lowest shelf (shelf 0). Shelf 7 was used only for the first measurements of xenon samples from sweep (a) in which there was a very intense activity due to ^{135g}Xe. From numerous determinations the relative efficiency of shelf 0 to shelf 7 was 9.9 ± 0.1. Table B1 also shows that the efficiencies determined for gas samples were a little higher than those determined for liquid samples (GRA 61), but the

small difference could be due to a difference in their method of drawing the background and obtaining the area under the photopeak.

TABLE B1. Measurement of Photopeak Efficiencies for ^{135g}Xe and ^{133g}Xe

(sweep (b) sample from) Experiment Number,	Exp. Method	Efficiency (Sample on shelf 0)	
		249-kev (^{135g}Xe)	80-kev (^{133g}Xe)
E2	i	-	0.25 ± .02
E5	i	-	0.29 ± .02
R5	i	0.20 ± .03	-
R6	i	0.21 ± .03	-
R7	i	0.23 ± .02	-
R16	ii	-	0.27 ± .02
Mean value used:		0.22 ± .02	0.27 ± .02
Comparative values from efficiency curves for liquid samples (GRA 61) :		0.20	0.23

The efficiency curves of Grant et al. (GRA 61) suggested that the efficiencies of the 233- and 249-kev photopeaks would not be very different. An efficiency of 0.225 was therefore used for the former photopeak due to ^{133m}Xe.

B.2 BETA MEASUREMENT OF XENON PRODUCED IN FISSION

In the present work, beta counting was used only to calibrate the gamma counting method used to measure the activities of ^{135}Xe, ^{133m}Xe and ^{133g}Xe. Although previous studies by Storms (STO 62) and by James et al. (JAM 64) have measured the xenon formed in fission with a beta counter, this technique was not used here because of the complexity of the beta decay curves obtained for the sample from sweep (a). As well as the activity of ^{135g}Xe (9.2 hours) there were three components due to (1) independently formed ^{133g}Xe (5.3 days), (2) independently formed ^{133m}Xe (2.3 days), and (3) ^{133g}Xe produced in the decay of the independently formed ^{133m}Xe. A FORTRAN program based on simple decay equations was used to obtain theoretical decay curves for these three components, with different isomer ratios for ^{133}Xe and different values for the α_T of ^{133m}Xe. Fig. B3 shows a good example of such a set of curves, where $\alpha_T = 6.3$ and the isomer ratio was equal to one. It shows the three components and the total beta activity, (4a). Apparently only after several days would the latter activity have a half life of 5.3 days. The observed beta decay curves were due to a curve similar to (4a) in Fig. B3 together with a high initial activity of ^{135g}Xe (9.2 hours) and small but significant

FIGURE B3.

Theoretical beta decay curves for ^{133}Xe, with an isomer ratio of one and $\alpha_T = 6.3$.

The curves are for

(1) independently formed ^{133g}Xe (5.3 days),

(2) independently formed ^{133m}Xe (2.3 days),

(3) ^{133g}Xe grown from the decay of independently formed ^{133m}Xe.

Curve (4a) is the sum of the above three components. It is the theoretical total beta activity of ^{133}Xe. If all the ^{133}Xe were formed as ^{133g}Xe, then curve (4b) would represent the total beta activity.

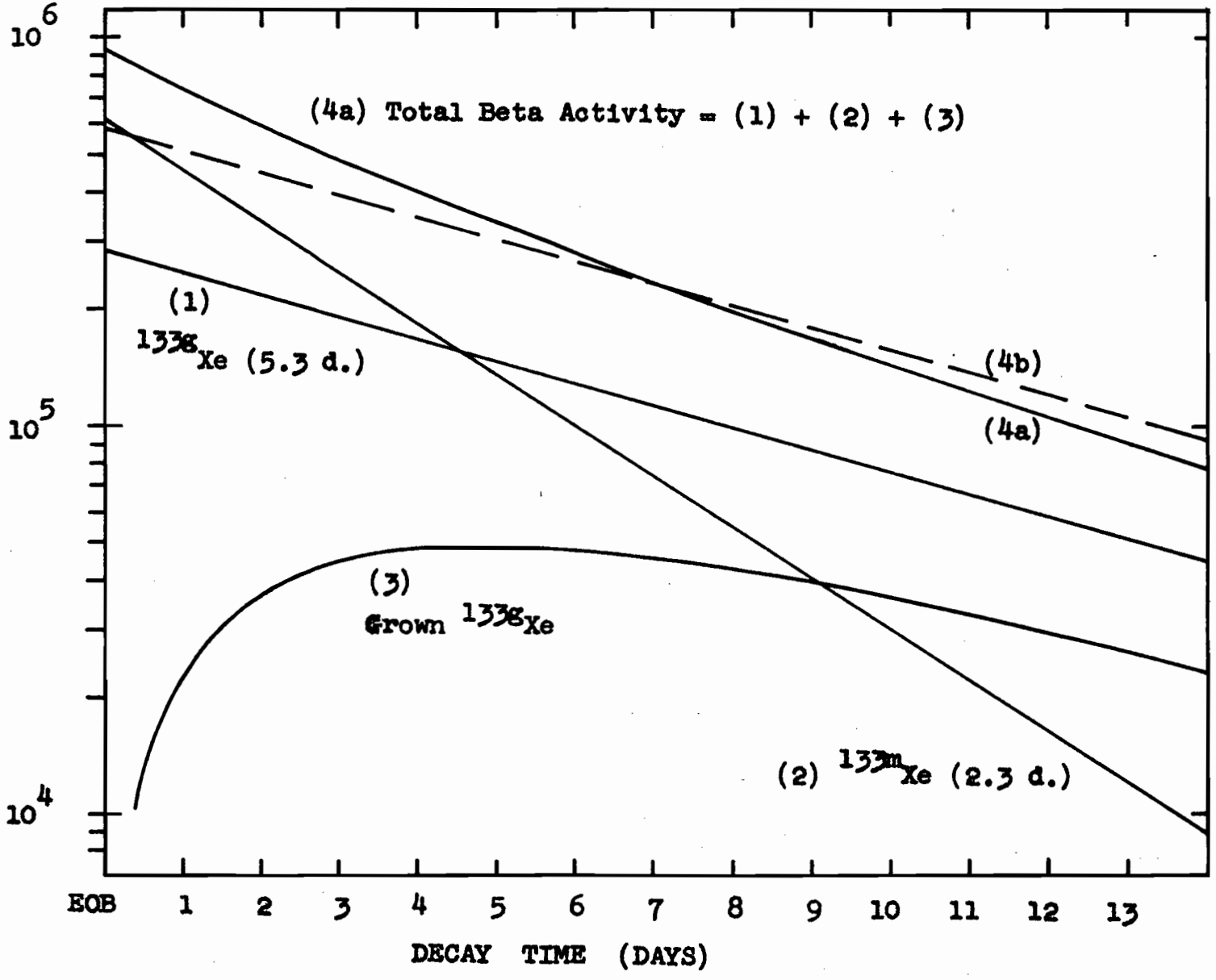
(4a) Total Beta Activity = (1) + (2) + (3)
(1)
133g Xe (5.3 d.)
(4b)
(4a)
(3)
Grown 133g Xe
(2) 133m Xe (2.3 d.)
BETA
ACTIVITY
(Arbitrary
Units)
10^6
10^5
10^4
EOB
1
2
3
4
5
6
7
8
9
10
11
12
13
DECAY TIME (DAYS)

activities of longer-lived xenon isotopes (Table 5). Obviously the latter activities would become more important at higher fission energies.

Storms measured his xenon sample from sweep (a) for only the first two days because his sample from sweep (b) was then measured in the same counter. This was a very unsatisfactory method, because of the complexity of the beta decay curve in this early period (Fig. B3), especially as his sample (a) often had considerable krypton contamination which introduced short-lived activities due to ^{85m}Kr (4.4 hours), ^{87}Kr (78 minutes) and ^{88}Kr (2.8 hours). It was not surprising that the data from his beta measurements gave no indication of the activity of half-life 2.3 days, but it was surprising that no 233-kev gamma ray was detected in a test that he made. On the basis of his evidence he assumed that there was a negligible yield of ^{133m}Xe in medium-energy fission. This assumption now appears to be wrong as a result of the present work on ^{133}Xe and of the work on isomeric yields for the similar nuclides ^{131}Te and ^{133}Te (SAR 65). The results of the present work have been communicated to Storms and he has recently proposed (STO 65) that he should revise his results for the mass chain 133. It would be difficult to do this here because of the

complexity of his activity data. He estimated (STO 62) that if the isomeric yield ratio of ^{133}Xe was 1.0 his yields, based on an isomer ratio of zero, would be too high by 30-40%.

The dashed line (4b) in Fig. B3 represents the theoretical decay curve for the total beta activity if all the ^{133}Xe was formed as ^{133g}Xe. Fortuitously the right-hand tails of the theoretical curves (4a) and (4b) are very close. This suggests that if Storms had counted his sample (a) for longer periods his errors would probably have been smaller.

James, Martin and Silvester (JAM 64) measured the beta activity of ^{133}Xe and ^{135}Xe produced in fission of ^{238}U with 14.7-MeV neutrons. Their samples were part of the gas filling in a Geiger-Muller tube. They have drawn important conclusions about fine structure (Section 1A.3.1) in the mass distribution curve, because they obtained an unexpectedly high yield for the mass chain of A = 133. It is therefore important that their data be reviewed in view of the present work on ^{133}Xe. They have not reported the interpretation of their data in sufficient detail for this review to be made here. If they did assume that the isomer yield ratio for ^{133}Xe was very small, fortuitously the corresponding error may be small, as shown above.

In the present work for a few early experiments with ^{238}U, the beta activity of xenon samples taken from sweep (a) was measured, but the decay curves gave no evidence for the presence of ^{133m}Xe. This might be expected from the above discussion. In the present research, the formation of this isomer in reasonable yield was first established by the detection of a 233-kev photopeak which decayed with a half-life of 2.3 days.

A disadvantage of gamma counting in the present work was that the measured independent cross sections for ^{133m}Xe, and therefore for ^{133g}Xe, were very dependent on the poorly defined (Sections 4A.1 and 4B.1) total conversion coefficient, α_T, for the highly converted gamma rays of ^{133m}Xe. Integral beta counting has been shown to be an unsuitable alternative method of measurement. However, there would be many advantages to using a beta spectrometer to measure the conversion electrons. This could eliminate some of the difficulties due to other xenon isotopes and to low gamma activity of ^{133m}Xe. Furthermore the isomer ratios obtained would be far less sensitive to the value of α_T.

APPENDIX C

METHOD (2) TO DETERMINE Z_p. BATEMAN EQUATIONS FOR GROWTH AND DECAY IN CHAIN 133

Section 4A.2 outlined the principles of method (2) to determine Z_p, and showed that the simpler method (1) was satisfactory to interpret most of the present data. Since method (2) was used to check method (1) and may prove useful in future work at lower energy, some further details are described briefly. Storms (STO 62) described in detail a very similar method to determine Z_p in chain 133, from data similar to those in this work. The present method (2) differed only in that it used more recent parameters and used a different stepwise reiteration method from that used by Storms to solve essentially the same two simultaneous equations.

These two equations describing the activities of ^{133g}Xe, measured in the xenon samples from sweeps (a) and (b), were constructed simply from the early Bateman equations (BAT 10, FRI 64). In a Bateman decay chain of n radioactive members, only the first member must be present initially ($t = 0$). If the initial number of atoms of this first member was N_1^o, then the number of atoms of the nth member after time t is given by,

$$N_n^t = C_1 e^{-\lambda_1 t} + C_2 e^{-\lambda_2 t} + ... + C_n e^{-\lambda_n t} , \qquad (C1)$$

where

$$C_1 = \frac{\lambda_1 \lambda_2 \cdots \lambda_{(n-1)}}{(\lambda_2-\lambda_1)(\lambda_3-\lambda_1)\cdots(\lambda_n-\lambda_1)} N_1^o ,$$

and

$$C_2 = \frac{\lambda_1 \lambda_2 \cdots \lambda_{(n-1)}}{(\lambda_1-\lambda_2)(\lambda_3-\lambda_2)\cdots(\lambda_n-\lambda_2)} N_1^o .$$

This convenient equation (C1) was applied to chain 133 by dividing the latter into nine Bateman chains with values of n from 1 to 5. Table C1 describes schematically these nine chains and gives the N_1^o used for each chain. The various parameters are represented by the names which were used in the FORTRAN program. These are defined here for the chain 133.

1 = ^{133}Sb (2.64 mins)

2M = ^{133m}Te (53 mins)

2G = ^{133g}Te (12.5 mins)

3 = ^{133}I (20.8 hours)

4M = ^{133m}Xe (2.3 days)

4G = ^{133g}Xe (5.3 days)

(N.B. The FORTRAN names of the decay constants were AL1, AL2M, AL2G, etc.)

TABLE C1.

The Nine Bateman Chains Used for the Mass Chain 133

Bateman Chain No.	Length, n		N_1^o = (X. f. Y) X =	f =
1	4	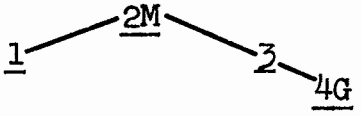	FBR1 x FBR2	f_1^{cum}
2	3	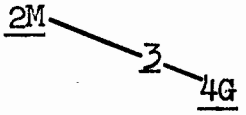	$\frac{TEISR}{(1+TEISR)}$ x FBR2	f_2^{ind}
3	2	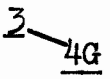	1	f_3^{ind}
4	1		$\frac{1}{(1 + XEISR)}$	f_4^{ind}
5	5	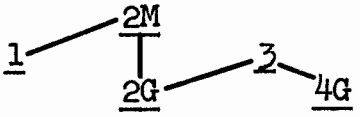	(1-FBR2) x FBR1	f_1^{cum}
6	4	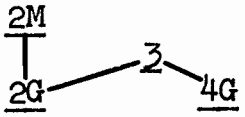	(1-FBR2) $\frac{TEISR}{(1+TEISR)}$	f_2^{ind}
7	4	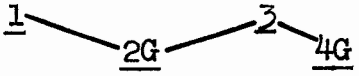	(1 - FBR1)	f_1^{cum}
8	3	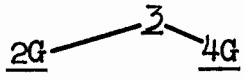	$\frac{1}{(1 + TEISR)}$	f_2^{ind}
9	2		$\frac{XEISR}{(1 + XEISR)}$	f_4^{ind}

Branching ratios,

FBR1 = 0.72,

and FBR2 = 0.87.

Isomer ratios,

TEISR = 2.0 (for $^{133m}Te/^{133g}Te$),

and XEISR = 1.0 (for $^{133m}Xe/^{133g}Xe$).

In the expression for N_1^o,

f = the fractional chain yield of an isobar

X = a factor introduced in the Bateman chain to account for branching and isomeric yield ratios

Y is proportional to the total number of fission product atoms of mass 133 formed in an experiment.

Using equation (C1) for these nine Bateman chains, an expression of twenty-seven terms was constructed to give the activity of ^{133g}Xe (= 4G) at the end of sweep (a). This expression will be referred to here as equation (C2) and the latter activity had the FORTRAN name AEO14G, where AEO14G = ($C^a_{^{133g}Xe}$/YA) (cf. Table 7). In all these terms, t = T1, where T1 = (t_1 + (t_o/2)) (cf. Table 6). In the Bateman chain (9), ^{133m}Xe was not separated from ^{133g}Xe and this was

accounted for by neglecting the corresponding first term in equation (C1) (cf. equation A6, Appendix A).

Some of the twenty-seven terms made a negligible contribution to the activity AE014G. However, no approximations were made, since this would have saved very little execution time on the computer and could have introduced errors.

The activity of ^{133g}Xe at the end of sweep (b) was given by another expression, referred to here as equation (C3). This activity had the FORTRAN name AE024G, where AE024G = ($C^{b}_{133g_{Xe}}$/YB) (cf. Table 7). Equation (C3) was constructed using two equations like (C2) except that Bateman chains (4) and (9) were excluded, because the xenon activity from sweep (b) resulted purely from precursor decay. The number of atoms of ^{133g}Xe present at the end of sweep (b) was calculated by subtracting the number formed in precursor decay in the time t = T1, from the number similarly formed in time t = (T1 + T2), where T2 = t_2 (Table 6).

The essential details of method (2) have now been given above and in Section 4A.2.3. For possible use in future work, more exact details are contained in the thesis of Storms (STO 62). Further, the FORTRAN source list is reproduced here and this complements the other descriptions

of method (2). Briefly, method (2) was programed as follows.

The subprogram SUBROUTINE NEWXEI computed XEOLD, Y, and XENEW using methods described elsewhere in this thesis. The main program iterated this subprogram until a value of $(Z - Z_p)$ gave XENEW $\approx$ XEOLD. The main program contains READ and FORMAT statements which describe the necessary input data. The output data included the final values for XEOLD and XENEW and the corresponding $(Z - Z_p)$ value for ^{133}Xe. These results have been discussed in Section 4A and given in Table 12.

FORTRAN SOURCE LIST

Main Program

133 CHAIN

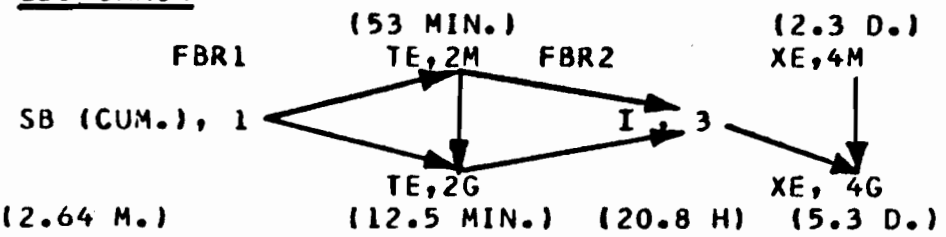


```
      COMMON DZ,ZMZP,XEOLD,XENEW,FCUMI,Y,C,AEO14G,AEO24G,NUMBER,A,
     1 FC157(2),FC268(2),FC3(2),FC49(2)
      AL1 = 0.6931 / (2.64 / 60.0 )
      AL2M = 0.6931 / (53.0 / 60.0 )
      AL2G = 0.6931 / ( 12.5 / 60.0 )
     AL3 = 0.6931 / 20.8
      AL4M = 0.6931 / ( 2.3 *24.0            )
       AL4G = 0.6931 / (5.3 * 24.0 )
      FBR1 =  0.72
      FBR2 = 0.87
      TEISR = 2.0
     C1P1     = ALF4 ( AL1,AL2M,AL3,AL4G )
     C1P12M   = ALF4 ( AL2M,AL1,AL3,AL4G )
     C1P13    = ALF4 ( AL3,AL1,AL2M,AL4G )
     C1P14G   = ALF4 ( AL4G,AL1,AL2M,AL3 )
     C2P2M    = ALF3(AL2M,AL3,AL4G )
     C2P2M3   = ALF3(AL3,AL2M,AL4G )
     C2P2M4   = ALF3(AL4G,AL2M,AL3 )
      C3P3     = ALF2 (AL3,AL4G )
      C3P34G   = ALF2 (AL4G,AL3 )
      C4P4G = AL4G
     C5P1    = ALF5 (AL1,AL2M,AL2G,AL3,AL4G )
     C5P12M = ALF5 (AL2M,AL1,AL2G,AL3,AL4G )
     C5P12G = ALF5 (AL2G,AL1,AL2M,AL3,AL4G )
     C5P13     = ALF5 (AL3,AL1,AL2M,AL2G,AL4G )
     C5P14G    = ALF5 (AL4G,AL1,AL2M,AL2G,AL3 )
      C6P2M     = ALF4 (AL2M,AL2G,AL3,AL4G )
      C6P2MG    = ALF4 (AL2G,AL2M,AL3,AL4G )
      C6P2M3    = ALF4 (AL3,AL2M,AL2G,AL4G )
      C6P2M4    = ALF4 (AL4G,AL2M,AL2G,AL3 )
       C7P1     = ALF4 (AL1,AL2G,AL3,AL4G )
       C7P12G   = ALF4 (AL2G,AL1,AL3,AL4G )
       C7P13    = ALF4 (AL3,AL1,AL2G,AL4G )
       C7P14G   = ALF4 (AL4G,AL1,AL2G,AL3 )
       C8P2G    = ALF3 (AL2G,AL3,AL4G )
       C8P2G3   = ALF3 (AL3,AL2G,AL4G )
       C8P2G4   = ALF3 (AL4G,AL2G,AL3 )
      C9P4MG = ALF2 (AL4G,AL4M )
      DIMENSION   D(28)
      D(1) = C1P1*FBR1*FBR2
```

```
      D(2) = C1P12M  *FBR1*FBR2
      D(3) = C1P13   *FBR1*FBR2
     D(4) = C1P14G   *FBR1*FBR2
     D(5) = C2P2M     *FBR2*TEISR/(1.0 + TEISR )
     D(6) = C2P2M3    *FBR2*TEISR/(1.0 + TEISR )
     D(7) = C2P2M4    *FBR2*TEISR/(1.0 + TEISR )
     D(8) = C3P3
     D(9) = C3P34G
     D(11) = C5P1 * FBR1*(1.0-FBR2)
     D(12) = C5P12M      *FBR1*(1.0 - FBR2)
     D(13) = C5P12G      *FBR1*(1.0 - FBR2)
    D(14)= C5P13         *FBR1*(1.0 - FBR2)
    D(15) = C5P14G       *FBR1*(1.0 - FBR2)
    D(16) = C6P2M    *(1.0-FBR2)*TEISR /(1.0 + TEISR)
    D(17) = C6P2MG   *(1.0-FBR2)*TEISR /(1.0 + TEISR)
    D(18) =C6P2M3    *(1.0-FBR2)*TEISR /(1.0 + TEISR)
    D(19) =C6P2M4    *(1.0-FBR2)*TEISR /(1.0 + TEISR)
    D(20) =  C7P1       *(1.0-FBR1)
    D(21) = C7P12G      *(1.0-FBR1)
    D(22) = C7P13       *(1.0-FBR1)
    D(23) = C7P14G      *(1.0-FBR1)
    D(24) = C8P2G       *1.0 /(1.0 + TEISR )
    D(25) = C8P2G3      *1.0 /(1.0 + TEISR )
    D(26) = C8P2G4      *1.0 /(1.0 + TEISR )
     WRITE(6,800) (II,D(II), II = 1,27 )
800 FORMAT(1H1,(I10, E15.5,//)   )
 15  READ(5,100) NAME,ENERGY, XEISR, AEO14G, AEO24G, T1,T2, C, YA,YB
100  FORMAT (2A6, F6.2,2F9.0,2F6.3, 11X, F5.2,2F4.2 )
       WRITE (6,300)
300  FORMAT(1H1,5X,100H  XEISR.   AEO14G    AEO24G   T1       T2     YA
   1     YB              C              RUN  E.MEV.                    )
      WRITE(6,200)            XEISR, AEO14G, AEO24G, T1, T2,   YA,YB
   1, C, NAME, ENERGY
200  FORMAT(1HO,5X,F7.2, 2F10.0,2F7.3,2F6.2,10X, F6.2,10X,2A6  )
     D(10) = C4P4G*1.0/(1.0 + XEISR )
     D(27) = C9P4MG *XEISR /(1.0 + XEISR )
     I10 = 10
     I27 = 27
     WRITE(6,850) I10, D(10), I27, D(27)
850   FORMAT(1HO,2(I10       ,E15.5,//))
      F ( C , AL,T)= C * EXP ( - AL *          T )
      T =  T1
      DO  2  I = 1,2
      F1P1      = F ( C1P1,AL1 ,T)
      F1P12M    = F ( C1P12M,AL2M ,T)
      F1P13     = F ( C1P13, AL3 ,T)
      F1P14G    = F ( C1P14G, AL4G ,T)
      F2P2M     = F ( C2P2M,AL2M ,T)
      F2P2M3    = F ( C2P2M3, AL3 ,T)
      F2P2M4    = F ( C2P2M4,AL4G ,T)
       F3P3      = F (C3P3,AL3,T)
       F3P34G    = F (C3P34G,AL4G,T)
      F4P4G  = F(C4P4G ,AL4G ,T)
      F5P1     =  F ( C5P1,AL1 ,T)
      F5P12M   =  F ( C5P12M,AL2M ,T)
```

```
      F5P12G  =  F ( C5P12G,AL2G ,T)
      F5P13   =  F ( C5P13,AL3 ,T)
      F5P14G  =  F ( C5P14G,AL4G ,T)
      F6P2M    = F(C6P2M,AL2M ,T)
      F6P2MG   = F(C6P2MG,AL2G ,T)
      F6P2M3   = F(C6P2M3,AL3 ,T)
      F6P2M4   = F(C6P2M4,AL4G ,T)
      F7P1    =  F(C7P1,AL1 ,T)
      F7P12G  =  F(C7P12G,AL2G ,T)
      F7P13   =  F(C7P13,AL3 ,T)
      F7P14G  =  F(C7P14G,AL4G ,T)
      F8P2G    =  F(C8P2G,AL2G ,T)
      F8P2G3   =  F(C8P2G3,AL3 ,T)
      F8P2G4   =  F(C8P2G4,AL4G ,T)
        F9P4MG  = F( C9P4MG,AL4G ,T)
      FC1 = FBR1*FBR2* (F1P1 +F1P12M + F1P13 +F1P14G )
      FC2 = FBR2*TEISR /(1.0 + TEISR)*(F2P2M+F2P2M3+F2P2M4 )
     FC3(I)= (F3P3 + F3P34G )
     FC4 = 1.0 / (1.0 + XEISR )*(F4P4G )
     FC5 = FBR1*(1.0 -FBR2)*( F5P1+F5P12M+F5P12G+F5P13+F5P14G )
     FC6 = (1.0 -FBR2)*TEISR / (1.0 +TEISR)*(F6P2M+F6P2MG
    1+ F6P2M3 +F6P2M4 )
      FC7= (1.0 -FBR1)*(F7P1 + F7P12G +F7P13 +F7P14G )
     FC8 = 1.0 /(1.0+ TEISR)*(F8P2G + F8P2G3 + F8P2G4 )
      FC9 = XEISR /(1.0 + XEISR ) *F9P4MG
      FC157 (I) = FC1 +FC5 + FC7
      FC268(I) = FC2 + FC6+FC8
      FC49 (I) = FC4 + FC9
      WRITE (6,977) C3P3,C3P34G,C9P4MG,F9P4MG,FC9
 977   FORMAT(1HO,5E20.5 )
     WRITE (6,700)   FC4, FC9
 700   FORMAT (1HO,     6H FC4=     ,E20.5 ,6H FC9=         ,E20.5  )
   2   T = T2     + T1
     WRITE(6,111)FC157(2),FC157(1),FC268(2),FC268(1),FC3(2),FC3(1)
 111 FORMAT(1HO,8X,23H Y = AEO24G/ (SBFCUM*(      ,E14.5,3H -  ,E14.5,2H
    1H ) ,14H  + TEFIND*(    ,E14.5, 3H -   ,E14.5, 2H ) ,    //,
    2 11H + FINDI* (
    3      ,E14.5, 3H - ,E14.5,5H ) )   )
     WRITE(6,1111) FC157(1),FC268(1),FC3(1),FC49(1)
1111  FORMAT    (1HO,8X,      32H   XENEW =((AEO14G/Y) -(SBFCUM*     ,
    1E14.5,11H + TEFIND*   ,E14.5,11H  + FINDI *     ,E14.5,3H))/   ,
    2   E20.5 )
     WRITE (6,8888 )
8888 FORMAT( 110HO STEP NO.    XENEW        XEOLD       FCUM       FCUMI
    1/XEOLD         Z - ZP   ATOM CH. Y.                              )
      AEO14G = AEO14G / YA
     AEO24G = AEO24G / YB
       NUMBER = 0.0
     ZMZP = 2.1
       A = 1. / SQRT ( 3.142 * C )
     DZ = 0.1
     DO 25  L= 1,25
      CALL      NEWXEI
     IF (XENEW/XEOLD .LE. 1.0)  GO TO 22
     IF (ZMZP.GE.0.0 ) GO TO 25
```

```
998    WRITE (6,997)
997    FORMAT (80H0  Z-ZP WENT NEGATIVE IN FIRST 0.1 DO LOOP THIMK
   1                                                              )
 25    CONTINUE
 22     ZMZP = ZMZP + 0.15
       DZ = 0.01
       WRITE (6,1)  L
  1    FORMAT (8H0 L =        , I3 , ///)
       DO 35   K = 1,20
 35     CALL       NEWXEI
        GO TO 15
        END
```

```
       SUBROUTINE  NEWXEI
       COMMON DZ,ZMZP,XEOLD,XENEW,FCUMI,Y,C,AE014G,AE024G,NUMBER,A,
     1 FC157(2),FC268(2),FC3(2),FC49(2)
       NUMBER = NUMBER + 1
       GSSFI ( ZZMZP ) = A * EXP (- ZZMZP **2 / C )
       ZMZP = ZMZP - DZ
       XEOLD = GSSFI( ZMZP)
       FINDI= GSSFI( ZMZP - 1.0 )
        TEFIND= GSSFI(ZMZP - 2.0 )
       SBFIND = GSSFI(ZMZP - 3.0 )
       SBPIND= GSSFI (ZMZP - 4.0 )
        SBGPI = GSSFI( ZMZP - 5.0 )
        SBFCUM = SBFIND +  SBPIND + SBGPI
       FCUMI = FINDI + TEFIND + SBFCUM
       RATIO = FCUMI / XEOLD
      Y= AE024G /(SBFCUM*(FC157(2) - FC157(1)) +TEFIND* ( FC268(2) -
     1 FC268(1)) + FINDI*(FC3(2) - FC3(1)))
      XENEW = (AE014G / Y -(SBFCUM *FC157(1) + TEFIND * FC268(1) +
     1 FINDI * FC3(1)))/ FC49(1)
       WRITE(6,888) NUMBER,XENEW,XEOLD,FCUMI, RATIO, ZMZP, Y
888    FORMAT( 1H ,I10,3F12.6 ,E17.5 , F10.4, E16.5  )
       RETURN
         END
```

```
      FUNCTION ALF2 (A1,A2)
      ALF2 = A1*A2 /(A2 - A1 )
      RETURN
     END
```

```
      FUNCTION ALF3 (A1,A2,A3 )
     ALF3 = A1*A2*A3 /((A2-A1)*(A3-A1))
      RETURN
    END
```

```
      FUNCTION  ALF4 (A1,A2,A3,A4 )
      ALF4                = A1*A2*A3*A4 /((A2-A1)*(A3-A1)*(A4-A1))
       RETURN
     END
```

```
      FUNCTION  ALF5 (A1,A2,A3,A4,A5 )
      ALF5 = A1*A2*A3*A4*A5 /((A2-A1)*(A3-A1)*(A4-A1)*(A5-A1))
       RETURN
     END
```

BIBLIOGRAPHY

AECL Atomic Energy of Canada Ltd. (Model, AEP 1109).

ALB 57 D.E. Alburger, in "Encyclopedia of Physics", Vol. XLII, p.1-108 (published by Springer-Verlag, Berlin, 1957).

ALE 57 J.M. Alexander and C.D. Coryell, Phys. Rev., 108, 1274 (1957).

APA 60 V.F. Apalin, U.P. Dobrynin, V.P. Zakharova, I.E. Kutikov and L.A. Mikaelyan, Atomnaya Energia 8, 15 (1960)

APA 62 V.F. Apalin, Y.N. Gritsyuk, I.Y. Kutikov, V.I. Lebedev and L.A. Mikaelyan, Nucl. Phys., 38, 193 (1962); and Soviet Phys. -JETP 16, 235, 1451 (1963).

APA 64 V.F. Apalin, Y.N. Gritsyuk, I.Y. Kutikov, V.I. Lebedev and L.A. Mikaelyan, Nucl. Phys., 55, 249 (1964).

APO 62 A.N. Apollonova, I.T. Krisyuk and V.N. Ushatskii, Radiokhimiya, 4, 711 (1962) (in Russian) - Nuclear Science Abstract 17-15306.

ARA 65 N.K. Aras, M.P. Menon and G.E. Gordon, Nucl. Phys., 69, 337 (1965).

ARM 64 P. Armbruster, D. Hovestadt, H. Meister and H.J.Specht, Nucl. Phys., 54, 586 (1964).

ARM 65 P. Armbruster, Symposium on the Physics and Chemistry of Fission, I.A.E.A., Salzburg, Paper SM-60/11 (1965).

ARN 47 J.R. Arnold and N. Sugarman, J. Chem.Phys.,15, 703 (1947).

AUB 61 R. Aubeau, L. Champeix et Mme J. Reiss, J. Chromatog., 6, 209 (1961).

BAI 59 S.M. Bailey, Ph.D. Thesis, Department of Chemistry, University of California, UCRL-8710 (1959).

BAI 60 "A Handbook of Scintillation Spectrometry" by Baird-Atomic Inc., Massachusetts (1960).

BAR 65 E. Barnard, A.T.G. Ferguson, W.R. McMurray, I.J. Van Heerden, Nucl. Phys., 71, 228 (1965).

BAT 10 H. Bateman, Proc. Cambridge Phil.Soc. 15, 423 (1910).

BAT 65 R. Batchelor, W.B. Gilboy, J.H. Towle, Nucl. Phys., 65, 236 (1965).

BAY 61 J.G. Bayly, M.F. Duret, N.B. Poulsen and R.H.Tomlinson, Can.J. Phys., 39, 1391 (1961).

BEN 65 P.P. Benjamin, Ph.D. Thesis, Department of Chemistry, McGill University (1965).

BER 50 W. Bernstein and R. Ballentine, Rev. Sci. Instr., 21, 158 (1950).

BER 52 I. Bergstrom, Arkiv For Fysik, 5, 191 (1952).

BER 54 I. Bergstrom, S. Thulin, A.H. Wapstra and B. Astrom, Arkiv For Fysik, 7, 255 (1954).

BIS 61 C.T. Bishop, Argonne National Laboratory Report, ANL-6405 (1961) (unpublished).

BIS 64a C.T. Bishop, H.K. Vonach and J.R. Huizenga, Nucl.Phys., 60, 241 (1964).

BIS 64b C.T. Bishop, J.R. Huizenga and J.P. Hummel, Phys. Rev., 135, B401 (1964).

BJO 58 F. Bjorklund and S. Fernbach, Phys. Rev., 109, 1295 (1958).

BLA 52 J.M. Blatt and V.F. Weisskopf, Theoretical Nuclear Physics, John Wiley and Sons Inc., New York (1952).

BLA 60 H.M. Blann, Ph.D. Thesis, University of California Radiation Laboratory, Report UCRL-9190 (unpublished); Phys. Rev., 123, 1356 (1961).

BLI 63 M.V. Blinov, N.M. Kazarinov, A.N. Protopopov and B.M. Shiryaev, Soviet Phys. -JETP, 16, 1159 (1963)

BLU 65 L. Blumberg, J. Gursky and R.B. Leachman, Symposium on the Physics and Chemistry of Fission, I.A.E.A., Salzburg, Paper SM-60/6 (1965).

BOD 62 D. Bodansky, Ann.Rev.Nucl.Sci., 12, 79 (1962).

BOH 39 N. Bohr and J.A. Wheeler, Phys. Rev., 56, 426 (1939).

BOW 63 H.R. Bowman, J.C.D. Milton, S.G. Thompson and W.J. Swiatecki, Phys. Rev., 129, 2133 (1963).

BOW 65 H.R. Bowman, S.G. Thompson, R.L. Watson, S.S. Kapoor and J.O. Rasmussen, Symposium on the Physics and Chemistry of Fission, I.A.E.A., Salzburg, Paper SM-60/53 (1965).

BRI 64 H.C. Britt and S.L. Whetstone, Jr., Phys. Rev., 133, B603 (1964).

BRO 53 F. Brown and L. Yaffe, Can. J. Chem., 31, 242 (1953).

BRU 62 C. Brun and G.N. Simonoff, Le Journale de Physique et Le Radium, 23, 12 (1962).

CHA 62 R. Chaudhry, R. Vandenbosch and J.R. Huizenga, Phys. Rev., 126, 220 (1962).

CHO 63 G.R. Choppin and T.J. Klingen, Phys. Rev., 130, 1990 (1963).

CHU 59 Y.Y. Chu, University of California Radiation Laboratory Report, UCRL-8926 (1959).

COH 55 B.L. Cohen, B.L. Ferrell-Bryan, D.J. Coombe and M.K. Hullings, Phys. Rev., 98, 685 (1955).

COH 63 S. Cohen and W.J. Swiatecki, Ann. Phys., 22, 406 (1963).

COL 61 L.J. Colby, Jr., and J.W. Cobble, Phys. Rev., 121, 1410 (1961).

COR 51 C.D. Coryell and N. Sugarman, Radiochemical Studies, "The Fission Products", National Nuclear Energy Series Div. IV, 9, McGraw Hill Co. Inc., New York (1951).

COR 53 C.D. Coryell, Ann. Rev. Nucl. Sci., 2, 305 (1953).

COR 61 C.D. Coryell, M. Kaplan and R.D. Fink, Can. J. Chem., 39, 646 (1961).

CRO 60 I.F. Croall, U.K.A.E.A. Report, A.E.R.E.- R3209 (1960).

CRO 62 I.F. Croall and H.H. Willis, J. Inorg. Nucl. Chem., 24, 221 (1962).

CRO 63 I.F. Croall and H.H. Willis, J. Inorg. Nucl. Chem., 25, 1213 (1963).

DAV 63 J.H. Davies and L. Yaffe, Can. J. Phys., 41, 762 (1963); Can. J. Chem., 41, 1836 (1963).

DELM Delmar Scientific Laboratories, Chicago (Automatic Toepler pump, 0.5 litres).

DIL 51 C.R. Dillard, R.M. Adams, H. Finston and A. Turkevich, National Nuclear Energy Series, Div. IV, 9, Paper 68 McGraw Hill Co. Inc., New York (1951).

DOS 62 I. Dostrovsky (Private communications 1962, 1963).

DOS 64 I. Dostrovsky, S. Katcoff and R.W. Stoenner, Phys. Rev., 136, B44 (1964).

DRO 61 J.R.S. Drouin, Ph.D. Thesis, Department of Chemistry, McGill University (1961).

DUD 65 N.D. Dudey and T.T. Sugihara, Phys. Rev., 139, B896 (1965).

EIS 63 V.P. Eismont, Soviet Phys.-JETP, 17, 502 (1963).

ERB 63 M.T. Erben, L.E. Glendenin, H.C. Griffin and E.P. Steinberg (Private communication 1965).

ERI 59 T. Ericson, Nucl. Phys., 11, 481 (1959).

ERI 60 T. Ericson, Phil. Mag. Supplement 9, 425 (1960).

EWA 65 H. Ewald, Symposium on the Physics and Chemistry of Fission, I.A.E.A., Salzburg, Paper SM-60/38 (1965).

FAR 62 H. Farrar and R.H. Tomlinson, Can.J.Phys., 40, 943 (1962).

FAR 62b H. Farrar and R.H. Tomlinson, Nucl.Phys., 34, 367 (1962).

FAR 64 H. Farrar, W.B. Clarke, H.G. Thode and R.H. Tomlinson, Can. J.Phys., 42, 2063 (1964).

FEL 51 B.T. Feld, H. Feshbach, M.L. Goldberger, H. Goldstein and V.F. Weisskopf, Atomic Energy Commission Report, NYO-636 (1951).

FEL 62 F. Felix and P. Schmeling, Joint Euratom/United States Program, EUR 111.e, Brussels (1962).

FER 65 J.M. Ferguson and P.A. Read, Phys. Rev., 139, B56 (1965).

FES 53 H. Feshbach, M.M. Shapiro and V.F. Weisskopf, Atomic Energy Commission Report, NYO-3077 (1953).

FIC 59 H.R. Fickel and R.H. Tomlinson, Can.J. Phys., 37, 531 (1959).

FIE 63 J. Fiedler and G. Herrmann, Z. Naturforsch, 18a, 553 (1963).

FON 56 P. Fong, Phys. Rev., 102, 434 (1956).

FOR 58 B.M. Foreman, Ph.D. Thesis, University of California Radiation Laboratory Report, UCRL-8223, 1958 (Unpublished).

FOR 60 G.P. Ford, Phys. Rev., 118, 1261 (1960).

FOR 65 G.P. Ford and R.B. Leachman, Symposium on the Physics and Chemistry of Fission, I.A.E.A., Salzburg, Paper SM-60/24 (1965).

FRA 54 J.S. Fraser and J.C.D. Milton, Phys. Rev., 93, 818 (1954).

FRA 65 J.S. Fraser, Symposium on the Physics and Chemistry of Fission, I.A.E.A., Salzburg, Paper SM-60/34 (1965).

FRI 58 K. Fritze, C.C. McMullen and H.G. Thode, Second U.N. I.C.P.U.A.E., 15, P/187 (1958).

FRI 63 G. Friedlander, L. Friedman, B. Gordon and L. Yaffe, Phys. Rev., 129, 1809 (1963).

FRI 64 G. Friedlander, J.W. Kennedy, J.M. Miller, Nuclear and Radiochemistry, John Wiley and Sons, Inc., New York (2nd Edition, 1964).

FRI 65 G. Friedlander, Symposium on the Physics and Chemistry of Fission, I.A.E.A., Salzburg, Paper SM-60/63 (1965).

FUK 61 F. Fukuzawa, J. Phys. Soc. Japan, 16, 2371 (1961).

GIB 56 W.M. Gibson, Ph.D. Thesis, University of California Radiation Laboratory, UCRL-3493 (1956).

GLE 51 L.E. Glendenin, C.D. Coryell and R.R. Edwards, National Nuclear Energy Series, Div. IV, 9, Paper 52, McGraw Hill Co. Inc., New York (1951).

GLE 54 L.E. Glendenin and E.P. Steinberg, Ann. Rev. Nucl.Sci., 4, 69 (1954).

GLE 65 L.E. Glendenin, J.P. Unik, and H.C. Griffin, Symposium on the Physics and Chemistry of Fission, I.A.E.A., Salzburg, Paper SM-60/31 (1965).

GOE 49 R.H. Goeckermann and I. Perlman, Phys. Rev., 73, 1127 (1948); Phys. Rev., 76, 628 (1949).

GOR 57 B. Gordon and L. Friedman, Phys. Rev., 108, 1053 (1957).

GOR 65 G.E. Gordon and N.K. Aras, Symposium on the Physics and Chemistry of Fission, I.A.E.A., Salzburg, Paper SM-60/48 (1965).

GOW Gow-Mac Instruments Co., New Jersey (cell specification, AEL 9677).

GRA 60 D.L. Gray, U.S.A.E.C., Report HW-62639 (1960).

GRA 61 G. Grant, Ph.D. Thesis, Department of Chemistry, McGill University (1961).

GRA 65 G. Graff, A. Lajtai and L. Nagy, Symposium on the Physics and Chemistry of Fission, I.A.E.A., Salzburg, Paper SM-60/55 (1965).

GRO 60 V.M. Strutinski, L.V. Groshev and M.K. Akimova, Nucl. Phys., 16, 657 (1960).

GRO 61 J.R. Grover, Phys. Rev., 123, 267 (1961).

GRO 62 J.R. Grover, Phys. Rev., 127, 2142 (1962).

GRU 57 W.E. Grummitt and G.M. Milton, AECL Report CRC-694 (1957).

GUN 59 R. Gunnink and J.W. Cobble, Phys. Rev., 115, 1247 (1959).

HAF 62 W.L. Hafner, Jr., J.R. Huizenga and R. Vandenbosch, Argonne National Laboratory Report, ANL-6662 (1962).

HAG 63 E. Hagebo, J. Inorg. Nucl. Chem., 25, 1201 (1963).

HAG 64 E. Hagebo, A.C. Pappas and P. Aagaard, J. Inorg. Nucl. Chem., 26, 1639 (1964).

HAG 65 E. Hagebo, J. Inorg. Nucl. Chem., 27, 927 (1965).

HAH 39 O. Hahn and F. Strassmann, Naturwiss., 27, 11, 89 (1939); H.G. Graetzer, Am. J. Phys., 32, 9 (1964).

HAL 58 I. Halpern and V.M. Strutinski, in Proceedings of the International Conference on the Peaceful Uses of Atomic Energy, Geneva, 1958 (United Nations, New York, 1958), Vol. 15, 408

HAL 59 I. Halpern, Ann. Rev., Nucl. Sci., 9, 245 (1959).

HAL 61 I.B. Haller and G. Andersson, J. Inorg. Nucl. Chem., 20, 12 (1961).

HAMN Hamner Electronics Co. (Model, N-351).

HARS Harshaw Chemical Co., U.S.A.

HEWL Hewlett Packard, California (Digital Recorder Model H43 562A).

HIC 55 H.G. Hicks and R.S. Gilbert, Phys. Rev., 100, 1286 (1955).

HIC 62 H.G. Hicks, H.B. Levy, W.E. Nervik, P.C. Stevenson, J.B. Niday and J.C. Armstrong, Jr., Phys. Rev., 128, 700 (1962).

HOA 51 E.J. Hoagland and N. Sugarman, Radiochemical Studies, "The Fission Products", National Nuclear Energy Series Div. IV, 9, Paper 147, McGraw Hill Co. Inc., New York (1951).

HOD 65 R.C. Barrett, A.D. Hill and P.E. Hodgson, Nucl. Phys., 62, 133 (1965).

HOF 64 M.M. Hoffman, Phys. Rev., 133, B714 (1964).

HUI 60 J.R. Huizenga and R. Vandenbosch, Phys. Rev., 120, 1305 (1960).

HUI 62 J.R. Huizenga and R. Vandenbosch, in "Nuclear Reactions" (Edited by P.M. Endt and P.B. Smith) North-Holland, Amsterdam vol. 2 (1962).

HYD 60 E.K. Hyde, A Review of Nuclear Fission (Medium Energy) Part II, University of California Radiation Laboratory Report UCRL-9065 (1960) (Unpublished).

HYD 62 E.K. Hyde, A Revised Version of a Review of Nuclear Fission (Low Energy) Part I, University of California Radiation Laboratory Report UCRL-9036, revised 1962 (Unpublished).

HYD 64 E.K. Hyde, The Nuclear Properties of the Heavy Elements, Vol. III; Fission Phenomena, Prentice Hall Inc., Englewood Cliffs, N.J., 401 (1964).

JAM 64 R.H. James, G.R. Martin and D.J. Silvester, Radiochim. Acta 3, 1/2, 76 (1964).

JOH 64 S.A.E. Johansson, Nucl. Phys., 60, 378 (1964).

JOH 65 S.A.E. Johansson, Nucl. Phys., 64, 147 (1965).

JON 55 W.E. Jones, A. Timnick, J.H. Paehler and T.H. Handley, Phys. Rev., 99, 184 (1955).

KAP 61 M. Kaplan and C.D. Coryell, Phys. Rev., 124, 1949 (1961).

KAP 64 S.S. Kapoor and R. Ramanna, Phys. Rev., 133, B598 (1964).

KAT 52 S. Katcoff, Phys. Rev., 87, 886 (1952).

KAT 53 S. Katcoff and W. Rubinson, Phys. Rev., 91, 1458 (1953).

KAT 60 S. Katcoff, Nucleonics, 18, 201 (1960).

KAT 65 S. Katcoff and W. Rubinson, J. Inorg. Nucl. Chem., 27, 1447 (1965).

KAU 63 S. Kaufman, Phys. Rev., 129, 1866 (1963).

KIE 63 R.L. Kiefer, University of California Radiation Laboratory Report, UCRL-11049 (1963) (Unpublished).

KIR 54 J.S. Kirkaldy, Ph.D. Thesis, Foster Radiation Laboratory, McGill University (1954); and more recent private communications with Radiation Laboratory.

KJE 61 A. Kjelberg, H. Taniguchi and L. Yaffe, Can. J. Chem., 39, 635 (1961).

KOC 61 R.C. Koch and G.L. Grandy, Anal. Chem., 33, 43 (1961).

KON 65 E. Koneczny, H.D. Opower, H. Gunther, and H. Gobel, Symposium on the Physics and Chemistry of Fission, I.A.E.A., Salzburg, Paper SM-60/33 (1965).

KOW 64 L. Kowalski, Ann. de Physique, 9, 211 (1964).

KRA 53 K.A. Kraus and G.E. Moore, J. Am. Chem. Soc., 75, 1460 (1953).

KRI 61 W.R. Kritz, Nucleonics, 19, 106 (1961).

LEA 62 R.B. Leachman, Paper for the Boston Meeting of the American Nuclear Society, June 1962.

LEI 65a H. Maier-Leibnitz, P. Armbruster and H.J. Specht, Symposium on the Physics and Chemistry of Fission, I.A.E.A., Salzburg, Paper SM-60/52 (1965).

LEI 65b H. Maier-Leibnitz, H.W. Schmitt and P. Armbruster, Symposium on the Physics and Chemistry of Fission, I.A.E.A., Salzburg, Paper SM-60/54 (1965).

LEV 53 H.B. Levy, Ph.D. Thesis, University of California Radiation Laboratory Report, UCRL-2305 (1953) (Unpublished).

LEV 61 H.B. Levy, H.G. Hicks, W.E. Nervik, P.C. Stevenson, J.B. Niday and J.C. Armstrong, Jr., Phys. Rev., 124, 544 (1961).

LIN 60 M. Lindner and A. Turkevich, Phys. Rev., 119, 1632 (1960).

MAC 50 J. Macnamara, C.B. Collins, and H.G. Thode, Phys. Rev., 78, 129 (1950).

MANO The Manostat Corporation, New York (Flowmeter, M9142B).

MARC Marconi Co. (Model AEP 908).

MAT 65 D.S. Mather, P. Fieldhouse and A. Moat, Nucl. Phys., 66, 149 (1965).

MATH Matheson of Canada Ltd., Whitby, Ontario

MATS 65 T. Matsuo, J.M. Matuszek, Jr., N.D. Dudey and T.T. Sugihara, Phys. Rev., 139, B886 (1965).

MATU 65 J.M. Matuszek (Private communication December 1965).

MCC 54 G.H. McCormick and B.L. Cohen, Phys. Rev., 96, 722 (1954).

MCH 63 J.A. McHugh, Jr., Ph.D. Thesis, University of California Radiation Laboratory Report, UCRL-10673 (1963).

MEG 62 S. Meghir, Ph.D. Thesis, Department of Chemistry, McGill University (1962); and more recent communications.

MET 58 N. Metropolis, R. Bivins, M. Storm, A. Turkevich, J.M. Miller and G. Friedlander, Phys. Rev., 110, 185 (1958).

MIL 58 J.C.D. Milton and J.S. Fraser, Phys. Rev., 111, 877 (1958).

MIL 62 J.C.D. Milton, University of California Radiation Laboratory Report, UCRL-9883 (1962).

MIL 65 J.C.D. Milton and J.S. Fraser, Symposium on the Physics and Chemistry of Fission, I.A.E.A., Salzburg, Paper SM-60/45 (1965).

MILF 62 J.C.D. Milton and J.S. Fraser, Can. J. Phys., 40, 1626 (1962).

MOL 62 J.F. Mollenauer, Phys. Rev., 127, 867 (1962).

MOM 60 F.F. Momyer, Jr., "The Radiochemistry of the Rare Gases", Nuclear Science Series NAS-NS 3025, National Research Council, Washington D.C., (1960).

MOSE Moseley Co. (Hewlett Packard) California (Autograf, X-Y Recorder, Model 2D-2).

NAR 63 V. Narang, Ph.D. Thesis, Department of Chemistry, McGill University (1963).

NATL National Bureau of Standards, U.S. Department of Commerce, Washington D.C.

NDS Nuclear Data Sheets, edited by K. Way (National Academy of Sciences - National Research Council, Washington D.C. 1962, with later supplements).

NET 65 D.R. Nethaway and H.B. Levy, Phys. Rev., 139, B1505 (1965).

NICH R.H. Nicholls Ltd. (Model, AEP 1007B).

NIX 65 J.R. Nix and W.J. Swiatecki, Nucl. Phys., 71, 1 (1965).

PAP 53 A.C. Pappas, Massachusetts Institute of Technology Report No.63 (1953).

PAP 55 A.C. Pappas, U.N. I.C.P.U.A.E., 7, 19 (1955).

PAP 61 A.C. Pappas and J. Alstad, J. Inorg. Nucl. Chem., 17, 195 (1961).

PAR 66 S. Parikh, Ph.D. Thesis, Department of Chemistry, McGill University (1966).

PAT 55 B.D. Pate and L. Yaffe, Can. J. Chem., 33, 15; 610; 929; 1656 (1955); 34, 265 (1956).

PAT 58a B.D. Pate, J.S. Foster and L. Yaffe, Can. J. Chem., 36, 1691 (1958).

PAT 58b B.D. Pate, Can. J. Chem., 36, 1707 (1958).

PAT 65 P. Patzelt and G. Herrmann, Symposium on the Physics and Chemistry of Fission, I.A.E.A., Salzburg, Paper SM-60/60 (1965).

PER 63 F.G. Perey, Phys. Rev., 131, 745 (1963).

PET 65 G.A. Petrov, Soviet Phys. -JETP, 20, 1387 (1965).

POL 60 S.M. Polikanov and Y.T. Chubarkow, Zh. Eksperim. Teor. Fiz. (USSR), 38, 295 (1960).

POR 57 N.T. Porile, Phys. Rev., 108, 1526 (1957).

PORS 57 N.T. Porile and N. Sugarman, Phys. Rev., 107, 1410 (1957).

POW 62 J.A. Powers, Ph.D. Thesis, Purdue University (1962).

PRE 47 R.D. Present, Phys. Rev., 72, 7 (1947).

RIDL Radiation Instrument Development Laboratory, Illinois, (400 channel analyser, Model 34-12B).

ROS 58 M.E. Rose, International Conversion Coefficients, North-Holland, Amsterdam (1958).

RUD 65 G. Rudstam, Symposium on the Physics and Chemistry of Fission, I.A.E.A., Salzburg, Paper SM-60/65 (1965).

SAC 65 D.R. Sachdev (Private communication 1965).

SAH 65 G.B. Saha, Ph.D. Thesis, Department of Chemistry, McGill University (1965).

SAR 65 D.G. Sarantites, C.D. Coryell and G.E. Gordon, Phys. Rev., 138, B353 (1965).

SCIE Scientific Glass Apparatus Co., New Jersey (pressure stopcock, JS-5205).

SCH 54 R.A. Schmitt and N. Sugarman, Phys. Rev., 95, 1260 (1954).

SEE 63 D.W. Seegmiller, University of California Radiation Laboratory Report, UCRL-10850 (1963) (Unpublished).

SEG 49 E. Segrè and A.C. Helmholz, Revs. Modern Phys., 21, 271 (1949).

SER 47 R. Serber, Phys. Rev., 72, 1114 (1947).

SHA 59 R.A. Sharp and A.C. Pappas, J. Inorg. Nucl. Chem., 10, 173 (1959).

SIK 65 T. Sikkeland and G.R. Choppin, J. Inorg. Nucl. Chem., 27, 13 (1965).

SKA 65 K. Skarsvag and J. Singstad, Nucl. Phys., 62, 103 (1965).

SPE 53 R.W. Spence and G.P. Ford, Ann. Rev. Nucl. Sci., 2, 399 (1953).

SPE 65 H.J. Specht and H. Seyfarth, Symposium on the Physics and Chemistry of Fission, I.A.E.A., Salzburg, Paper SM-60/61 (1965).

STE 55 E.P. Steinberg and L.E. Glendenin, U.N. I.C.P.U.A.E., 3 (1955).

STE 58 P.C. Stevenson, H.G. Hicks, W.E. Nervik and D.R. Nethaway, Phys. Rev., 111, 886 (1958).

STE 59 R.M. Sternheimer, Phys. Rev., 115, 137 (1959).

STE 65 W.E. Stein, Symposium on the Physics and Chemistry of Fission, I.A.E.A., Salzburg, Paper SM-60/37 (1965).

STO 62 H.A. Storms, Ph.D. Thesis, Massachusetts Institute of Technology, September 1962 (Unpublished).

STO 65 H.A. Storms (Private communication 1965).

STR 60 V.M. Strutinski, Soviet Phys. -JETP, 10, 613 (1960).

STR 65 P.O. Strom, G.R. Grant and A.C. Pappas, Can. J. Chem., 43, 2493 (1965).

SUG 44 N. Sugarman and A. Turkevich (Private communication to C.D. Coryell, cf. reference COR 61).

SWI 65 W.J. Swiatecki, Symposium on the Physics and Chemistry of Fission, I.A.E.A., Salzburg, Paper SM-60/1 (1965).

TAL 63 M. Talat-Erben and B. Guven, Phys. Rev., 129, 1762 (1963); Phys. Rev., 134, B972 (1964).

TER 62 J. Terrell, Phys. Rev., 127, 880 (1962).

TER 65 J. Terrell, Symposium on the Physics and Chemistry of Fission, I.A.E.A., Salzburg, Paper SM-60/43 (1965).

TEW 52 H.A. Tewes and R.A. James, Phys. Rev., 88, 860 (1952).

TEX Texas Instruments Inc., U.S.A. (Rectilinear recorder, No. 882).

THO 64 T.D. Thomas, Nucl. Phys., 53, 577 (1964).

THOGP 65 T.D. Thomas, R.A. Atneosen, W.M. Gibson and M.L.Perlman, Symposium on the Physics and Chemistry of Fission, I.A.E.A., Salzburg, Paper SM-60/57 (1965).

THOGS 65 T.D. Thomas, W.M. Gibson and G.J. Safford, Symposium on the Physics and Chemistry of Fission, I.A.E.A., Salzburg, Paper SM-60/36 (1965).

THOV 64 T.D. Thomas and R. Vandenbosch, Phys. Rev., 133, B976 (1964).

TIL 63a R.S. Tilbury, Ph.D. Thesis, Department of Chemistry, McGill University (1963).

TIL 63b R.S. Tilbury and L. Yaffe, Can. J. Chem., 41, 1956 (1963).

TOB 61 W. Tobocman, "Theory of Direct Nuclear Reactions", Oxford University Press, London (1961).

TOW 61 C.W. Townley, J.E. Howes, Jr., G.E. Raines, W.S. Diethorn and D.N. Sunderman, Nucl. Sci. and Eng., 10, 346 (1961).

TRO 64 D.E. Troutner, A.C. Wahl and R.L. Ferguson, Phys. Rev., 134, B1027 (1964).

TUR 51 A. Turkevich and J.B. Niday, Phys. Rev., 84, 52 (1951).

VAN 58 R. Vandenbosch and J.R. Huizenga in Proceedings of the International Conference on the Peaceful Uses of Atomic Energy, Geneva, 1958, Vol. 15, 212.

VAN 60 R. Vandenbosch and J.R. Huizenga, Phys. Rev., 120, 1313 (1960).

VAN 65 R. Vandenbosch, L. Haskin and J.C. Norman, Phys. Rev., 137, B1134 (1965).

VIO 65 V.E. Viola, J.M. Alexander and A.R. Trips, Phys. Rev., 138, B1434 (1965).

VON 64 H.K. Vonach, R. Vandenbosch and J.R. Huizenga, Nucl. Phys.,60, 70 (1964).

WAH 55 A.C. Wahl, Phys. Rev., 99, 730 (1955).

WAH 58 A.C. Wahl, J. Inorg. Nucl. Chem., 6, 263 (1958).

WAH 62 A.C. Wahl, R.L. Ferguson, D.R. Nethaway, D.E. Troutner and K. Wolfsberg, Phys. Rev., 126, 1112 (1962).

WAH 65 A.C. Wahl, Symposium on the Physics and Chemistry of Fission, I.A.E.A., Salzburg, Paper SM-60/22 (1965).

WAR 64 H. Warhanek and R. Vandenbosch, J. Inorg. Nucl. Chem., 26, 669 (1964).

WEA 63 L.E. Weaver, P.O. Strom and P.A. Killeen, Report USNRDL-TR-633 (1963).

WEB 63 J.W. Weber, J. Nucl. Materials, 10, 67 (1963).

WEL 59 L.A. Weller, U.S.A.E.C. Research and Development Report MLM-1092 (1959).

WEL 58 F.J. Welcher, "The Analytical Uses of Ethylenediamine-tetra-acetic acid", (D. Van Nostrand Co. Inc., Princeton, New Jersey, 1958 (reprinted)).

WELCH W.M. Welch Manufacturing Co., Chicago (Duo-Seal vacuum pump).

WHE 56 J.A. Wheeler, International Conference on the Peaceful Uses of Atomic Energy, U.N., New York, 2, 155, P/593 (1956).

WHE 64 S.L. Whetstone, Jr., Phys. Rev., 133, B613 (1964).

WHI 52 W.J. Whitehouse, "Progress in Nuclear Physics", 2, 120 Pergamon Press, New York (1952).

WIL 57 E.J. Wilson, C. Evans, J. Chadwick, J. Eakins and K.J. Taylor, Harwell Report, A.E.R.E. 1/R 2216 (1957).

WIN 62 J. Wing, Argonne National Laboratory Report, ANL-6598 (1962, with corrections and additions).

WOL 65 K. Wolfsberg, Phys. Rev., 137, B929 (1965).

Ph.D. JOHN H. FORSTER Chemistry

XENON YIELDS AND ISOMER RATIOS IN THE FISSION OF HEAVY ELEMENTS BY MEDIUM-ENERGY PROTONS

ABSTRACT

The independent yields of ^{135}Xe, ^{133m}Xe and ^{133g}Xe and the cumulative yields of ^{135}I and ^{133}I have been measured radiochemically for twenty-seven fission systems, consisting of the targets ^{232}Th, ^{238}U, ^{235}U and ^{233}U with 20-85-MeV protons. Absolute yields were measured by monitoring the proton beam with the reaction $^{65}Cu(p,pn)^{64}Cu$.

Isomeric yield ratios of ^{133}Xe were of primary interest. They were apparently independent of the spin and type of the target and were more weakly dependent on fission energy than expected. Crude statistical computations were made for three spin-pair classes of isomers.

Two empirical methods assumed a Gaussian charge distribution and gave Z_p values for chains 133 and 135. Corresponding neutron yields were approximated semi-empirically. The behaviour of ^{235}U and ^{233}U was considerably different from that of ^{238}U and ^{232}Th for which more data exist. Total chain yields were obtained for A = 133 and 135.